

VOLUME 80

JANUARY 1, 1976

NUMBER 1

JPCA_x

THE JOURNAL OF
PHYSICAL
CHEMISTRY



PUBLISHED BIWEEKLY BY THE AMERICAN CHEMICAL SOCIETY

Announcing:

SUPER SERVICE

Now your J.T. Baker distributor can also ship you things he doesn't have!

How can your Baker distributor ship you things he doesn't have? Easy. He now can immediately contact the Baker Super Service Center and—in almost every instance—have the desired item shipped directly to you within 24 hours. *It's as though your J. T. Baker distributor has just added the largest reagent warehouse in the world to his backyard to serve you.* (To super-serve you.)

Now depend on your nearest Baker distributor for *all* of your laboratory reagent needs. He's listed on the facing page.

And do you have our new 428-page Catalog 750 featuring thousands of Baker quality laboratory chemicals? If not, please use coupon below. Thanks.

J. T. Baker Chemical Co.
222 Red School Lane
Phillipsburg, N.J. 08865

Please forward a copy of your new Catalog 750.

Name _____

Title _____

Dept. _____

Organization _____

Address _____

_____ Zip _____

Check Baker first!



J. T. Baker Chemical Co.
222 Red School Lane
Phillipsburg, N.J. 08865
201/859-5411

J.T. Baker

SUPER SERVICE DISTRIBUTORS

ALABAMA

Sargent-Welch Scientific Co.
Birmingham
205 / 251-5125

ARIZONA

VWR Scientific
Phoenix
602 / 272-3272

VWR Scientific
Tucson
602 / 624-8371

CALIFORNIA

Sargent-Welch Scientific Co.
Anaheim
714 / 772-3550

VWR Scientific
Los Angeles
213 / 265-8123

VWR Scientific
San Diego
714 / 262-0711

VWR Scientific
San Francisco
415 / 469-0100

Curtin-Matheson Scientific Co.
Brisbane
415 / 467-1040

Curtin-Matheson Scientific Co.
Fountain Valley
714 / 963-6761

COLORADO

VWR Scientific
Denver
303 / 388-5651

Sargent-Welch Scientific Co.
Denver
303 / 399-8220

CONNECTICUT

Brand-Nu Laboratories, Inc.
Meriden
203 / 235-7989

DELAWARE

John G. Merkel & Sons
Wilmington
302 / 654-8818

FLORIDA

Curtin-Matheson Scientific Co.
Orlando
305 / 859-8281

GEORGIA

Curtin-Matheson Scientific Co.
Atlanta
404 / 349-3710

VWR Scientific
Atlanta
404 / 351-3872

Estes Surgical Supply Co.
Atlanta
404 / 521-1700

HAWAII

VWR Scientific
Honolulu
808 / 847-1361

ILLINOIS

Sargent-Welch Scientific Co.
Skokie
312 / 267-5300

A. Daigger & Co.
Chicago
312 / 644-9438

LaPine Scientific Co.
Chicago
312 / 735-4700

Macmillan Science Co., Inc.
Chicago
312 / 488-4100

SGA Scientific Inc.
Elk Grove Village
312 / 439-2500

Technical Industrial Products
East Peoria
309 / 694-6226

Wilkins-Anderson Co.
Chicago
312 / 384-4433

Curtin-Matheson Scientific Co.
Elk Grove Village
312 / 439-5880

Rascher & Betzold, Inc.
Chicago
312 / 275-7300

INDIANA

General Medical of Indiana
Indianapolis
317 / 634-8560

KENTUCKY

Preiser Scientific Inc.
Louisville
304 / 343-5515

LOUISIANA

Curtin-Matheson Scientific Co.
New Orleans
504 / 524-0475

MARYLAND

Curtin-Matheson Scientific Co.
Beltsville
301 / 937-5950

VWR Scientific
Baltimore
301 / 796-8500

MASSACHUSETTS

Doe & Ingalls, Inc.
Medford
617 / 391-0090

Curtin-Matheson Scientific Co.
Woburn
617 / 935-8888

Healthco Scientific
Canton
617 / 828-3310

SciChemCo
Everett
617 / 389-7000

VWR Scientific
Newton Upper Falls
617 / 969-0900

MICHIGAN

Curtin-Matheson Scientific Co.
Detroit
313 / 964-0310

Curtin-Matheson Scientific Co.
Midland
517 / 631-9500

Rupp & Bowman Company
Detroit
313 / 491-7000

Sargent-Welch Scientific Co.
Detroit
313 / 931-0337

MINNESOTA

Curtin-Matheson Scientific Co.
Minneapolis
612 / 378-1110

Hawkins Chemical Co.
Minneapolis
612 / 331-6910

Lerlab Supply Co.
Hibbing
218 / 262-3456

Physicians & Hosp. Supply Co.
Scientific & Laboratory Div.
Minneapolis
612 / 333-5251

MISSOURI

Curtin-Matheson Scientific Co.
Kansas City
816 / 561-8780

Curtin-Matheson Scientific Co.
Maryland Heights
314 / 872-8100

MONTANA

Northwest Scientific Co.
Billings
406 / 252-3269

NEW JERSEY

Ace Scientific Supply Co., Inc.
Linden
201 / 925-3300

Amend Drug & Chem. Co., Inc.
Irvington
201 / 926-0333
212 / 228-8920

J. & H. Berge, Inc.
South Plainfield
201 / 561-1234

Beckman Instruments Inc.
Mountainside
201 / 232-7600

Curtin-Matheson Scientific Co.
Wayne
201 / 278-3300

Macalaster Bicknell of N.J., Inc.
Millville
609 / 825-3222

Sargent-Welch Scientific Co.
Springfield
201 / 376-7050

SGA Scientific Inc.
Bloomfield
201 / 748-6600
212 / 267-9451

Seidler Chem. & Supply Co.
Newark
201 / 622-4495

NEW MEXICO

VWR Scientific
Albuquerque
505 / 842-8650

NEW YORK

Albany Laboratories, Inc.
Albany
518 / 434-1747

Ashland Chemical Co.
Binghamton
607 / 723-5455

Berg Chemical Co.
New York
212 / 563-2684

Kem Chemical
Mt. Vernon
914 / 699-3110

New York Lab. Supply Co.
West Hempstead
516 / 538-7790

Riverside Chemical Co.
N. Tonawanda
716 / 692-1350

VWR Scientific
Rochester
716 / 288-5881

NORTH CAROLINA

Carolina Biological Supply Co.
Burlington
919 / 584-0381

OHIO

Curtin-Matheson Scientific Co.
Cincinnati
513 / 671-1200

Curtin-Matheson Scientific Co.
Cleveland
216 / 883-2424

VWR Scientific
Columbus
614 / 445-8281

Sargent-Welch Scientific Co.
Cincinnati
513 / 771-3850

Sargent-Welch Scientific Co.
Garfield Heights, Cleveland
216 / 587-3300

OKLAHOMA

Curtin-Matheson Scientific Co.
Tulsa
918 / 622-1700

Melton Company, Inc.
Labco Scientific Div.
Oklahoma City
405 / 235-3526

OREGON

VWR Scientific
Portland
503 / 225-0400

PENNSYLVANIA

Arthur H. Thomas Company
Philadelphia
215 / 627-5600

Bellevue Surgical Supply Co.
Reading
215 / 376-2991

Bowman-Mell Co., Inc.
Harrisburg
717 / 238-5235

Dolbey Scientific
Philadelphia
215 / 748-8600

Para Scientific Co.
Fairless Hills
609 / 882-4545

Reading Scientific Co.
Reading
215 / 921-0221

Scientific Equipment Co.
Philadelphia
215 / 222-5655

RHODE ISLAND

Eastern Scientific Co.
Providence
401 / 831-4100

TENNESSEE

Durr-Fillauer Surgical
Supplies, Inc.
Chattanooga
615 / 267-1161

Nashville Surgical Supply Co.
Nashville
615 / 255-4601

TEXAS

Curtin-Matheson Scientific Co.
Dallas
214 / 747-2503

Curtin-Matheson Scientific Co.
Houston
713 / 923-1661

Sargent-Welch Scientific Co.
Dallas
214 / 357-9381

Capitol Scientific
Austin
512 / 836-1167

VWR Scientific
Houston
713 / 641-0681

VWR Scientific
El Paso
915 / 778-4225

UTAH

VWR Scientific
Salt Lake City
801 / 328-1112

VIRGINIA

General Medical
Vienna
703 / 938-3500

General Scientific
Richmond
804 / 264-2861

WEST VIRGINIA

Preiser Scientific
Charleston
304 / 343-5515

WASHINGTON

VWR Scientific
Seattle
206 / 447-5811

WISCONSIN

Genetec Hospital Supply Co.
Div. of McKesson & Robbins
Milwaukee
414 / 271-0468

Drake Brothers
Menomonee Falls
414 / 781-2166



THE JOURNAL OF PHYSICAL CHEMISTRY

BRYCE CRAWFORD, Jr., *Editor*
STEPHEN PRAGER, *Associate Editor*
ROBERT W. CARR, Jr., **FREDERIC A. VAN-CATLEDGE**, *Assistant Editors*

EDITORIAL BOARD: C. A. ANGELL (1973–1977), F. C. ANSON (1974–1978), V. A. BLOOMFIELD (1974–1978), J. R. BOLTON (1976–1980), L. M. DORFMAN (1974–1978), H. L. FRIEDMAN (1975–1979), H. L. FRISCH (1976–1980), W. A. GODDARD (1976–1980), E. J. HART (1975–1979), W. J. KAUZMANN (1974–1978), R. L. KAY (1972–1976), D. W. McCLURE (1974–1978), R. M. NOYES (1973–1977), W. B. PERSON (1976–1980), J. C. POLANYI (1976–1980), S. A. RICE (1976–1980), F. S. ROWLAND (1973–1977), R. L. SCOTT (1973–1977), W. A. STEELE (1976–1980), J. B. STOTHERS (1974–1978), W. A. ZISMAN (1972–1976)

Published by the
AMERICAN CHEMICAL SOCIETY
BOOKS AND JOURNALS DIVISION
D. H. Michael Bowen, Director

Editorial Department: Charles R. Bertsch,
Head; Marianne C. Brogan, Associate
Head; Celia B. McFarland, Joseph E.
Yurvati, Assistant Editors

Graphics and Production Department:
Bacil Guiley, Head

Research and Development Department:
Seldon W. Terrant, Head

Advertising Office: Centcom, Ltd., 50 W.
State St., Westport, Conn. 06880.

© Copyright, 1976, by the American
Chemical Society. No part of this publica-
tion may be reproduced in any form with-
out permission in writing from the Ameri-
can Chemical Society.

Published biweekly by the American
Chemical Society at 20th and Northamp-
ton Sts., Easton, Pennsylvania 18042. Sec-
ond class postage paid at Washington, D.C.
and at additional mailing offices.

Editorial Information

Instructions for authors are printed in
the first issue of each volume. Please con-
form to these instructions when submitting
manuscripts.

Manuscripts for publication should be
submitted to *The Journal of Physical
Chemistry*, Department of Chemistry, Uni-
versity of Minnesota, Minneapolis, Minn.
55455. Correspondence regarding accepted
papers and proofs should be directed to
the Editorial Department at the ACS East-
on address.

Page charges of \$60.00 per page are as-
sessed for papers published in this journal.
Ability to pay does not affect acceptance or
scheduling of papers.

Bulk reprints or photocopies of indi-
vidual articles are available. For informa-
tion write to Business Operations, Books
and Journals Division at the ACS Wash-
ington address.

Requests for **permission to reprint**
should be directed to Permissions, Books
and Journals Division at the ACS Wash-
ington address. The American Chemical
Society and its Editors assume no responsi-
bility for the statements and opinions ad-
vanced by contributors.

Subscription and Business Information

1976 Subscription rates—including sur-
face postage

	U.S.	PUAS	Canada, Foreign
Member	\$24.00	\$29.75	\$30.25
Nonmember	96.00	101.75	102.25
Supplementary material	15.00	19.00	20.00

Air mail and air freight rates are avail-
able from Membership & Subscription Ser-
vices, at the ACS Columbus address.

New and renewal subscriptions
should be sent with payment to the Office
of the Controller at the ACS Washington
address. Changes of address must include
both old and new addresses with ZIP code
and a recent mailing label. Send all ad-
dress changes to the ACS Columbus ad-
dress. Please allow six weeks for change to
become effective. Claims for missing num-
bers will not be allowed if loss was due to
failure of notice of change of address to be
received in the time specified; if claim is

dated (a) North America—more than 90
days beyond issue date, (b) all other foreign
—more than 1 year beyond issue date; or if
the reason given is “missing from files”.
Hard copy claims are handled at the ACS
Columbus address.

Microfiche subscriptions are available
at the same rates but are mailed first class
to U.S. subscribers, air mail to the rest of
the world. Direct all inquiries to Business
Operations, Books and Journals Division,
at the ACS Washington address or call
(202) 872-4444. Single issues in hard copy
and/or microfiche are available from Spe-
cial Issues Sales at the ACS Washington
address. Current year \$4.75. Back issue
rates available from Special Issues Sales.
Back volumes are available in hard copy
and/or microform. Write to Special Issues
Sales at the ACS Washington address for
further information. Microfilm editions of
ACS periodical publications are available
from volume 1 to the present. For further
information, contact Special Issues Sales
at the ACS Washington address. **Supple-
mentary material** must be ordered direct-
ly from Business Operations, Books and
Journals Division, at the ACS Washington
address.

	U.S.	PUAS, Canada	Other Foreign
Microfiche	\$2.50	\$3.00	\$3.50
Photocopy			
1–7 pages	4.00	5.50	7.00
8–20 pages	5.00	6.50	8.00

Orders over 20 pages are available only on
microfiche, 4 × 6 in., 24X, negative, silver
halide. Orders must state photocopy or mi-
crofiche if both are available. Full biblio-
graphic citation including names of all au-
thors and prepayment are required. Prices
are subject to change.

American Chemical Society
1155 16th Street, N.W.
Washington, D.C. 20036
(202) 872-4600

Member & Subscription Services
American Chemical Society
P.O. Box 3337
Columbus, Ohio 43210
(614) 421-7230

Editorial Department
American Chemical Society
20th and Northampton Sts.
Easton, Pennsylvania 18042
(215) 258-9111

Notice to Authors printed in this issue

NOTICE TO AUTHORS

I. General Considerations

The Journal of Physical Chemistry is devoted to reporting both experimental and theoretical research dealing with fundamental aspects of physical chemistry. Space limitations necessitate giving preference to research articles dealing with previously unanswered basic questions in physical chemistry. Acceptable topics are those of general interest to physical chemists, especially work involving new concepts, techniques, and interpretations. Research that may lead to reexaminations of generally accepted views is, of course, welcome.

Authors reporting data should include an interpretation of the data and its relevance to the theories of the properties of matter. However, the discussion should be concise and to the point and excessive speculation is to be discouraged. Papers reporting redeterminations of existing data will be acceptable only if there is reasonable justification for repetition: for example, if the more recent or more accurate data lead to new questions or to a reexamination of well known theories. Manuscripts that are essentially applications of chemical data or reviews of the literature are, in general, not suitable for publication in *The Journal of Physical Chemistry*. Detailed comparisons of methods of data analysis will be considered only if the paper also contains original data, or if such comparison leads to a genesis of new ideas.

Authors should include an introductory statement outlining the scientific rationale for the research. The statement should clearly specify the questions for which answers are sought and the connection of the present work with previous work in the field. All manuscripts are subject to critical review. It is to be understood that the final decision relating to a manuscript's suitability rests solely with the editors.

Symposium papers are sometimes published as a group, but only after special arrangement with the editor.

II. Types of Manuscripts

The Journal of Physical Chemistry publishes two types of manuscripts: *Articles* and *Communications*.

A. *Articles* should cover their subjects with thoroughness, clarity, and completeness. However, authors should also strive to make their *Articles* as concise as possible, avoiding unnecessary historical background. Abstracts to *Articles* should be brief—300 words is a maximum—and should serve to summarize the significant data and conclusions. The abstract should convey the essence of the *Article* to the reader.

B. *Communications* are of two types, *Letters* and *Comments*. Both types are restricted to three-quarters of a page (750 words or the equivalent) including tables, figures, and text, and both types of *Communications* are subject to critical review, but special efforts will be made to expedite publication.

Letters should report preliminary results whose immediate availability to the scientific community is deemed important, and whose topic is timely enough to justify the double publication that usually results from the publication of a *Letter*.

Comments include significant remarks on the work of others. The editors will generally permit the authors of the work being discussed to reply.

The category of *Notes* has been discontinued since the handling of such manuscripts was precisely the same as that of *Articles* save for the requirement of an Abstract, and since even a short *Article* will need an Abstract ultimately, it seems as well to ask the author to provide this. Short *Articles* will of course continue to be welcome contributions.

III. Introduction

All manuscripts submitted should contain brief introductory remarks describing the purpose of the work and giving sufficient background material to allow the reader to appreciate the state-of-knowledge at the time when the work was done. The introductory remarks in an *Article* should constitute the first section of the paper and should be labeled accordingly. In *Communications*, the introductory material should not be in such a separate section. To judge the appropriateness of the manuscript for *The Journal of Physical Chemistry*, the editors will place considerable weight on the author's intentions as stated in the Introduction.

IV. Microform Material

From time to time manuscripts involve extensive tables, graphs, spectra, mathematical derivations, expanded discussions of peripheral points, or other material which, though essential to the specialized reader who needs all the data or all the detail, does not help and often hinders the effective presentation of the work being reported. Such "microform material" can be included in the *microfilm* edition of this Journal, available in many scholarly libraries, and also in the *microfiche* edition. In some instances the microform material may also be included in the printed issue in *miniprint*, in which the manuscript pages are reproduced directly in reduced size. All microform material may be obtained directly by the interested reader at nominal cost, either in full size photocopy or in microfiche (in which miniprint material appears at standard reduction, i.e., one manuscript page per microfiche frame). Authors are encouraged to make use of this resource, in the interest of shorter articles (which mean more rapid publication) and clearer more readable presentation.

Microform material should accompany a manuscript at the time of its original submission to an editor. It should be clipped together and attached at the end of the manuscript, along with a slip of paper clearly indicating the material is "microform material". Copy for microform material should preferably be on 8½ × 11 in. paper, and in no case on sheets larger than 11 × 14 in.; if typed it should be one and one-half spaced, and in any event the smallest character should be at least one-eighth inch in size; good contrast of black characters against a white background is required for clear photoprocess reproduction. A duplicate copy is required for indexing purposes.

A paragraph should appear at the end of the paper indicating the nature of the material and the means by which the interested reader may obtain copies directly. The following is an example.

Supplementary Material Available: description of the material (no. of pages). Ordering information is given on any current masthead page.

V. Functions of Reviewers

The editors request the scientific advice of reviewers who are active in the area of research covered by the manuscript. The reviewers act only in an advisory capacity and the final decision concerning a manuscript is the responsibility of the editors. The reviewers are asked to comment not only on the scientific content, but also on the manuscript's suitability for *The Journal of Physical Chemistry*. With respect to *Communications*, the reviewers are asked to comment specifically on the urgency of publication. **Authors are encouraged to suggest, when submitting a manuscript, names of scientists who could give a disinterested and informed and helpful evaluation of the work.** All reviews are anonymous and the reviewing process is most effective if reviewers do not reveal their identities to the authors. An exception arises in connection with a manuscript submitted for publication in the form of a comment on the work of another author. Under such circumstances the first author will, in general, be allowed to review the communication and to write a rebuttal, if he so chooses. The rebuttal and the original communication may be published together in the same issue of the journal. Revised manuscripts are generally sent back to the original reviewers, who are asked to comment on the revisions. If only minor revisions are involved, the editors examine the revised manuscript in light of the recommendations of the reviewers without seeking further opinions. For the convenience of reviewers, authors are advised to indicate clearly, either in the manuscript or in a covering letter, the specific revisions that have been made.

VI. Submission of Manuscripts

All manuscripts must be submitted in triplicate to expedite handling. Manuscripts must be typewritten, double-spaced copy, on 8½ × 11 in. paper. Legal sized paper is not acceptable. Authors should be certain that copies of the manuscript are clearly reproduced and readable. **Authors submitting figures must include the original drawings or photographs thereof, plus three xerographic copies for review purposes. These reproductions of the figures should be on 8½ × 11 in. paper.** Graphs must be in black ink on white or blue paper. Figures and tables should be held to a minimum consistent with adequate presentation of information. All original data which the author deems pertinent must be submitted along with the manuscript. For example, a paper reporting a crystal structure should include structure factor tables for use by the reviewers.

All references and explanatory notes, formerly set up as footnotes on individual pages, are now grouped at the end of the article in a section called "References and

Notes." They should be numbered consecutively in the order in which they are first mentioned in the text, and the complete list of notes and literature citations should appear at the end of the manuscript. Nomenclature should conform to that used in *Chemical Abstracts* and mathematical characters should be underlined for italics, Greek letters should be annotated, and subscripts and superscripts clearly marked.

Papers should not depend for their usefulness on unpublished material, and excessive reference to material in press is discouraged. References not readily available (*e.g.*, private technical reports, preprints, or articles in press) that are necessary for a complete review of the paper must be included with the manuscript for use by the reviewers.

VII. Revised Manuscripts

A manuscript sent back to an author for revision should be returned to the editor within 6 months; otherwise it will be considered withdrawn and treated as a new manuscript when and if it is returned. Revised manuscripts returned to the editor must be submitted in triplicate and all changes should be made by typewriter. **Unless the changes are very minor, all pages affected by revision must be re-typed.** If revisions are so extensive that a new typescript of the manuscript is necessary, it is requested that a copy of the original manuscript be submitted along with the revised one.

VIII. Proofs and Reprints

Galley proofs, original manuscript, cut copy, and reprint order form are sent by the printer directly to the author who submitted the manuscript. The attention of the authors is directed to the instructions which accompany the proof, especially the requirement that all corrections, revisions, and additions be entered on the proof and not on the manuscript. Proofs should be checked against the manuscript (in particular all tables, equations, and formulas, since this is not done by the editor) and returned as soon as possible. No paper is released for printing until the author's proof has been received. Alterations in an article after it has been set in type are made at the author's expense, and it is understood that by entering such alterations on proofs the author agrees to defray the cost thereof. The filled-out reprint form must be returned with the proof, and if a price quotation is required by the author's organization a request for it should accompany the proof. Reprint shipments are made a month or more after publication, and bills are issued by the printer subsequent to shipment. Neither the editors nor the Washington office keeps any supply of reprints. Therefore, only the authors can be expected to meet requests for single copies of papers.

A page charge is assessed to cover in part the cost of publication. Although payment is expected, it is not a condition for publication. Articles are accepted or rejected only on the basis of merit, and the editor's decision to publish the paper is made before the charge is assessed. The charge per journal page is \$60.

COMMUNICATIONS TO THE EDITOR

Polymorphism of Cholesteryl Acrylate	Shinichi Yano,* Junji Yasue, and Koichiro Aoki 88
Experimental Confirmation of the Gronwall-Friedman Limiting Law for Unsymmetrical Electrolytes	H. Frank Gibbard and Michael J. Wilson 89

■ Supplementary material for this paper is available separately (consult the masthead page for ordering information): it will also appear following the paper in the microfilm edition of this journal.

* In papers with more than one author, the asterisk indicates the name of the author to whom inquiries about the paper should be addressed.

AUTHOR INDEX

Akazawa, H., 33	Hara, I., 64	Lévay, B., 37	Slagle, I. R., 14
Alegriá, A. E., 69	Heicklen, J., 1		Smith, G. R., 25
Aoki, K., 88	Hino, T., 33	Masuhara, H., 33	Stevenson, G. R., 69
Bauer, S. H., 73	Hopkins, H. P., Jr., 25	Mataga, N., 33	
Boskey, A. L., 40	Hoshino, M., 30	Morita, T., 30	Takezaki, Y., 8
Burgess, A. W., 52			Tsuji, A., 8
Carstensen, E. L., 55	Ibuki, T., 8	Norman, A. B., 25	Valko, L., 19
Chen, N. Y., 60	Ishii, Y., 30	Okazaki, M., 64	Vértes, A., 37
			Vigee, G. S., 83
Fujiyama, T., 64	Johnsen, R. H., 46	Posner, A. S., 40	Watkins, C. L., 83
	Jordan, F., 76		Wilson, M. J., 89
Gibbard, H. F., 89	Joshi, A., 46	Scheraga, H. A., 52	
Gilbert, J. R., 14		Shipman, L. L., 52	Yano, S., 88
Graham, R. E., 14	Koide, G. T., 55	Shizuka, H., 30	Yasue, J., 38
Gutman, D., 14	Kovářik, P., 19	Simonaitis, R., 1	Yokozeki, A., 73

THE JOURNAL OF PHYSICAL CHEMISTRY

Registered in U. S. Patent Office © Copyright, 1976, by the American Chemical Society

VOLUME 80, NUMBER 1 JANUARY 1, 1976

Reactions of HO₂ with NO and NO₂ and of OH with NO

R. Simonaitis and Julian Heicklen*

Department of Chemistry and Ionosphere Research Laboratory, The Pennsylvania State University, University Park, Pennsylvania 16802
(Received July 7, 1975)

The reaction of HO₂ with NO was studied at room temperature (~23°C) in competition with the reaction 2HO₂ → H₂O₂ + O₂ (3) and the competition for HO₂ between NO and NO₂ was studied by monitoring NO removal via the chemiluminescent detection of NO. The HO₂ radicals were produced either by N₂O or NO photolysis at 213.9 nm in the presence of O₂ and excess H₂. Two possible paths for the HO₂-NO reaction are HO₂ + NO → HO + NO₂ (1a) and HO₂ + NO → HONO₂ (1b). If k_3 is taken as 3.3×10^{-12} cm³/sec, then $k_{1a} = (1.0 \pm 0.2) \times 10^{-12}$ cm³/sec and $k_{1b} < 2 \times 10^{-15}$ cm³/sec. If an HO₂NO intermediate is formed in reaction 1, its lifetime is <2 sec. With NO₂ a complex set of reactions occurs: HO₂ + NO₂ → HONO + O₂ (2a) and HO₂ + NO₂ ⇌ HO₂NO₂ (2b, -2b) and possibly HO₂NO₂ → HONO + O₂ (10b). The intermediate HO₂NO₂ has a lifetime of about 50 sec and causes NO to be oxidized after the irradiation is terminated. A detailed analysis of the mechanism relates the lifetime of HO₂NO₂, τ_B , with the fundamental rate coefficients as $\tau_B^{-1} \approx k_{10b} + k_{-2b}k_{2a}/k_2 \sim 0.02$ sec⁻¹. The competition between reactions 1 and 2 gives $k_1/k_2' = 9.5 \pm 1.5$ where $k_2' = k_2 - k_{2b}k_{-2b}/(k_{-2b} + k_{10b})$. Thus $k_2' = (9.8 \pm 3.5) \times 10^{-14}$ cm³ sec⁻¹. Furthermore $k_2' \sim k_{2b}$, and $k_2 \sim 2k_2'$. Information was also obtained on the reaction OH + NO (+M) → HONO (+M) (4). The values obtained for k_4 were 3.7×10^{-12} cm³ sec⁻¹ at ~100 Torr of H₂ and 1.1×10^{-11} cm³ sec⁻¹ at ~730 Torr of H₂, in good agreement with recent literature values.

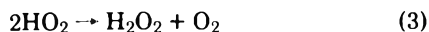
Introduction

The reactions of HO₂ with NO and NO₂ are important in atmospheric chemistry.



However, rate coefficients for these reactions are not yet known with sufficient accuracy for aeronomic purposes.

The reaction of HO₂ with NO has been studied by several groups. Davis et al.¹ give $k_{1a} = 3 \times 10^{-13}$ cm³ sec⁻¹ (with an uncertainty of a factor of 3) measured relative to

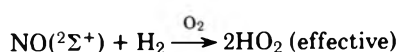
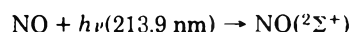


Hack et al.² found $k_{1a} = (2.0 \pm 0.5) \times 10^{-11} \exp\{-(1200 \pm 150)/T\}$ cm³ sec⁻¹ by monitoring OH production by EPR in a stirred flow reactor. At 300 K this gives a value of 3.7×10^{-13} cm³ sec⁻¹.

Lower limits to the rate coefficient for reaction 1a have been measured in our laboratory. In a competitive study with reaction 3 and monitoring NO₂ production, $k_{1a} \geq 1.1 \times 10^{-13}$ cm³ sec⁻¹ (based on $k_3 = 3.3 \times 10^{-12}$ cm³ sec⁻¹)

was obtained.³ Later the competition with reaction 2a was studied.⁴ It was found that $k_{2a} > 2 \times 10^{-13}$ cm³ sec⁻¹ (based on $k_3 = 3.3 \times 10^{-13}$ cm³ sec⁻¹) and $k_{1a}/k_{2a} = 7 \pm 1$; therefore $k_{1a} > 1.4 \times 10^{-12}$ cm³ sec⁻¹. Recently Cox,⁵ using a flow system at atmospheric pressure and monitoring NO, found $k_{1a} = 1.2 \times 10^{-12}$ cm³ sec⁻¹ and $k_{2a} = 1.2 \times 10^{-13}$ cm³ sec⁻¹ in reasonable agreement with our lower limits.

In order to obtain precise values of the rate coefficients for reactions 1a and 2a and to resolve the discrepancy between the measurements from the several laboratories, we have undertaken further studies of these systems. As in the earlier studies, the reactions of HO₂ with NO are studied by competitive methods with reaction 3 and with the reactions of HO₂ with NO₂. The HO₂ radicals are generated by photolysis of N₂O at 213.9 nm in the presence of H₂ and O₂,^{3,4} or by photolysis of NO at 213.9 nm also in the presence of H₂ and O₂. The reaction scheme assumed for the latter system is the following:



The reactions are monitored by the measurement of the NO removal rate using chemiluminescent detection of NO.

By proper adjustment of reaction conditions, the reaction of OH radicals with NO could also be studied.



There is good agreement in the literature for the rate coefficient for reaction 4 at low pressures, but very little work has been done near the high-pressure limit.⁶ Results for the rate coefficient of reaction 4 at $\sim 100 \pm 5$ Torr and $\sim 730 \pm 40$ Torr total pressure ($\sim 95\%$ H₂) are also presented in this paper.

Experimental Section

Apparatus and Procedure. A conventional high-vacuum line utilizing Teflon stopcocks with Viton O rings was used. The reaction vessel was a 2-l. Pyrex bulb provided with two quartz windows opposite each other for the passage of 213.9-nm radiation obtained from two Phillips Zn resonance lamps (TYP 93106E). Two lamps were used to obtain uniform illumination of the reaction vessel. Experiments performed with one lamp (under conditions where the quantum yields depend on the absorbed intensity, I_a) gave essentially the same results as with two lamps indicating that any remaining nonuniformity in illumination does not affect the results.

The contents of the reaction vessel could be sampled into the chemiluminescent detector either continuously or intermittently by a capillary bleed from the center of the vessel. The flow rate through the capillary was ~ 30 cm³/min.

The chemiluminescent analyzer was similar to the one described by Stedman et al.⁷ The analyzer was a cylindrical ~ 500 -cm³ vessel equipped with a quartz window for viewing the red emission, and with two nozzles for sample gas containing NO (from the reaction vessel) and O₃ injection. The analyzer was pumped with a Welch (No. 1402) high-velocity pump. Typically the analyzer pressures ranged from ~ 1 –3 Torr. Ozonized O₂ was prepared by a high-voltage discharge through O₂. The O₂–O₃ flow rate was ~ 130 cm³/min.

The red emission was viewed with an EMI photomultiplier Model No. (9558B) operated at 1600 V. The photomultiplier current was measured with a Keithly Picoammeter Model 410A, and the signal could be monitored continuously with a strip chart recorder.

The detector was calibrated with known pressures of NO. The lower detectability limit was about 10 ppb. The detector was linear in the measured range of 10 ppb to 200 ppm. The time constant of the electronics and the pumping system was always much less than that of the reaction. In experiments in which the time of reaction was short, continuous sampling of the reaction mixture was done. However, for long time experiments the reaction mixture was sampled intermittently in order to maintain a constant pressure in the reaction vessel.

Actinometry for the N₂O and NO photolysis experiments was done by measuring the rate of NO production from the photolysis of pure N₂O. For this system $\phi\{\text{NO}\} = 1.2$.⁸ To determine the absorbed light intensity, I_a , in the NO photolysis system, the relative absorption coefficients $\epsilon\{\text{NO}\}/\epsilon\{\text{N}_2\text{O}\} = 8 \pm 0.5$ ⁶ were used. When NO₂ was present in the NO photolysis experiments, an appreciable amount of light was absorbed by the NO₂. To compute I_a under these conditions, $\phi\{0(^1\text{D})\} = 0.5$ was taken for the photolysis of NO₂ at 213.9 nm,⁹ and the absorption cross section for NO₂ at 213.9 nm was taken to be 5.3×10^{19} cm².¹⁰

Materials. All gases except H₂ were from the Matheson Co. N₂O was purified by degassing at -196°C . Cylinder H₂ was purified by passage over traps maintained at -196°C . O₂ was used directly from the cylinder. NO was purified by distillation from a trap maintained at -186°C to a trap at -196°C ; the color of the frozen NO was white indicating it to be free of NO₂. Cylinder NO₂ was stored by mixing with excess O₂ to oxidize any NO. Analysis showed a negligible amount of NO.

Results

N₂O Photolysis. Photolysis of N₂O–H₂–O₂–NO mixtures at 213.9 nm and 23°C leads to the consumption of NO. There is no measurable induction period (< 1 sec) for NO removal. The initial NO loss quantum yields, $-\Phi_i\{\text{NO}\}$, for photolysis of N₂O–H₂–O₂–NO mixtures at 213.9 nm are presented in Tables I and II. Experiments were done at ~ 700 and ~ 90 Torr H₂ pressure. At very low [NO] (Table I), $-\Phi_i\{\text{NO}\}$ is almost proportional to the $[\text{NO}]/I_a^{1/2}$ ratio over a range of 1 – 10×10^7 cm^{-3/2} sec^{1/2}. In this range I_a was varied by a factor of 5.6. At relatively high [NO] (Table II), $[\text{NO}]/[\text{H}_2] \geq 6 \times 10^{-7}$, and $-\Phi_i\{\text{NO}\}$ decreases with increasing $[\text{NO}]/[\text{H}_2]$. In between these two extremes the variation in $-\Phi_i\{\text{NO}\}$ is complex.

If NO₂ is present initially, the oxidation shows (1) an induction period, i.e., the rate is slow at first and accelerates as the reaction proceeds, and (2) the rate of oxidation is greatly reduced. The results in the presence of NO₂ are presented in Table III. Figure 1 shows [NO] as a function of time for a run in which [NO₂] = 11 mTorr initially.

NO Photolysis. In the photolysis of NO–H₂–O₂ mixtures, light absorption is by NO. However, since [NO] is very low, I_a is very low; consequently conditions for which $-\Phi_i\{\text{NO}\}$ depends on $[\text{NO}]/I_a^{1/2}$ could not be achieved. The results are presented in Table IV. As [NO] increases, $-\Phi_i\{\text{NO}\}$ declines, at first slowly, and then more rapidly. Experiments were done at ~ 700 and ~ 90 Torr H₂. $-\Phi_i\{\text{NO}\}$ at low [H₂] is generally higher than at high [H₂] for comparable [NO]/[H₂].

If NO₂ is present initially, light absorption is by NO and NO₂. In this system, NO₂ inhibits the oxidation of NO as in the N₂O system. The results are presented in Table V.

Dark Removal of NO. In the photolysis of N₂O–H₂–O₂–NO or N₂O–H₂–O₂–NO–NO₂ mixtures, NO removal continues to occur even after the radiation is terminated. Figure 2 shows two typical runs. For NO–H₂–O₂ or NO–H₂–O₂–NO₂ mixtures, dark removal of NO also occurs, but the amount removed in the dark is much less than for the N₂O system.

A study of this dark rate was done over a range of conditions. The results are presented in Table VI. Since NO₂ is a product of the light reaction, it was always present when the dark reaction commenced. The amount of NO₂ present at the beginning of the dark reaction, [NO₂]₀, when none is present initially is given by $[\text{NO}]_i - [\text{NO}]_0$, where [NO]_i is the NO concentration at the beginning of the light run and [NO]₀ is the concentration when radiation is terminated. In some experiments NO₂ was added at the beginning of the light run. The duration of the light runs was varied from about 54 to 15% conversion of the initial NO.

From the data in Table VI it is apparent that the amount of NO consumed in the dark is not very dependent on reaction conditions. The approximate initial rates of NO removal $-R_i\{\text{NO}\}$ are also given in Table VI. It is apparent that in spite of the variation in conditions there is not

TABLE I: Photolysis of N₂O-H₂-O₂-NO Mixtures at 213.9 nm and 23°C (Low [NO])

$10^{-7}[\text{NO}]/I_a^{1/2}$, $\text{cm}^{-3/2}\text{sec}^{-1/2}$	$10^{-13}[\text{NO}]$, cm^{-3}	$[\text{O}_2]$, Torr	$10^{-11}I_a$, $\text{cm}^{-3}\text{sec}^{-1}$	$-\Phi_1\{\text{NO}\}$
[H ₂] = 700 ± 60 Torr				
1.25	0.48	29	1.48	4.5
1.65	0.48	41	0.843	8.3
1.65	0.48	41	0.843	9.65
1.66	0.48	33	0.830	6.5
2.11	0.48	25	0.519	13.2
2.40	0.48	26	0.411	12.5
2.40	0.48	41	0.411	13.7
2.70	0.45	38	0.275	14.3
2.87	0.86	32	0.896	11.2
3.66	0.45	38	0.152	19.5
4.15	0.99	43	0.237	24.6
4.32	0.90	22	0.496	24.0
6.60	0.99	35	0.237	31.5
9.07	2.02	43	0.492	41
12.3	2.27	43	0.338	48
13.1	2.02	47	0.237	55
[H ₂] = 90 ± 10 Torr				
3.35	0.90	9.6	0.720	17
3.80	1.06	12.4	0.777	23.3
5.35	1.25	9.3	0.540	26.0
10.1	2.63	8.0	0.670	53
10.6	2.55	13.2	0.573	31.7
21.8	2.70	8.8	0.156	95

TABLE II: Photolysis of N₂O-H₂-O₂-NO Mixtures at 213.9 nm and 23°C (High [NO])

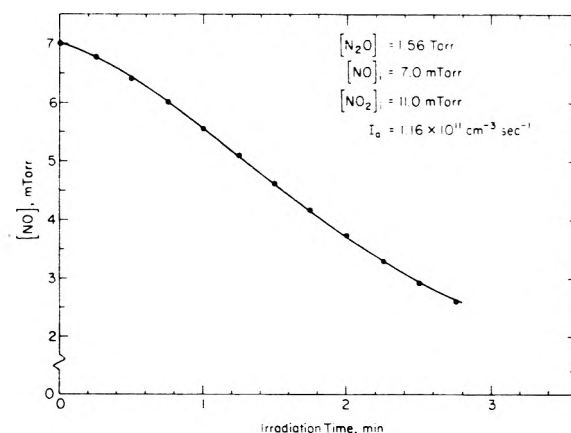
$10^6[\text{NO}]/[\text{H}_2]$	$10^{-13}[\text{NO}]$, cm^{-3}	$[\text{O}_2]$, Torr	$10^{-11}I_a$, $\text{cm}^{-3}\text{sec}^{-1}$	$-\Phi_1\{\text{NO}\}$
[H ₂] = 700 ± 60 Torr				
6.92	15.2	27	0.0425	110
8.03	17.7	24	0.086	108
12.2	26.9	33	0.347	79
16.2	35.7	23	0.369	67
32.2	70.8	24	0.107	40
[H ₂] = 90 ± 10 Torr				
47.7	13.7	10.8	0.042	95
53.4	14.6	15.0	0.23	65
54.4	15.3	12.4	0.70	53
56.0	15.2	15.8	0.021	67
56.2	15.6	12.4	0.089	57
135	39.7	9.0	0.133	24

TABLE III: Photolysis of N₂O-H₂-O₂-NO-NO₂ Mixtures at 213.9 nm and 23°C^a

$[\text{NO}_2]/[\text{NO}]$	$10^{-13}[\text{NO}]$, cm^{-3}	$10^{-13}[\text{NO}_2]$, cm^{-3}	$[\text{O}_2]$, Torr	$10^{-10}I_a$, $\text{cm}^{-3}\text{sec}^{-1}$	$-\Phi\{\text{NO}\}$
0.30	16.5	5.0	33	7.5	30.9
0.42	22.5	9.5	25	6.7	29.1
0.61	18.0	10.9	42	8.0	20.5
1.14	16.6	18.9	41	9.0	12.5
1.58	22.4	35.4	30	11.6	7.1
1.59	22.2	35.4	23	9.4	8.6

^a [H₂] = 700 ± 60 Torr; [N₂O] = 1.4 ± 0.1 Torr.

much change in $-R_1\{\text{NO}\}$. Figure 2 shows a typical NO decay plot in the dark for a run in which NO₂ is initially absent, and for a run in which NO₂ is initially present. From Figure 2 it appears that [NO₂] has very little effect

Figure 1. Typical plot of [NO] vs. irradiation time in the photolysis of N₂O-H₂-O₂-NO-NO₂ mixtures at 213.9 nm and 23°C.TABLE IV: Photolysis of NO-H₂-O₂ Mixtures at 213.9 nm and 23°C

$10^6[\text{NO}]/[\text{H}_2]$	$10^{-13}[\text{NO}]$, cm^{-3}	$[\text{O}_2]$, Torr	$10^{-8}I_a$, $\text{cm}^{-3}\text{sec}^{-1}$	$-\Phi_1\{\text{NO}\}$
[H ₂] = 700 ± 60 Torr				
0.42	0.93	25	1.31	457
0.70	1.55	23	2.19	462
0.73	1.60	22	2.27	444
0.73	1.60	17	2.27	287
0.95	2.09	13	2.96	505
2.02	4.45	22	5.94	326
4.25	9.44	16	13.3	321
4.79	10.5	21	14.9	215
4.86	10.7	19	15.2	256
15.2	33.5	22	47.3	109
26.0	57.1	23	80.8	61
[H ₂] = 90 ± 10 Torr				
4.97	1.45	12	2.04	602
5.11	1.66	19	2.35	455
11.6	3.35	15	4.73	405
38.4	11.1	14	13.9	115
64.0	18.5	15	26.2	64
93.5	27.2	13	38.5	43

TABLE V: Photolysis of NO-H₂-O₂-NO₂ Mixtures at 213.9 nm and 23°C^a

$[\text{NO}_2]/[\text{NO}]$	$10^{-13}[\text{NO}]$, cm^{-3}	$10^{-13}[\text{NO}_2]$, cm^{-3}	$[\text{O}_2]$, Torr	$10^{-10}I_a$, $\text{cm}^{-3}\text{sec}^{-1}$	$-\Phi\{\text{NO}\}$
0.12	12.4	1.42	20	0.26	122
0.30	11.0	3.26	15	0.41	67
0.36	17.9	6.40	24	0.75	44
0.64	2.36	1.50	13	0.16	55.4
0.75	10.1	7.60	24	0.76	28.7
1.28	11.3	14.5	18	1.28	17.8
1.52	9.75	14.8	24	1.36	13.3

^a [H₂] = 700 ± 60 Torr.

on the rate of the dark reaction. However, since I_a during the light period was a factor of 2 higher in the NO₂ run, the intermediate causing the dark decay of NO should be about a factor of 2 higher, which would tend to increase the NO decay rate by the same factor. That the rate was not increased shows that the NO₂ has an inhibiting effect (at the beginning of the dark run, the NO₂ pressures should be about a factor of 3-4 different). One experiment was done

TABLE VI: Light-Induced Dark Oxidation of NO at 23°C^{a, b}

$10^{-13}[\text{NO}]_i$, cm^{-3}	$10^{-13}[\text{NO}_2]_i$, cm^{-3}	$10^{-13}[\text{NO}_2]_0$, cm^{-3}	$10^{-13}[\text{NO}]_0$, cm^{-3}	$10^{-13}[\text{NO}]_\infty$, cm^{-3}	$10^{-11}I_a$, $\text{cm}^{-3} \text{sec}^{-1}$	$-10^{-11}R_i\{\text{NO}\}$, $\text{cm}^{-3} \text{sec}^{-1}$
95.3		33.2	62.1	53.1	1.0	9.7
46.0		9.02	37.0	29.0	1.0	13-21
42.2		21.2	21.0	7.41	1.1	9.7
26.0	33.8	45.4	14.3	3.22	1.3	8.1
24.9		4.31	20.6	12.9	0.77	
24.5		6.21	18.3	8.95	1.6	
24.2		9.02	15.1	3.86	0.69	10.1
23.0		3.54	19.5	12.2	0.86	6-24
22.7		9.50	13.2	2.64	0.80	
22.3		12.0	10.3	0.74	0.76	7.0
21.1		8.44	12.7	5.70	0.25	5.8
21.0	19.9	23.2	16.9	5.92	0.94	6.8
20.5	32.2	43.4	9.79	0.32	1.3	6.9

^a $[\text{N}_2\text{O}] \sim 1-3$ Torr; $[\text{O}_2] 22 \pm 5$ Torr; $[\text{H}_2] = 700 \pm 60$ Torr. ^b The subscripts *i* and *0* refer to the concentrations at the beginning and end of the irradiation, respectively. The subscript ∞ refers to infinite time.

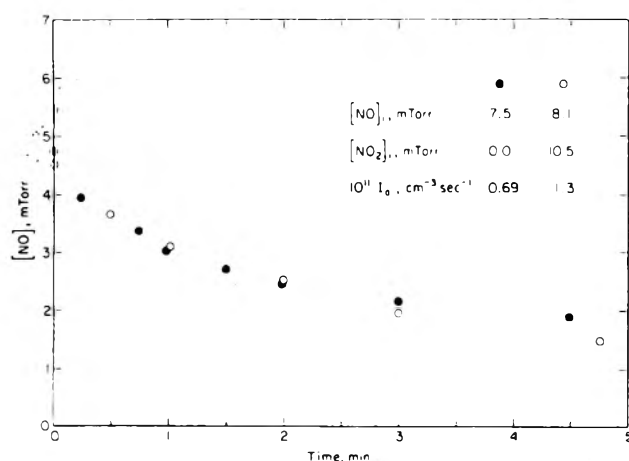
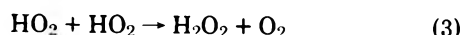
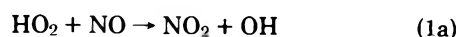
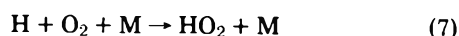
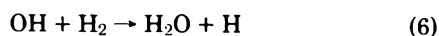
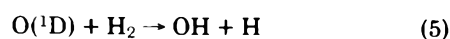
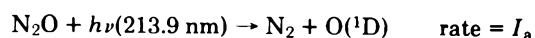


Figure 2. Plot of $[\text{NO}]$ vs. time in light-induced dark oxidation of NO. The listings in the legend refer to conditions at the beginning of irradiation.

in which the temperature of the reaction vessel was increased by about 10–15°C. The initial rate of oxidation increased dramatically (a factor of 3–4). For this reason the dark oxidation results are only approximate, since room temperature fluctuations were ~5°C. These room temperature fluctuations have no effect on the light reaction. Further experiments are planned in which the dark reaction will be studied under carefully controlled temperature conditions.

Discussion

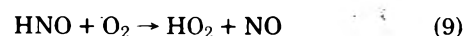
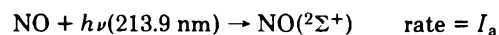
NO₂ Absent. The photolysis of $\text{N}_2\text{O}-\text{H}_2-\text{O}_2-\text{NO}$ mixtures at 213.9 nm may be discussed in terms of the mechanism:



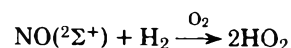
The mechanism above is a chain process for oxidizing NO to NO_2 . The chain-propagating steps are reactions 6, 7 and 1a, and the chain-terminating steps are reactions 3, 4, and 1b. The only reaction of importance for $\text{O}({}^1\text{D})$ atoms is with H_2 ($\geq 97\%$), since H_2 is in large excess over all other gases in the system. In this system OH can only react with H_2 and NO. H atoms will react entirely with O_2 since the $[\text{O}_2]/[\text{NO}]$ ratio is very large. Reactions of OH and H with N_2O are known to be very slow at room temperature.

All radical-radical terminating reactions of H and OH with themselves and with HO_2 are entirely unimportant compared to reactions 3 and 4, as their steady state concentrations compared to $[\text{HO}_2]$ or $[\text{NO}]$ are very low. Reactions 3, 4, 6, and 7 are well known and for which rate coefficients are available.^{6,11} Reaction 1b has only recently been claimed to have been observed,⁵ though it has been suggested numerous times as a possibly important reaction between HO_2 and NO.

When radical production is induced by NO photolysis instead of N_2O photolysis, the reactions are



The subsequent steps are as before. The deactivation of $\text{NO}({}^2\Sigma^+)$ will be by H_2 only, since the rate coefficient is very large, $\geq 4.8 \times 10^{-11} \text{ cm}^3 \text{ sec}^{-1}$,¹² and $[\text{H}_2]/[\text{O}_2] \geq 16$. Furthermore deactivation leads to HNO with unit efficiency.¹³ HNO might react in other ways than in reaction 9. However, as we shall see, the present results are consistent with reaction 9 being the exclusive reaction. Therefore for the sake of simplicity other reactions of HNO will be ignored for the present. The net effect of reactions 8 and 9 in the presence of O_2 is the production of 2 HO_2 radicals.



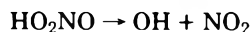
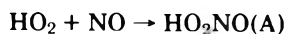
It is convenient to consider two limiting cases of the mechanism: case (a) when chain termination is by reaction 3 only, i.e., at low $[\text{NO}]$ and high I_a , the rate law for NO removal is

$$-\Phi_i\{\text{NO}\} = k_{1a}[\text{NO}]/(k_3I_a)^{1/2} \quad (a)$$

case (b) when chain termination is by reactions 4 and 1b, i.e., at high $[\text{NO}]/I_a^{1/2}$, the rate law for NO removal is

$$-\Phi_i\{\text{NO}\}^{-1} = k_{1b}/2k_1 + k_4[\text{NO}]/2k_6[\text{H}_2] \quad (\text{b})$$

In deriving eq a and b, the steady state assumption for all radicals and intermediates was made including the possible intermediate formed by the reaction of HO₂ with NO



The steady state assumption is justified because no induction period (<2 sec) for NO removal was observed under all conditions. Thus the experimental lifetime for A is <2 sec.

A plot of $-\Phi_i\{\text{NO}\}$ vs. $[\text{NO}]/I_a^{1/2}$ at low values of $[\text{NO}]/I_a^{1/2}$ is shown in Figure 3. The plot for $[\text{NO}]/I_a^{1/2} \leq 8 \times 10^7 \text{ cm}^{-3/2} \text{ sec}^{1/2}$ is linear as required by eq a. The slope of the plot gives $k_{1a}/k_3^{1/2} = 5.1 \times 10^{-7} \text{ cm}^{3/2} \text{ sec}^{-1/2}$, with an uncertainty of $\pm 10\%$. Since $k_3 = 3.3 \times 10^{-12} \text{ cm}^3 \text{ sec}^{-1}$,¹⁴ $k_{1a} = 9.3 \times 10^{-13} \text{ cm}^3 \text{ sec}^{-1}$. This value of k_{1a} is nearly a factor of 2.5 larger than the value given by Hack et al.,² and more than a factor of 3 larger than the value given by Davis et al.,¹ though the latter value has uncertainty of a factor of 3. However, our value is in good agreement with the value of $1.2 \times 10^{-12} \text{ cm}^3 \text{ sec}^{-1}$ measured by Cox⁵ and it is close to our lower limit measured earlier.⁴

Equation b predicts that a plot of $-\Phi_i\{\text{NO}\}^{-1}$ vs. $[\text{NO}]/[\text{H}_2]$ should be linear with a slope of $k_4/2k_6$ and an intercept of $k_{1b}/2k_1$. Plots of eq b for total pressures of ~ 730 and 100 Torr are given in Figures 4 and 5, respectively, for both the N₂O and NO photolysis experiments. The plots in Figure 4 are reasonably linear for both systems. Although the slopes of both plots in Figure 4 are nearly the same, the intercepts are slightly different. The points for the NO photolysis system at very low $[\text{NO}]/[\text{H}_2]$ are slightly above the line determined by the rest of the points, since under these conditions termination by reaction 3 is not entirely negligible. From the slopes of the plots $k_4/k_6 = 1.20 \times 10^3$ (NO photolysis) and $k_4/k_6 = 1.37 \times 10^3$ (N₂O photolysis) are obtained. The agreement between these two numbers is good; the difference being within the $\pm 10\%$ uncertainty for each value. Since $k_6 = 7.6 \times 10^{-15} \text{ cm}^3 \text{ sec}^{-1}$,¹³ $k_4 = 9.2 \times 10^{-12}$ and $1.1 \times 10^{-11} \text{ cm}^3 \text{ sec}^{-1}$ for the two systems, respectively. The average value of $1.0 \times 10^{-11} \text{ cm}^3 \text{ sec}^{-1}$ compares well with the recently determined value of 7.8×10^{-12} by Sie et al.⁶ using a different technique at a pressure of ~ 770 Torr, and the results of Atkinson et al.¹⁵ who found $k_4 = (6.1 \pm 1.0) \times 10^{-12} \text{ cm}^3 \text{ sec}^{-1}$ at 760 Torr N₂. The reason for the slightly lower values of $-\Phi_i\{\text{NO}\}$, and hence a larger intercept in the N₂O system, is not clear. The assumption that two HO₂ radicals are produced per photon absorbed by NO in the presence of H₂ cannot be the reason, because if that assumption was incorrect then the discrepancy would be worse. Probably the discrepancy can be attributed to systematic errors, i.e., error in the relative absorption coefficients of NO and N₂O, errors in calibration, etc. From the intercepts $k_{1b}/k_1 \sim 8.0 \times 10^{-3}$ (N₂O photolysis) and $k_{1b}/k_1 \sim 2 \times 10^{-3}$ (NO photolysis). Since the data for the NO system are closer to the intercept, the value of k_{1b}/k_1 obtained for this system is probably more accurate; therefore we conclude that $k_{1b}/k_1 \leq 2 \times 10^{-3}$, and since $k_{1a} = 9.3 \times 10^{-13}$, $k_{1b} \leq 2 \times 10^{-15} \text{ cm}^3/\text{sec}$ at a total pressure of 730 ± 40 Torr. Our upper limit for k_{1b} is in sharp disagreement with the value of $1.4 \times 10^{-13} \text{ cm}^3 \text{ sec}^{-1}$ recently measured by Cox⁵ at 1 atm O₂ + N₂.

In Figure 4 our earlier measurements of $\Phi\{\text{NO}_2\}$ are also included. (Note that according to the mechanism $-\Phi_i\{\text{NO}\}$

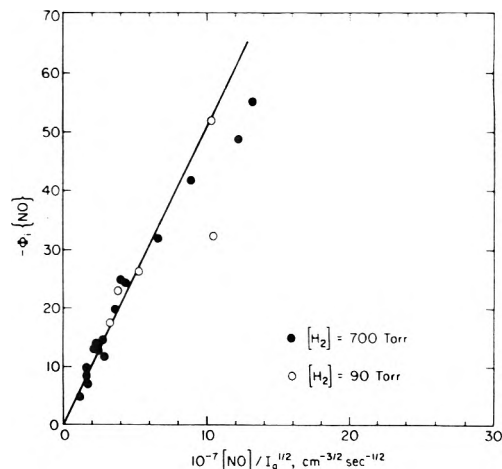


Figure 3. Plot of $-\Phi_i\{\text{NO}\}$ vs. $[\text{NO}]/I_a^{1/2}$ in the photolysis of N₂O-H₂-O₂-NO mixtures at 213.9 nm and 23°C.

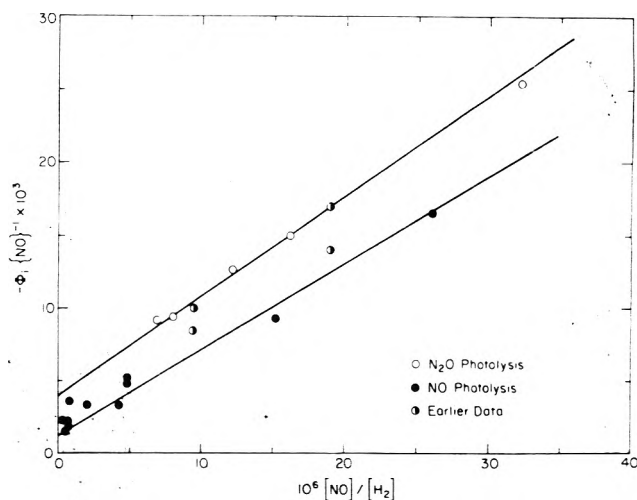


Figure 4. Plot of $-\Phi_i\{\text{NO}\}^{-1}$ vs. $[\text{NO}]/[\text{H}_2]$ in the photolysis of N₂O-H₂-O₂-NO mixtures and NO-H₂-O₂ mixtures at 213.9 nm and 730 ± 40 Torr total pressure. Earlier data from ref 3.

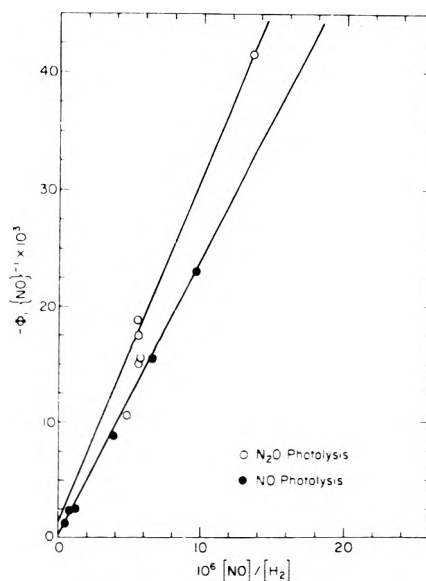
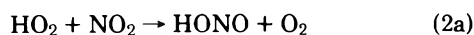


Figure 5. Plot of $-\Phi_i\{\text{NO}\}^{-1}$ vs. $[\text{NO}]/[\text{H}_2]$ in the photolysis of NO-H₂-O₂ mixtures and N₂O-H₂-O₂-NO mixtures at 213.9 nm and 100 ± 5 Torr total pressure.

= $\Phi\{\text{NO}_2\}$.) The agreement between the earlier measurements and the present results is good.

Figure 5 presents a plot of $-\Phi\{\text{NO}\}^{-1}$ vs. $[\text{NO}]/[\text{H}_2]$ for the data at total pressure of about 100 Torr. For the NO photolysis system, the data fall on a reasonably straight line as required. The data for the N_2O photolysis system are insufficient to define a line, but as before these points lie somewhat higher. As $[\text{N}_2\text{O}]$ is reduced, $-\Phi\{\text{NO}\}$ appears to approach the NO photolysis line. The slope of the line (NO photolysis) gives $k_4/k_6 = 483 \pm 50$; since $k_6 = 7.6 \times 10^{-15} \text{ cm}^3 \text{ sec}^{-1}$, $k_4 = 3.7 \times 10^{-12} \text{ cm}^3 \text{ sec}^{-1}$. This value is also in acceptable agreement with the value of $2.7 \times 10^{-12} \text{ cm}^3 \text{ sec}^{-1}$ measured by Sie et al.⁶ at ~ 95 Torr total pressure (mainly H_2). The intercept of this plot gives $k_{1b}/k_1 \leq 2 \times 10^{-3}$; thus $k_{1b} \leq 2 \times 10^{-15} \text{ cm}^3 \text{ sec}^{-1}$, the same as obtained from the 730 Torr total pressure data.

NO₂ Present. The addition of NO_2 to the N_2O or NO photolysis systems reduces $-\Phi\{\text{NO}\}$ sharply (Tables III and V). This is in agreement with our earlier study⁴ that NO_2 inhibits the chain oxidation of NO to NO_2 . To account for this inhibition the reaction

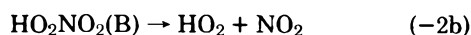


was proposed with $k_{1a}/k_{2a} = 7 \pm 1$ and $k_{2a} \geq 3 \times 10^{-13} \text{ cm}^3 \text{ sec}^{-1}$ (based on $k_3 = 6 \times 10^{-12} \text{ cm}^3 \text{ sec}^{-1}$).

In this study two important additional observations are made: (1) the oxidation shows a marked induction period in the presence of NO_2 , and (2) the oxidation continues even after termination of radiation. Both observations imply that a complex of appreciable lifetime is formed which can decompose to products capable of continuing the chain oxidation of NO. The first observation suggests that the complex is between HO_2 and NO_2 .



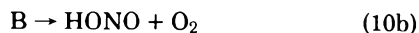
Complex B may decompose



Thus the chain carrying radical HO_2 is regenerated. The decomposition of the complex B via the reaction



is neglected, since reaction $-2b$ is favored energetically. However, even if (10a) were dominant the conclusions would be the same. The decomposition of B via



may be important, and this reaction must be included in the analysis. The second observation is necessarily a consequence of the first observation.

Since the induction period for the oxidation during irradiation in the absence of NO_2 is very short (< 2 sec), it follows that the experimental lifetime of complex A is very short (< 2 sec). Therefore complex A can only play a role in the dark reaction in the first few seconds. This implies that the half-time for NO oxidation in the dark would be of the order of < 2 sec if complex A was responsible, whereas the observed half-lives are of the order of 1 min. Complex B must be the responsible agent.

The mechanism consisting of reactions 1, 2, 4, 5 (or 8 and 9), 6, 7, and 11, which must be introduced in the presence of NO_2



leads to the following rate law during irradiation

$$-\Phi\{\text{NO}\} = \frac{2k_1[\text{NO}]}{k_2[\text{NO}_2] + (\beta k_{1a} + k_{1b})[\text{NO}]} \times \frac{1}{[1 - k_{-2b}\alpha\tau_B(\exp\{-t/\tau_B\} - 1)]} \quad (c)$$

where

$$\alpha = k_{2b}[\text{NO}_2]/(k_2[\text{NO}_2] + (\beta k_{1b} + k_{1b})[\text{NO}])$$

and

$$\beta = (k_4[\text{NO}] + k_{11}[\text{NO}_2])/(k_6[\text{H}_2] + k_4[\text{NO}] + k_{11}[\text{NO}_2])$$

and τ_B is the lifetime of B

$$\tau_B^{-1} = k_{10b} + k_{-2b}(1 - \alpha)$$

At $t = 0$, when $[\text{B}] = 0$

$$-\Phi\{\text{NO}\}^{-1} - \frac{k_{1a}\beta}{2k_1} = \frac{k_{1b}}{2k_1} + \frac{k_2[\text{NO}_2]}{2k_1[\text{NO}]} \quad (d)$$

and later in the reaction when B reaches its steady state

$$-\Phi\{\text{NO}\}^{-1} - \frac{k_{1a}\beta}{2k_1} = \frac{k_{1b}}{2k_1} + \frac{k_2'[\text{NO}_2]}{2k_1[\text{NO}]} \quad (e)$$

where k_2' is given by

$$k_2' = k_2 - k_{2b}k_{-2b}/(k_{-2b} + k_{10b})$$

Since $k_{1a}/k_1 \approx 1.0$, a plot of $-\Phi\{\text{NO}\}^{-1} - \beta/2$ vs. $[\text{NO}_2]/[\text{NO}]$ should be linear after the steady state in B is reached (eq e). Such a plot is shown in Figure 6 for both the N_2O and NO photolysis data ($-\Phi\{\text{NO}\}$ is evaluated after the induction period is over). The correction factor β was computed with $k_4 = 1.0 \times 10^{-11} \text{ cm}^3 \text{ sec}^{-1}$ given before, $k_{11} = 8 \times 10^{-12} \text{ cm}^3 \text{ sec}^{-1}$ and $k_6 = 7.6 \times 10^{-15} \text{ cm}^3 \text{ sec}^{-1}$.¹¹ The plot obeys eq e quite well, though the slope for the NO- NO_2 photolysis system is somewhat lower than that for the N_2O system. The difference in slopes is probably outside the experimental error of the measurements. However, it is within the expected error if the error in $\Phi\{\text{O}^1\text{D}\}$ for NO_2 photolysis, the error in computing I_a for the NO- NO_2 system from absorption coefficients, and the error in the steady state concentration of B (10-20%) are included. The slopes give $k_1/k_2' = 8.0$ and 11 for the N_2O and NO- NO_2 systems, respectively. The average value is 9.5. Since $k_{1a} = 9.3 \times 10^{-13} \text{ cm}^3 \text{ sec}^{-1}$ determined above, $k_2' = 9.8 \times 10^{-14} \text{ cm}^3 \text{ sec}^{-1}$. The intercept of the plots in Figure 6 gives $k_1/k_{1b} \geq 250$; thus $k_{1b} \leq 4 \times 10^{-15} \text{ cm}^3 \text{ sec}^{-1}$. The present value of $k_2' = 9.8 \times 10^{-14} \text{ cm}^3 \text{ sec}^{-1}$ is close to the lower limit determined in our earlier study,⁴ and is in excellent agreement with $k_2' = 1.2 \times 10^{-13} \text{ cm}^3 \text{ sec}^{-1}$ determined recently by Cox.⁵

The induction period should depend only on the temperature, since $\tau_B^{-1} \approx k_{10b} + k_{-2b}k_{2a}/k_2$ (note that $k_2[\text{NO}_2] > \beta k_1[\text{NO}]$). The measured induction period is variable. The reason for this is not entirely clear, but it is possible that the variability may be due to variation in room temperature ($\sim 5^\circ\text{C}$ variability), since k_{-2b} is expected to be strongly temperature dependent (the dark oxidation is greatly accelerated by small changes in temperature). For the run in Figure 1 in which the induction period is most readily apparent, $-\Phi\{\text{NO}\} \sim -\Phi\{\text{NO}\}/2$; therefore from eq d and e it is deduced that $k_2' \sim k_{2b}$.

Dark Reaction. Based on the mechanism, the initial rate of NO oxidation in the presence of NO_2 in the dark is described by the differential equation:

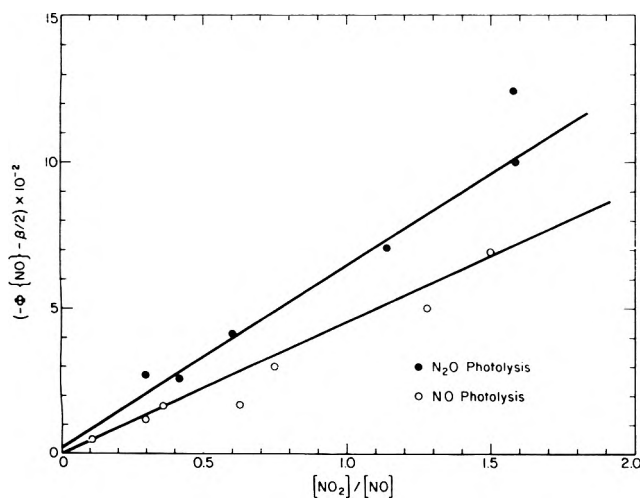


Figure 6. Plot of $-\frac{d[\text{NO}]}{dt} - \beta/2$ vs. $[\text{NO}_2]/[\text{NO}]$ in the photolysis of $\text{N}_2\text{O}-\text{H}_2-\text{O}_2-\text{NO}-\text{NO}_2$ and $\text{NO}-\text{H}_2-\text{O}_2-\text{NO}_2$ mixtures at 213.9 nm and 23°C.

$$-\left(\frac{d[\text{NO}]}{dt}\right)_i = \frac{k_1[\text{NO}]k_{-2b}[\text{B}]_0}{k_2[\text{NO}_2] + (\beta k_{1a} + k_{1b})[\text{NO}]} \quad (\text{f})$$

where $[\text{B}]_0$ is the concentration of B at $t = 0$ of the dark period. Since during the light part of the run B is in the steady state, $[\text{B}]_0 = [\text{B}]_{\text{ss}}$. Thus

$$[\text{B}]_0 = \frac{2I_a k_{2b} [\text{NO}_2] / (k_{-2b} + k_{10b})}{(k_2' [\text{NO}_2] + (\beta k_{1a} + k_{1b}) [\text{NO}])} \quad (\text{g})$$

Combining eq f and g, and noting that $k_{2a}[\text{NO}_2] > (\beta k_{1a} + k_{1b})[\text{NO}]$, we find that the initial rate in the dark is given by

$$-\left(\frac{d[\text{NO}]}{dt}\right)_i = \frac{2I_a \gamma k_1 k_{2b} [\text{NO}]}{(k_2 - \gamma k_{2b}) k_2 [\text{NO}_2]} \quad (\text{h})$$

where

$$\gamma = k_{-2b} / (k_{-2b} + k_{10b})$$

Equation h predicts that the initial dark rate should be proportional to $[\text{NO}]/[\text{NO}_2]$ for constant I_a . Examination of the data in Table VI shows that $-R_i[\text{NO}]$ is less than proportional to $[\text{NO}]/[\text{NO}_2]$ even when the variation in I_a is taken into account. Part of the problem is lack of temperature control; small changes in temperature have a large effect on the rate. However, for the last two runs in Table VI, the temperature was known to be constant ($\pm 0.5^\circ\text{C}$), yet the rate was reduced by only a factor of ~ 2 (note that I_a is different) for a change of a factor of ~ 5 in $[\text{NO}]/[\text{NO}_2]$. Since k_1 and k_2' have been determined before, an order of

magnitude estimate of $k_{2b}/k_2 = 0.3-1$ is obtained from the initial rates and eq h. Therefore $k_{2b} \sim 1 \times 10^{-13} \text{ cm}^3 \text{ sec}^{-1}$, which is consistent with the value $\sim 1 \times 10^{-13} \text{ cm}^3 \text{ sec}^{-1}$ estimated from the induction period. An estimate of τ_B^{-1} can be made from the time necessary for $-R_i[\text{NO}]$ to decrease by $1/2$. This time is approximately $\sim 0.5-1.5$ min, so that $\tau_B^{-1} = k_{10} + k_{-2b}k_{2a}/k_2 \sim 0.02 \text{ sec}^{-1}$.

Attempts to treat the dark oxidation data in more detail do not lead to significantly better agreement between the mechanism and the dark oxidation data. It appears that the general features of the mechanism are probably correct as it is difficult to explain the light induced dark oxidation by other mechanisms, but the complete details are not yet clear. Further work in understanding the dark oxidation is planned. Particularly useful will be studies at low temperatures since complex B should be more stable.

The formation of a long-lived complex between HO₂ and NO₂ could be important in a complete understanding of the influence of nitrogen oxides on stratospheric ozone. If τ_B^{-1} is as low as $\sim 0.02 \text{ sec}^{-1}$ at 25°C , then complex B would be essentially stable to thermal decomposition at stratospheric temperatures. If a significant portion of NO₂ is removed as the complex, and if it reacts to produce more stable nitrogen oxides, the effect of the NO_x catalytic cycle on ozone removal could be reduced.

Acknowledgment. This work was supported by the National Science Foundation through Grants No. GA-42856 and the Department of Transportation through Contract No. DOT-OS-40051, for which we are grateful.

References and Notes

- (1) D. D. Davis, W. A. Payne, and L. J. Stief, *Science*, **179**, 280 (1973); W. A. Payne, L. J. Stief, and D. D. Davis, *J. Am. Chem. Soc.*, **95**, 7614 (1973).
- (2) W. Hack, K. Hoyermann, and H. G. Wagner, presented at the CODATA Symposium, "Chemical Kinetics Data for the Lower and Upper Atmosphere," Warrenton, Va., Sept 16-18, 1974.
- (3) R. Simonaitis and J. Heicklen, *J. Phys. Chem.*, **77**, 1096 (1973).
- (4) R. Simonaitis and J. Heicklen, *J. Phys. Chem.*, **78**, 653 (1974).
- (5) R. A. Cox, and R. G. Derwent, *J. Photochem.*, **4**, 139 (1975).
- (6) B. K. T. Sie, R. Simonaitis, and J. Heicklen, *Int. J. Chem. Kinet.*, in press.
- (7) D. H. Stedman, E. E. Daby, F. Stuhl, and H. Niki, *J. Air Pollut. Control Assoc.*, **22**, 260 (1972).
- (8) R. Simonaitis, R. I. Greenberg, and J. Heicklen, *Int. J. Chem. Kinet.*, **4**, 497 (1972).
- (9) W. M. Uselman and K. C. Lee, *Chem. Phys. Lett.*, **30**, 212 (1974).
- (10) H. S. Johnston and R. Graham, *Can. J. Chem.*, **52**, 1415 (1974).
- (11) D. Garvin and R. F. Hampson, National Bureau of Standards Report NBSIR 74-430, Chemical Kinetics Data Survey VII, 1974.
- (12) J. Heicklen, *Adv. Photochem.*, **5**, 157 (1968).
- (13) J. Heicklen, *J. Phys. Chem.*, **70**, 2456 (1966).
- (14) A. C. Lloyd, *Int. J. Chem. Kinet.*, **6**, 169 (1974).
- (15) R. Atkinson, D. A. Hansen, and J. N. Pitts, Jr., *J. Chem. Phys.*, **62**, 3284 (1975).

Isomerization of Chemically Activated 1-Buten-1-yl and 1-Buten-4-yl Radicals

Toshio Ibuki,* Akira Tsuji, and Yoshimasa Takezaki

Institute for Chemical Research, Kyoto University, Gokanoshō, Uji, Kyoto, Japan (Received June 17, 1975)

Publication costs assisted by the Institute for Chemical Research

Chemically activated 1-buten-1-yl radicals were generated by the addition of ethyl radicals produced by the photolysis of diethyl ketone to acetylene at 75 and 123°. The unimolecular rate constant for the isomerization of the excited 1-buten-1-yl to 1-buten-4-yl radicals through 1,4-hydrogen atom migration was measured. In addition, it was found that the 1-buten-4-yl formed can isomerize to methylallyl radicals via 1,2-H atom shift. The average rate constants for isomerization were found to be 1.00×10^9 and 1.05×10^9 sec^{-1} for 1-buten-1-yl and 3.47×10^7 and 6.20×10^7 sec^{-1} for 1-buten-4-yl radicals at 75 and 123°, respectively. The best agreement between the rate constants as calculated by the RRKM theory and the experimental results was found when the threshold energies, E_0 , were chosen as 17.1 and 33.0 kcal/mol for 1,4- and 1,2-H atom shifts, respectively. It is shown that these values satisfy the expression, $E_0 = E_{ab} + E_s$, where E_{ab} is the activation energy for a bimolecular H atom abstraction and E_s is the ring strain energy.

Introduction

Isomerization of vibrationally excited radicals via intramolecular hydrogen atom migration forms an important class of the reactions of alkyl¹⁻⁹ and alkenyl radicals¹⁰⁻¹⁴ both in thermal⁶⁻⁹ and chemical activation systems.^{1-5,10-14} Especially 1,4- and 1,5-hydrogen atom migrations which occur via five- and six-membered cyclic transition states have been well studied, the activation energies of which have been found to be in the range 15–21^{1-4,6,7,10,13} and 8–11 kcal/mol,^{3,8,9} respectively. Study of the isomerization of nonyl-2 to nonyl-3 radical through 1,6-H atom shift has given the value of 16.0 kcal/mol as the threshold energy.³ Recently, 1,2- and 1,3-H atom shifts have been substantiated in chemical activation systems and they have high threshold energies, 30–34.5 kcal/mol.^{5,13,14}

In the calculation of the RRKM specific reaction rate, two factors are required; one is the vibrational frequency assignments of the radical and H-atom transfer activated complex, and the other is the critical energy for isomerization. The former can be obtained by using the formulation developed by Rabinovitch and coworkers.^{3,15} For the latter we proposed in a previous paper¹⁴ that the critical energy can be approximately estimated by the expression, $E_0 = E_{ab} + E_s$, where E_0 is the critical energy, E_{ab} the activation energy for a bimolecular H atom abstraction, and E_s the ring strain energy.

In previous work,⁵ the rate constant for a 1,2-H atom shift was measured by the relative yields of the decomposition products. The object of this work is to substantiate 1,2-H atom shift by measuring the relative yields of stabilized isomers and to ascertain the above expression in the case of isomerization of vibrationally excited 1-buten-1-yl and 1-buten-4-yl radicals.

Experimental Section

The experimental details were the same as described previously.¹⁴ 1-Buten-1-yl radicals were generated by the vapor phase photolysis of diethyl ketone in the presence of acetylene. A quartz reactor of 206 cm³ was used. The cell was illuminated with the output from a 500-W high-pressure mercury lamp with a Matsuda UV-27 filter interposed to cut off radiation of wavelength shorter than 2500 Å.

Analyses were carried out by gas chromatography using a 2.25-m phenylisocyanate-Porasil C (Waters Associates Inc.) and a 2.25-m Porapak Q columns. Reaction products were identified by the retention time of authentic substances and also by means of Shimadzu Model LKB-9000 gas chromatograph-mass spectrometer.

Results

Reaction of Excited 1-Buten-1-yl Radicals. The products measured were ethane, ethylene, *n*-butane, 1-butene, 1,3-butadiene, 3-methyl-1-pentene, *cis*- and *trans*-3-hexene (and/or *cis*- and *trans*-2-hexene), *cis*- and *trans*-1,3-hexadiene, and benzene. Despite efforts to detect further products, none could be found (i.e., no substantial chromatographic peaks eluted after benzene). The peaks were well resolved except *cis* and *trans* isomers and 3-hexene overlapped completely with 2-hexene. The rate of formation of each product is given in Tables I and II.

The addition of ethyl radicals to acetylene at 75 and 123° produces a 1-buten-1-yl radicals with about 33 kcal/mol in average (see Discussion section). The excited radical can either react or be stabilized by collisional energy transfer. The presence of 1-hexene and 3-methyl-1-pentene seems to be an evidence for the existence of 1-buten-4-yl and methylallyl radicals, respectively.

Stabilized 1-buten-1-yl radicals abstract a H atom from diethyl ketone to yield 1-butene. Combination of 1-buten-1-yl with ethyl radicals produces 3-hexene. Cross disproportionation products may be 1-butyne and ethane. However, the amount of 1-butyne was too small to be measured. Subsequent addition of 1-buten-1-yl to acetylene results in 1,3-hexadiene and benzene which appear in the steps of typical free-radical-initiated polymerization of acetylene.¹⁶ Methylallyl radicals may react with ethyl radicals to produce 2-hexene, 2-butene, and 1,2-butadiene in addition to 3-methyl-1-pentene. However, 2-hexene could not be resolved and cross disproportionation products were also too small to be measured in the present conditions.

A reaction scheme which can explain the products distribution shown in Tables I and II and their dependence on pressure is given as

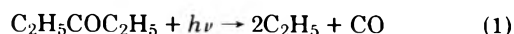


TABLE I: Experimental Results at 75°C

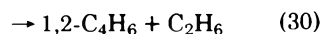
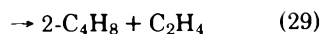
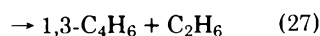
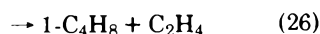
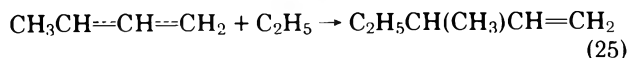
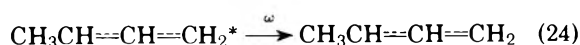
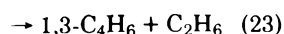
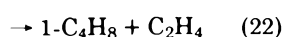
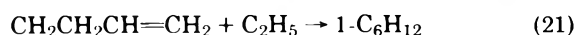
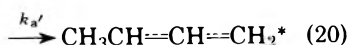
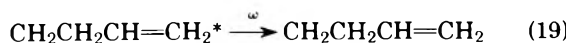
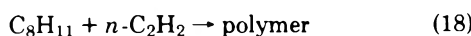
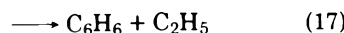
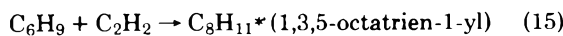
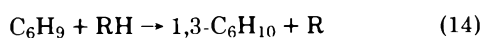
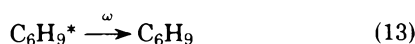
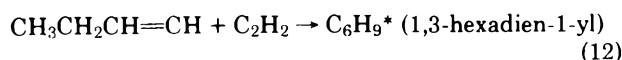
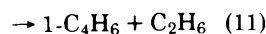
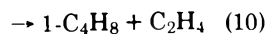
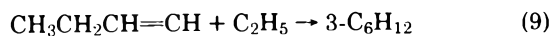
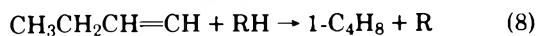
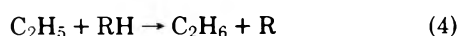
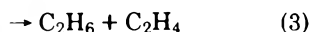
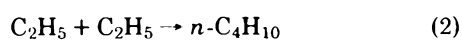
No.	DEK pressure ^a	C ₂ H ₂ pressure	Total pressure	Temp, °C	t, sec	C ₂ H ₆ ^c	C ₂ H ₄	n-C ₄ H ₁₀	1-C ₄ H ₈	1,3-C ₄ H ₆	3MPI ^d	1-C ₆ H ₁₂	2-C ₆ H ₁₂ ⁺ 3-C ₆ H ₁₂	1,3-C ₆ H ₁₀	C ₆ H ₆
11	34.2	104.0	138.2	74.3	300	12.2	7.73	58.3	8.37	0.335	0.0321	3.14	0.213	1.14	0.233
12	30.6	68.1	98.7	75.7	300	11.8	7.00	56.3	5.64	0.290	0.0325	2.69	0.164	0.666	0.122
13	34.6	42.4	77.0	75.8	300	12.7	7.67	63.9	3.87	0.201	0.0275	2.02	0.121	0.232	0.0451
14	14.2	41.8	56.0	74.3	300	5.66	3.88	32.5	1.69	0.203	0.0369	1.79	0.112	0.212	0.0555
15	9.8	45.4	55.2	74.1	300	3.80	2.70	21.5	1.19	0.194	0.0354	1.64	0.108	0.186	0.0868
16	26.6	28.0	54.6	74.7	360	10.3	6.75	57.1	2.10	0.161	0.0284	1.60	0.0947	0.130	0.0326
17	11.4	43.0	54.4	75.7	300	4.38	3.14	25.3	1.41	0.208	0.0352	1.72	0.110	0.208	0.0709
18	18.0	36.1	54.1	75.1	300	7.07	4.83	40.4	1.92	0.207	0.0353	1.83	0.112	0.184	0.0367
19	35.7	18.0	53.7	75.2	300	13.8	8.31	73.4	1.80	0.113	0.0173	1.16	0.0619	0.0535	~0
20	13.9	38.3	52.2	74.7	300	5.26	3.84	31.5	1.57	0.216	0.0369	1.74	0.108	0.195	0.0399
21	9.1	37.6	46.7	74.1	300	3.40	2.46	20.5	1.01	0.192	0.0341	1.50	0.0962	0.166	0.0646
22	14.9	22.7	37.6	74.0	300	5.94	4.29	34.8	0.992	0.147	0.0288	1.26	0.0819	0.0736	~0
23	20.5	11.3	31.8	74.9	300	8.51	5.75	49.9	0.596	0.0751	0.0155	0.722	0.0407	~0	~0
24	7.0	22.7	29.7	75.0	300	2.52	1.86	14.6	0.396	0.139	0.0310	0.963	0.0662	0.0467	0.0310
25	10.9	12.1	23.0	75.9	300	3.89	2.83	23.6	0.333	0.0876	0.0236	0.653	0.0500	0.0220	0.0103

^a Pressures are expressed in Torr. ^b Photolysis time. ^c Products are expressed in terms of their rates of formation in mol cm⁻³ sec⁻¹ × 10¹². ^d 3-Methyl-1-pentene.

TABLE II: Experimental Results at 123°C^a

No.	DEK pressure	C ₂ H ₂ pressure	Total pressure	Temp, °C	t, sec	C ₂ H ₆	C ₂ H ₄	n-C ₄ H ₁₀	1-C ₄ H ₈	1,3-C ₄ H ₆	3MPI	1-C ₆ H ₁₂	2-C ₆ H ₁₂ ⁺ 3-C ₆ H ₁₂	1,3-C ₆ H ₁₀	C ₆ H ₆
31	33.5	100.0	133.5	123.9	180	14.0	6.06	28.2	19.3	1.42	0.158	6.51	0.478	3.32	1.41
32	32.0	66.2	98.2	122.1	180	15.2	6.63	36.2	14.5	1.29	0.179	6.99	0.458	2.11	0.634
33	35.7	36.4	72.1	122.5	60	38.2	17.0	103.4	20.9	2.07	0.306	11.9	0.554	1.00	0.480
34	29.0	29.8	58.8	123.3	60	14.8	6.92	42.5	7.12	0.975	0.164	5.12	0.334	0.588	0.135
35	13.6	44.9	58.5	123.0	300	6.09	3.65	19.8	4.49	1.10	0.211	5.03	0.425	0.755	0.553
36	14.3	43.9	58.2	123.0	180	5.85	3.36	18.7	4.25	1.03	0.186	4.38	0.379	0.702	0.501
37	18.0	39.6	57.6	121.3	180	8.56	4.62	28.1	5.25	1.06	0.200	5.44	0.438	0.744	0.336
38	9.3	48.3	57.6	122.5	300	4.01	2.65	13.2	3.03	1.01	0.195	4.25	0.409	0.645	0.898
39	11.3	45.7	57.0	123.2	300	4.05	2.67	13.0	3.08	0.993	0.187	4.04	0.373	0.592	0.713
40	20.4	36.0	56.4	122.2	300	10.2	5.23	33.0	6.06	0.988	0.222	5.74	0.508	0.679	0.279
41	25.0	30.3	55.3	124.1	180	13.1	6.09	41.0	6.70	0.991	0.211	5.88	0.449	0.610	0.156
42	33.1	21.5	54.6	122.2	180	19.4	7.98	61.2	6.54	0.712	0.161	5.36	0.356	0.358	0.0376
43	15.9	31.1	47.0	122.5	180	7.54	3.99	26.1	3.86	0.882	0.183	4.24	0.297	0.372	0.198
44	21.0	23.4	44.4	122.0	60	10.6	5.20	33.5	3.93	0.772	0.155	3.96	0.297	0.303	~0
45	13.5	24.1	37.6	121.8	180	6.43	3.65	23.4	2.52	0.785	0.185	3.65	0.340	0.272	0.130
46	20.0	11.5	31.5	122.5	180	10.9	5.24	41.9	2.07	0.450	0.135	2.98	0.257	0.110	~0
47	14.7	15.8	30.5	121.4	60	8.67	4.25	27.8	1.92	0.638	0.154	3.04	0.271	0.166	~0
48	6.4	19.5	25.9	123.0	180	2.61	1.96	10.7	0.842	0.722	0.168	2.16	0.277	0.112	0.189

^a See Table I for units.



where RH and R represent the $(\text{C}_2\text{H}_5)_2\text{CO}$ molecule and the $\text{C}_2\text{H}_5\text{COC}_2\text{H}_4$ radical, respectively.

Kinetic Treatments. In order to obtain rate constants for isomerization, it is required to estimate the portion of stabilized 1-buten-1-yl radicals which are consumed in polymerization reactions and the rate of formation of 2-hexene produced by the cross combination reaction of isomerized methylallyl with ethyl radicals.

For reactions 1–30, steady-state treatments are applied, which lead to the following equation

$$R^{1/2}(n\text{-C}_4\text{H}_{10})[\text{C}_2\text{H}_2]/R_8(1\text{-C}_4\text{H}_8) = \{(\omega + k_a)/\omega\}(k_2^{1/2}/k_5)\{(k_{12}/k_8)[\text{C}_2\text{H}_2]/[\text{DEK}] + 1 + (k_9 + k_{10} + k_{11})/k_8[\text{C}_2\text{H}_2]/[\text{DEK}]\}$$

where $R_8(1\text{-C}_4\text{H}_8)$ is the rate of 1-butene formation via reaction 8, DEK diethyl ketone, and ω the effective stabilization rate constant.

Since $R(3\text{-C}_6\text{H}_{12}) < 0.05R(1\text{-C}_4\text{H}_8)$ in every run (3-hexene formation see the next section), the above equation is rewritten as

$$R^{1/2}(n\text{-C}_4\text{H}_{10})[\text{C}_2\text{H}_2]/R_8(1\text{-C}_4\text{H}_8) = \{(\omega + k_a)/\omega\}(k_2^{1/2}/k_5)\{(k_{12}/k_8)[\text{C}_2\text{H}_2]/[\text{DEK}] + 1\} \quad (\text{A})$$

Although 1-butene is formed by reactions 8, 10, 22, and 26, the fraction formed by reactions 10 and 26 can be neglected because formation of 3-hexene and 3-methyl-1-pentene was very small as compared with other products.

The rate constant ratios of k_{22}/k_{21} and k_{23}/k_{21} were estimated to be 0.06 and 0.08, respectively, in accord with the known disproportionation to combination ratios of *n*-alkyl and ethyl radicals.¹⁷ Thus

$$R_8(1\text{-C}_4\text{H}_8) = R(1\text{-C}_4\text{H}_8) - 0.06R(1\text{-C}_6\text{H}_{12})$$

On the condition that the ratio of $(\omega + k_a)/\omega$ is constant (i.e., total pressure are kept approximately constant), plots of $R^{1/2}(n\text{-C}_4\text{H}_{10})[\text{C}_2\text{H}_2]/\{R(1\text{-C}_4\text{H}_8) - 0.06R(1\text{-C}_6\text{H}_{12})\}$ vs. [acetylene]/[diethyl ketone] from the data in Table I (runs 14–20) and Table II (runs 34–42) gave values of k_{12}/k_8 as 0.311 and 0.382 at 75 and 123°, respectively. Then the portions of 1-buten-1-yl radicals consumed in polymerization are calculated by the following equation:

$$R_{12}(\text{polymerization})/\{R(1\text{-C}_4\text{H}_8) - 0.06R(1\text{-C}_6\text{H}_{12})\} = (k_{12}/k_8)[\text{C}_2\text{H}_2]/[\text{DEK}] \quad (\text{B})$$

The value of k_{28}/k_{25} can be obtained from the equation

$$R(2\text{-C}_6\text{H}_{12} + 3\text{-C}_6\text{H}_{12})/R(3\text{MP1}) = (k_9/k_2^{1/2}k_8)R^{1/2}(n\text{-C}_4\text{H}_{10})R_8(1\text{-C}_4\text{H}_8)/R(3\text{MP1})[\text{DEK}] + k_{28}/k_{25} \quad (\text{C})$$

where 3MP1 is 3-methyl-1-pentene. Figure 1 shows the plots of eq C by using the experimental data from Tables I and II. A least-squares treatment gave a slope of 3.91×10^{-3} , and $k_{28}/k_{25} = 1.67$ at 75°; and a slope of 3.05×10^{-3} , and $k_{28}/k_{25} = 1.55$ at 123°. In the case of reactions of mutual interaction of radicals, the activation energies are considered to be small.¹⁸ Then the value of k_{28}/k_{25} should show temperature independence. Accordingly the mean value 1.61 was used in the following calculations.

Isomerization of Chemically Activated 1-Buten-1-yl Radicals. In a chemically activated system the average rate constant k_a for a unimolecular reaction is given by $k_a = \omega(I/S)$,¹⁹ where ω is the specific collision frequency of the excited radical, I is the total rate of formation of the isomerized products, and S is the total rate of formation of the stabilized products. In the present case I and S are given by

$$I = R(1\text{-buten-4-yl products}) + R(\text{methylallyl products})$$

$$S = R(1\text{-buten-1-yl products})$$

Concerning methylallyl products, the ratios of disproportionation to combination were estimated to be $(k_{25} + k_{26} + k_{27})/k_{25} = (k_{28} + k_{29} + k_{30})/k_{28} = 1.18$ assuming that the ratios are equal to that of allyl and ethyl radicals.²⁰ Then I

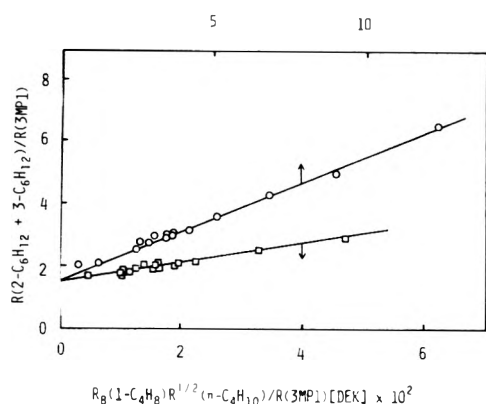


Figure 1. Experimental plot of eq C: O, 75°; □, 123°.

is rewritten as below by using the obtained value $k_{28}/k_{25} = 1.61$

$$I = R(1-C_6H_{12}) + R_{22}(1-C_4H_8) + R(1,3-C_4H_6) + 1.18R(3MP1) + 1.18R(2-C_6H_{12}) = 1.06R(1-C_6H_{12}) + R(1,3-C_4H_6) + 3.08R(3MP1)$$

On the other hand S was calculated by using eq B

$$S = R_8(1-C_4H_8) + R(3-C_6H_{12}) + R_{12}(\text{polymerization}) = \{1 + (k_{12}/k_8)[C_2H_2]/[DEK]\}R(1-C_4H_8) - 0.06R(1-C_6H_{12}) + R(2-C_6H_{12} + 3-C_6H_{12}) - 1.61R(3MP1)$$

A plot of I/S vs. $1/\omega$ from the data in Table I is shown in Figure 2. The calculation of collision rates is given in Appendix. The values 1.00×10^9 and $1.05 \times 10^9 \text{ sec}^{-1}$ were obtained as k_a at 75 and 123°, respectively.

Isomerization of Chemically Activated 1-Buten-4-yl Radicals. The rate constant for isomerization of chemically activated 1-buten-4-yl radicals k_a' is given by

$$k_a' = \omega(I'/S') = \frac{\omega R(\text{methylallyl products})}{R(1\text{-buten-4-yl products})}$$

As mentioned in the previous sections, the rates of formation of methylallyl and 1-buten-4-yl products are

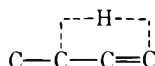
$$R(\text{methylallyl products}) = 1.18R(3MP1) + 1.18R(2-C_6H_{12}) = 3.08R(3MP1)$$

$$R(1\text{-buten-4-yl products}) = 1.14R(1-C_6H_{12})$$

A plot of I'/S' vs. $1/\omega$ (Figure 3) and a least-squares treatment gave values of $k_a' = 3.47 \times 10^7$ and $6.20 \times 10^7 \text{ sec}^{-1}$ at 75 and 123°, respectively.

Discussion

If isomerized methylallyl radicals can be formed by direct isomerization of chemically activated 1-buten-1-yl radicals, the possible course is formation through a four-membered cyclic transition state



In this case, we can see easily that the ratio, $I'/S' = R(\text{methylallyl products})/R(1\text{-buten-1-yl products})$, should be in direct proportion to ω^{-1} , i.e.

$$I'/S' = k/\omega \quad (D)$$

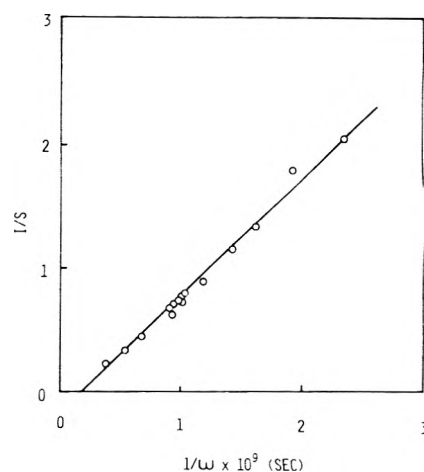


Figure 2. Plots of I/S vs. $1/\omega$ at 75°.

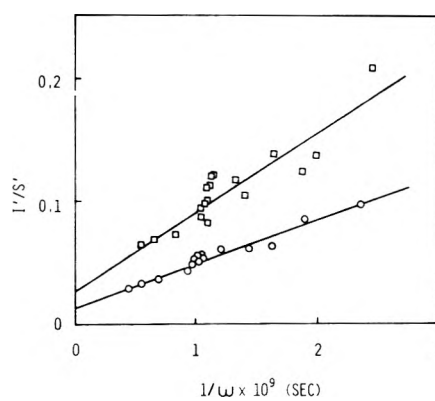


Figure 3. Plots of I'/S' vs. $1/\omega$: O, 75°; □, 123°.

On the other hand, when the proposed reaction scheme in which isomerized 1-buten-4-yl radicals are assumed to isomerize successively to the methylallyl radicals is correct, a plot of I'/S' vs. ω^{-1} should give a parabolic curve. That is, using the relations $k_a = \omega(I/S)$, $k_a' = \omega(I'/S')$, and $I = I' + S'$, one can obtain

$$I'/S' = k_a k_a' / \omega(\omega + k_a')$$

where k_a' is negligibly small as compared with ω (see Results section). Thus we can write

$$I'/S' = k_a k_a' / \omega^2 \quad (E)$$

or

$$(I'/S')^{1/2} = (k_a k_a')^{1/2} / \omega \quad (F)$$

Figure 4 shows plots of I'/S' vs. ω^{-1} and of $(I'/S')^{1/2}$ vs. ω^{-1} at 75° (similar curves are also obtained at 123° runs). From this figure it is clear that the data are well described by eq E and F, but not by eq D. The slope of the straight line in Figure 4 gives values of $k_a k_a' = 3.40 \times 10^{16}$ and $5.09 \times 10^{16} \text{ sec}^{-2}$ at 75 and 123°, respectively, which agree with those obtained separately in the Results section, i.e., 3.47×10^{16} and $6.51 \times 10^{16} \text{ sec}^{-2}$.

In addition, the critical energy for the isomerization of 1-buten-1-yl to methylallyl radicals via 1,3-H atom shift is estimated to be in the range 34–37 kcal/mol both by using eq G (see the following discussion section) and by analogy with the critical energy for the isomerization of chemically activated propenyl to allyl radicals,¹⁴ $E_0(4pp) = 34.5 \text{ kcal/}$

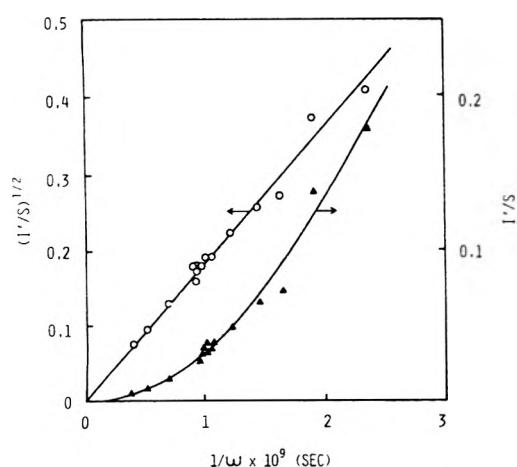


Figure 4. Plots of I'/S and $(I'/S)^{1/2}$ vs. $1/\omega$ at 75° : \blacktriangle , I'/S vs. $1/\omega$; \circ , $(I'/S)^{1/2}$ vs. $1/\omega$.

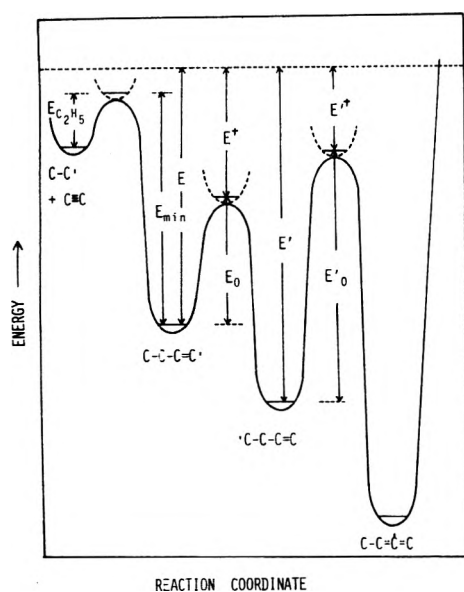


Figure 5. Schematic potential energy diagram.

TABLE III: Comparison of Calculated and Experimental Results

Temp, $^\circ\text{C}$	E' , kcal/mol	$k_a(\text{obsd})$, sec^{-1}	E_0 , kcal/mol	$k_a(\text{calcd})$, sec^{-1}
1,4-H Atom Shift				
75	33.1	1.00×10^9	17.1	0.99×10^9
123	33.5	1.05×10^9	17.1	1.06×10^9
1,2-H Atom Shift				
75	43.3	3.47×10^7	33.0	3.64×10^7
123	43.7	6.20×10^7	33.0	4.68×10^7

mol, which undergoes a similar 1,3-H atom shift. The 1-buten-1-yl radicals isomerize to 1-buten-4-yl via 1,4-H atom shift by reaction 7 with a low critical energy, 17.1 kcal/mol (see the following RRKM calculation section). Thus the ratio of the rate constant for the 1,3-H atom shift isomerization of the 1-buten-1-yl radicals to that of reaction 7 results in smaller than 10^{-10} . This implies that the formation of methylallyl radicals by 1,3-H atom shift of 1-buten-1-yl is negligible under the present conditions.

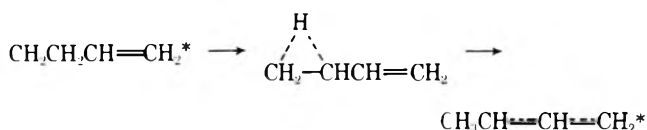
Therefore, it is concluded that the methylallyl radicals

TABLE IV: Parameters Used in Collision Calculations^a

Species	σ , Å	ϵ/k , K
C_2H_3	4.11	212
$\text{C}_2\text{H}_3, \text{COC}_2\text{H}_3$	5.91	413
$\text{CH}_3\text{CH}_2\text{CH}=\text{CH}$	5.20	319
$\text{CH}_2\text{CH}_2\text{CH}=\text{CH}_2$	5.20	319

^a Reference 27, parameters for radicals are assumed to be equal to those for 1-butene.

are formed by the succeeding isomerization of the 1-buten-4-yl radicals. The only energetically possible process is the isomerization through a three-membered cyclic activated complex



In order to obtain estimates of isomerization critical energies of 1,4- and 1,2-H atom shifts, RRKM calculations were carried out.¹⁹ Computational procedures were described in detail previously when data for the addition of methyl radicals to acetylene were reported.¹⁴ Figure 5 is a schematic potential energy diagram starting with $\text{C}_2\text{H}_5 + \text{C}_2\text{H}_2$ and leading to the observed products. Energy parameters for isomerization are given in the Appendix. Details of frequency assignments of the radicals, association complex, and isomerization complexes are also given in the Appendix.

The best agreement between the theoretical and experimental rate constants was obtained when the threshold energies were chosen as 17.1 and 33.0 kcal/mol for 1,4- and 1,2-H atom shifts, respectively. The calculated average rate constants k_a are shown in Table III.

The nonzero intercept in Figure 2 has about a 25% increasing effect on the value of k_a , and in Figure 3 about a 40% decreasing effect on k_a' as compared with those obtained on the assumption that the straight lines in the figures would have a zero intercept. However, the uncertainty caused by the nonzero intercept does not cause an uncertainty in the critical energies greater than 0.5 kcal/mol.

The critical energy for 1,4-H atom shift, $E_0 = 17.1$ kcal/mol, agrees well with the values reported in exothermic reactions.^{2-4,10,11,13} Stabilized isomers of 1,2-H atom shift have not been found hitherto. The only evidence for 1,2-H atom shift is the work of Tardy⁵ in which the decomposition products in H + 1-pentene system were analyzed, and the value of approximately $E_0(3\text{ss}) = 33 = 1$ kcal/mol has been proposed as its critical energy, which agrees with that obtained in the present work $E_0(3\text{sp}) = 33.0$ kcal/mol.

Abnormally low critical energies have been found when the so-called homoallylic rearrangement is included in the cyclic transition states.¹¹⁻¹³ The above agreement in 1,2-H atom shift suggests that the activation complex for the isomerization of 1-buten-4-yl to methylallyl radicals has very little or no stabilization by allylic conjugation, though the isomerized methylallyl radicals are stabilized. The same matter was observed in the isomerization of chemical-ly activated propenyl to allyl radicals.¹⁴

Estimation of critical energies E_0 for isomerization of alkyl and alkenyl radicals is given by

$$E_0 = E_{ab} + E_s - Q, \text{ if any (for endothermic reaction)} \quad (\text{G})$$

TABLE V: Enthalpies of Formation and Bond Energy at 0 K (kcal/mol)

$\Delta H_f^\circ(\text{C}_4\text{H}_5)$	28.86 ^a	$D^\circ(\text{vinylic C-H})$	106.5
$\Delta H_f^\circ(\text{C}_4\text{H}_7)$	54.33 ^b	$D^\circ(\text{primary C-H})$	96.2
$\Delta H_f^\circ(1\text{-C}_4\text{H}_8)$	4.96 ^a	$D^\circ(\text{secondary C-H})$	92.8
$\Delta H_f^\circ(\text{H})$	51.62 ^a	$D^\circ(\text{secondary allylic C-H})$	81.5
$\Delta H_f^\circ(\text{CH}_2\text{CH}_2\text{CH}=\text{CH})$	59.8		
$\Delta H_f^\circ(\text{CH}_2\text{CH}_2\text{CH}=\text{CH}_2)$	49.5		
$\Delta H_f^\circ(\text{CH}_2\text{CH}=\text{CH}=\text{CH}_2)$	34.8		

^a Reference 19. ^b Reference 11.

TABLE VI: Frequency Changes for Radical \rightarrow Activated Complex^a

(A) Association Complex					
C-C stretch	Skeletal bend for C=C...C	C=C stretch \rightarrow C=C stretch	Libration	Frequencies lowering	Torsion for forming C=C
826 \rightarrow 0	469 \rightarrow 234	1649 \rightarrow 1811	102 \rightarrow 51	1445 \rightarrow 722 1333 \rightarrow 666 301 \rightarrow 150	995 \rightarrow 1200
(B) 1,4· and 1,2-H atom Shifts Complexes					
Mode		Frequencies deleted from radical assignments		Replaced ring deformation modes	
		C-C-C=C	C-C-C=C	C-C-C=C ^b	
CC	tors	102		1623	
CH ₃	tors	237	237	937 (2)	
C=C	twist	995		1116	
C=CC	bend	469		386	
CCC	bend	301		662	
CC	str	1046	1046	1100 (3)	
=CC	str	826		C-C-C=C	
C=C	str	1649		850 (2)	
CH	str	2972	2982	1100	
CH ₂	rock	967			
CH	bend		1333		

^a Frequencies are in units of cm^{-1} . ^b Taken from C. W. Bekett, N. K. Freeman, and K. S. Pitzer, *J. Am. Chem. Soc.*, **70**, 4227 (1948).

where E_{ab} and E_s are already stated and Q is the "thermal effect"²¹ which is the difference between the zero-point energies of the initial and final states (Q is negative when the reaction is endothermic). Although accurate critical energies for isomerization of radicals have not been obtained in endothermic reactions, 1,5-H atom shifts of the 6ps type show somewhat higher critical energies than those expected.³ This seems to correspond to the thermal effect.

In the present case, we can adopt for a 1,4-H atom shift $E_{ab} = 9.1$ kcal/mol²² and $E_s = 8.5$ kcal/mol, the strain energy for cyclopentene,²³ and for 1,2-H atom shift $E_{ab} = 7.6$ kcal/mol²⁴ and $E_s = 28.7$ kcal/mol, the strain energy for cyclopropane,²³ where the values of E_s are corrected to 0 K.

The difference between the experimental and calculated critical energies by means of eq G is approximately $\pm 10\%$ through three-, four-,^{13,14} five-,^{2-4,10,11,13} six-,⁹ and seven-membered³ ring activated complexes. The errors do not have large effects on the value of k_a when the activation energies of the activated complexes (E^\ddagger in Figure 5) are large (five-, six-, and seven-membered ring), but when they are small, k_a is affected considerably. In the present case, when the calculated $E_0 = 36.3$ kcal/mol and the same calculational procedures are adopted, the rate constant for the 1,2-H atom shift becomes approximately 10% of that when $E_0 = 33.0$ kcal/mol.

There is an allowance of more than ± 1 kcal/mol in choosing the values E_{ab} ²⁵ and E_s .^{23,26} Therefore it seems natural that there are approximately $\pm 10\%$ errors between the calculated and experimental critical energies. Nevertheless eq G is considered convenient in order to estimate

the activation energies for isomerization of alkyl and alkenyl radicals via ring complexes.

Appendix

Calculation of Collision Rates. Collision rates were calculated by the standard kinetic relationship

$$\omega = \{(s_a + s_b)/2\}^2 \{(M_a + M_b)/M_a M_b\}^{1/2} (8\pi kT)^{1/2} N_b$$

where s is the effective collision diameter, M the molecular weight, and N_b the concentration of B molecules. The s values were derived from the Lennard-Jones parameters σ and ϵ/k .

$$s_{ab}^2 = \sigma_{ab}^2 [\Omega^{(2,2)}(T^*)]$$

where

$$T^* = T[(\epsilon/k)_a(\epsilon/k)_b]^{-1/2}$$

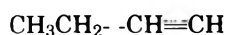
and the collision integrals $\Omega^{(2,2)}(T^*)$ were obtained from standard tables.²⁷ The values used are given in Table IV.

Thermochemical Parameters. Heats of formation of radicals are obtained from the appropriate bond dissociation energies and the 0 K heat of formation of 1-butene (Table V). C-H bond dissociation energies used are 96.2 and 92.8 kcal/mol for primary and secondary bonds, respectively,²⁸ 106.5 kcal/mol for the vinylic bond,²³ and 81.5 kcal/mol for the secondary allylic C-H bond.²⁹ The activation energy for the addition of ethyl radicals to acetylene $E_{C_2H_5}$ has been found to be 7.0 kcal/mol.³⁰

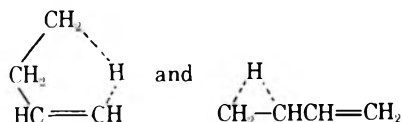
Frequency Assignments. The frequency assignments for

1-buten-1-yl and 1-buten-4-yl radicals were taken from 1-butene,³¹ in which the torsional mode about the central C-C bond was lowered to 102 cm⁻¹ as pointed out by Pearson and Rabinovitch,¹⁵ and the following three frequencies were removed: CH stretch, 3011 cm⁻¹, and two HCH bends, 1443 and 913 cm⁻¹, for 1-buten-1-yl; 2972, 1045, and 1470 cm⁻¹ for 1-buten-4-yl radicals.

For the calculation of k_a , the association complex was specified as



and the isomerization complexes as



and modifications of their frequency assignments were made according to those by Rabinovitch and coworkers.^{3,15} The modified frequencies are given in Table VI. These frequencies give $\log A(\text{sec}^{-1}) = 12.11$ and $\log A(\text{sec}^{-1}) = 12.68$ for 1,4- and 1,2-H atom shifts, respectively.

References and Notes

- E. A. Hardwidge, C. W. Larson, and B. S. Rabinovitch, *J. Am. Chem. Soc.*, **92**, 3278 (1970).
- K. W. Watkins and D. R. Lawson, *J. Phys. Chem.*, **75**, 1632 (1971).
- C. W. Larson, P. T. Chua, and B. S. Rabinovitch, *J. Phys. Chem.*, **76**, 2507 (1972).
- K. W. Watkins, *Can. J. Chem.*, **50**, 3738 (1972).
- D. C. Tardy, *Int. J. Chem. Kinet.*, **6**, 291 (1974).
- L. Endrenyi and D. J. LeRoy, *J. Phys. Chem.*, **70**, 4081 (1966).
- K. W. Watkins, *J. Am. Chem. Soc.*, **93**, 6355 (1971).
- K. W. Watkins and L. A. Ostereko, *J. Phys. Chem.*, **73**, 2080 (1969).
- K. W. Watkins, *J. Phys. Chem.*, **77**, 2938 (1973).
- K. W. Watkins and D. K. Olsen, *J. Phys. Chem.*, **76**, 1089 (1972).
- K. W. Watkins and L. A. O'Deen, *J. Phys. Chem.*, **75**, 2665 (1971).
- W. P. L. Carter and D. C. Tardy, *J. Phys. Chem.*, **78**, 1245 (1974).
- W. P. L. Carter and D. C. Tardy, *J. Phys. Chem.*, **78**, 2201 (1974).
- T. Ibuki, T. Murata, and Y. Takezaki, *J. Phys. Chem.*, **78**, 2543 (1974).
- M. J. Pearson and B. S. Rabinovitch, *J. Chem. Phys.*, **42**, 1624 (1965).
- C. W. Drew and A. S. Gordon, *J. Chem. Phys.*, **31**, 1417 (1959).
- (a) J. O. Terry and J. H. Futrell, *Can. J. Chem.*, **45**, 2327 (1967); (b) J. Grotowold and J. A. Kerr, *J. Chem. Soc.*, 4337 (1963); (c) Y. Ined, *J. Phys. Chem.*, **74**, 2581 (1970); (d) R. A. Holrcyd and T. E. Pierce, *ibid.*, **68**, 1392 (1964).
- J. A. Kerr and A. F. Trotman-Dickenson, "Progress in Reaction Kinetics", Vol. 1, Pergamon Press, New York, N.Y., 1961.
- B. S. Rabinovitch and D. W. Setser, "Advances in Photochemistry", Vol. 3, Wiley, New York, N.Y., 1964.
- D. G. L. James and G. E. Troughton, *Trans Faraday Soc.*, **62**, 145 (1966).
- N. M. Emanuel and D. G. Knorre, "Chemical Kinetics," Wiley, New York, N.Y., 1960, p 58.
- M. H. Jones and E. W. R. Steacie, *Can. J. Chem.*, **31**, 505 (1953).
- S. W. Benson, "The Foundation of Chemical Kinetics", Wiley, New York, N.Y., 1960.
- A. F. Trotman-Dickenson and E. W. R. Steacie, *J. Chem. Phys.*, **19**, 169 (1951).
- A. F. Trotman-Dickenson and G. S. Milne, *Natl. Stand. Ref. Data Ser., Natl. Bur. Stand., No. 9* (1967).
- P. v. R. Schleyer, J. E. Williams, and K. R. Elanchard, *J. Am. Chem. Soc.*, **92**, 2377 (1970).
- J. O. Hirschfelder, C. F. Curtiss, and R. B. Bird, "Molecular Theory of Gasses and Liquids", Wiley, New York, N.Y., 1964.
- C. W. Larson and B. S. Rabinovitch, *J. Chem. Phys.*, **50**, 871 (1969).
- D. M. Golden and S. W. Benson, *Chem. Rev.*, **69**, 125 (1969).
- J. A. G. Dominguez and A. F. Trotman-Dickenson, *J. Chem. Soc.*, 940 (1962).
- L. M. Sverdlov, M. G. Borisov, and N. V. Tarasova, *Opt. Spectrosc.*, **5**, 354 (1958).

Direct Identification of Reactive Routes and Measurement of Rate Constants in the Reactions of Oxygen Atoms with the Fluoroethylenes

James R. Gilbert, Irene R. Slagle, Ronald E. Graham, and David Gutman*

Department of Chemistry, Illinois Institute of Technology, Chicago, Illinois 60616 (Received June 13, 1975)

Publication costs assisted by the Petroleum Research Fund

The room temperature reactions between oxygen atoms and monofluoro-, difluoro (1,1 and 1,2)-, trifluoro-, and tetrafluoroethylene have been studied in crossed jets to directly identify their reactive routes. Free radical and stable products were detected using photoionization mass spectrometry and were assigned to reactive routes. The routes identified were of three types: $\cdot\text{O} + \text{WXC}=\text{CYZ} \rightarrow \text{WXC}\cdot + \text{CYZO}$; $\cdot\text{O} + \text{WXC}=\text{CYZ} \rightarrow \text{WXYC}\cdot + \cdot\text{CZO}$ (or $\text{Z}\cdot + \text{CO}$); $\cdot\text{O} + \text{WXC}=\text{CYZ} \rightarrow \text{WX} + \text{C}_2\text{YZO}$, where W, X, Y, and Z are either H or F atoms. Individual O + fluoroethylene reactions were found to proceed by either one, two, or three of these distinctly different kinds of routes. The results of this study are interpreted using an expanded version of a mechanism proposed by Cvetanović for O + olefin reactions. Overall rate constants for several of these reactions were also measured at 300 K and are reported.

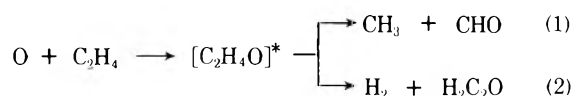
Introduction

The reactions of oxygen atoms with unsaturated organic molecules proceed via the formation of extremely energy rich adducts which are capable of decomposing or undergoing rapid internal rearrangements.¹ These reactions have

long been recognized as important steps in thermal and photochemical combustion mechanisms and are now receiving new attention as potential chemical lasers.² Although today there is considerable information on the overall rate constants for many of these reactions, knowledge of the products they produce is still quite sparse.^{3,4} We are

currently investigating the reactions of O atoms with alkenes and alkynes both in crossed jets and in a flow system specifically to directly detect and identify the reactive and stable intermediates they produce as well as to determine the importance of the various reactive routes by which these same reactions proceed.³⁻⁷ We have now completed a study at ambient temperature of the reactions of O atoms with each of the fluorinated ethylenes (FE) and have identified their open reactive channels. The results of this study are reported here.

The two extreme members of the series of reactions $O + C_2H_xF_y$ ($x = 0-4$, $y = 4 - x$) proceed by entirely different paths. Products of the $O + C_2H_4$ reaction have been detected and identified in experiments using crossed jets and the reaction was shown to proceed by two routes, a principal one involving internal H-atom migration in the $O-C_2H_4$ adduct followed by decomposition into two free radicals, and a secondary one in which H_2 is eliminated from the excited adduct^{3,5}



The $O + C_2F_4$ reaction has been extensively studied and there is strong indirect evidence that it proceeds exclusively by direct C-C bond cleavage of the $O-C_2F_4$ adduct to produce difluorocarbene⁸



The present study was undertaken partially because it was anticipated that the knowledge gained of the mechanistic differences among the $O + C_2H_xF_y$ reactions might indicate some of the factors which govern access to the different kinds of energetically allowed reactive routes in the reactions of O atoms with unsaturated organic molecules. We feel some additional details were revealed regarding how these reactions proceed, and we have discussed our results with an expanded version of a mechanism first proposed by Cvetanović.¹

Experimental Section

Two kinds of experiments were performed on each $O +$ fluoroethylene reaction. First each was studied in high-intensity crossed jets to directly detect and identify products of the reaction. Second, the room temperature rate constant was measured using a fast-flow reactor. In the crossed-jet experiments, an uncollimated and indiscriminated room temperature beam containing ~5% O atoms intersected a similar beam containing the FE. Products scattered in the direction of the O-atom beam were detected with a photoionization mass spectrometer. Details of the crossed-jet reactor, the detection system, the experimental conditions, and the data reduction procedure followed are all as described previously.³⁻⁷ Special tests to assure that detected products were not the result of secondary reactions or the result of possible hyperthermal kinetic energy of the reactant molecules were done as in previous studies.^{6,7}

The FE gases used were obtained from PCR Inc. (Gainesville, Fla.) except 1,1-difluoroethylene and C_2F_4 which were obtained from Matheson Gas Co. All FE reactants were condensed with liquid N_2 , degassed, and fractionally distilled, the middle third being retained for the experiments.

The overall rate constants of the $O + FE$ reactions were measured at 300 ± 2 K using a fast-flow reactor described before.⁹ Oxygen atoms were generated by flowing $He + O_2$ gas mixtures through a microwave discharge. Rate constants were obtained by monitoring the first-order decay of FE along the reactor in the presence of a large O-atom excess. In the experiments involving fluoroethylenes which were found to produce carbenes (CHF or CF_2) in their reactions with O atoms ($1,2-C_2H_2F_2$, C_2HF_3 , C_2F_4) extremely high $[O]/[FE]_0$ (>90) had to be used to obtain "rate constants" which were independent of reactant concentrations. A similar observation was reported by Huie, Herron, and Davis in their flow-reactor study of these same reactions.¹⁰ Our sensitivity for detecting C_2F_4 by photoionization was lower than for the other fluoroethylenes, so we were unable to accurately monitor C_2F_4 under the required conditions and to obtain accurate rate constants for the $O + C_2F_4$ reaction. A possible explanation of this interference is that carbenes add so readily to the FE reactants that the subsequent reaction of these products cannot be adequately suppressed until extremely low FE concentrations are used. By contrast, carbenes were not detected as products of the $O + 1,1-C_2H_2F_2$ reaction and measurements of its rate constant required only the normal $[O]/[FE]_0$ ratios which are needed to assure negligible depletion of O atoms during reaction (~ 20).

The results of the crossed-jet experiments are given in Table I, and the measured rate constants are listed in Table II.

Discussion

Overall Rate Constants. The overall rate constants for the $O + FE$ reactions measured in this study at room temperature are in excellent agreement with those measured by Huie, Herron, and Davis in a similar flow reactor study.¹⁰ Jones and Moss have determined rate constant ratios for all the $O + FE$ reactions relative to the $O + 2$ -(trifluoromethyl)-propene reaction.¹² Using their data we have calculated quotients of the $O + FE$ rate constants divided by that for $O + C_2H_3F$. These ratios are in good agreement with similar quotients using the results of our study. A comparison of these ratios as well as of the overall rate constants is given in Table III.

Reactive Routes. Every product detected and identified in the study of each $O +$ fluoroethylene reaction has been assigned to a reactive route. These routes are listed in Table I. Those products which were not detected in each of the routes listed generally could not be detected either due to their having ionization potentials which were too high to be detected with our photoionization mass spectrometer (H , F , CO , HF , H_2 , F_2 , $CHFO$, and CF_2O), or due to their having mass numbers which are at or adjacent to that of the reactant (e.g., CFO in the $O + C_2H_3F$ reaction), or due to their having the same mass number as that of an impurity in one of the reactant beams (e.g., CHO in most of the reactions).

There have been no earlier studies of these reactions under conditions where subsequent reactions of initial products were suppressed and hence comparison of our results can only be done with the indirect evidence for reactive routes reported by others. What secondary evidence exists generally supports the results of this study. Hecklen and coworkers have extensively studied the $O + C_2F_4$ reaction through measurements of the ultimate stable products produced (CF_2O and $c-C_3F_6$).⁸ Their results suggested to

TABLE I: List of Products Detected and Assigned Reactive Routes for O + Fluoroethylene Reactions

Reaction	Products detected ^a	Assigned reactive routes
O + HFCCCH ₂	CH ₃ , ^b CH ₂ F, CHO C ₂ H ₂ O C ₂ HFO ^b	CH ₃ + CFO (F + CO) CH ₂ F + CHO C ₂ H ₂ O + HF C ₂ HFO + H ₂
O + F ₂ CCH ₂	CHF ₂ , C ₂ HFO	CHF ₂ + CHO (H + CO) C ₂ HFO + HF
O + HFCCCHF ^c (cis and trans)	CH ₂ F, C ₂ HFO CHF	CH ₂ F + CFO (F + CO) C ₂ HFO + HF CHF + CHFO (CO + HF)
O + HFCCF ₂	CF ₂ , ^d CHF	CF ₂ + CHFO (CO + HF) CHF + CF ₂ O (CO + F ₂)
O + F ₂ CCF ₂	CF ₂	CF ₂ + CF ₂ O

^a Products sought with photoionization energies of 11.6 eV (Ar lamp), 10.2 eV (H lamp), and 9.5 eV (O lamp).

^b These products probably of minor importance. Ion signal ~1% that detected for all products combined. ^c Ion signals detected from reactions of cis and trans isomers were not significantly different. Differences in relative ion signals among products were measurable to ±30% with 95% confidence. ^d The detection of CF₂ may possibly indicate the presence of the reactive route O + C₂HF₃ → C₂F₂O (CF₂ + CO) + HF. The molecule C₂F₂O is believed to be unstable and decomposes into CF₂ + CO.¹¹

TABLE II: Results of Experiments to Measure the Overall Rate Constant for O + Fluoroethylene Reactions^{a,b}

Pressure, ^c Torr	Flow velocity, m/sec	10 ⁻¹⁴ [O], p cm ⁻³	10 ⁻¹² [Fluoroethyl- ene] ₀ , p cm ⁻³	10 ¹³ k, ^d cm ³ p ⁻¹ sec ⁻¹
O + <i>trans</i> -1,2-C ₂ H ₂ F ₂				
1.45	11.8	3.25	2.96	6.1
1.46	11.9	9.55	9.31	5.6
1.46	11.9	9.03	7.17	5.7
				Av k for O + <i>trans</i> -1,2-C ₂ H ₂ F ₂ 5.8
O + <i>cis</i> -1,2-C ₂ H ₂ F ₂				
1.45	11.8	3.25	2.94	3.8
1.46	11.9	9.55	9.44	3.6
1.46	11.9	9.03	7.10	3.8
				Av k for O + <i>cis</i> -1,2-C ₂ H ₂ F ₂ 3.7
O + 1,1-C ₂ H ₂ F ₂				
1.49	12.0	3.36	16.2	3.3
1.49	12.0	3.36	6.57	3.2
1.46	12.6	10.8	10.7	2.6
1.46	12.6	10.8	15.8	2.8
1.46	12.6	10.8	7.5	2.5
1.46	12.6	10.8	53.	2.8
1.46	12.6	4.1	11.2	3.6
1.46	12.7	4.1	5.32	4.0
1.46	12.7	4.6	5.45	3.0
				Av k for O + 1,1-C ₂ H ₂ F ₂ 3.1
O + C ₂ HF ₃				
1.46	12.8	7.84	6.52	9.1
1.45	12.6	3.51	2.67	7.8
1.45	12.6	3.58	4.03	8.2
1.46	12.8	3.59	3.42	8.2
				Av k for O + C ₂ HF ₃ 8.3

^a Rate constants for O + C₂H₂F₂ reaction reported in ref 7. Average k for O + C₂H₂F₂ at 302 ± 2 K is 4.1 × 10⁻¹³ cm³ p⁻¹ sec⁻¹. ^b T in all experiments 300 ± 2 K. ^c Average pressure along flow reactor. Total pressure drop along tube less than 5%. ^d Average rate constants are estimated accurate to ±20%.

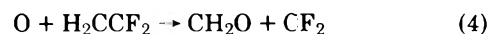
TABLE III: Comparison of Overall Rate Constants for O + Fluoroethylene Reactions

Fluoroethylene	This study		Huie, Herron, and Davis ^a		Jones and Moss ^b
	10 ¹³ k, cm ³ p ⁻¹ sec ⁻¹	k/ k _{C₂H₃F}	10 ¹³ k, cm ³ p ⁻¹ sec ⁻¹	k/ k _{C₂H₃F}	k/ k _{C₂H₃F}
H ₂ CCHF	4.1 ^c	1.00	4.36	1.00	1.00
HFCCHF (cis) (mixture) ^d	3.7	0.90	4.48	1.03	0.76
(trans)	5.8	1.41			1.38
H ₂ CCF ₂	3.1	0.76	3.63	0.83	0.52
HFCCF ₂	8.3	2.02			1.40

^a Reference 10, T = 307 K. ^b From data in ref 12, T = 298 K. ^c k for O + C₂H₃F reaction from ref 7. ^d An equilibrium mixture of cis and trans isomers would contain about 82% cis isomer (calculated using equilibrium constant in ref 13).

the authors that the only route of this reaction is the one directly observed in this study, reaction 3. Mitchell and Simons¹⁴ as well as Tyerman¹⁵ have seen CF₂ in absorption in the flash initiated O + C₂F₄ reaction and also concluded it was produced by reaction 3.

Mitchell and Simons have also studied the O + 1,1-difluoroethylene reaction in a similar flash-initiated experiment, and they also observed CF₂ production from this reaction.¹⁴ They conclude that the route



is an important one. As we did not detect CF₂ in our study of this reaction, we conclude that this route, if present, must be a minor one (<10% of the total reaction). This opinion is supported by our additional observation that no "carbene interference" was encountered in the flow reactor study of the O + H₂CCF₂ reaction.

Huie et al. list aldehydic products (CH₂O, CHFO, and CF₂O) detected in their flow reactor studies of the O + FE reactions.¹⁰ However, they drew no conclusions regarding the origin of these products since they could have been produced by either the primary or by secondary reactions. Recently Umstead, Lin, and Woods observed HF laser emission from the O + C₂H₃F reaction and reported evidence that the lasing HF was produced by the initial reaction.² Such a conclusion would be consistent with our observation of the other product produced by this route (C₂H₂O) in our crossed-jet study of this reaction.

The Mechanism. In this section we interpret our experimental findings on the O + FE reactions with a detailed mechanism which is an outgrowth of what is already known about the course of O + olefin reactions. Cvetanović has extensively studied this latter class of reactions and has proposed a mechanism which has adequately accounted for his major observations.¹ We have broadened his scheme to include two additional types of reactive routes which are not included in Cvetanović's mechanism because they are not observed to occur to a significant degree in O + olefin reactions. In addition we have attempted to be more specific about the stages at which various types of decompositions occur. The expanded mechanism which we feel "explains" our observations is shown in Figure 1 and is discussed below.

Addition. The initial step for all O + FE reactions is the electrophilic addition of the O atom to the double bond to form an excited biradical intermediate. This is the same

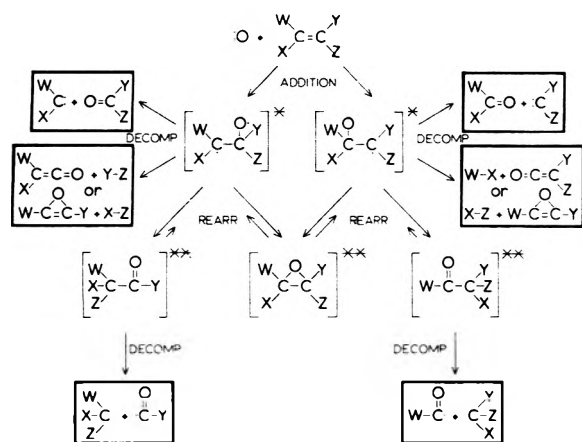


Figure 1. Mechanism for the reactions of oxygen atoms with the fluorinated ethylenes. Products in boxes are the products produced under the conditions of the crossed-jet experiments.

initial step proposed by Cvetanović for all O + olefin reactions, who further suggest a transition complex involving a partial charge transfer of one of the π electrons from the olefin to the attacking atom. To support this model Cvetanović¹⁶ and Sato and Cvetanović¹⁷ have shown that the logarithms of the room temperature rate constants for these reactions are linearly related to various electronic properties of the olefins such as ionization potential and electronic excitation energy.

The trend and magnitudes of the O + FE rate constants support a similar rate-determining step for these reactions. A small decrease in ionization potential of the FE with increasing fluorination correlates with the small increase in the O + FE room temperature rate constant. In fact the O + FE rate constants lie quite near the line on a semilog plot formed by plotting the O + olefin rate constants vs. the ionization potential of the olefin. Apparently the marked differences in the types of products produced by the different O + FE reactions have no significant effect on the overall reaction rate constant.

Biradical Decomposition. The biradical adduct may either unimolecularly decompose or intramolecularly rearrange. Two types of decomposition are possible: C-C bond cleavage to form a carbene or molecular elimination of H₂ or HF. Our suggestion that these two decompositions occur from the biradical adduct rather than from species formed by rearrangements (the carbonyl and epoxide compounds) is supported by some evidence. DeMore has studied the O + C₂F₄ reaction in liquid argon and found that even in the condensed phase this reaction proceeds entirely by decomposition to form CF₂ + CF₂O.¹⁸ He found no trace of CF₂CF₂O or CF₃CFO, the two possible stabilized products of this reaction. The absence of stabilized products, especially CF₂CF₂O, when this reaction is run in the liquid phase suggests that this reaction did not proceed through an internally excited carbonyl or epoxide structure. Indeed the decomposition to form difluorocarbene and carbonyl fluoride is apparently so rapid in the O + C₂F₄ reaction that any electronic or structural rearrangement prior to decomposition seems unlikely. Molecular elimination of H₂ and hydrogen halides occur quite readily from some diradicals (e.g., electronically excited haloethylenes^{19,20}), but happens not to occur to any significant extent from carbonyl compounds and epoxides (the rearrangement products of

the O + FE reactions) which are photochemically excited to energies comparable to those contained in these compounds when they are produced by the O + FE reactions.²¹ Epoxides such as ethylene oxide do decompose partially by H₂ elimination when excited to much higher energies.²² However, there is reason to believe photochemical and thermal decompositions of epoxides begin with ring opening to form the biradical intermediate.²³

The substitution of fluorine for hydrogen in ethylene enhances the probability for unimolecular decomposition of the excited biradical adduct relative to the probability for rearrangement to a carbonyl or epoxide structure for two reasons. First the addition of F atoms to the adduct creates the possibility of molecular HF elimination from the adduct. The loss of HF is less endothermic than the loss of H₂ from the same compound and is more important than H₂ elimination wherever these processes are both capable of occurring.^{20,24} Our initial quantitative studies of the importance of the different O + FE reactive routes indicate a like trend. We have found that molecular elimination of H₂ in the O + C₂H₄ reaction accounts for only 5% of the overall reaction⁵ but accounts for 11% of the O + C₂H₃F reaction.⁷ The diatomic expelled in the O + C₂H₃F reaction is almost entirely HF.

Apparently both 1,1 and 1,2 elimination of HF occurs from the excited O-FE adducts. The product CHF₂O was detected with about equal intensity from both the reactions



and



The presence of reaction 6 is the evidence for a 1,2 elimination process. The elimination of H₂ from the O-C₂H₄ has already been shown to be overwhelmingly a 1,1 process,³ and we presume 1,1 elimination of HF from the carbon to which the O atom adds is also a very likely process in O + FE reactions. The comparable ion signals from C₂HFO produced by reactions 5 and 6 suggest that 1,1 and 1,2 HF elimination from O-FE adducts may occur with comparable probabilities. Such behavior would be consistent with the observations that HF photoelimination lasers can be produced by either 1,1 or 1,2 removal of HF from FE.^{19,25}

The second factor which enhances the probability of unimolecular decomposition of the O + FE diradical adduct is the weakening of the C=C bond in the FE with increasing degree of fluorination. The C=C bond energy drops (presumably monotonically²⁶) 101 kcal/mol from 171 kcal/mol in C₂H₄ to 70 kcal/mol in C₂F₄. Both σ and π bond energies are lowered²⁷ so with increasing degree of fluorination of the reacting ethylene, the O-FE biradical adduct has more internal energy (a weaker π bond is broken) which enhances the rate constants of all unimolecular decomposition routes and also has a weaker C-C bond which makes the decomposition into a carbene and a carbonyl compound a more likely prospect. The reactions of oxygen with C₂H₄ and C₂H₃F do not proceed by C-C bond breakage of the diradical adduct, but the reactions with C₂HF₃ and C₂F₄ appear to proceed exclusively by this route. The energetics of the two extreme reactions offers an explanation of this behavior. The O + C₂H₄ reaction produces a diradical with 30 kcal/mol of internal energy and the decomposition by C-C bond cleavage is 22 kcal/mol endothermic from the unexcited adduct.²⁸ In the O + C₂F₄ reaction the diradical adduct has about 54 kcal/mol of internal energy and decom-

position by C-C bond cleavage is *exothermic* from the unexcited adduct. The inability to stabilize the O-C₂F₄ adduct even in condensed phase suggests there may also be no barrier to this exothermic decomposition. By contrast the O-C₂H₄ adduct is completely stabilized when the O + C₂H₄ reaction is run in liquid phase.²⁹

The reactions of O with the difluoroethylenes are ones in which all three possible fates of the adduct which lead to products occur: the two unimolecular decompositions and the H-atom migration to form a carbonyl compound (the fourth process shown in Figure 1, the formation of an epoxide, does not lead to products in the beam experiments. This route is included in the mechanism for completeness since adducts can be collisionally stabilized as the epoxide¹). In our study of the O + 1,2-difluoroethylene reaction, we actually observed products from all three processes. In the reaction involving 1,1-difluoroethylene, only products from two routes were detected, but spectroscopic evidence for the third occurring at least to some extent has been reported as mentioned before.¹⁴ These intermediate reactions in the O + FE series will be the most interesting for future quantitative study of the relative importance of the several reactive routes and for an analysis of the factors controlling the course of the O + FE reactions. It is not possible now to make a reasonable assessment of how the thermodynamics of the various reactive paths of these reactions might be related to their importance due to a lack of adequate thermodynamic data on some of the reactants and products and on the diradical intermediates.

Biradical Rearrangement. The O-FE biradical adduct in addition to decomposing may also rearrange either by ring formation to form an epoxide or by H-atom migration from the addition site to the adjacent carbon atom to form an aldehydic product. No evidence was found for F-atom migration in any of these reactions.³⁰ Both products of rearrangement have sufficient internal energy to break a bond. In the case of the epoxide we have suggested that the most likely process is the breaking of a C-O bond and thus a return to the biradical state. The most likely decomposition route for an aldehydic product with the internal energies they contain is by a cleavage to yield a substituted or unsubstituted methyl and formyl radical.²¹

Since F atoms do not migrate in these reactions, the identities of the methyl radicals formed give indications of the site of the initial O-atom addition. In the O + C₂H₃F reaction, addition must be virtually completely at the unfluorinated carbon since CH₂F is detected as a major product and CH₃ is a very minor one (the CH₃ product ion signal was 1/80 that from CH₂F). In the O + 1,1-difluoroethylene reaction at least a major portion of the O atom addition is at the unfluorinated carbon. In this reaction addition to the fluorinated carbon could not yield a substituted methyl radical product (since F atoms do not migrate), so we are unable to conclude that addition to this carbon is insignificant.

Other Routes. The three types of reactive routes which are shown in Figure 1 are the only kinds which were detected in our studies of the O + FE reactions. All these reactions, however, have sufficiently low rate constants that products of some minor routes (accounting for less than 10% of the overall reaction) could have passed undetected in our experiments. Other minor routes were detected in our studies of O + olefin reactions and the O + C₂H₃Cl reaction. These reactions have higher rate constants than the

O + FE reactions and hence increase the effective sensitivity for detection of their less important reactive routes.

Possible Chemical Lasers. The reactions of O with C₂H₃F, C₂H₂F₂, and possibly C₂HF₃ proceed at least to some extent by HF ejection from the diradical O-FE adduct. These reactions are very exothermic ($\Delta H \sim -105$ kcal/mol for the reaction O + C₂H₃F → C₂H₂O + HF) and hence possess the potential for producing HF with considerable internal energy. One of these, the O + C₂H₃F reaction, has recently been reported to have produced HF laser emission. The addition of O atoms to most halogen substituted unsaturated organic molecules probably proceeds to some extent by hydrogen halide elimination,³¹ and hence many more of these reactions will probably be used to produce chemical lasers in the future.

Acknowledgments. The authors gratefully acknowledge support for this research from the Donors of the Petroleum Research Fund, administered by the American Chemical Society, and from the National Science Foundation.

References and Notes

- (1) R. J. Cvetanović, "Advances in Photochemistry", Vol. I, W. A. Noyes, Jr., G. Hammond, and J. N. Pitts, Jr., Ed., Interscience, New York, N.Y., 1963, p 115.
- (2) M. E. Umstead, M. C. Lin, and F. J. Woods, Paper No. 123 presented at 169th American Chemical Society National Meeting, Philadelphia, Pa., April, 1975.
- (3) J. R. Kanofsky and D. Gutman, *Chem. Phys. Lett.*, **15**, 236 (1972); J. R. Kanofsky, D. Lucas, and D. Gutman, *Symp. (Int.) Combust., [Proc.]* **14**, 1972, 285 (1973).
- (4) J. R. Kanofsky, D. Lucas, F. Pruss, and D. Gutman, *J. Phys. Chem.*, **78**, 311 (1974).
- (5) F. J. Pruss, Jr., I. R. Slagle, and D. Gutman, *J. Phys. Chem.*, **78**, 663 (1974).
- (6) I. R. Slagle, D. Gutman, and J. R. Gilbert, *Chem. Phys. Lett.*, **26**, 111 (1974).
- (7) I. R. Slagle, D. Gutman, and J. R. Gilbert, *Symp. (Int.) Combust., [Proc.]* **15**, 1974, 785 (1975).
- (8) N. Cohen and J. Heicklen, *J. Phys. Chem.*, **70**, 3082 (1966).
- (9) I. R. Slagle, F. J. Pruss, Jr., and D. Gutman, *Int. J. Chem. Kinet.*, **6**, 111 (1974).
- (10) R. E. Huie, J. T. Herron, and D. D. Davis, *Int. J. Chem. Kinet.*, **4**, 521 (1972).
- (11) D. C. England and C. G. Krespan, *J. Org. Chem.*, **33**, 816 (1968).
- (12) D. S. Jones and S. J. Moss, *Int. J. Chem. Kinet.*, **6**, 443 (1974).
- (13) N. C. Craig and E. A. Entemann, *J. Am. Chem. Soc.*, **83**, 3047 (1961).
- (14) R. C. Mitchell and J. P. Simons, *J. Chem. Soc. E*, 1005 (1968).
- (15) W. J. R. Tyerman, *Trans. Faraday Soc.*, **65**, 163 (1969).
- (16) R. J. Cvetanović, *J. Chem. Phys.*, **30**, 19 (1959); *Can. J. Chem.*, **38**, 1678 (1960).
- (17) S. Sato and R. J. Cvetanović, *J. Am. Chem. Soc.*, **81**, 3223 (1959).
- (18) W. B. DeMore, *Chem. Phys. Lett.*, **16**, 608 (1972).
- (19) M. J. Berry and G. C. Pimentel, *J. Chem. Phys.*, **51**, 2274 (1969).
- (20) W. A. Guillory and G. H. Andrews, *J. Chem. Phys.*, **62**, 3208 (1975).
- (21) J. G. Calvert and J. N. Pitts, Jr., "Photochemistry", Wiley, New York, N.Y., 1966, Chapter 5.
- (22) M. Kawasaki, T. Ibuki, M. Iwasaki, and Y. Takezaki, *J. Chem. Phys.*, **59**, 2076 (1973).
- (23) S. W. Benson, *J. Chem. Phys.*, **40**, 105 (1964).
- (24) G. E. Millward, R. Hartig, and E. Tschuikow-Roux, *J. Phys. Chem.*, **75**, 3195 (1971); J. M. Simmie and E. Tschuikow-Roux, *ibid.*, **74**, 4075 (1970).
- (25) E. Cuellar, J. H. Parker, and G. C. Pimentel, *J. Chem. Phys.*, **61**, 422 (1974).
- (26) E. Tschuikow-Roux and K. R. Maltman, *Int. J. Chem. Kinet.*, **7**, 363 (1975).
- (27) The σ and π bond energies of C₂H₄ and C₂F₄ calculated using JANAF thermodynamic data and the definitions of these bond energies in S. W. Benson, "Thermochemical Kinetics", Wiley, New York, N.Y., 1968, p 50. In kcal/mol the σ bond energies are 108 for C₂H₄ and 34 for C₂F₄. The π bond energies are 62 for C₂H₄ and 35 for C₂F₄.
- (28) Thermochemistry of C₂H₄-O and C₂F₄-O adducts calculated as in ref 23.
- (29) C.-I. Hirokami and R. J. Cvetanović, *Can. J. Chem.*, **51**, 373 (1973).
- (30) In the O + HFCCHF reaction F migration would yield CHF₂, and H migration would yield CH₂F. Only CH₂F was detected as a product. In the O + H₂CCF₂ reaction F migration would produce CH₂F, and H migration would yield CHF₂. Only CHF₂ was detected as a product.
- (31) The elimination of HCl inverted between its $\nu = 1$ and $\nu = 2$ vibrational levels has been reported to occur in the reactions of O atoms with two chloroolefins (J. T. Gleaves and J. D. McDonald, *J. Chem. Phys.*, **62**, 1582 (1975)).

On Thermal Dehydrochlorination of Model Compounds for Poly(vinyl Chloride). III. Activation Entropy and Frequency Factor Calculations

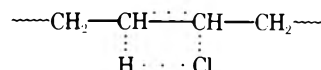
L. Valko* and P. Kovařík

Institute of Physical Chemistry of the Slovak Technical University, 880 37 Bratislava, Czechoslovakia (Received April 23, 1975)

A study has been made of the thermal stability of model compounds containing secondary and tertiary chlorine and also of unsaturated models which correspond to abnormal structures in poly(vinyl chloride). By considering in more detail the entropy changes taking place in the four-center hydrogen chloride elimination processes, we have applied and modified a simple, general entropy bond additivity method by which fairly reliable a priori estimates of the A factors for such reactions can be made. The activated entropies for elimination of hydrogen chloride were calculated on the principle of the additivity of bond entropies in the ground and in the fully developed cyclic-four-center transition state, respectively. On the basis of a few simple rules for assigning the corresponding bond entropies and entropy correction terms it is shown that quantitative estimates of A factors can be made to within the average experimental uncertainty of ± 0.3 unit $\log A/\text{sec}^{-1}$. The extreme range of A values extends over ± 0.5 in $\log A$ units. In a few isolated cases the discrepancy between estimated and observed A factors extends 0.9 $\log A$ unit and the weight of evidence suggests that the experimental values may not be reliable. In general, the entropic π bond effect is a stabilizing character since it markedly decreases the unimolecular dehydrochlorination frequency factor in comparison with other model compounds, and so partially compensates the destabilizing energy effect of the internal π bond on the activation energy.

Introduction

In the first paper¹ of this series we were concerned with the stability of some model compounds containing various defects in the structure order of poly(vinyl chloride) (PVC), and in the second paper² the semiempirical methods of the molecular orbital theory were used to study the mechanism of β -cis elimination of hydrogen chloride from ethyl chloride. We took into consideration the ideal structure, branched structures involving a tertiary chlorine and hydrogen, as well as structures containing a double bond at the end or inside the chain. The semiempirical evaluation of the activation energies has been carried out for the monomolecular elimination of hydrogen chloride and thus the stability of model compounds studied was evaluated. The overall conception of the stability of the model compounds for PVC may be obtained provided the individual structures are characterized not only by the energies of activation, but also the entropies of activation. The activation energies for elimination of hydrogen chloride were successfully calculated on the principle of the additivity of bond energies of the transition state.¹ The properties of homolytic and heterolytic full-frequency models of the transition states are widely discussed in this journal with the connection of the unimolecular dehydrohalogenation of chemically activated partially halogenated alkanes. It therefore seems interesting also to seek some method for the activation entropy calculations which provides a check on the internal consistency with the method used for the activation energy calculations.¹ Muljava and Ševčuk³ described a simple method based on the additivity of bond entropies for estimating Arrhenius A factors of many radical and monomolecular reactions. It is this reason why in the present paper the activation entropies for elimination of hydrogen chloride were calculated on the basis of the additivity of bond entropies of the fully developed cyclic four-center transition state



for various irregular structures present in the model compounds. However, in a more fully developed cyclic transition state, i.e., one having close to half-bond character between the reacting (H \cdots Cl) ends, the internal rotations of the reactants transform to out-of-plane ring vibrations involving all of the atoms of the ring. The ring vibrations in this case become not only difficult to visualize from the point of view of the group frequency method of O'Neal and Benson but also impossible to assign in any simple fashion. The tight cyclic transition state proposed here, then, is energetically reasonable, operationally convenient, and, as we intend to show, gratifyingly consistent with the data. Its use, if anything, should provide a lower limit to the Arrhenius A factor since a loose cyclic transition state would mean a looser structure and, therefore, a lower entropy loss. The ultimate purpose of this work is to compare the predictions of the group frequency method of O'Neal and Benson with the results of the entropy-bond additivity method used here.

Theoretical Part

Activation Entropy Calculations. The pyrolytic dehydrochlorination of some chloroethanes was shown to be homogeneous and unimolecular 20 years ago.⁴ Since that time a large body of experimental data had been built up on the unimolecular dehydrohalogenation of chlorine and bromine compounds.⁵ Several different models for the transition state for this class of the homogeneous unimolecular dehydrohalogenations have been proposed⁵⁻¹² and the Rice-Ramsperger-Kassel-Marcus (RRKM) theory has been used to test these models.^{13,14} The models range from a four-centered ring structure to one with only bond stretching prior to the transition state. Neither model can be elim-

inated solely on the basis of the values calculated for observable quantities in pyrolysis reactions,¹³ but the possibility exists that chemical activation together with kinetic isotope effects will allow a discrimination between these models. Trends in the reactivities of different haloalkanes have also been used to argue in favor of a highly polar transition state.^{11,12}

Let us consider a set of separated atoms which form a molecule or transition state. Such a set of nonbonded atoms always shows a higher entropy than a set of atoms bonded in a molecule. The entropy of a given molecule is to be regarded as the difference between the entropies of an equal number free and bonded atoms, thus

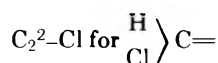
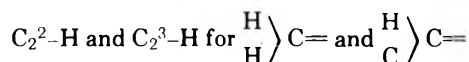
$$S^\circ = \sum_{\text{at}} S^\circ_{\text{at}} - \sum_{\text{bond}} S^\circ_{\text{bond}} - R \ln \sigma \quad (1)$$

where S° represents the entropy of the molecule under standard conditions at a given temperature, S°_{at} is the entropy of individual atoms under equal conditions at a given temperature, S°_{bond} is the entropy of the bond, and σ is the symmetry number. Modern usage has separated this factor into two portions, the symmetry number of the molecule as whole σ_w and the symmetry of a rotating portion σ_r . The total symmetry number σ_t , is the product of all of the symmetry numbers of the molecule

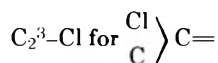
$$\sigma_t = \sigma_w \prod_i \sigma_{r_i}$$

We consider three groups of the investigated model compounds: (i) saturated nonbranched chloroalkanes, (ii) saturated branched chloroalkanes, and (iii) the unsaturated chloroalkanes with a double bond at the end of or inside the chain. We shall apply eq 1 to each of above-mentioned types of model compounds.

From several existing classifications of bonds we shall use the classification according to Bagdasarjan.¹⁵ In this classification all σ C-C bonds are regarded as equivalent in all unsubstituted hydrocarbons and the effect of the close proximity on the σ C-C bonds is taken into consideration in the case of heteroalkanes. The atoms of hydrogen and chlorine (X = H or Cl) bonded to primary, secondary, and tertiary carbon in saturated compounds will be denoted C_1 -X, C_2 -X, and C_3 -X, respectively. For unsaturated chlorinated alkanes we use following group notation



and



For saturated chloroalkanes including branched chloroalkanes eq 1 assumes the following form

$$S^\circ_{C_n H_m Cl_p} = nS^\circ_C + \sum_{i=1}^3 n_i S^\circ_{C_i-H} + \sum_{i=1}^3 n'_i S^\circ_{C_i-Cl} - (n-1)S^\circ_{C-C} - \sum_{i=1}^3 n_i S^\circ_{C_i-H} - \sum_{i=1}^3 n'_i S^\circ_{C_i-Cl} - R \ln \sigma \quad (2)$$

where n is the total number of carbon atoms; n_1, n_2, n_3 , and n'_1, n'_2, n'_3 denote the number of C-X (X = H or Cl) bonds on the primary, secondary, or tertiary carbon. For the sum of n_i and n'_i the following relations must hold

$$\alpha = \sum_{i=1}^3 n_i$$

$$\beta = \sum_{i=1}^3 n'_i$$

and

$$\sum_{i=1}^3 (n_i + n'_i) = 2(n+1) \quad (3)$$

By applying eq 1 to the chloroalkenes we obtain

$$S^\circ_{C_n H_m Cl_p} = nS^\circ_C + \sum_{i=1}^3 \sum_{j=2}^3 (n_i + m_j) S^\circ_{C_i-H} + \sum_{i=1}^3 \sum_{j=2}^3 (n_i + m_j) S^\circ_{C_i-Cl} - pS^\circ_{C=C} - (n-1-p)S^\circ_{C-C} - \sum_{i=1}^3 (n_i S^\circ_{C_i-H} + n'_i S^\circ_{C_i-Cl}) - \sum_{j=2}^3 (m_j S^\circ_{C_2^j-H} + m'_j S^\circ_{C_2^j-Cl}) - R \ln \sigma \quad (4)$$

where m_2, m_3 as m'_2 and m'_3 represent the numbers of the bonds of type C_2^2 -X and C_2^3 -X, where X = H or Cl. Thus

$$\mu = \sum_{i=1}^3 \sum_{j=2}^3 (n_i + m_j)$$

$$\nu = \sum_{i=1}^3 \sum_{j=2}^3 (n'_i + m'_j)$$

and

$$\sum_{i=1}^3 (n_i + n'_i) + \sum_{j=2}^3 (m_j + m'_j) = 2n \quad (5)$$

The principle of additivity rests on the assumption that, for additive bound unit, its "local" properties remain unchanged in a series of homologous compounds. That is, there is no significant interaction with more distant bonds. Linear molecules, such as normal paraffins and their substituted derivatives, are ideally suited to such an assumption; it is not surprising, therefore, that these fit additivity rules extremely well (Table II). However, as soon as we introduce structural features into a molecule to bring more distant units into proximity, we may expect departures from additivity laws. In order to accommodate unsaturated and cyclic model compounds of PVC in a certain spin state into an additivity entropy scheme, we must add "corrections" for these second-order interactions.

Considering the more complicated haloalkanes in a certain spin state in which rings and conjugated bonds occur a "correction" for such higher order interactions must be introduced into eq 1. In general the following equation is valid

$$S^\circ = \sum_k S^\circ_{\text{at},k} - \sum_l S^\circ_{\text{bond},l} - \sum_m \Delta S^\circ_{\text{ring},m} - \sum_n \Delta S^\circ_{\text{conj},n} + R \ln (ng_e/\sigma) \quad (6)$$

$\Delta S^\circ_{\text{ring}}$ and $\Delta S^\circ_{\text{conj}}$ being the corrections for rings and conjugated bond, respectively, while n is the total number of energetically equivalent 2^p optical isomers, where p is the number of structurally different asymmetric carbons in a molecule, g_e is the electronic degeneracy.

Equation 6 expressing the additivity of entropic contributions may be also applied to the four-center transition state. The cyclic activated molecule may be regarded as a molecule in which certain atoms are bonded by a definite

number of γ activated bonds forming δ activated rings conjugated by ϵ activated double bonds, while the rest of the molecule contains $l - \gamma$ normal bonds, $n - \delta$ nonactivated rings conjugated by $\nu - \epsilon$ ordinary double bonds. On the basis of this assumption equations similar to eq 2 and 4 may be put forward for the entropy of the transition state in the case of chloroalkanes and chloroalkenes. Nevertheless, we shall limit ourselves to the general form of the equation for the transition state entropy

$$S^\ddagger = \sum_k S^\circ_{\text{at},k} - \sum_{p=l-\gamma} S^\circ_{\text{bond},p} - \sum_{r=1}^{\gamma} S^\ddagger_{\text{bond},r} + \sum_{s=m-\delta}^m \Delta S^\circ_{\text{ring},s} + \sum_{t=1}^{\delta} \Delta S^\ddagger_{\text{ring},t} - \sum_{u=n-\epsilon}^n \Delta S^\circ_{\text{conj},u} - \sum_{\nu=1}^{\epsilon} \Delta S^\ddagger_{\text{conj},\nu} + R \ln (n^\ddagger g_e^\ddagger / \sigma^\ddagger) \quad (7)$$

Combining eq 6 and 7 gives the following relationship for the entropy of activation

$$\Delta S^\ddagger = S^\ddagger - S^\circ = \sum_{r=1}^{\gamma} S^\circ_{\text{bond},r} - \sum_{r=1}^{\gamma} S^\ddagger_{\text{bond},r} + \Delta \Delta S + R \ln (\sigma n^\ddagger g_e^\ddagger / \sigma^\ddagger n g_e) \quad (8)$$

where

$$\Delta \Delta S = \sum_{t=1}^{\delta} (\Delta S^\ddagger_{\text{ring},t} - \Delta S^\circ_{\text{ring},t}) - \sum_{\nu=1}^{\epsilon} (\Delta S^\ddagger_{\text{conj},\nu} - \Delta S^\circ_{\text{conj},\nu}) \quad (9)$$

The ratio $(\sigma n^\ddagger g_e^\ddagger / \sigma^\ddagger n g_e)$ is usually equivalent to the reaction path degeneracy,¹⁹ where n^\ddagger corresponds to the transition state and has the same meaning as n for molecules in the ground state. The electronic degeneracy g_e for all the model compounds studied in the ground state as well as in the transition states are equal, i.e., $g_e = g_e^\ddagger$, hence the term $R \ln (g_e^\ddagger / g_e)$ vanishes.

The frequency factor of a unimolecular reaction can be written, in terms of transition state theory, in the form

$$A = \mathcal{H} \frac{ekT}{h} \exp \left(\frac{\Delta S^\ddagger}{R} \right) \quad (10)$$

where the transmission coefficient \mathcal{H} is assumed to be unity.

Results

Entropy of Bonds in Ground and Transition State. For the calculation of the entropies of reactants and transition states, respectively, it is necessary to know all terms in eq 6 and 7. The entropies of the atoms constituting the reactants were taken from Gurvich and Chackuruzov,¹⁶ the entropies of bonds and the second-order corrections appertaining to our model compounds for PVC in the ground as well as transition states were calculated as follows.

The entropies of the bonds $S^\circ_{\text{C-C}}$, $S^\circ_{\text{C}_1\text{-H}}$, $S^\circ_{\text{C}_2\text{-H}}$, and $S^\circ_{\text{C}_3\text{-H}}$ were calculated by means of eq 1 applied to normal alkanes. The calculation was performed by using 15 branched and 15 nonbranched alkanes while the experimental values of $S^\circ_{\text{C}_n\text{H}_{2n+2}}$ were taken from Vvedenskij.¹⁷

The reliability of the calculated bond entropies was carried out by calculating the entropies for the series of hydrocarbons and comparing them with the experimental values. The calculated entropies are within an average of ± 0.49 gibbs mol⁻¹; the maximum deviation is 1.24 gibbs mol⁻¹. This corresponds to an average deviation of 2.72% and a

maximum deviation of 4.24% in the absolute values of the activation entropies.

The entropies of bonds $S^\circ_{\text{C}_2^2\text{-H}}$, $S^\circ_{\text{C}_2^3\text{-H}}$, and $S^\circ_{\text{C}=\text{C}}$ were calculated in the same manner. Equation 1 was applied to the alkenes and the experimental values of $S^\circ_{\text{C}_n\text{H}_{2n}}$ were taken again from ref 17. The calculation of the entropies of diene hydrocarbons also necessitated an estimate of the correction for the conjugation effect $\Delta S^\circ_{\text{conj}}$ which was found by using the experimental data pertaining to diene hydrocarbons. The agreement with experimental data was checked again by the calculations for the whole series of alkenes. The calculated entropies are within an average of ± 0.46 gibbs mol⁻¹; the maximum of deviation is 1.53 gibbs mol⁻¹. This corresponds to an average deviation of 2.70% and a maximum deviation of 4.62% in the absolute values of the activation entropies.

The entropies of bonds $S^\circ_{\text{C}_1\text{-Cl}}$, $S^\circ_{\text{C}_2\text{-Cl}}$, and $S^\circ_{\text{C}_3\text{-Cl}}$ were calculated using eq 2. The experimental data for chlorinated hydrocarbons $S^\circ_{\text{C}_n\text{H}_n\text{Cl}_\beta}$ were taken from literature sources¹⁸ or because of scanty experimental data the values of some $S^\circ_{\text{C}_n\text{H}_n\text{Cl}_\nu}$ were calculated using the thermochemical kinetic estimation techniques developed by Benson and coworkers.¹⁹⁻²¹ The activation entropies were determined from the experimental frequency factors by means of eq 10 and then the entropies of activated bonds were calculated from eq 8 (see Table I). Since the experiments showed a great fluctuation, as much as 10² sec⁻¹ in the A factors we chose as a criterion of correctness of the frequency factor that measurement for which the experimental activation energy was in agreement with the theoretical activation energy calculated by the method described in our first paper.¹

For the calculation of the entropy of the activated C...H bond we started from the dehydrogenation reactions of alkanes and cycloalkanes and furthermore we used the experimental frequency factors for the model compounds for PVC. A more detailed analysis of the frequency factors of the chloroalkenes reveals the intramolecular interaction of a four-center transition state with the π electrons of the double bond at the β position to the transition state. This effect is rather significant if the double bond occurs inside the hydrocarbon chain. Therefore, we evaluated $\Delta S^\ddagger_{\text{conj}}$ separately for the double bond at the end of the chain. This behavior may be understood, using the arguments given by Thomas,²² that the lower frequency factors obtained for the dehydrochlorination of the chloroalkenes can be ascribed to the effect of the partially formed double bond and that already present in the molecule.^{1,23}

The entropies of all the calculated nonactivated and activated bonds and correction contributions are reported in Table I.

Calculated Frequency Factors

Now we are going to present the results involving the calculations of activation entropies and frequency factors of the model compounds for PVC as well as the comparison of these values with experimental data. The calculation of the entropies of activation and then calculation of frequency factors are governed by eq 6-9.

Comparison of the observed and predicted activation entropies demands the adjustment of the calculated and observed values from the experimental temperature to some common temperature which we have chosen as 298 K. These adjustments are contingent on estimating the heat capacity of the transition states. The corrections are never larger than 0.06 eu, and the error in them was estimated to

TABLE I: Bond Entropies, Activation Bond Entropies, and Corrections

Bond	Bond entropy, gibbs mol ⁻¹	Activated bond and corrections	Activated bond entropy and correction contributions, gibbs mol ⁻¹
S ^o _{C-C}	35.83	S [‡] _{C⁺...C⁺} ^a	35.20
S ^o _{C₁-H}	24.03	S [‡] _{C₁...H}	31.83
S ^o _{C₂-H}	23.55	S [‡] _{C₂...H}	28.32
S ^o _{C₃-H}	22.11	S [‡] _{C₃...H}	27.23
S ^o _{C=C}	27.04	S [‡] _{C₁...C₁}	31.50
S ^o _{C₂²-H}	25.71	S [‡] _{C₂...C₁}	30.46
S ^o _{C₂³-H}	25.66	S [‡] _{C₃...C₁}	29.06
ΔS ^o _{conj}	3.00	S [‡] _{H...C₁}	24.00
S ^o _{C₁-C₁}	28.76	ΔS [‡] _{4,ring} ^a	32.50
S ^o _{C₂-C₁}	28.16	ΔS [‡] _{conj} ^b	1.06
S ^o _{C₃-C₁}	27.95	ΔS [‡] _{conj} ^c	11.81

^a The values are taken from ref 3. ^b The correction for the conjugation with a double bond at the end of the chain. ^c The correction for the conjugation with a double bond inside the chain.

be less than the expected inaccuracies from other sources. Since some model compounds for PVC are able to split off a hydrogen atom from a primary or secondary carbon atom we shall use the notation α for the splitting from secondary carbon and the notation β for the splitting from primary carbon. The results of calculations as well as the comparison of the calculated frequency factors with experimental findings are reported in Tables II-IV.

Mean Values

In the experimental work of the rate of a thermally activated process within the experimental accuracy, the rate of a given process can be described according to the theory of absolute reaction rates as formulated by Eyring,³⁹ and the rate constant k_i is given by the equation

$$k_i(T) = \mathcal{H}(kT/h) \exp(\Delta S_i^\ddagger/R) \exp(-E_i/RT) = A_i \exp(-E_i/RT) \quad \mathcal{H} = 1; i = 1, 2 \quad (11)$$

where (kT/h) is a universal frequency dependent only on temperature and independent of the nature of the reactants and the type of reaction.

If, in fact, the process occurs by the simultaneous operation of a number of mechanisms each of which has the same activation energy then eq 11 is correct. However, the same treatment could not be extended to cases where there are competing mechanisms of different activation energies. The term mechanism is used here, in a very general sense, to mean any reaction path by which the process can occur. It is our purpose now to consider what physical interpretation can be given to the measured frequency factor A_{exptl} and activation energy E_{exptl} values in such cases when the thermal dehydrochlorination mechanism of the model compounds for PVC consists of a set of mechanisms not all of the same activation energy.

As shown previously, there are two possible mechanisms for the elimination of hydrogen chloride from some model compounds.

In this connection we shall use a discrete distribution function of activation energies, limiting ourselves to two distinct activation energies, E_1 and E_2 , e.g., a two-dimensional problem. Knowing the distribution function of acti-

vation energies, one can define the mean value of measured activation energy. We shall designate this quantity by the notation $\langle E \rangle$ and it is evident that

$$\langle E \rangle = \sum_k p_k E_k \quad k = 1, 2 \quad (12)$$

where p_k is the occurrence of distinct activation energies E_k , i.e.

$$p_i = \frac{k_i}{\sum_i k_i} \quad (13)$$

where k_i is its rate constant and $\sum_i p_i = 1$.

Having checked the consistency of our definition of p_i 's, we may use them to calculate the mean activation energy. For $\langle E \rangle$ we obtain the expression

$$\langle E \rangle = E_1 + RT \frac{r}{r+1} \quad (14)$$

where

$$\epsilon = (E_2 - E_1)/RT$$

and

$$r = (A_2/A_1) \exp(-\epsilon) \quad (15)$$

Since a discrete spectrum of the occurrence of activation energies is available, using the definitions of the Dirac δ "function", the average value of the frequency factor $\langle A \rangle$ is

$$\langle A \rangle = \sum_{i=1}^2 \int_0^\infty A_i \exp[(\langle E \rangle - E)/RT] \times \delta(E - E_i) dE = A_1(1+r) \exp\left(\frac{\epsilon r}{1+r}\right) \quad (16)$$

The competing mechanism of the splitting-off of hydrogen chloride is possible in the case of some model compounds introduced in Table V. For the calculation of the mean values of activation energies we employed the data previously published.¹ The mean values of activation energies and frequency factors as well as their comparison with experimental data are presented in Table V.

Discussion

The agreement between the calculated and observed frequency factors for the first-order dehydrochlorination of ideal structures for PVC and also for model compounds having tertiary chlorine (Tables II and III) is remarkable, the differences in most cases being correct within a factor of $10^{\pm 0.5} \text{ sec}^{-1}$ (i.e., $\Delta \log(A/\text{sec}^{-1}) = \pm 0.5$). These are very acceptable error limits considering their relative ease of acquisition and the experimental and interpretational difficulties to be overcome in their determination by conventional means. Thus, since the calculational procedure requires the estimation of some physical parameters of the activated complex, it must be realized that it is no substitute for highly reliable rate data. Consequently, however, the calculations render obsolete all but the most precise experimental rate determinations. From the results summarized in Tables II and III, it follows that the frequency factors for elimination of hydrogen chloride for saturated model compounds having tertiary chlorine are in principle the same as for saturated ideal structures. The frequency factors for unsaturated compounds, evaluated similarly by our procedure, are given in Table IV, from which it follows

TABLE II: Evaluation of Entropies of Activation ΔS^\ddagger at 298 K (Frequency Factors) of Nonbranched Chloroalkanes and Comparison with Experimental Results

Model compound	σ	S°	S^\ddagger , gibbs mol ⁻¹	ΔS^\ddagger	$\log A_{\text{calcd}}/\text{sec}^{-1}$	$\log A_{\text{exptl}}/\text{sec}^{-1}$	Ref
2-Chloropropane		72.60	75.19	2.59	13.78	13.40	4
						13.64	24
						11.10	25
2-Chlorobutane	α^a	82.21	85.65	3.44	13.98	13.62	26
						14.00	27
						14.07	28
	β^a	82.21	84.80	2.59	13.78	13.62	26
						14.00	27
						14.07	28
3-Chloropentane		91.82	95.26	3.44	13.98	12.29	29
4-Chlorododecane		159.09	162.53	3.44	13.98	11.95	29
2,4-Dichloropentane	α_{cis}^a	99.30	103.64	4.34	14.17	13.38 ± 0.29	30
	α_{trans}^a	18	97.91	103.64	5.13	14.35	30
	β_{cis}^a	9	99.30	100.61	1.31	13.51	30
	β_{trans}^a	18	97.91	100.61	2.70	13.82	30
5,7-Dichlorododecane		166.55	170.91	4.36	14.19	14.25	29
2,4,6-Trichloroheptane	α^a	125.97	131.25	5.28	14.38	14.17 ± 0.27	30
	β^a	9	125.97	130.39	4.42	14.19	30

^a Estimated A factors for the two possible elimination mechanisms.

TABLE III: Evaluation of Entropies of Activation ΔS^\ddagger at 298 K (Frequency Factors) of Branched Chloroalkanes and Comparison with Experimental Results

Model compound	σ	S°	S^\ddagger , gibbs mol ⁻¹	ΔS^\ddagger	$\log A_{\text{calcd}}/\text{sec}^{-1}$	$\log A_{\text{exptl}}/\text{sec}^{-1}$	Ref
2-Methyl-2-chloropropane		76.64	81.22	4.58	14.22	14.20	31
						12.40	32
						13.77	33
						13.70	34
						13.74	24
						13.90	35
						14.41	36
						12.85	25
2-Methyl-2-chlorobutane	α^a	27	88.43	91.68	3.25	13.93	31
						13.82	33
	β^a	27	88.43	90.83	2.40	13.75	31
						14.82	33
2,3-Dimethyl-2-chlorobutane	α^a	81	95.89	93.57	-2.30	12.72	37
	β^a	81	95.89	98.29	2.40	13.75	37
3-Ethyl-3-chloropentane		81	105.47	110.90	5.43	14.41	25
3-Methyl-3-chloropentane	α^a	27	117.26	120.51	3.25	13.93	29
	β^a	27	117.26	119.65	2.39	13.75	29

^a Estimated A factors for the two possible elimination mechanisms.

that the preexponential factors decrease markedly in comparison with saturated model compounds.

However, the transition state for the chloroalkenes with the internal π bond can be stabilized through the partly formed double bond and that already present in the molecule,^{1,23} whereas such interaction involves stiffening of large internal rotation about the C-C bond yielding a net $\Delta S^\ddagger < 0$ corresponding to the "tighter" transition state complex. However, the hydrogen chloride elimination reaction in the case of 2,3-dimethyl-2-chlorobutane is characterized also with a small negative entropy of activation (Table III). Indeed, the entropic internal π bond effect is a

stabilizing character since it decreases the unimolecular dehydrochlorination rate constant in comparison with other model compounds, and so partially compensates the destabilizing energetic effect of the internal π bond on the activation energy.^{1,23}

It is proposed that the serious discrepancy between experimentally observed Arrhenius parameters for the elimination kinetic in the case of 3-chloro-1-pentene and 4-chloro-2-hexene and those presented in this paper and the activation energies in paper I of this series, predicted by the transition state calculations assuming a monomolecular four-center mechanism for the dehydrochlorination reac-

TABLE IV: Evaluation of Entropies of Activation ΔS^\ddagger at 298 K (Frequency Factors) of Chloroalkenes and Comparison with Experimental Results

Model compound	σ	S°	S^\ddagger , gibbs mol ⁻¹	ΔS^\ddagger	log $A_{\text{calcld}}/\text{sec}^{-1}$	log $A_{\text{expt}}/\text{sec}^{-1}$	Ref
3-Chloro-1-butene	3	80.55	82.02	1.47	13.55	13.35	22
3-Chloro-2-methyl-1-butene	9	88.61	90.14	1.53	13.56	13.28	22
3-Chloro-3-methyl-1-butene	9	86.66	88.06	1.40	13.53	13.30	39
3-Chloro-1-pentene	3	90.11	92.49	2.38	13.75	9.20	25
						14.60 ± 0.19	
4-Chloro-2-pentene	9	88.13	79.47	-9.26	11.21	12.03 ± 0.19	30
4-Chloro-2-hexene	9	98.33	89.97	-8.36	11.40	9.50	25
						10.75	29
6-Chloro-2,4-heptadiene	9	101.85	95.63	-6.22	11.87	11.43 ± 0.41	30

TABLE V: Mean Values of Activation Energies and Frequency Factors and Comparison with Experimental Results

Model compound	E_1 , kcal mol ⁻¹	E_2 , kcal mol ⁻¹	A_1 , sec ⁻¹	A_2 , sec ⁻¹	$\langle E \rangle$, kcal mol ⁻¹	log $\langle A \rangle/\text{sec}^{-1}$	log $A_{\text{expt}}/\text{sec}^{-1}$	Ref
2-Chlorobutane	49.70	49.40	6.07×10^{13}	9.52×10^{13}	49.50	14.18	13.62	26
							14.00	27
							14.07	28
<i>trans</i> -2,4-Dichloropentane	49.40	49.00	6.58×10^{13}	2.23×10^{14}	49.05	14.45	13.38 ± 0.29	30
2,4,6-Trichloroheptane	49.10	48.70	1.55×10^{14}	2.39×10^{14}	49.90	14.57	14.17 ± 0.27	30
2-Methyl-2-chlorobutane	44.10	44.30	5.66×10^{13}	8.62×10^{13}	44.20	14.15	14.65	31
							13.82	33
2,3-Dimethyl-2-chlorobutane	43.30	42.80	5.66×10^{13}	5.23×10^{12}	43.10	13.77	13.54	37
3-Methyl-3-chloropentane	42.70	42.50	5.60×10^{13}	8.62×10^{13}	42.60	14.14	12.38	29

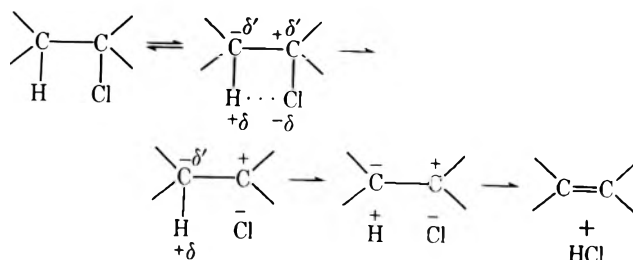
tions, can be explained in terms of the unusually large systematic errors in the rate constants given in the original experimental study.²⁵

In using the bond entropy additivity method, it is necessary to fix the values of correction parameters, which appear in the entropy expressions for the reactant eq 6 and the transition state eq 7. The correction factors include the effects of electron path degeneracy, quite naturally, the effects of conjugative stabilization. We followed the procedure of searching for the values of correction parameters which give agreement between the calculated and observed activation entropies.

From the results it follows that the activation entropies for the elimination of hydrogen chloride for the unsaturated model compounds with the double bond inside the chain are the lowest with respect to other model compounds of PVC. We suggest that to treat the frequency factors in terms of transition state theory, it is necessary to assume that the transmission coefficient for the unsaturated model compounds with the double bond inside the chain is much less than unity. Laidler⁴⁰ points out two classes of reactions for which the transmission coefficient may be considerably less than unity. The first comprises the bimolecular recombination of atoms in the gas phase. The second is for the electronically or vibrationally nonadiabatic reactions, which probably operates also in the process of the monomolecular elimination of hydrogen chloride. The small A factor can be identified in each case with a low probability of the transition state reaching the final state, rather than a low probability that the transition state is formed. It is probable that in the unimolecular dehydrochlorinations of chemically activated alkanes, quantum

mechanical tunneling should become important in the four centered complex.

From the point of view of electronic reorganization which is occurring within the system, the heterolytic transition state can be depicted as



The conclusion that we may draw from our calculations is that the activation entropies calculated in this work for dehydrochlorination reactions are, within experimental uncertainty, the same as those found from the application of the group frequency method of Benson and O'Neal.¹⁹

The internal consistency of the monomolecular dehydrochlorination mechanism is thus guaranteed, and the good fits between the experimental and the calculated activation entropies demonstrate that the monomolecular theory is consistent with the experimental results.

Acknowledgment. The authors are grateful to Eva Poláková for her kind assistance.

References and Notes

- (1) L. Valko and I. Tvaroska, *Europ. Polym. J.*, **7**, 41 (1971).

- (2) I. Tvaroska, V. Klimo, and L. Valko, *Tetrahedron*, **30**, 3275 (1974).
 (3) M. P. Muljava and V. J. Ševčuk, *TECH*, **5**, 498 (1969).
 (4) D. R. H. Barton and K. E. Howlet, *J. Chem. Soc.*, 165 (1949).
 (5) A. Maccoll, *Chem. Rev.*, **69**, 33 (1969).
 (6) H. E. O'Neal and S. W. Benson, *J. Phys. Chem.*, **71**, 2903 (1967).
 (7) H. W. Chang and D. W. Setser, *J. Am. Chem. Soc.*, **91**, 7648 (1969).
 (8) G. O. Pritchard and J. M. Perona, *J. Phys. Chem.*, **73**, 2944 (1969).
 (9) J. A. Kerr and D. M. Timlin, *Trans. Faraday Soc.*, **67**, 1376 (1971).
 (10) C. K. Ingolo, *Proc. Chem. Soc., London* 279 (1957).
 (11) S. W. Benson and A. N. Bose, *J. Chem. Phys.*, **39**, 3463 (1963).
 (12) A. Maccoll and P. J. Thomas, *Prog. React. Kinet.*, **4**, 119 (1967).
 (13) N. Noble, H. Carmichael, and C. L. Bumgardner, *J. Phys. Chem.*, **76**, 1680 (1972).
 (14) P. N. Clough, J. C. Pclanyi, and R. T. Taguchi, *Can. J. Chem.*, **48**, 2919 (1970).
 (15) Ch. S. Bagdasarjan, *ŽFCH*, **24**, 1326 (1950).
 (16) L. V. Gurvich and G. A. Chackuruzov, "Termodynamiceskie svojstva individualnykh molekul", Izdat. AN SSSR, 1962.
 (17) A. A. Vvedenskij, "Thermodynamic Calculations of Petrochemical Processes", SNTL, Praha, 1963.
 (18) J. A. Treger, I. F. Pimenov, and E. A. Golfand, "Spravocnik po fizikochemiceskim svojstvam chloralifateskich soeninenij C₁-C₅", Chimia, Leningrad, 1973.
 (19) S. W. Benson, "Thermochemical Kinetics", Wiley, New York, N.Y., 1968.
 (20) S. W. Benson, F. R. Cruickshank, D. M. Golden, G. R. Haugen, H. E. O'Neal, A. S. Rodgero, R. W. Shaw, and R. Walsh, *Chem. Rev.*, **69**, 278 (1969).
 (21) H. E. O'Neal and S. W. Benson, *J. Chem. Eng. Data*, **15**, 266 (1970).
 (22) P. J. Thomas, *J. Chem. Soc. B*, 1238 (1967).
 (23) L. Valko and I. Tvaroska, *Angew. Makromol. Chem.*, **23**, 173 (1972).
 (24) W. Tsang, *J. Chem. Phys.*, **40**, 1171 (1964).
 (25) M. Asahina and M. Ozonuka, *J. Polym. Sci., Part A2*, 3503, 3515 (1964).
 (26) A. Maccoll and R. H. Stone, *J. Chem. Soc.*, 2756 (1961).
 (27) H. Heydtmann and G. Rinck, *Z. Phys. Chem. (Frankfurt am Main)*, **30**, 250 (1961).
 (28) H. Heydtmann and G. Rinck, *Z. Phys. Chem. (Frankfurt am Main)*, **36**, 75 (1963).
 (29) F. Erbe, T. Grewer, and K. Wehage, *Angew. Chem.*, **74**, 985 (1962).
 (30) V. Chytrý, B. Obereigner, and D. Lim, International Conference on Chemical Transformation of Polymers, Bratislava, 1968.
 (31) F. Daniels and P. L. Veltman, *J. Chem. Phys.*, **7**, 756 (1939).
 (32) D. R. H. Barton and F. P. Onyon, *Trans. Faraday Soc.*, **45**, 752 (1949).
 (33) S. C. Wong, Ph.D. Thesis, University of London, 1958.
 (34) R. L. Failes and V. R. Stimson, *Aust. J. Chem.*, **15**, 437 (1962).
 (35) W. Tsang, *J. Chem. Phys.*, **40**, 1948 (1964).
 (36) B. Roberts, Ph.D. Thesis, University of London, 1968.
 (37) G. D. Harden and A. Maccoll, *J. Chem. Soc.*, 5028 (1957).
 (38) C. J. Harding, Ph.D. Thesis, University of London, 1968.
 (39) S. Glasstone, K. J. Laidler, and H. Eyring, "The Theory of Rate Processes", McGraw-Hill, New York, N.Y., 1941.
 (40) K. J. Laidler, "Chemical Kinetics", McGraw-Hill, New York, N.Y., 1965, p. 80.

Interaction of Alkali Metal Cations with *cis*- and *trans*-1-Benzyl-2,3-dibenzoylaziridine in Acetonitrile

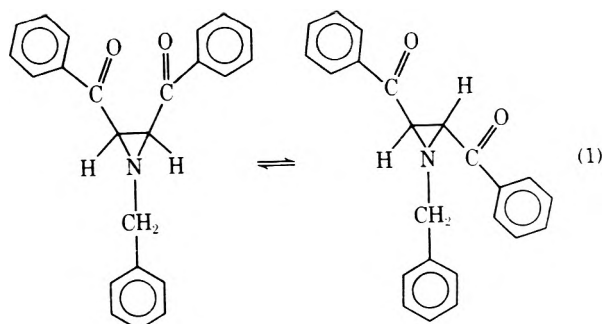
Alan B. Norman, Gregory R. Smith, and Harry P. Hopkins, Jr.*

Department of Chemistry, Georgia State University, Atlanta, Georgia 30303 (Received June 4, 1975)

The interaction of alkali metal ions with *cis*- and *trans*-1-benzyl-2,3-dibenzoylaziridine in acetonitrile has been studied by means of NMR and infrared spectroscopy. For all cations studied, association with the *cis* isomer is preferred. In the presence of alkali metal ions the chemical shift of the ring hydrogens of *cis*-aziridine moves down field, whereas the corresponding chemical shift of the *trans* isomer is virtually unaffected. From this observation, it is concluded that the association is occurring at the carbonyl oxygens via chelation. This conclusion is further substantiated by the observation that the frequency of the carbonyl stretching mode for the *cis* isomer is shifted to lower wavenumbers upon the addition of LiBr and NaI. For the *cis* isomer-LiBr solutions an isobestic point is evident, whereas in the NaI solutions an isobestic point is absent. At a ratio of LiBr to *cis* isomer above 0.4 at 25°C a white crystalline solid precipitated which was found to be the 2:1 *cis* isomer adduct of LiBr. Analysis of the NMR data by means of a best fit procedure provided approximate values for the equilibrium constants for the association processes. From these values the order of association is found to be $\text{Li}^+ > \text{Na}^+ > \text{K}^+$.

Introduction

The base-catalyzed *cis*-*trans* equilibrium (eq 1) for 1-benzyl-2,3-dibenzoylaziridine (AZ) has been reported by Lutz and Turner¹ to be influenced by the polarity of the medium and by the presence of lithium or sodium chloride. The equilibrium constant, $K = [\text{cis}]/[\text{trans}]$, increases as the polarity of the solvent increases but a corresponding increase in K was observed when LiCl or NaCl were present in alcoholic solvents. Since K increases with the polarity of the solvent without salts present, Lutz and Turner postulated that the observed salt induced increase in K was also a medium effect related to the presence of the ions. How-



ever, over the last several years, numerous workers²⁻¹⁰ have shown that both the lithium and sodium cation in a variety of environments can strongly interact with organic molecules containing basic moieties to form specific ion-molecule complexes. These results would suggest that the observations of Lutz and Turner are due to a specific cation-ligand interaction. Therefore, in order to determine if the variation of the *cis*-*trans* equilibria with cations is indeed due to a specific cation interaction with the dibenzoylaziridines, spectroscopic studies were performed on acetonitrile solutions containing varying amounts of *cis* and *trans* AZ and alkali metal salts. The results of these studies are reported here and interpreted to provide a unique explanation for the observations of Lutz and Turner.

Experimental Section

A Varian A-60A NMR spectrometer was employed to record all spectra at $40 \pm 1^\circ\text{C}$. Chemical shifts were measured relative to tetramethylsilane (Me_4Si) with a Hewlett-Packard oscillator (Model 2000D) and frequency counter (Model 5512A).

Infrared spectra were run on a Beckman IR-12 infrared spectrophotometer with variable path length KBr cells at ambient temperature.

Fisher technical grade acetonitrile was purified by refluxing over calcium hydride for 10-12 hr followed by distillation onto freshly activated (600°C) molecular sieves. The water content in the acetonitrile prepared in this manner was determined by a gas chromatographic procedure¹¹ to be less than 0.2 ppm. All solutions used in the NMR and infrared studies were prepared in a nitrogen flushed dry-box.

The *cis*- and *trans*-1-benzyl-2,3-dibenzoylaziridines were prepared as described by Turner¹² and were found to have melting points and spectral characteristics identical with literature values.

Lithium bromide and sodium iodide (Fisher) were fused at 500°C for 1 hr and stored in a vacuum desiccator. Sodium tetraphenylborate (Fisher ACS grade) was dried in a vacuum desiccator and used without further purification. Potassium hexafluorophosphate (Alpha Products) was recrystallized from 95% ethanol and dried in a vacuum desiccator.

Results and Discussion

For both *cis*- and *trans*-AZ in acetonitrile two singlets appear between 215 and 250 Hz which were tentatively assigned to the aziridine ring and methylene hydrogens based on chloroform¹² NMR studies. When either *cis*- or *trans*-AZ was equilibrated in CH_3OD with sodium methoxide, the low-frequency peak disappeared, producing an unequivocal assignment for the chemical shift of the ring hydrogens. Consequently, the remaining signals can be assigned to the methylene hydrogens. The assignments for the ring and methylene hydrogens for *cis*- and *trans*-AZ are given in Table I and compared with the literature values in CDCl_3 .

Both the ring and methylene chemical shifts were monitored in acetonitrile solutions at a constant AZ concentration as the alkali metal salt was increased. The chemical shifts found in these experiments for the ring hydrogens are tabulated in Table II and plotted vs. the mole ratio of salt to AZ in Figure 1. The chemical shift of the methylene hydrogens for both the *cis* and *trans* isomers did not vary outside of experimental error in the concentration range of alkali metal salts used in these experiments. The same rela-

TABLE I: Chemical Shift^a Assignments for Ring and Methylene Hydrogens of 1-Benzyl-2,3-dibenzoylaziridine

Isomer	Ring, Hz		Methylene, Hz	
	CH_3CN	CDCl_3	CH_3CN	CDCl_3
<i>Cis</i>	197.7	202.5	213.6	238.0
<i>Trans</i>	218.4	238.4	226.6	244.6

^a Relative to Me_4Si in CDCl_3 as external standard.

TABLE II: Chemical Shift^a of the Ring Hydrogens as a Function of the Alkali Metal Ion Concentrations in Acetonitrile

	LiBr		NaB(Ph)_4 ^b		KPF_6 ^b		
	<i>cis</i> -AZ	<i>trans</i> -AZ	<i>cis</i> -AZ	<i>cis</i> -AZ	<i>cis</i> -AZ	<i>cis</i> -AZ	
<i>R</i> ^c	δ , Hz	<i>R</i> ^c	δ , Hz	<i>R</i> ^c	δ , Hz	<i>R</i> ^c	δ , Hz
0.07	222.0	0.2	238.6	0.2	222.6	0.1	218.6
0.14	226.0	0.3	238.7	0.4	225.6	0.4	220.2
0.20	229.0	0.5	239.2	0.6	229.2	0.5	220.4
0.34	233.2	0.8	239.3	0.8	230.5	1.2	222.8
0.40	235.0	1.0	239.9	1.0	233.2	2.0	225.0
0.47	236.2	1.3	240.3	1.2	234.4	2.5	226.8
0.60	237.2	1.7	240.9	1.6	236.4	3.8	229.0
0.80	242.6	2.0	241.1	2.0	239.2		
1.00	244.2			4.0	243.8		
1.20	247.2			6.0	247.2		
1.45	251.0			8.0	249.2		
1.60	251.9						
1.80	253.8						
2.00	255.5						

$C_{\text{AZ}} = 0.0136 \text{ M}$ $C_{\text{AZ}} = 0.03 \text{ M}$ $C_{\text{AZ}} = 0.0125 \text{ M}$ $C_{\text{AZ}} = 0.019 \text{ M}$

^a Relative to Me_4Si internal standard. ^b The *trans* isomer did not show any measurable change in chemical shift over the same mole ratio range. ^c $R = (\text{salt})/(\text{AZ})$.

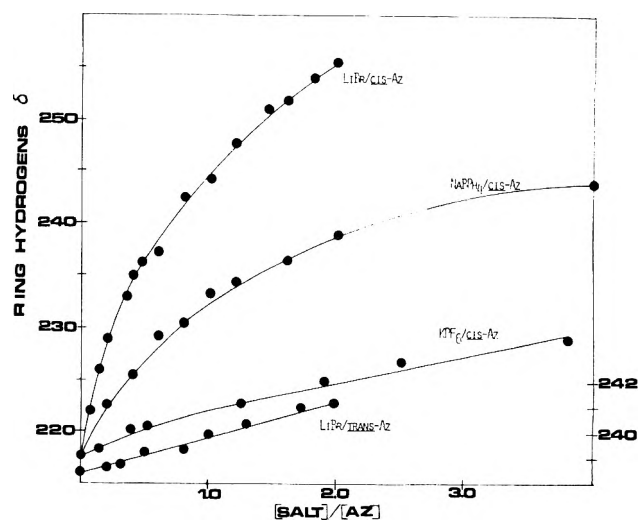


Figure 1. A plot of the chemical shift of the ring hydrogens of *cis*-AZ as a function of the mole ratio $[\text{salt}]/[\text{cis-AZ}]$. The right-hand scale is for the variation of the *trans*-AZ ring hydrogen chemical shift as a function of the mole ratio $[\text{LiBr}]/[\text{trans-AZ}]$. The concentrations and chemical shift data are given in Table II.

tive changes in chemical shifts were found for either an external or internal Me_4Si standard, indicating that Me_4Si does not influence the observed chemical shifts. The uncertainty of the δ values based on several independent measurements on identical solutions is estimated to be ± 0.5 Hz. This rather large uncertainty for the chemical shifts in

the acetonitrile solutions where the salts were present could be due to small but variable concentrations of water. The effect of added water on the chemical shift of the ring hydrogens of cis-AZ with LiBr present was investigated by adding small amounts of water to a sample which was 0.013 *M* cis-AZ and 0.026 *M* LiBr. The addition of water caused the chemical shift of the ring hydrogens to move upfield toward its original value. At an added water concentration of 10^{-3} *M*, the signal due to the ring hydrogen was 4 Hz downfield from the value with no LiBr present.

Since the variation of the ring hydrogens' chemical shift is considerably greater for the cis isomer than for the trans isomer when LiBr is added, this seems to suggest that the cis isomer interacts with the lithium cation to a substantially greater degree than the trans isomer (Figure 1). A similar conclusion can be reached for the interaction of the sodium cation with the two isomers since the chemical shift of the ring hydrogens moves downfield with addition of sodium ions (Figure 1), but the chemical shift of the ring hydrogens does not change appreciably for the trans isomer when sodium ions are added to the solution. The results for the potassium ion are similar to those found for the sodium ion except the magnitude of the observed changes in chemical shift are greatly reduced. While these results were obtained in acetonitrile and not in the alcoholic solutions where the equilibrations were performed, it is expected that the relative preference of the cis isomer for the alkali metal ions would be maintained in the alcohol solutions. Consequently the observations of Lutz et al. can be attributed to the preferential complexation of the cis isomer by alkali metal ions.

The actual site of complexation is suggested by the observation in the NMR experiments that the methylene hydrogens' chemical shift does not change upon adding LiBr. This would indicate that the carbonyl oxygens are complexing the lithium ion, but not the aziridine ring nitrogen, if the observed changes in chemical shift are attributed to an electrostatic induction effect.¹³ If the alkali metal cation is complexed to the carbonyl oxygens of the cis isomer, the electron density at the ring and methylene hydrogens would be reduced via the electrostatic field of the cation. However, the methylene hydrogens are at least 1 Å further away on the average from the center of the cation than are the ring hydrogens when complexation occurs simultaneously to both oxygens of the cis isomer. Since the electric field around a monopole varies as $1/r^2$, the through space induction or polarization effect at the methylene C-H bond would be considerably reduced. Furthermore, a bond polarization mechanism predicts a reduced effect at the methylene hydrogens when complexation occurs simultaneously at the cis carbonyl oxygens since the methylene hydrogens are two bonds more removed from the site of the cation complexation than the ring hydrogens.

The infrared spectrum in the carbonyl region for cis-AZ in acetonitrile was recorded in the presence of varying amounts of LiBr and NaI to determine if the carbonyl band was affected by the interaction of the cation with cis-AZ. The cis-AZ carbonyl absorption is a doublet in acetonitrile but in the presence of LiBr, the band at higher wavenumbers decreases in intensity while the second band increases and shifts slightly to a lower wavenumber value as the concentration of LiBr is increased (Figure 2). An isobestic point is evident near 1687 cm^{-1} . The effect on the spectrum when NaI is added is not as pronounced as in the LiBr experiments, furthermore, an isobestic point was not

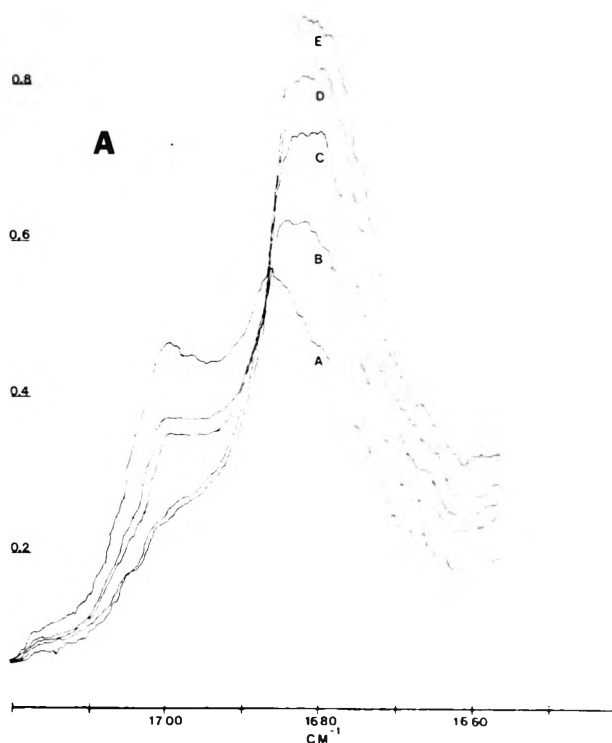


Figure 2. The carbonyl absorption region of cis-AZ at several mole ratios of LiBr in acetonitrile. Concentration of AZ = 0.0058 *M*. Mole ratios (LiBr/AZ) are (A) 0, (B) 0.8, (C) 1.6, (D) 4.0, and (E) 6.0. The cell path length was 0.1 mm.

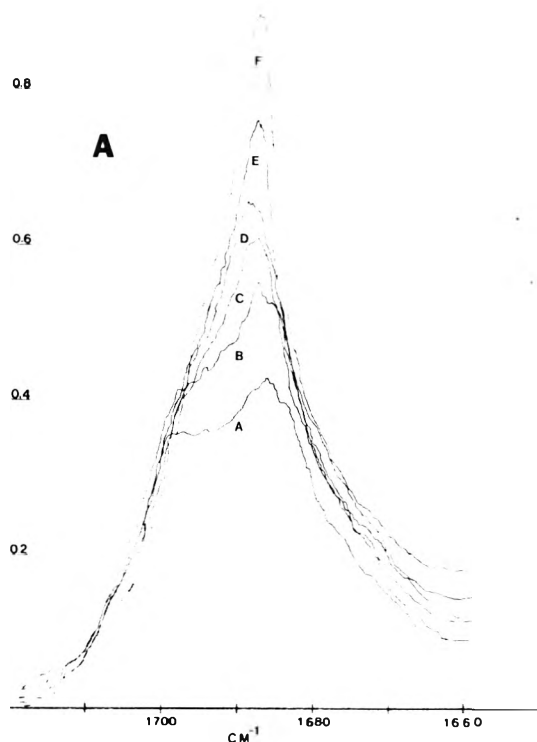


Figure 3. The carbonyl absorption region of cis-AZ at several mole ratios of NaI in acetonitrile. Concentration of AZ = 0.0063 *M*. Mole ratios (NaI/AZ) are (A) 0, (B) 1.2, (C) 2.4, (D) 3.6, (E) 10, and (F) 20. The cell path length was 0.07 mm.

observed (Figure 3). When similar experiments were performed on trans-AZ, the spectrum in the carbonyl region was virtually unaffected. The complex shape of the carbon-

yl absorption band for *cis*-AZ in acetonitrile could be due to rotational isomers and/or Fermi resonance. However, the gradual coalescence of the two peaks and the overall shift to lower wavenumbers upon addition of LiBr, is clear evidence for the involvement of the carbonyl oxygens at the site of complexation to the lithium cation. A less pronounced change is observed for the addition of NaI to the *cis*-AZ solutions, but a similar conclusion can be inferred. Since the carbonyl stretching frequency did not change appreciably on the addition of potassium ions, a definite conclusion concerning the site of complexation for this cation can not be reached from the infrared studies.

A white crystalline solid precipitated from solutions of 0.013 *M* *cis*-AZ when the mole ratio (LiBr/*cis*-AZ) was above 0.4 at room temperature (~25°C). At 40°C, where the NMR experiments were performed, the precipitate did not appear in the 0.013 *M* *cis*-AZ solutions at or below a 2:1 mole ratio. A sample of this material was prepared for analysis by mixing 10 ml of 0.03 *M* *cis*-AZ with 10 ml of 0.1 *M* LiBr. The precipitate was dissolved in a chloroform solution which was filtered and evaporated to dryness. The residue was then recrystallized from dry acetonitrile. The analysis of this material by combustion analysis indicates that the precipitate is a 2:1 *cis*-AZ-LiBr adduct (Calcd for the 2:1 complex: N, 3.6; Br, 10.3; C, 71.8; H, 4.9. Found: N, 3.4; Br, 10.9; C, 68.2; H, 5.1). The low value of the percent C is due to the formation of Li₂CO₃ which could not be completely suppressed by the addition of a catalyst. The infrared spectrum of the adduct (KBr pellet) in the carbonyl region compared with the spectrum of *cis*-AZ reveals that the adduct carbonyl band is much narrower and shifted slightly to lower wavenumbers (Figure 4). The remainder of the spectrum was virtually identical with that of *cis*-AZ. The NMR spectrum of the adduct in chloroform has singlet signals at 252 and 248 Hz. The signal at 252 Hz can be assigned to the ring hydrogens and the 248-Hz signal to the methylene hydrogens by comparing these values with the data found in Table II.

The stoichiometry of the lithium cation-*cis*-AZ complex in acetonitrile solutions is probably 2:1 (AZ:Li⁺) since a solid *cis*-AZ adduct of LiBr is obtained from these solutions with a 2:1 formula. Furthermore, the infrared studies in the carbonyl region show the existence of a definite isobestic point, indicating that there is only one major complexed species being formed when LiBr is added. However, a finite amount of a 1:1 complex must be present in these solutions which would not necessarily be discernible in the infrared spectra: In the case of the sodium and potassium cation, neither an isobestic point (Figure 3) nor a solid adduct was observed.

Since the spectroscopic data do not provide an unambiguous assignment of the stoichiometry of the species present in the alkali metal salt-acetonitrile solutions of *cis*-AZ, a curve fitting procedure was applied to the NMR data, assuming three different models, i.e., a 1:1 complex only, a 2:1 complex only, and a mixture of both the 2:1 and 1:1 complexes being present. In each model the best fit of the observed chemical shifts (δ_m) to the equilibrium and chemical shift parameters was determined by minimizing the quantity CHISQ

$$\text{CHISQ} = \sum(\delta_c - \delta_m)^2$$

where δ_c and δ_m are the calculated and measured chemical shifts as each mole ratio. The calculated chemical shifts at each mole ratio (δ_c) were evaluated from the equilibrium

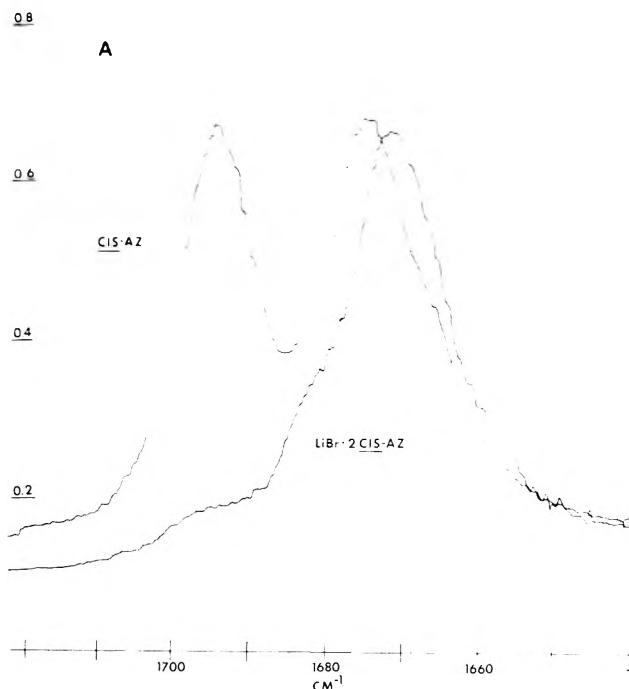


Figure 4. Carbonyl region of the infrared spectrum of *cis*-AZ and the 2:1 LiBr adduct in KBr pellets. The samples were 1% by weight AZ:KBr.

constants and chemical shifts of the complexes, assuming a fast exchange on the NMR time scale was occurring in these solutions. For the initial calculation of CHISQ, reasonable guesses for the equilibrium constants and chemical shifts of the complexes were employed. The best fit of the data to a particular model was then sought by employing a minimization algorithm,¹⁴ STEPIT.¹⁵ The procedures and computer programs to perform this analysis were kindly provided by Henneke and Puhl¹⁶ and slightly modified to apply to the NMR data.

For the KPF₆-*cis*-AZ system, a CHISQ value of less than 0.52 was obtained for all three models for the seven points in Table II. Consequently, it is impossible at this time to distinguish between a 1:1 or 2:1 equilibrium model for the potassium cation since no corroborating evidence exists to support either model.

For both the lithium and sodium cation-*cis*-AZ systems, the 2:1 and mixture models gave almost identical CHISQ values (7.9 and 3.5, respectively). The CHISQ found for the lithium cation 1:1 model was 48 whereas the value for the 1:1 sodium cation system was 9. These results seem to further demonstrate that a 2:1 complex is substantially preferred for the lithium cation but only slightly preferred for the sodium cation. Therefore it seems reasonable to assume a mixture model for both the sodium and lithium cation-*cis*-AZ systems. However, the curve-fitting procedure did not provide unambiguous values for the four parameters of the mixture model for either the Li⁺ or Na⁺ *cis*-AZ systems. Consequently, only rough estimates of the concentration equilibrium constants, K_1 and K_2 , were obtained from the curve-fitting analysis. These estimates are $K_1(\text{Li}^+) = 0.96$; $K_2(\text{Li}^+) = 4879$; $K_1(\text{Na}^+) = 1.0$; and $K_2(\text{Na}^+) = 2969$. While these values must be viewed with considerable reservation, the relative magnitude of $K_1 \times K_2$ indicates that the cation-*cis*-AZ interaction is greatest for the lithium cation. Whereas, this interaction appears to be reduced by approximately a factor of 2 for the Na⁺-*cis*-AZ system rela-

tive to Li^+ . The corresponding estimate ($K_1 \times K_2$) obtained for the K^+ -cis-AZ system is nearly a factor of 11 smaller than the value for the Na^+ -cis-AZ system.

In the preceding curve-fitting analysis of the NMR data, corrections due to possible ion pairing and activity coefficient terms were neglected. Since the ion size parameter in the Debye-Hückel approximation for ionic activities is expected to increase upon complexation, the activity coefficient correction may not be negligible. Ionic association of sodium tetraphenylborate in acetonitrile has been reported by Kay et al.¹⁷ to be undetectable up to 0.005 M. Preliminary conductance data obtained in our laboratory on LiBr and KPF_6 indicate that these salts are approximately strong electrolytes in acetonitrile. The conductance data were obtained below 0.006 M and a small ion pairing effect at the concentration of the NMR experiments cannot be totally discounted.

Conclusion

The spectral data presented here suggest that both Li^+ and Na^+ in acetonitrile solutions selectively interact with two molecules of cis-AZ to form a chelated complex. This interaction appears to occur through the carbonyl oxygens of the benzoyl moiety. Both the concentration equilibrium constants ($K_1 \times K_2$) and the chemical shifts for the 2:1 complex are the largest for the lithium cation system. This result is qualitatively what would be expected for an electrostatic bonding model via ion-dipole and ion-induced dipole forces. Apparently, the lithium cation prefers the four coordinate complexation with the carbonyl oxygens which is only possible with the cis isomer. When a space-filling molecular model was constructed for cis-AZ a cavity only a little smaller than the lithium cation could be formed by appropriate arrangement of two cis-AZ models. In this configuration the carbonyl oxygens formed a tetrahedral array in which the lithium cation could be placed for maximum

coordination. With this model the carbonyl oxygens are in intimate contact with the alkali metal ion, at the Van der Waals radii, forming what is expected to be a stable¹⁸ ion-molecule complex due to electrostatic interactions. The sodium and potassium cations can also be readily surrounded by two molecules of cis-AZ to form a tetrahedral cavity, but the increased radii of these cations substantially reduces the electrostatic interaction of the cation with the carbonyl oxygens. For example, the total interaction energy of an alkali metal ion¹⁸ with CO_2 at the "kinetic theory collision diameter" decreases by 25% when lithium is replaced by sodium and by 60% when lithium is replaced by potassium.

References and Notes

- (1) R. E. Lutz and A. B. Turner, *J. Org. Chem.*, **33**, 516 (1968).
- (2) E. Schaschel and M. C. Day, *J. Am. Chem. Soc.*, **90**, 503 (1968).
- (3) C. Lassigne and P. Baine, *J. Phys. Chem.*, **75**, 3188 (1971).
- (4) M. K. Wong, W. J. McKinney, and A. I. Popov, *J. Phys. Chem.*, **75**, 56 (1971).
- (5) J. L. Wuepper and A. I. Popov, *J. Am. Chem. Soc.*, **91**, 4352 (1969).
- (6) E. C. Ashby, F. R. Dobbs, and H. P. Hopkins, Jr., *J. Am. Chem. Soc.*, **95**, 2823 (1973).
- (7) D. Balasubramanian, A. Goel, and C. N. R. Rao, *Chem. Phys. Lett.*, **17**, 482 (1972).
- (8) H. B. Flora, II, and W. R. Gilkerson, *J. Phys. Chem.*, **77**, 1421 (1973).
- (9) M. Szwarc, "Carbanions and Living Polymers and Electron Transfer Processes", Interscience, New York, N.Y., 1968.
- (10) M. Szwarc, Ed., "Ions and Ion Pairs in Organic Reactions", Wiley-Interscience, New York, N.Y., 1972.
- (11) J. M. Hogan, R. A. Engel, and H. F. Stevenson, *Anal. Chem.*, **42**, 249 (1970).
- (12) A. B. Turner, H. W. Heine, J. Irving, and J. B. Bush, *J. Am. Chem. Soc.*, **87**, 1050 (1965).
- (13) A. D. Buckingham, *Can. J. Chem.*, **38**, 300 (1960).
- (14) J. A. Nelder and R. Mead, *Computers J.*, **8**, 308 (1965).
- (15) J. P. Chandler, Quantum Chemistry Program Exchange, Indiana University, 1965.
- (16) W. H. Puhl and H. F. Henneke, *J. Phys. Chem.*, **77**, 558 (1973); a complete review of this method and a detailed explanation of the calculations can be found in the Ph.D. Thesis of W. H. Puhl, University of Minnesota, 1970.
- (17) R. L. Kay, B. J. Hales, and G. P. Cunningham, *J. Phys. Chem.*, **71**, 3925 (1967).
- (18) J. O. Hirschfelder, C. F. Curtiss, and R. B. Bird, "Molecular Theory of Gases and Liquids", Wiley, New York, N.Y., 1964.

Wavelength-Dependent Photochemical Behavior in 9,10-Dimethylenebianthracene

H. Shizuka,* Y. Ishii, M. Hoshino, and T. Morita

Department of Chemistry, Gunma University, Kiryu, Gunma 376, Japan (Received June 23, 1975)

Publication costs assisted by Gunma University

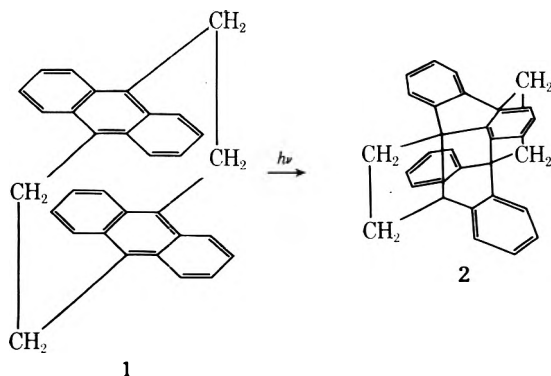
The photochemical reaction of 9,10-dimethylenebianthracene has been carried out in the wavelength range 260–470 nm. Wavelength-dependent phenomena were observed: the reaction quantum yields 0.70 ± 0.06 at 450–470 nm, 0.45 ± 0.04 at ≤ 420 nm, and the S_2 fluorescence ($\Phi_F = 1 \times 10^{-3}$). The results show that direct excitation to the transannular excited state at longer wavelengths is much more effective for the photochemical reaction than that to the locally excited state (1L_a or 1B_b) of anthracene. The reaction mechanism has been discussed in connection with the transannular interaction in the excited state.

1. Introduction

Since the discovery of the pyrene excimer by Förster and Kasper¹ in 1954, many studies on excimers have been reported and the results have been reviewed by Förster,^{2a} Birks,^{2b} and Klöpffer.^{2c} It is well known that an excimer (an electronically excited molecular complex) is dissociated in the ground state,³ and the geometry of an excimer, consisting of two identical aromatic hydrocarbon planes, is a sandwich configuration with an interplanar spacing of 3 Å.⁴

As for paracyclophanes, the original work has been carried out by Cram et al.,⁵ and the studies on paracyclophanes^{6–18} have become of interest in recent years from the following viewpoints. Since the sandwich structure in these molecules is fixed by a more or less rigid link in both the excited and the ground states, it may be responsible for the excimer formation.^{2c} The proximity of two aromatic hydrocarbon planes makes it possible to overlap the molecular π orbital resulting in an electronic interaction between the planes (transannular interaction) even in the ground state.^{5,8,9} In the closest contact between the planes, the aromatic ring is distorted and bent out of plane.^{5,6}

However, only a few studies have been concerned with the photochemical reaction: the photochemical ring-opening reactions of [2.2]paracyclophane studied by Helgeson and Cram,¹⁰ the photosensitized autoxidation reported by Wasserman et al.,¹² and the intramolecular bridge formation of 9,10-dimethylenebianthracene (1) upon irradiation reported by Golden.⁷



It seems that the photochemical reaction $1 \rightarrow 2$ has a close relation to the photodimerization of anthracenes.^{19–23} No mechanistic work on 1 has been given. Furthermore, it was of interest to determine whether the absorption and

emission spectra of 1, as well as the photochemical behavior are similar to those of the anthracene dimer reported by Chandross et al.²⁴ We report the photochemistry of 1 in some detail.

2. Experimental Section

Starting material 1 was synthesized⁷ and purified by repeated recrystallizations from chloroform in dim red light. Tetrahydrofuran (THF) and 2-methyltetrahydrofuran (MTHF) were Tokyo Kasei Co. G.R. grade products and were used without further purification.

A xenon lamp (an Ushio 150-W UXL-150D-SS), equipped with a diffraction grating, was used as the 2600–4700-Å range radiation sources. The diffraction grating admitted only a narrow band of wavelengths (± 70 Å). Actinometry was carried out using a ferric oxalate solution.²⁵ Reaction quantum yields were measured in the initial stage of the reaction. The fluorescence quantum yield was measured by comparison with quinine bisulfate 0.1 N H₂SO₄. The absolute value was determined to be 0.54 by Melhuish.²⁶

All samples were thoroughly degassed on a high-vacuum line by the freeze-pump-thaw method. The amount of photoproduct was determined spectrophotometrically, which was equal to the decrease of the starting material. The absorption and emission spectra were measured by Hitachi 139 and 124 spectrophotometers and Hitachi MPF-2A fluorimeter, respectively.

3. Results and Discussion

The absorption spectrum of 1 in tetrahydrofuran (THF) at 293 K is shown in Figure 1. In addition to the 1L_a (λ_{\max} 380 nm, ϵ 8.30×10^3) and 1B_b (λ_{\max} 263 nm, ϵ 3.81×10^4) bands,²⁷ a new band was observed at longer wavelengths (ϵ 5.0×10^2 at 465 nm). This band was assigned to the transannular band in 1 judging from the weak, broad, and structureless band. In comparison with theoretical results obtained by Azumi, Armstrong, and McGlynn²⁸ and by Murrell and Tanaka,²⁹ the transannular excited state (TA state) with a transition energy of 2.67 eV resembles that of the anthracene excimer in electronic character.

Figure 2 shows the spectral change of 1.5×10^{-4} M THF solution of 1 upon the 366-nm irradiation at 293 K, indicating the photochemical transformation $1 \rightarrow 2$. Similar spectral changes at longer wavelengths (450–470 nm) were observed. Quantum yields for the reaction $1 \rightarrow 2$ at several

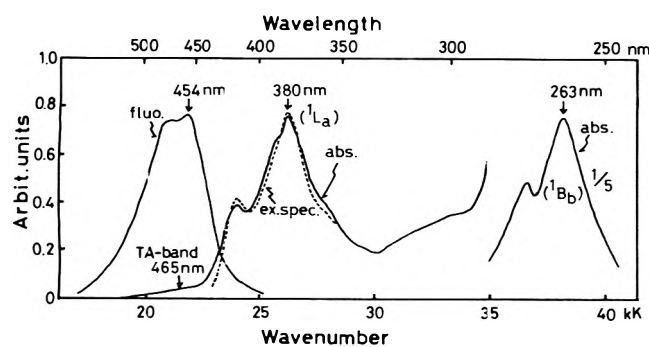


Figure 1. Absorption and fluorescence spectra of **1** in THF; abs.: absorption spectrum; fluo.: fluorescence spectrum; ex. spec.: excitation spectrum.

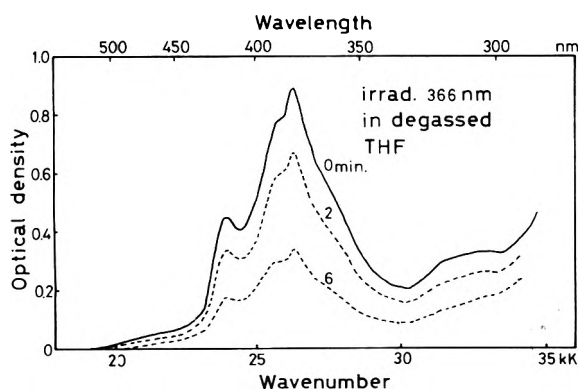


Figure 2. Spectral change of 1.5×10^{-4} M THF solution of **1** with lapse of irradiation time at 366 nm. Numbers refer to time in minutes.

wavelengths were measured spectrophotometrically in degassed THF at 293 K. The reaction quantum yield Φ_R ($=0.70 \pm 0.06$) at direct excitation to the TA-state was larger than that of Φ_R ($=0.45 \pm 0.04$) at the excitation to the locally excited state (1L_a or 1B_b) of anthracene as shown in Figure 3.

It may be assumed that at room temperature there are sufficient molecules of **1** vibrationally compressed to give a long wavelength absorption. If the "hot bands" arise from a compressed geometry, it is reasonable that the quantum yield of Φ_R is high. However, this assumption was denied, because long wavelength absorption was observed at 77 K in a MTHF rigid matrix as shown in Figure 4. The photochemical reaction occurred even at 77 K at 450 nm. Moreover, no temperature effect on Φ_R at 366 nm was observed in the temperature range 203–300 K (Figure 5).

The fluorescence and excitation spectra of **1** is also shown in Figure 1. The fluorescence at 454 nm did not originate from the S_1 (TA) state, but from the S_2 (1L_a) state. The fluorescence quantum yield Φ_F was $(1 \pm 0.1) \times 10^{-3}$ in degassed THF at 366 nm. Similar fluorescence was observed in a MTHF rigid matrix at 77 K (see Figure 4). Recently, similar S_2 fluorescence of **1** has been reported by Morita et al.³³

The absorption and fluorescence spectra of **1** are different from those of anthracene dimers, which are made by irradiation of rigid glasses of methylcyclohexane containing dianthracene with 254-nm light from a low-pressure Hg lamp.²⁴ It is known that there are two types of anthracene dimers: a sandwich dimer and a "55 deg dimer"; the absence of a transannular band at 465 nm is observed in these dimers.²⁴ These differences can be understood by the fact

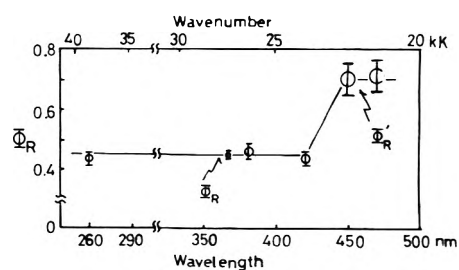


Figure 3. Reaction quantum yields as a function of excitation wavelength.

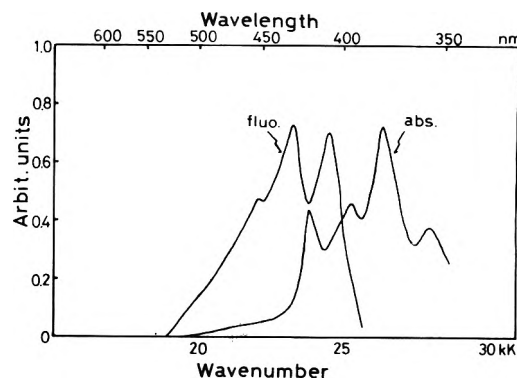


Figure 4. Absorption and fluorescence spectra of **1** in a MTHF rigid matrix at 77 K.

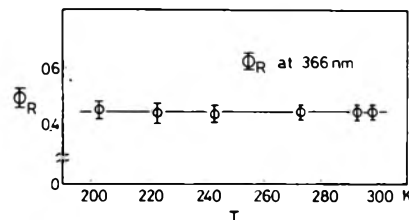


Figure 5. Temperature effect on the reaction quantum yield Φ_R at 366 nm and 293 K.

that the proximity of two anthracene planes fixed by dimethylene in **1** makes it possible to overlap the molecular π orbital to give the TA band.

The addition of piperylene ($\leq 10^{-2}$ M) as a triplet quencher did not affect both the Φ_R and Φ_F values at 366 nm and 293 K, supporting a singlet mechanism. In order to confirm the singlet pathway, the photosensitized reaction of **1** (1×10^{-4} M) by benzophenone (0.1 M) in degassed benzene at room temperature has been carried out. About 95% incident light was absorbed by benzophenone molecules and the efficiency for the triplet-triplet energy transfer was ca. 90% considering the triplet lifetime (12 μsec)³¹ of benzophenone and the diffusion-controlled rate constant ($1.0 \times 10^{10} \text{ M}^{-1} \text{ sec}^{-1}$)³² of the solvent. The reaction quantum yield sensitized by triplet benzophenone was less than 0.001. This result is evidence for the singlet mechanism.

From these results, the photochemical and photophysical processes can be accounted for by the scheme shown in Figure 6. A thermal relaxation in the TA state (S_1) may give an intramolecular singlet excimer (1E) which is responsible for the photochemical reaction. The rate constant k_i for the internal conversion S_n (1B_b) \rightarrow S_2 (1L_a) is very large on the basis of the result of the wavelength effect on Φ_P . The re-

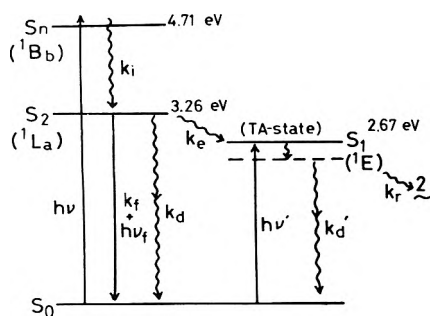


Figure 6. Schematic energy state diagram for the photochemical reaction $1 \rightarrow 2$.

verse process from S_1 to S_2 may be negligible, since the energy gap between the S_1 and S_2 levels is appreciable (0.59 eV).

Using a steady state approximation, the following equations are obtained:

$$\Phi_R = 0.45 = \frac{k_e}{k_d + k_e + k_f k_d' + k_r} = \varphi_e \Phi'_R \quad (1)$$

where $\varphi_e = k_e / (k_d + k_e + k_f)$.

$$\Phi'_R = 0.70 = k_r / (k_d' + k_r) \quad (2)$$

$$\Phi_F = 1 \times 10^{-3} = k_f / (k_d + k_e + k_f) \quad (3)$$

Because of the low value of Φ_F , the main deactivation processes in the $S_2(^1L_a)$ state comprise k_e and k_d . From eqs. 1–3, the efficiency φ_e and the rate constant k_e for TA-state formation from S_2 can be derived:

$$\varphi_e = \Phi_R / \Phi'_R \simeq 0.64 \quad (4)$$

$$k_e = 6.4 \times 10^2 \times k_f = 5.3 \times 10^{10} \text{ sec}^{-1} \quad (5)$$

where the radiative rate constant k_f was estimated to be $8.3 \times 10^7 \text{ sec}^{-1}$ from the 1L_a band. The values of k_d , $(k_d + k_e)^{-1}$, and k_r/k_d' can be also evaluated as follows:

$$k_d \simeq 3 \times 10^{10} \text{ sec}^{-1} \quad (6)$$

$$\tau_{S_2} = (k_d + k_e)^{-1} \simeq 1.2 \times 10^{-11} \text{ sec} \quad (7)$$

$$k_r/k_d' \simeq 2.3 \quad (8)$$

The lifetime of the 1L_a state (~ 12 psec) of **1** becomes much shorter than that of isolated anthracene (4.9 nsec^{2b}), indicating a large transannular interaction in the S_2 state of **1**.

Finally, the wavelength-dependent photochemical behavior of **1** has been revealed. Direct excitation to the transannular excited state at longer wavelengths (450–470 nm) is much more effective for the photochemical reaction from **1** to **2** than that to the locally excited state (1L_a or 1B_b) of anthracene at shorter wavelengths (< 420 nm).

References and Notes

- (1) Th. Förster and K. Kasper, *Z. Phys. Chem. (Frankfurt am Main)*, **1**, 275 (1954); *Z. Elektrochem.*, **59**, 976 (1955).
- (2) (a) Th. Förster, *Angew. Chem.*, **81**, 364 (1969); *Angew. Chem., Int. Ed. Engl.*, **8**, 333 (1969); (b) J. B. Birks, "Photophysics of Aromatic Molecules", Wiley-Interscience, London, 1970; (c) W. Klöpffer, "Organic Molecular Photophysics", Vol. 1, J. B. Birks, Ed., Wiley-Interscience, London, 1973; and many references therein.
- (3) B. Stevens, *Nature (London)*, **192**, 725 (1961).
- (4) E. g. H. Braun and Th. Förster, *Ber. Bunsenges. Phys. Chem.*, **70**, 1091 (1966); *Z. Phys. Chem. (Frankfurt am Main)*, **78**, 40 (1971); J. B. Birks and L. G. Christophorou, *Proc. R. Soc. London, Ser. A*, **277**, 571 (1964).
- (5) D. J. Cram and H. Steinberg, *J. Am. Chem. Soc.*, **73**, 5691 (1951); D. J. Cram, N. L. Allinger, and H. Steinberg, *ibid.*, **76**, 6132 (1954).
- (6) C. J. Brown, *J. Chem. Soc.*, 3265 (1953); K. Lonsdale, H. J. Milledge, and K. V. K. Rao, *Proc. R. Soc. London, Ser. A*, **255**, 82 (1960).
- (7) J. H. Golden, *J. Chem. Soc.*, 3741 (1961). It was confirmed by means of the TLC method that there were no impurities in starting material **1**: it gave only one spot in the TLC experiment (silica gel; benzene:acetone = 1:2).
- (8) J. Koutecky and J. Padlus, *Collect. Czech. Chem. Commun.*, **27**, 599 (1962).
- (9) M. T. Vala, Jr., J. Haebig, and S. A. Rice, *J. Chem. Phys.*, **43**, 886 (1965); M. T. Vala, I. H. Hillier, S. A. Rice, and J. Jorter, *ibid.*, **44**, 23 (1966).
- (10) R. C. Helgeson and D. J. Cram, *J. Am. Chem. Soc.*, **88**, 509 (1966).
- (11) A. Ron and O. Schnepf, *J. Chem. Phys.*, **37**, 2540 (1962); **44**, 19 (1966).
- (12) H. H. Wasserman and A. R. Doumaux, *J. Am. Chem. Soc.*, **88**, 4517 (1966); H. H. Wasserman and P. M. Keehn, *ibid.*, **88**, 4522 (1966).
- (13) W. Rebaika and H. A. Staab, *Angew. Chem.*, **85**, 831 (1973); *ibid.*, **86**, 234 (1974); *Angew. Chem., Int. Ed. Engl.*, **12**, 776 (1973); M. Haenel and H. A. Staab, *Chem. Ber.*, **106**, 2203 (1973).
- (14) A. Iwana, T. Toyoda, T. Otsubo, and S. Misumi, *Chem. Lett.*, 587 (1973); H. Hirota, N. Kannen, T. Otsubo, and S. Misumi, *Tetrahedron Lett.*, 501 (1974); T. Otsubo, S. Misogami, Y. Sakata, and S. Misumi, *Bull. Chem. Soc. Jpn.*, **46**, 3831 (1973); S. Iwata, K. Fuke, M. Sasaki, S. Nagakura, T. Otsubo, and S. Misumi, *J. Mol. Spectrosc.*, **46**, 1 (1973).
- (15) M. A. Hassloch, M. J. Nugent, and O. E. Weigang, Jr., *J. Am. Chem. Soc.*, **96**, 2619 (1974); P. H. Hoffman, E. C. Ong, O. E. Weigang, Jr., and M. J. Nugent, *ibid.*, **96**, 2620 (1974).
- (16) J. L. Marshall and B.-H. Bong, *J. Org. Chem.*, **39**, 1342 (1974).
- (17) S. E. Potter and I. O. Sutherland, *J. Chem. Soc., Chem. Commun.*, 520 (1973).
- (18) E. Heilbronner and J. P. Maier, *Helv. Chim. Acta*, **57**, 151 (1974).
- (19) J. Fritzsche, *J. Prakt. Chem.*, **101**, 337 (1866).
- (20) F. D. Greebe, S. L. Misrock, and J. R. Wolfe, Jr., *J. Am. Chem. Soc.*, **77**, 3852 (1955).
- (21) E. J. Bowen and D. W. Tanner, *Trans. Faraday Soc.*, **51**, 475 (1955); E. J. Bowen, *Adv. Photochem.*, **1**, 23 (1963).
- (22) R. L. Barnes and J. B. Birks, *Proc. R. Soc. London, Ser. A*, **291**, 570 (1966).
- (23) J. Bertran, V. Forero, F. Mora, and J. I. Fernandez-Alonso, *Tetrahedron*, **30**, 427 (1974).
- (24) E. A. Chandross, *J. Chem. Phys.*, **43**, 4175 (1965); E. A. Chandross, J. Ferguson, and E. G. McRae, *ibid.*, **45**, 3546 (1965); E. A. Chandross and J. Ferguson, *ibid.*, **45**, 3973 (1966); J. Ferguson, *ibid.*, **44**, 2677 (1966); J. Ferguson, A. W. H. Mau, and J. M. Morris, *Aust. J. Chem.*, **26**, 91 (1973).
- (25) C. G. Hatchard and C. A. Parker, *Proc. R. Soc. London, Ser. A*, **235**, 518 (1956).
- (26) W. H. Melhuish, *J. Phys. Chem.*, **65**, 229 (1961).
- (27) These two electronic transitions $^1L_a \leftarrow ^1A$ ($^1B_{2u} \leftarrow ^1A_{1g}$) and $^1B_b \leftarrow ^1A$ ($^1B_{3u} \leftarrow ^1A_{1g}$) in anthracene have been well characterized. See, e.g., J. W. Sidman, *J. Chem. Phys.*, **25**, 115 (1956); D. P. Craig and P. C. Hobbins, *J. Chem. Soc.*, 539, 2309 (1955).
- (28) T. Azumi, A. T. Armstrong, and S. P. McGlynn, *J. Chem. Phys.*, **41**, 3839 (1964).
- (29) J. N. Murrell and J. Tanaka, *Mol. Phys.*, **7**, 363 (1964).
- (30) S. Morita, J. Tanaka, M. Tanaka, T. Hayashi, N. Mataga, Y. Sakata, and S. Misumi, presented at the Symposium on Molecular Structure of Japan, Tokyo, October 1974.
- (31) S. L. Murov, "Handbook of Photochemistry", Marcel Dekker, New York, N.Y., 1973, p 3.
- (32) J. G. Calvert and J. N. Pitts, Jr., "Photochemistry", Wiley, New York, N.Y., 1967, p 627.

Ionic Photodissociation of Excited Electron Donor-Acceptor Systems.

II. The Importance of the Chemical Property of Donor-Acceptor Pairs

T. Hino, H. Akazawa, H. Masuhara,* and N. Mataga

Department of Chemistry, Faculty of Engineering Science, Osaka University, Toyonaka, Osaka 560, Japan (Received June 9, 1975)

The relationship between the ionic photodissociation yield and the electron donor-acceptor interaction of pyrene-quencher systems was investigated by nanosecond laser photolysis and transient photocurrent measurements. While no general relation was obtained, the chemical property of donor-acceptor pairs was found to be reflected in the yield. On the basis of the present and previous results it was concluded that the ionic photodissociation process consists of two steps, namely, the encounter collisional electron transfer and the orientational relaxation of solvents. With the latter process some other radiationless transitions depending on the chemical property compete in the dissociative excited state. It was shown in the case of pyrene-nitrile systems that an unknown quenching process, other than ionic dissociation as well as triplet formation, increases with the electron affinity.

Introduction

The fluorescence quenching process of aromatic hydrocarbons due to electron transfer has been extensively studied in solution. A quantitative analysis was given by Rehm and Weller,¹ who established an equation on the relationship between the quenching rate constant (k_q) and the free energy change of the electron transfer process in acetonitrile solution. A number of systems of aromatic hydrocarbon-quencher (amines, methoxybenzenes, nitriles) were examined and confirmed to satisfy the proposed equation. On the other hand, the fate of the transient ion pair produced by the electron transfer still seems unclear. It may dissociate into free ions, disappear by reverse electron transfer from the anion to the cation, or convert into another chemical species. Moreover, these primary processes are expected to be explained in terms of the electron donor-acceptor (EDA) interaction in the excited state. These are the problems associated with the mechanism of ionic photodissociation of EDA systems, which have been investigated in detail by the present authors.²⁻⁵

In the present work the quantum yields of ionic photodissociation of 21 pyrene-quencher systems in polar solvents have been obtained by using nanosecond laser photolysis and transient photocurrent measurements. The relationship between the yield and the EDA interaction will be examined, and the importance of the chemical property of donor-acceptor pairs will be pointed out. The ionic photodissociation mechanism will be discussed in general.

Experimental Section

Transient absorption spectra were obtained by using a nitrogen laser constructed in the present work. A double parallel-plate transmission line was used for a low inductance capacitor,⁶ and a single triggered spark gap was made of an aluminum block and a motor car plug (NGK BUHX). Dielectrics were polyethylene terephthalate films (Toray Lumirror). The output of 337-nm pulse was 1.5 mJ and its pulse duration was 5.5 nsec. The monitoring light source was a Xe flash lamp (Ushio US-240B) or a pulsed Xe lamp (500 W, Ushio). The electronic circuit for the latter was constructed by referring to the pulser circuit designed by Thomas.⁷ A block diagram of the present laser photolysis

apparatus is given in Figure 1. Transient photocurrent measurements were performed by the method and the apparatus reported previously.^{3,5} For excitation, a frequency-doubled ruby pulse of 80-mJ output and 15-20-nsec duration was used.

Pyrene was chromatographically purified. *N,N*-Dimethylaniline (DMA), *N,N*-diethylaniline (DEA), and *N,N*-dimethyl-*m*-toluidine (DMT) were refluxed with acetic anhydride, distilled under reduced pressure, washed with water, dried over potassium hydroxide, distilled under reduced pressure, vacuum distilled, and stored in vacuo. Aniline (AN) and *N*-methylaniline (NMA) were distilled, vacuum distilled, and stored in vacuo. Benzonitrile and diethylphthalate were used after distillation. All other electron acceptors were purified by several recrystallizations and sublimation. Acetone (Dotite spectrograde) and acetonitrile (Merck spectrograde) were used without further purification. Acetone solutions were bubbled with nitrogen gas saturated with acetone, and acetonitrile solutions were degassed by the usual freeze-pump-thaw method.

Results

1. *Transient Absorption Spectral Measurements on Pyrene-Amine and Pyrene-Nitrile Systems in Acetonitrile.* The transient spectra obtained at 200 nsec after excitation are shown in Figures 2 and 3. The concentration of pyrene was adjusted so as to give an appropriate optical density (0.1~0.4) at 347 nm for the present photolysis method. The concentration of quenchers was determined so as to quench the pyrene fluorescence more than 90% for nitriles and 98% for amines. These spectra can be reproduced by the superposition of the bands of the donor cation, the acceptor anion, and the triplet pyrene,⁸⁻¹⁰ which means that ionic photodissociation of the present EDA systems occurs. Quantum yields of the dissociation process were obtained by examining the pyrene anion (492 nm) and the pyrene cation (445 nm) bands for amine and nitrile quenchers, respectively. Details of the procedure for evaluating the yield are the same as reported previously.² The values obtained are listed in Table I and accompanied with the free energy change of the ionic photodissociation process. The change was calculated according to the following equation:¹

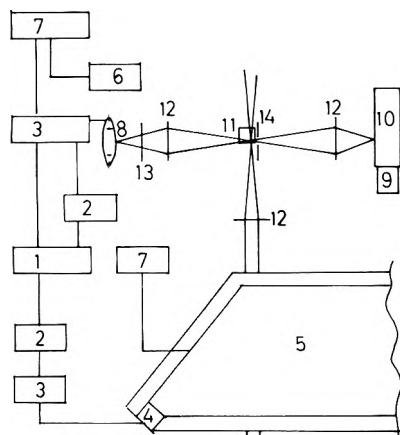


Figure 1. A block diagram of the nitrogen laser photolysis apparatus with a pulsed Xe lamp as a monitoring light source: (1) pulser, (2) delay circuit, (3) triggering circuit, (4) single triggered spark gap, (5) nitrogen gas laser, (6) starter, (7) power supply, (8) Xe lamp, (9) photomultiplier, (10) monochromator, (11) sample cell, (12) lens, (13) filter, (14) slit.

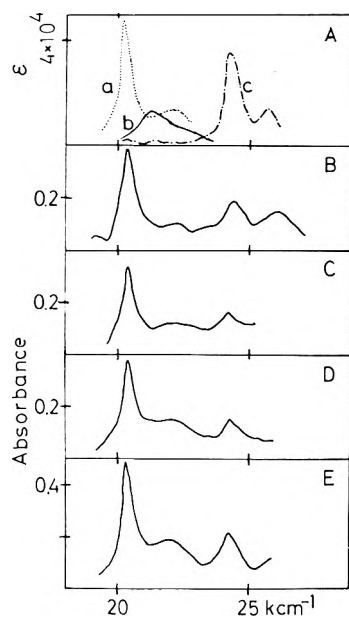


Figure 2. Transient absorption spectra of the pyrene-amine-acetonitrile systems obtained 200 nsec after laser excitation. (A) The literature spectra of the pyrene anion (a), the DEA cation (b), and the triplet pyrene (c) are from ref 8 and 9. The amines are as follows: (B) aniline, (C) *N*-methylaniline, (D) *N,N*-diethylaniline, (E) *N,N*-dimethylaniline.

$$\Delta G = E(D/D^+) - E(A^-/A) - \Delta E_{0,0}(A^*) - e^2/\epsilon a$$

where $E(D/D^+)$ and $E(A^-/A)$ represent the oxidation potential of the donor and the reduction potential of the acceptor, respectively. $\Delta E_{0,0}(A^*)$ and $e^2/\epsilon a$ are the energy of the zero-zero transition of pyrene and the Coulomb energy obtained due to the formation of ion pairs in the solvent of dielectric constant ϵ . The yields obtained by the usual method of photocurrent measurements⁵ are also shown in Table I. Here the yield determined with the photocurrent data (ψ_{pc}) was set equal to the value obtained by examining absorption spectral measurements (ψ_{abs}), since most of the anions and the cations produced are separately solvated in the case of pyrene-DMA and pyrene-*p*-dicyanobenzene (DCNB) systems in acetonitrile.³⁻⁵ The values of ψ_{pc} for

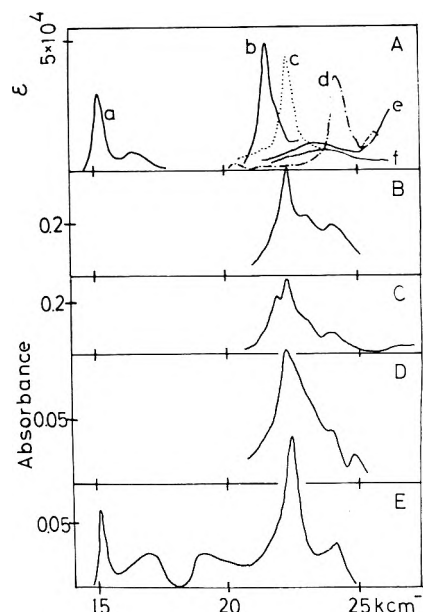


Figure 3. Transient absorption spectra of the pyrene-acceptor-acetonitrile systems obtained 200 nsec after laser excitation. (A) The literature spectra of the pyromellitic dianhydride anion (a), the tetracyanobenzene anion (b), the pyrene cation (c), the triplet pyrene (d), the *p*-dicyanobenzene anion (e), and the tetracyanoethylene anion (f) are from ref 8-10. The acceptors are as follows: (B) *p*-dicyanobenzene, (C) tetracyanobenzene, (D) tetracyanoethylene, (E) pyromellitic dianhydride.

TABLE I: Quantum Yields of Ionic Photodissociation of Pyrene-Amine and -Nitrile Systems in Acetonitrile

Quencher	ψ_{abs}^a	ψ_{pc}^b	$E(D/D^+)$ or $E(A^-/A)$, eV	ΔG , eV
<i>N,N</i> -Dimethylaniline	0.5 ^c	0.5	0.78	-0.47
<i>N,N</i> -Diethylaniline	0.5	0.5	0.76	-0.49
<i>N,N</i> -Dimethyl- <i>m</i> -toluidine	0.53	0.6	0.65	-0.60
<i>N</i> -Methylaniline	0.37	0.4	1.03	-0.22
Aniline	0.45	0.5	1.28	+0.03
Triethylamine	0.28	0.2	0.98	-0.27
<i>p</i> -Dicyanobenzene	0.38 ^c	0.38 ^c	-0.65	-0.50
<i>sym</i> -Tetracyanobenzene	0.20	0.25	-0.66	-1.49
Tetracyanoethylene	0.10	0.16	+0.24	-2.39
Pyromellitic dianhydride	0.11		-0.55	-1.60

^a ψ_{abs} are the absolute yields obtained by calculating the absorption spectral data. The value of 0.5 of the pyrene-DMA system was determined by Taniguchi et al.⁵ ^b ψ_{pc} are the yields obtained from the photocurrent data. ^c For pyrene-DAM and pyrene-DCNB systems ψ_{pc} is set equal to ψ_{abs} . See text.

some quencher systems are roughly equal to those of ψ_{abs} , which means that most of the ionic species are solvated as free ions in this solvent. In the case of pyrene-amine systems the yield is rather small when NMA and TEA are used as quenchers and it is almost constant when DMA, DEA, AN, and DMT are used as quenchers. In the case of pyrene-nitrile systems the yield decreases as the free energy change increases.

2. The Photocurrent Measurement on Pyrene-Acceptor Systems in Acetone. The observed laser-induced current shows rapid rise and rather slow decay in nanosecond time regions. Therefore the value of peak photocurrent attained immediately after excitation may be regarded as proportional to the yields of ions produced. All results are summa-

TABLE II: Relative Quantum Yields of Ionic Photodissociation of Pyrene-Acceptor Systems in Acetone

Acceptors	$E_{1/2}^a$, eV	E_f^b , eV	$E_f'^c$, eV	ϕ^d	Decay ^e	Reaction ^f
<i>p</i> -Benzoquinone	-0.51 ^h	2.04	1.37	0.63	Second order	No
Benzonitrile	-3.25 ⁱ	-0.80		0.27		
Fumaronitrile			0.79	0.45		
<i>o</i> -Dicyanobenzene	-2.63 ⁱ	-0.16		0.94	Second order	No
<i>p</i> -Dicyanobenzene	-2.48 ⁱ	-0.00	1.11	1.00		
<i>m</i> -Dicyanobenzene				0.65		
<i>sym</i> -Tetracyano-benzene	-0.71 ^h	1.84	2.20	0.68		
Phthalic anhydride	-1.31 ^h	1.21		0.20	Not clear	Yes
Tetrachlorophthalic anhydride	-0.86 ^h	1.70		0.17		
Maleic anhydride	-0.84 ^h	1.71		0.15		
Pyromellitic dianhydride	-0.55 ^h	2.02		0.12		
Diethyl isophthalate	-1.47 ⁱ	1.04		0.43	Second order	No
Diethyl phthalate	-1.45 ⁱ	1.07		0.33		
Diethyl terephthalate	-1.16 ⁱ	1.36		0.41		
Without acceptors				0.26	Not clear	No
Py-(CH ₂) ₃ -DMA ^g				0.16		

^a $E_{1/2}$ represents the reduction potential of acceptors. ^b E_f is the electron affinity of the acceptors obtained by using the following relations: $E_f = 1.04E_{1/2} + 2.58$, which is obtained by plotting the data of 21 acceptors. ^c E_f' is the electron affinity given by the magnetron method. See A. L. Farragher and F. M. Page, *Trans. Faraday Soc.*, 63, 2369 (1967). ^d ϕ is the relative quantum yield obtained in the present work. ^e The decay mode of transient photocurrent. ^f Photoproducts were checked by examining the change in uv absorption spectra. ^g Py-(CH₂)₃-DMA represents 1-pyrenyl-(CH₂)₃-(*p*-*N,N*-dimethylaminophenyl). This sample was supplied by Professor S. Misumi of this university. ^h M. E. Peover, *Trans. Faraday Soc.*, 58, 2370 (1962). ⁱ P. H. Rieger, I. Bernal, W. H. Reinmuth, and G. K. Fraenkel *J. Am. Chem. Soc.*, 85, 683 (1963). ^j These are values of corresponding dimethyl esters, which were kindly given by Dr. M. Yamamoto of Kyoto University.

ized in Table II. The concentrations were 1×10^{-4} M for pyrene and 1×10^{-3} M for acceptors throughout all measurements, and no appreciable excimer formation was detected. These acceptors do not show any considerable absorption at 347 nm, the wavelength of excitation by frequency-doubled ruby laser. The observed current in the case of pyrene solution without quenchers is due to the pyrene cation and the solvated electron produced by one- and two-photon absorption.¹¹ Since absorption of the second photon and quenching by acceptors compete with each other in the case of pyrene-acceptor systems, the photocurrent value for the system without quencher suggests an upper limit for the ionization of pyrene in the present pyrene-acceptor systems. The 1-pyrenyl-(CH₂)₃-(*p*-*N,N*-dimethylaminophenyl) system shows exciplex emission even in rather polar solvents¹² and the transient photocurrent is suppressed compared to the case of pyrene without quenchers. Quenching by the *N,N*-dimethylaminophenyl moiety may be efficient because of the short distance between the latter and pyrene. The peak photocurrent of the pyrene-acceptor systems may be due to ionization of pyrene as well as ionic photodissociation. Although the precise contribution from the dissociation of the donor-acceptor pair to the observed photocurrent cannot be determined, qualitative conclusions will be given in the present work.

When an excited pyrene is quenched by anhydrides the peak current obtained is only a little larger or even smaller than that of 1-pyrenyl-(CH₂)₃-(*p*-*N,N*-dimethylaminophenyl) and a change of absorption spectra after measurements was observed. This may be ascribed to a chemical reaction between fluorescent pyrene and anhydrides, whose rate is larger than that of dissociation. The transient current decay curve cannot be analyzed because of the low signal intensity. In the case of aromatic ester quenchers such a reaction was not detected and a second-order decay was analyzed. The yield is about 40% of that in the case of the py-

rene-DCNB system. It should be noted that the yield of pyrene-nitrile systems except benzonitrile and fumaronitrile quenchers decreases as the electron affinity increases. In the case of the latter quenchers, effective quenching does not occur because of a smaller kq value than the diffusion-controlled one¹ and the yield is lower than that of the pyrene-DCNB system.

Discussion

The relation between the ΔG value and the yield obtained in the present work is shown in Figure 4, where the fluorescence quenching rate constant is also given as a function of ΔG .¹ The yields of ester and anhydride quencher systems are due to data measured in acetone solution and the increase of the yield from acetone to acetonitrile was estimated by assuming the same solvent effect as in the pyrene-DCNB system. The increase is about 20% for the latter system.⁴ All examined quenchers are well known to have enough ability to quench the pyrene fluorescence and the rate constant is equal to the diffusion-controlled one. In the cases of NMA, AN, and TEA, corrections for smaller kq values are made by increasing the concentration of those amines. Therefore, a direct comparison of ionic photodissociation yield is possible and significant. The general relation between the yield and ΔG , which is related to the EDA interaction, was not obtained and the fluctuations of values in the $-0.5 \sim 0.7$ eV region of ΔG are noticeable. The data in Figure 4 may be classified into four groups, namely, nitriles, amines, esters, and anhydrides. It should be emphasized that the chemical property of donor-acceptor pairs plays an important role in the ionic photodissociation process.

Since the quenchers used here have large quenching ability due to electron transfer, transient ion pair may be produced at first although the nature of this ion pair is not very clear. However, different yields of free ions were observed as shown in the present work. Therefore, it is con-

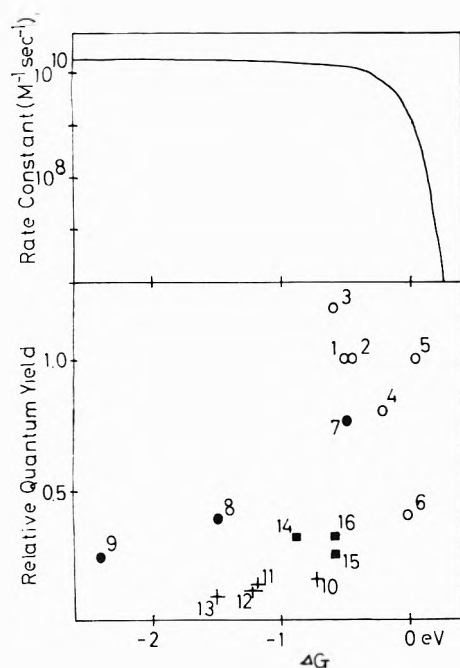
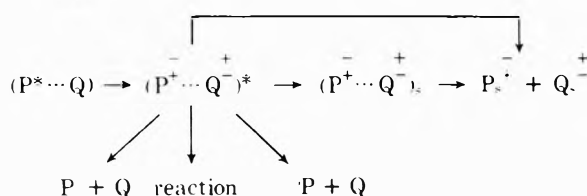
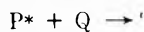


Figure 4. The relation between ΔG value and the ionic dissociation yield obtained immediately after excitation for several pyrene-quencher-acetonitrile systems. The representation of the fluorescence quenching rate constant as a function of ΔG is cited from ref 1. Quenchers are as follows: (1) *N,N*-dimethylaniline, (2) *N,N*-diethylaniline, (3) *N,N*-dimethyl-*m*-toluidine, (4) *N*-methylaniline, (5) aniline, (6) triethylamine, (7) *p*-dicyanobenzene, (8) tetracyanobenzene, (9) tetracyanoethylene, (10) phthalic anhydride, (11) tetrachlorophthalic anhydride, (12) maleic anhydride, (13) pyromellitic dianhydride, (14) diethylisophthalate, (15) diethylphthalate, (16) diethyl terephthalate. The data may be classified into four groups: amines (O), nitriles (●), esters (■), and anhydrides (+).

cluded that the encounter collisional electron transfer between the fluorescer and the quencher is not always followed by ionic dissociation into free ions. Electron transfer in the excited state may also be followed by some other primary processes. Namely, the primary processes to $P + Q$ as well as ${}^3P + Q$ and some chemical reactions from the state produced immediately after the electron transfer have been investigated in detail by Ottolenghi et al.¹³ and by us.³⁻⁵ According to those investigations and the present results, a schematic representation for the relevant processes may be as follows:



Here primary processes for about 10 nsec after excitation are summarized. P^* and Q are the excited pyrene molecule and quencher, respectively. $(P^* \cdots Q)$ is an encounter complex and $(P^+ \cdots Q^-)^*$ is the state formed immediately after electron transfer. The degree of relaxation of the latter state is not well known at the present stage of investigation. $(P^+ \cdots Q^-)_s$ and $P_s^+ + Q_s^-$ represent the solvated ion pair and free ions, respectively. Solvation to the ion pair or directly to free ions may compete with reverse electron transfer to the ground state, formation of the triplet py-

rene, and chemical reaction.¹⁴ The rate constants of such degradation processes may depend not only on the EDA interaction but also on the chemical property of the EDA pairs. Thus the yield of free ions formed widely from system to system even if electron transfer quenching occurs equally. It is concluded, therefore, that the dissociation process consists of two steps, namely, the encounter collisional electron transfer and the orientational relaxation of the solvent. This conclusion is consistent with the result on exciplex formation processes studied by time-resolved fluorescence spectra.¹⁵ The exciplex has been considered to be formed by encounter collisional electron transfer followed by solvation, as in the present case of ionic photodissociation.

The results on pyrene-nitrile systems showed that the yield decreases as the electron affinity increases. This tendency is confirmed with both photocurrent and spectral data. Since the rate of dissociation into free ions or the rate of formation of ion pairs should become larger as the electron affinity increases, the above result leads to the conclusion that there occurs some radiationless process which competes with ionic dissociation and becomes faster as the electron acceptor becomes stronger. Since the increase of the triplet pyrene was not observed with the decrease of the dissociation yield as one can see from Figure 3, this radiationless process is not the formation of the triplet pyrene. Moreover, the chemical reaction was not detected by absorption spectral measurements. Thus the nature of the degradation process in question is not clear at the present stage of investigation. Quite similar result was already reported by us on the tetracyanobenzene-methyl-substituted benzene charge-transfer complexes which is stable in the ground state.² As the ionization potential of the donor becomes higher and the CT degree in the excited Franck-Condon state is lowered, the yield of ionic dissociation was increased. This result was explained as due to the fact that the high CT degree leads to faster direct degradation to the ground state, which competes with ionic dissociation. It seems that such a radiationless transition is common to aromatic hydrocarbon-nitrile systems.

The influence of the chemical property of the quencher upon ionic photodissociation yield can be noticed also in the case of pyrene-amine systems. The dissociation yield of the pyrene-NMA system is lower than those of systems of pyrene-other aromatic amine quenchers. Recently it has been reported that hydrogen atom transfer from NMA to excited pyrene occurs,¹⁶ which seems to cause the low ionic dissociation yield. Moreover, the yield of the pyrene-TEA system is low compared to the case of other amine quenchers. This may be ascribed to the difference between aromatic and aliphatic amines. Dynamic behaviors of aromatic hydrocarbon-aliphatic amine exciplexes are rather distinct from those of aromatic hydrocarbon-aromatic amine exciplexes,¹⁷ and the same difference in the chemical nature may be reflected in the ionic photodissociation yield.

References and Notes

- (1) D. Rehm and A. Weller, *Ber. Bunsenges. Phys. Chem.*, **73**, 834 (1969); D. Rehm and A. Weller, *Isr. J. Chem.*, **8**, 259 (1970).
- (2) (a) H. Masuhara, M. Shimada, N. Tsujino, and N. Mataga, *Bull. Chem. Soc. Jpn.*, **44**, 3310 (1971); (b) M. Shimada, H. Masuhara, and N. Mataga, *ibid.*, **46**, 1903 (1973).
- (3) H. Masuhara, T. Hino, and N. Mataga, *J. Phys. Chem.*, **79**, 994 (1975); part I of the present series; Papers cited there.
- (4) T. Hino, H. Masuhara, and N. Mataga, *Bull. Chem. Soc. Jpn.*, in press.
- (5) Y. Taniguchi, Y. Nishina, and N. Mataga, *Bull. Chem. Soc. Jpn.*, **45**, 764 (1972); Y. Taniguchi, Ph.D. Thesis, Faculty of Engineering Science, Osaka University, Toyonaka, Osaka 560, Japan.
- (6) D. Basting, F. P. Schafer, and B. Steyer, *Opto-electronics*, **4**, 43 (1972);

- H. Sugikawa, M.S. Thesis, Faculty of Engineering, Osaka University, Suita, Osaka 565, Japan.
- (7) J. K. Thomas, private communication to H.M.
- (8) J. Langelaar, J. Wegdam-Van Beek, H. Ten Brink, and J. D. W. Van Voorst, *Chem. Phys. Lett.*, **7**, 368 (1970).
- (9) T. Shida and S. Iwata, *J. Am. Chem. Soc.*, **95**, 473 (1973); T. Shida and W. H. Hamill, *J. Chem. Phys.*, **44**, 2369 (1966); E. J. Land and G. Porter, *Trans. Faraday Soc.*, **59**, 2027 (1963).
- (10) A. Ishitani and S. Nagakura, *Theor. Chim. Acta*, **4**, 236 (1966).
- (11) Y. Taniguchi, Y. Nishina, and N. Mataga, *Bull. Chem. Soc. Jpn.*, **45**, 2923 (1972).
- (12) H. Masuhara, T. Okada, N. Mataga, Y. Sakata, and S. Misumi to be submitted for publication.
- (13) M. Ottolenghi, *Acc. Chem. Res.*, **6**, 153 (1973).
- (14) The true path of triplet formation is still unknown and a possibility of its formation from the solvated ion pair has been given recently by using the picosecond laser photolysis method. (N. Nakashima and N. Mataga, *Chem. Phys. Lett.*, to be submitted for publication; N. Mataga and N. Nakashima, *Spectrosc. Lett.*, in press). The formation through a geminate pair was suggested by Ottolenghi et al. See, *Chem. Phys. Lett.*, **26**, 365 (1974). On the other hand, the triplet pyrene was measured before the decay of ion pairs in the pyrene-DCNB system. See ref 4.
- (15) N. Nakashima, N. Mataga, F. Ushio, and C. Yamanaka, *Z. Phys. Chem. (Frankfurt am Main)*, **79**, 150 (1972).
- (16) T. Mori, T. Okada, and N. Mataga, Preprint for the Symposium on Photochemistry, Nagoya, Japan, 1974, p 13.
- (17) N. Nakashima, N. Mataga, and C. Yamanaka, *Int. J. Chem. Kinet.*, **5**, 833 (1973).

Bubble Formation Around Positronium Atoms in High Surface-Tension Aqueous Solutions of Inorganic Materials

Béla Lévy* and Attila Vértés

Department of Physical Chemistry and Radiology, L. Eötvös University, 1088 Budapest, Hungary (Received May 16, 1975)

Positron lifetime measurements were performed in concentrated aqueous solutions of various inorganic materials (KCl, NaCl, MgCl₂, NH₄OH, NaOH). Strong correlation was found between the orthopositronium lifetime and the surface tension of the solutions up to 101 dyn/cm, not depending on the kind of solute molecules. The results were interpreted by the bubble model, though it was not expected to be valid by other authors for high surface-tension solutions. The bubble parameters were calculated. Similar results were found also for concentrated solutions of NaI in methanol.

Introduction

The positronium atom (Ps), the bound state between a positron and an electron, is formed in a condensed medium when the positron, after its slowing down, captures an electron. Orthopositronium, in which the spins of the two particles are oriented parallel, annihilates into three γ quanta in vacuo with a lifetime of 140 nsec. In condensed matter, however, the most common way of the annihilation for the positrons of o-Ps atoms is the so called pick-off annihilation into two γ quanta with an electron of the medium (the spin of which is antiparallel to the spin of the positron). Thus the lifetime is reduced to a few nanoseconds depending strongly on the properties of the medium.¹

Many attempts have been made to explain this general annihilation phenomenon and to find correlations between annihilation parameters and the properties of the medium. An empirical and simple correlation was recently discovered by Tao concerning the surface tension in molecular liquids.² This correlation was found to be valid also for two component liquid mixtures by Lévy et al.³ and was interpreted by the bubble model.⁴

The bubble model, which was first applied by Ferrell⁵ to explain the unexpected long o-Ps lifetime in liquid helium, takes into consideration the effect of surface tension on the energy balance around the positronium atom formed in a cavity of the liquid. This model for liquid helium was improved by Roellig⁶ and extended to low surface-tension molecular liquids by Buchikhin et al.^{7,8} Buchikhin pointed out that the model cannot be applied to high surface-tension liquids.⁷

There are, however, some facts which are inconsistent with this opinion. First of all, the lifetime of pick-off annihilation measured in the high surface-tension water does not show any significant deviation from Tao's empirical relationship² or from the similar one found for water-methanol and water-dioxane mixtures.³

Recently we published our results⁹ on the ineffectiveness of surface-active materials in water on the o-Ps lifetime. This fact was accounted for by the very low concentration and very large size of the solute molecules, which thus could not take part in bubble formation around the positronium atoms.

Thus it seemed to be of interest to examine the effect of those small inorganic molecules on o-Ps lifetime in concentrated aqueous solutions which are not positronium quenchers and increase the surface tension of water significantly. These relatively small molecules, at high concentration, are expected to be able to take part in developing equilibrium conditions around o-Ps atoms.

Bertolaccini et al.¹⁰ have measured o-Ps lifetimes in aqueous solutions of various alkali halides which are known to increase the surface tension of water to a small degree. Almost all alkali halides, indeed, have caused a slight decrease in o-Ps lifetime, as could be expected. The highest effect was found in KF solutions. Unfortunately, however, surface-tension data for this system are not available.

On the other hand, Tao and Green¹¹ have published lifetime data for aqueous solutions of oxyacids and hydrogen compounds. In most of these solutions the o-Ps lifetime increased with increasing concentration. At the same time

the surface-tension data, which are available only for a few of these systems, showed slight decreases.

In the present work we report the results of our lifetime measurements in concentrated aqueous solutions of KCl, NaCl, MgCl₂, NaOH, and NH₄OH, together with measurements in concentrated solutions of NaI in methanol.

We shall show that the bubble model is not in contradiction with the experimental results even for high surface-tension solutions up to 101 dyn/cm, and that the surface tension is one of the most important physical parameters in determining the pick-off rate in these concentrated solutions.

Experimental Section

The positron lifetime spectra were measured with a conventional fast-slow coincidence system, where a commercial ORTEC 437A time-to-amplitude converter was used. The time resolution in these measurements was fwhm = 520 psec using 1 in. × 1 in. NE 111 plastic scintillators and XP 1021 photomultipliers. The ²²NaCl positron source (about 20 μCi) was deposited between two thin (1.2 mg/cm²) Melinex Type 442 (ICI Ltd.) polyester films.

At least 2 × 10⁵ counts were accumulated for each spectrum.

All the chemical materials were reagent grade and were used without further purification. The samples in methanol were carefully deoxygenated by bubbling purified nitrogen through the solution. The aqueous samples were measured without deoxygenation.

The lifetime spectra were analyzed by computer programs of SIRIUS program system. Either the MQPA or the SDO2 program was used, both were written by Horváth.¹²

The MQPA program uses a multiexponential (in our case a two exponential) fit. The SDO2 program is a modified version of POSITRONFIT.¹³ Both programs give practically identical results for the longest lifetime attributed to orthopositronium annihilation. The SDO2 program gives a better fit using three-component analysis, where the shortest lifetime of about 0.1 nsec corresponds to parapositronium, while the medium lifetime of about 0.4 nsec corresponds to free positron annihilation.

It was estimated that about 5% of the positrons were annihilated in the source supporting foils. The foil spectrum was not subtracted from the measured spectra.

Results and Discussion

The results of the two-exponential analysis of the lifetime spectra are presented in Table I.

All the dissolved inorganic materials decrease the orthopositronium lifetime as compared to the pure solvent except for NH₄OH in water. At the same time, all the dissolved materials increase the surface tension of the solvent except NH₄OH, which decreases it in water. (See Table II.)

This exception clearly indicates that the change in the lifetime cannot be accounted for by a chemical quenching reaction, but must be mainly due to the change of the surface tension caused by the solutes.

The strong correlation between the pick-off rate ($\lambda_p = 1/\tau_2$) and the surface tension (γ) of the solutions is shown in Figure 1, with logarithmic scales on both its axes.

The measured points are situated nearly along a straight line corresponding to Tao's empirical formula²

$$\lambda_p = \kappa \gamma^\alpha \quad (1)$$

not depending on the kind of solute molecules. Values of κ and α were calculated to be 0.062 ± 0.004 and 0.51 ± 0.02 ,

TABLE I: Results of Positron Lifetime Measurements in Concentrated Solutions of Inorganic Materials^a

No.	Solvent	Solute	Solute concn. wt %	τ_1 , nsec	τ_2 , nsec	I_2 , %
1	H ₂ O			0.414	1.87	25.3
2	H ₂ O	KCl	11	0.420	1.82	22.0
3	H ₂ O	KCl	25	0.417	1.70	22.7
4	H ₂ O	NaCl	15	0.409	1.72	22.4
5	H ₂ O	NaCl	25	0.406	1.68	21.1
6	H ₂ O	MgCl ₂	25	0.413	1.67	25.2
7	H ₂ O	NaOH	14	0.378	1.69	28.8
8	H ₂ O	NaOH	25	0.354	1.57	27.5
9	H ₂ O	NaOH	36	0.356	1.46	26.2
10	H ₂ O	NH ₄ OH	51.5	0.427	2.18	22.7
11	CH ₃ OH			0.457	3.33	21.5
12	CH ₃ OH	NaI	20	0.466	3.00	24.8
13	CH ₃ OH	NaI	40	0.472	2.75	18.3

^a The average errors of the measured values, expressed as two times the standard deviations calculated by the computer, are ± 1.5 , ± 2.0 , and ± 3.0 rel. % for τ_1 , τ_2 , and I_2 , respectively.

respectively, by least-squares analysis of the data (λ_p was measured in nsec⁻¹ and γ in dyn/cm). These values are in good agreement with those found by Tao² or by us³ for water-methanol and water-dioxane mixtures.

This correlation between the pick-off rate and surface tension of solutions, as was pointed out in our earlier paper,⁴ can be accounted for by the bubble model. Although Buchikhin et al.⁷ pointed out that their model is valid only for low-surface-tension molecular liquids, our experimental results indicate that there is every reason to extend it also to these high-surface-tension solutions.

This model approximates the bubble around a Ps atom as a square well with spherical geometry. This potential well has a radius R , a depth U , and the energy of Ps in it (measured from the bottom of the well) is E .

The basic relations between the bubble parameters and the physical parameters of the medium are expressed by the following equations^{7,8}

$$\lambda_p = \pi r_0^2 c n Z_{\text{eff}} P(kR) = \pi r_0^2 c N_A \frac{Z_{\text{eff}}}{V} P(kR) \quad (2)$$

$$P(kR) = \sin^2 kR / (1 - kR \cot kR) \quad (3)$$

$$\frac{\sin^4 kR}{kR(\tan kR - kR)} = -\frac{\pi \hbar^2 \gamma}{m U^2} \quad (4)$$

$$k = (4mE/2)^{1/2} \quad (5)$$

Here r_0 is the classical radius and m the mass of an electron, c is the velocity of light, n is the number of molecules in unit volume, N_A is Avogadro's number, and V is the molar volume. $P(kR)$ expresses the quantum mechanical probability for the Ps atom coming out of the well. Z_{eff} is the effective number of annihilating electrons per molecule, which proved to be equal to the number of valence electrons per molecule.^{7,8}

Recently it was pointed out⁴ that formal correlation can be found between empirical eq 1 and the theoretically derived equations of the bubble model. The connection between them is given by the following equation:

$$\alpha = \left(\log \frac{\sin^2 kR}{1 - kR \cot kR} \right) / \left(\log \frac{\sin^4 kR}{kR(kR - \tan kR)} \right) \quad (6)$$

TABLE II: Equilibrium Bubble Parameters Calculated from the Lifetime Data^a

No.	V , $\text{cm}^3 \text{M}^{-1}$	Z_{eff}	$P(kR)$	kR	γ , dyn/cm	U , eV	R , Å	κ	α
1	18.02	8	0.27	2.18	72.9	1.37	3.13	0.075	0.46
2	18.37	8	0.28	2.16	74.9	1.36	3.07	0.079	0.45
3	19.00	8	0.31	2.13	78.9	1.35	2.99	0.090	0.43
4	18.14	8	0.29	2.15	77.6	1.36	3.04	0.084	0.44
5	18.34	8	0.30	2.14	82.4	1.39	2.96	0.088	0.43
6	18.52	8.47	0.29	2.15	83.4	1.41	2.98	0.084	0.44
7	16.97	8	0.26	2.16	81.0	1.41	3.02	0.082	0.45
8	16.45	8	0.29	2.15	90.6	1.48	2.91	0.087	0.44
9	16.16	8	0.31	2.13	101.0	1.53	2.84	0.091	0.44
10	26.55	11.53	0.24	2.22	56.0	1.28	3.40	0.066	0.48
11	40.73	14	0.19	2.28	22.4	0.91	4.35	0.060	0.51
12	39.81	13.70	0.22	2.24	25.6	0.91	4.19	0.066	0.50
13	39.28	13.25	0.24	2.22	29.5	0.92	3.99	0.071	0.48

^a The average errors estimated from the error of lifetime data are ± 0.01 , ± 0.015 , ± 0.02 , and ± 0.02 for $P(kR)$, kR , U , and R , respectively.

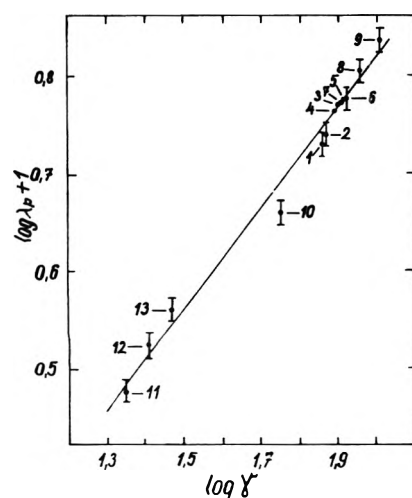


Figure 1. The pick-off rate (λ_p) of orthopositronium annihilation in concentrated solutions of inorganic materials in water or methanol as a function of the surface tension (γ). (The numbers refer to the numbers of measurements in Table I.)

e.g., the exponent in eq 1 is a function of the dimensionless quantity kR of the bubble model.

Using eq 2-6 and the well-known solutions for the finite potential well¹⁴ we have calculated the equilibrium bubble parameters and the corresponding κ and α values from our lifetime data. The results are presented in Table II. In the case of these solutions, average molecular weights (\bar{M}) and average effective electron numbers (\bar{Z}_{eff}), corresponding to the mole fractions of the systems, were used. The density and surface-tension data necessary to the calculations were taken from the literature.^{15,16}

With increasing surface tension the calculated bubble radius is decreasing, whereas the depth of the potential well is increasing.

It is surprising that kR , and as a consequence also α calculated by eq 6, show only moderate change with increasing surface tension. On the other hand, κ changes in higher degree, as was found also in the case of low-surface-tension liquids.⁴ In addition to this, κ depends to a greater degree also on the chemical character of the medium. As a consequence of these facts, the deviations from empirical eq 1 are probably due to this character of κ .

It is interesting to note that there is some correlation be-

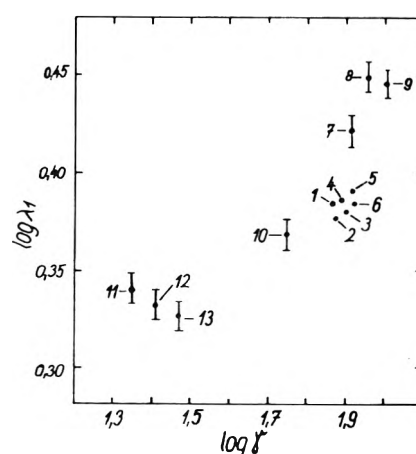


Figure 2. The annihilation rate of the short-lived component (λ_1) as a function of the surface tension (γ). (The numbers refer to the numbers of measurements in Table I.)

tween the surface tension and the shorter component of the lifetime spectra too. λ_1 increases with increasing surface tension (Figure 2). Unfortunately, however, this lifetime component is a mixed one, containing the parapositronium and free positron lifetimes. Thus it is difficult to say whether the annihilation of the very short-lived parapositronium or that of the free positrons account for this correlation.

As for the probability of o-Ps formation ($I_2\%$), we did not find any correlation with surface tension. KCl, NaCl, and NH_4OH showed a little inhibition while in aqueous solutions of NaOH the probability of Ps formation was a little bit higher than in pure water.

Conclusion

The main conclusion which can be drawn from the results is that the bubble model seems to be valid also for the high-surface-tension aqueous solutions, at least to the same extent as it was found to be valid for the low-surface-tension molecular liquids.⁷ The $R > 2.8 \text{ \AA}$ bubble radii for the solutions of highest surface tension are quite reasonable and do not suggest any impossibility of bubble formation. The other bubble parameters are also comparable to those found for the low surface-tension pure organic liquids.

The other conclusion to be drawn from our results is that

the small inorganic molecules (or small molecules in general) at high concentrations are able to take part in developing equilibrium conditions around o-Ps atoms in contrast to the large surface-active molecules that decreased the surface tension at small concentration, but did not affect the o-Ps lifetime.⁹ This fact, in our opinion, means that the surface tension does not always affect the o-Ps lifetime, but only if it can act in microscopic measures directly around the o-Ps atoms.

Our results show that the strong correlation between the surface tension and the pick-off quenching rate of o-Ps annihilation is a general phenomenon existing not only for the pure molecular liquids and their mixtures but for solutions with inorganic compounds as well.

Acknowledgment. We are grateful to Mrs. B. Jankó for technical assistance.

References and Notes

- (1) (a) J. H. Green and J. Lee, "Positronium Chemistry", Academic Press, New York, N.Y., 1964; (b) V. I. Goldanskii, *At. Energy Rev.*, **6**, 3 (1968);

- (c) J. A. Merrigan, J. H. Green, and S. J. Tao in "Physical Methods of Chemistry", A. Weissberger and B. R. Rositter, Ed., Vol. I, Part III, Wiley, New York, N.Y., 1972, p 501 ff; (d) J. H. Green, "Positronium and Mesonic Atoms" in "MTP International Review of Science", Vol. 8, Radiochemistry, A. G. Maddock, Ed., Butterworths, London, 1972.
- (2) S. J. Tao, *J. Chem. Phys.*, **56**, 5499 (1972).
- (3) B. Lévay, A. Vértes, and P. Hautojärvi, *J. Phys. Chem.*, **77**, 2229 (1973).
- (4) B. Lévay and A. Vértes, *Radiochem. Radioanal. Lett.*, **14**, 227 (1973).
- (5) R. A. Ferrell, *Phys. Rev.*, **108**, 167 (1957).
- (6) L. O. Roellig in "Positron Annihilation", L. O. Roellig and A. T. Stewart, Ed., Academic Press, New York, N.Y., 1965, p 127.
- (7) A. P. Buchikhin, V. I. Goldanskii, A. O. Tatur, and V. P. Shantarovich, *Zh. Eksp. Theor. Fiz.*, **60**, 1136 (1971) [*Sov. Phys. JETP*, **33**, 615 (1971)].
- (8) A. P. Buchikhin, V. I. Goldanskii, and V. P. Shantarovich, *Pis'ma Zh. Eksp. Teor. Fiz.*, **13**, 624 (1961) [*JETP Lett.*, **13**, 444 (1971)].
- (9) B. Lévay and A. Vértes, *J. Phys. Chem.*, **78**, 2526 (1974).
- (10) M. Bertolaccini, A. Bisi, and L. Zappa, *Nuovo Cimento*, **46**, 237 (1966).
- (11) S. J. Tao and J. H. Green, *J. Phys. Chem.*, **73**, 882 (1969).
- (12) D. Horváth in "Sirius Program System", KFKI, Budapest, 1972 (in Hungarian).
- (13) P. Kirkegaard and M. Eldrup, *Comput. Phys. Commun.*, **3**, 240 (1972).
- (14) L. I. Schiff, "Quantum Mechanics", McGraw-Hill, New York, N.Y., 1955.
- (15) For density data see J. Timmermans, "The Physico-Chemical Constants of Binary Systems in Concentrated Solutions", Interscience, New York, N.Y., 1960.
- (16) The surface-tension data are interpolated values from the "Handbook of Chemistry and Physics", 51st ed, R. C. Weast, Ed., The Chemical Rubber Co., Cleveland, Ohio, 1970-1971.

Formation of Hydroxyapatite at Low Supersaturation

A. L. Boskey* and A. S. Posner

Hospital for Special Surgery, Cornell University Medical College, New York, New York 10021 (Received March 10, 1975; Revised Manuscript Received September 26, 1975)

Publication costs assisted by the National Institutes of Health

The precipitation of hydroxyapatite, $\text{Ca}_{10}(\text{PO}_4)_6(\text{OH})_2$, from dilute solutions is discussed. The degree of supersaturation of these dilute solutions (10^5 to 10^9 , relative to hydroxyapatite) is in the range believed by some workers to exist at the sites of biological calcification. At these comparatively low supersaturations, hydroxyapatite is shown to be precipitated without the formation of the amorphous calcium phosphate precursor, which was previously believed obligatory. After initial formation, the hydroxyapatite crystals grow by a ripening process with little or no further nuclei forming. Calculations from electron microscope study of time-dependent crystal growth show the average crystal length l is related to time t as follows: $l = 13.7 \times 10^{-8} t^{0.37}$ (cm). Chemical analysis shows the precipitation and ripening process to be first order in Ca and OH and of order 1.25 in total PO_4 .

The precipitation of hydroxyapatite, $\text{Ca}_{10}(\text{PO}_4)_6(\text{OH})_2$, has been of great interest, particularly because of the relationship of this material to bone mineral.¹ In the presence of high concentrations of calcium and phosphate (total Ca and total PO_4 each greater than 10 mM) and at pH values greater than 6.8, the precipitation of hydroxyapatite is always preceded by the formation of an amorphous precursor,² distinct both chemically³ and structurally⁴ from the final product. The conversion of the amorphous precursor phase to hydroxyapatite has been shown to be an autocatalytic process with the rate of conversion at any given temperature dependent on the pH of the mediating solution.²

Preliminary studies indicated that in the presence of lower concentrations of calcium and phosphate (total Ca and total PO_4 each less than 2 mM), the first precipitate formed at pH 7.4 had an x-ray diffraction pattern, mor-

phology, and colloidal properties distinct from those of the amorphous calcium phosphate found in the presence of higher concentrations of reactants. However, after standing 24 hr, the hydroxyapatite found in these dilute solutions was comparable to the final product of the amorphous calcium phosphate transformation mentioned above. The purpose of this study was to determine the nature of the material precipitated initially from these dilute solutions and to determine the mechanism by which microcrystalline hydroxyapatite is produced under these conditions. Despite the fact that the exact calcium and phosphate concentration at the site of mineral formation is not known, the concentrations of the surrounding fluids are comparable to those used in this study, and therefore, an additional purpose of this study was to investigate a possible mechanism for the initial deposition of bone mineral.

Experimental Section

The precipitation of hydroxyapatite was initiated by the rapid mixing of CaCl_2 and Na_2HPO_4 solutions. Preliminary experiments were performed by adding 500 ml of 2.6 mM CaCl_2 to 500 ml of 2.0 mM Na_2HPO_4 . Prior to mixing, the pH of each of the reagents was adjusted to 7.4 by the addition of NaOH or HCl, as needed. The change in pH with time, after mixing, was monitored with a pH meter and the solution was maintained at pH 7.4 by the addition of 0.10 M NaOH. Aliquots (10 ml) for calcium and phosphate analysis and electron microscopy were removed immediately after mixing and at frequent intervals thereafter. No change in pH or initial calcium and phosphate concentrations was observed during the first 23–28 hr (induction period). In order to follow the reaction after this initial 23-hr period, the experimental set-up was modified so that the pH could be monitored by an automatic titrator (Mettler pH Stat). Using the titrator caused no changes in parameters measured after the induction period was completed, but did shorten the time during which no changes in solution concentrations were observable. (Since the reaction parameters after the completion of this induction period were independent of the method of mixing, for convenience, all subsequent experiments were performed using the automatic titrator.) Thus, in the bulk of the experiments, the desired volume of 0.133 M CaCl_2 was added to a solution of known ionic strength, described below, and the pH of the solution adjusted to 7.40. A solution of 0.100 M Na_2HPO_4 adjusted to pH 7.40 was added rapidly to the CaCl_2 solution. The reverse order of addition was also used with no change in results. The Ca/PO_4 molar ratio of the systems studied ranged from 1.0 to 1.7 while the $\text{Ca} \times \text{PO}_4$ mM products ranged from 0.25 to 1.7 mM². A number of solutions of different ionic strength (Table IV) and ionic species were used in the reaction to assess the effect of this parameter. Except for this series, all preparations were carried out at an approximately physiological ionic strength using 0.15 M NaCl.

All reactant solutions were prepared from Analytical Grade reagents and were filtered through fine sintered glass filters (4–5.5 μ) prior to use. Glassware was washed three times with 3 N HCl to remove any possible hydroxyapatite nuclei from the walls. Carbon dioxide was excluded from the reaction flask by bubbling prepurified nitrogen through the solution, or running the reaction in a nitrogen atmosphere. All experiments were performed in covered vessels at $26.5 \pm 0.3^\circ\text{C}$. After the initial mixing, solutions were stirred at a constant reproducible rate with a Teflon-coated, magnetic stirrer. The pH of the reaction solution was maintained at 7.40 using a Mettler automatic titrator capable of adding acid and/or base in volume aliquots as small as 5×10^{-4} ml. Fischer certified 0.1 N HCl and 0.1 N NaOH were used to adjust pH. The calibration of the combination electrode was checked prior to and after each experiment. The normality of the base was checked periodically against potassium hydrogen phthalate to ensure that no carbon dioxide had been absorbed.

The reaction was monitored in terms of the uptake of hydroxyl ions, the change in solution calcium and phosphate, and the changing nature of the solid as determined by electron microscopy and selected area electron diffraction. Calcium ion activity in the solution was measured with an Orion Select-ion electrode, placed directly in the reaction flask. The electrode was calibrated daily against standard

solutions of similar composition, pH, and ionic strength. (In order to maintain reproducibility the electrode's internal and external filling solutions were changed every 4 days.) At specific intervals, aliquots were removed from the reaction vessel, transferred to an ice bath to slow the reaction, and centrifuged at 2500 rpm for 15 min. The supernates were saved for analysis and the pellets weighed and analyzed. Solid material sufficient for analysis was present only after 24 hr.

In order to determine if the presence of the Select-ion electrode in the reaction flask had any effect on the observed decrease in calcium or hydroxyl uptake, an independent set of experiments was performed. In these, the Ca electrode was not placed in the reaction vessel, instead, small aliquots, which were not replaced, were taken from the reaction flasks, and the Ca activity determined using the Select-ion electrode outside of the reacting system. The data obtained from these experiments did not differ from that obtained when the Ca electrode was left in the reaction vessel.

Calcium was determined by atomic absorption spectrophotometry⁵ and inorganic phosphate by optical analysis of a molybdenum heteropolyphosphate complex.⁶ The analytical, as opposed to the Ca electrode values for Ca, were used in all kinetic analyses. The solution calcium activities calculated from these results agreed within $\pm 5\%$ with those measured with the calcium electrode, both internal and external to the reaction flask. Sintered-glass filters (4–6- μ pore diameter) did not remove the fine precipitates as efficiently as centrifugation, as evidenced by the fact that Ca analysis for the filtrate was 20% higher, on average, than for the centrifugate. The equilibrium concentrations of each of the phosphate ionic species and calcium phosphate ion pairs present at the pH of the experiment were calculated by an iterative process from the appropriate dissociation constants^{7,8} in order to evaluate the degree of supersaturation. Activity coefficients for Ca^{2+} , PO_4^{3-} , and OH^- were estimated from the Debye-Hückel equation.⁹

Single drop aliquots for electron microscope analysis were removed from the reaction flask immediately after mixing, at 2–5-min intervals during the first hour, at 30-min intervals for the next 8 hr, and at 8–12-hr intervals for the next 2–5 weeks. Electron microscopy was used to confirm that there were no solid phases of electron density comparable to hydroxyapatite in the reactant solutions before mixing. Electron microscopic examinations of the precipitate were carried out using a JEOL-100B transmission electron microscope operating at 80 kV with a liquid nitrogen cooled specimen holder. Samples were prepared for microscopy by placing one drop of solution on a 200 mesh copper grid coated with either formvar, collodion, colloidal carbon, or carbon alone. Excess water was removed by touching lint-free filter paper to the grid and immediately placing the grid in a vacuum desiccator.

The microscope magnification was calibrated using the resolution of a lattice image of a 8.2 \AA^{10} corresponding to the d spacing of the 100 planes of well-crystallized hydroxyapatite. Selected area diffraction of the precipitates was performed at a magnification of 50000 \times using a 20- μ limiting field aperture. The camera constant for each diffraction pattern was determined from the selected area diffraction of standard thallium chloride crystals already mounted in the multiple sample holder of the microscope so that the same electric and magnetic conditions prevailed. Dark field imaging was used to establish the monocrystalline nature

TABLE I: Comparative Degrees of Supersaturation Relative to Hydroxyapatite (HA) and Amorphous Calcium Phosphate (ACP) in Systems from which Hydroxyapatite is Formed

Solution concn, mM		Calcd supersaturations			First precipitate observed	Ref
Total calcium	Total phosphate	S_{CaP}^a	$S_{Ca(HA)}^a$	$S_{Ca(ACP)}^a$		
0.50	0.50	9.0×10^5	22	-0.7	HA dots ^a	This work
1.33	1.00	8.9×10^6	44	-0.1	HA dots ^a	This work
1.67	1.00	2.4×10^9	47	0.3	HA dots ^a	This work
1.562	0.973	$1.23 \times 10^{11} b$	43.6 ^b	10^{-3}	ACP	12
3	3	6×10^{11}			ACP	19
1.2	20	1×10^{18}			Octacalcium phosphate	20
12.0	10.8	1×10^{22}	500	7	ACP	2
1.46	2.58	2×10^4			c	11
2.35	2.80	2×10^7			d	11

^a These terms defined in text. ^b Values quoted from Nancollas and Tomazic, ref 12. ^c Extracellular fluid from hypertrophic rat cartilage. ^d Normal rat serum.

and orientation of certain hydroxyapatite crystallites, and through focus series photography was used for each field observed. The particle size measurements for each time period aliquot were made on at least ten fields within each grid so that a minimum of 100 particles was observed.

Results and Discussion

The range of calcium and phosphate concentrations used in this experiment (Table I) are comparable to those reported for synovial fluid¹¹ and are appreciably lower than those used in earlier studies² in which amorphous calcium phosphate was invariably a precursor to hydroxyapatite. In order to compare the composition of the solutions used in this study to those used by other researchers, and to predict what calcium phosphate phases were likely to form, the degree of supersaturation relative to hydroxyapatite (HA) and amorphous calcium phosphate (ACP) was calculated using Nancollas and Tomazic's method.¹² As in their work, two quantities were calculated, the supersaturation in terms of ionic activity product, S_{CaP} , and the supersaturation in terms of free ionic calcium S_{Ca} . The value of S_{CaP} was defined as $IP - K_{sp}/K_{sp}$ where the ion product, IP, for hydroxyapatite, in terms of the activity of ionic calcium a_{Ca} and ionic phosphate a_{PO_4} is equal to $a_{Ca}^5 a_{PO_4}^3 a_{OH}$. S_{Ca} was defined equal to $[Ca^{2+}]_t - [Ca^{2+}]_{\infty} / [Ca^{2+}]_{\infty}$ where $[Ca^{2+}]_t$ is the concentration of ionic calcium at the start of the experiment and $[Ca^{2+}]_{\infty}$ the concentration value at equilibrium. For hydroxyapatite, $[Ca^{2+}]_{\infty}$ was taken as the concentration of calcium at the end of the experiment (2-3 weeks). For amorphous calcium phosphate $[Ca^{2+}]_{\infty}$ had to be estimated since amorphous calcium phosphate transforms to hydroxyapatite in water and thus does not reach an equilibrium calcium level. In this case it was assumed that $[Ca^{2+}]_{\infty}$ was 1.51 mM, the highest calcium concentration observed above amorphous calcium phosphate in water at pH 7.4, prior to its transformation to hydroxyapatite.²

The supersaturation values for the experimental conditions reported in this paper are compared to values used by others and to those reported as *in vivo* concentrations in Table I. In each case where a precursor is observed prior to the formation of hydroxyapatite, its identity or composition is noted in this table. The solubility product K_{sp} used by Nancollas and Tomazic¹² was chosen to facilitate comparison of our results with theirs. It should be noted that this K_{sp} represents the value obtained for large hydroxyapatite crystals¹³ and it can be predicted from theory¹⁴ that the solubility product for the smaller synthetic and

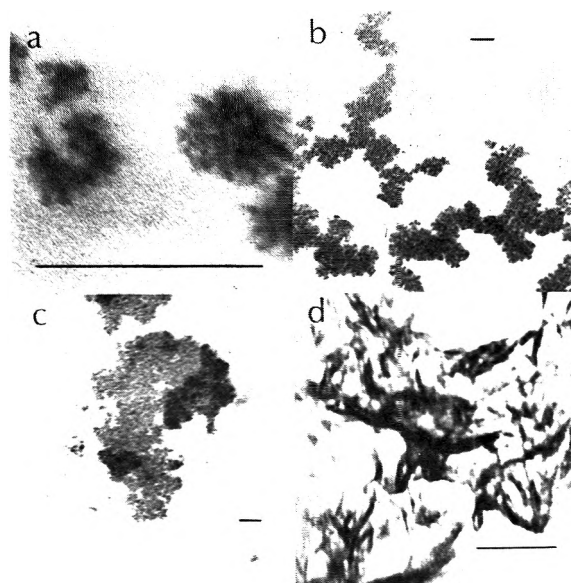


Figure 1. Electron micrographs selected from through focus series by sampling dilute solutions ($S_{CaP} = 10^6$) of Ca and PO_4 at pH 7.4 and 26°C. Scale shown represents 0.1 μ ; (a) 3 min, (b) 120 min, (c) 6 hr, and (d) 28 hr after the end of the induction period.

bone crystals dealt with in this paper would be larger. Thus, the supersaturation values in Table I should not be regarded as absolute, but just comparative numbers. From this table it can be seen that the solutions used in this experiment, as well as those reported *in vivo*, have a lower degree of supersaturation with respect to well-crystallized hydroxyapatite than those solutions from which amorphous precursor phases were obtained. In addition, the table shows that the solutions of this experiment are undersaturated, or only slightly saturated relative to the amorphous precursor.

Micrographs prepared from solution aliquots taken at intervals throughout the course of the reaction are shown in Figure 1. For the first 13-35 min after mixing of reactants all grids examined were blank. Between 13 and 35 min a "dot-like" material approximately 25 Å in diameter was observed (Figure 1a). The size and morphology of the initial material were independent of the type of grid coating, suggesting that the coating did not provide a nucleation site. The selected area electron diffraction pattern of this initial material, though broadened, was distinct from that

TABLE II: Diffraction Identification of Precipitated Materials

Major lines from x-ray diffraction of hydroxyapatite ^a			Observed selected area electron diffraction d spacings ^b				Hydroxyapatite	Amorphous calcium phosphate
			Experimental solids at corrected time, <i>t</i> , min					
<i>hkl</i>	<i>d</i>	<i>I/I</i> ₀	<i>t</i> = 3	<i>t</i> = 360	<i>t</i> = 1440			
100	8.17	12	7.9 w	8.0 w	8.0 w	8.2 w		
002	3.44	40	3.45 s,b	3.45 s	3.40 s	3.40 s		
210	3.08	18						
211	2.814	100						
112	2.778	60	2.78 s,b	2.77 s,b	2.75 s,b	2.78 s	3.0 s,b	
300	2.720	60						
222	1.943	30	1.82 w,b	1.88 w,b	1.90 w,b	1.95 w		
213	1.841	40				1.85 w	2.0, b	

^a Reference 14, ^b s = strong intensity; w = weak intensity; b = broad band, center used to approximate *d*.

observed for amorphous calcium phosphate. As the reaction proceeded the dots became larger and the diffraction pattern sharpened and after 24 hr long microcrystalline particles were observed (Figure 1d). The selected area diffraction pattern for this 24-hr microcrystalline material was identical with the pattern for synthetic hydroxyapatite prepared in more concentrated solutions at the same pH.

Table II lists the average "d" spacings calculated from the electron diffraction data of the initial "dot-like" material as well as from solid material observed throughout the experiment. For comparative purposes the table lists the *d* spacings of a calculated pattern of well-crystallized hydroxyapatite.¹⁵ The electron diffraction pattern of the "dot-like" material is distinct from that observed for amorphous calcium phosphate and comparable with those of synthetic hydroxyapatite. The two strongest bands in the diffraction pattern of the "dot-like" material can be attributed to the 002 plane and to a combination of the poorly resolved 211, 112, and 300 planes of hydroxyapatite, respectively. Although the broad band of amorphous calcium phosphate spans the region in which these peaks occur (2.7–3.5 Å), the strong lines at 3.45 (002) and 2.75–2.78 Å (211, 112, 300) clearly distinguish the "dot-like" material from amorphous calcium phosphate. Furthermore, the weak 100 reflection of hydroxyapatite was present in the diffraction patterns prepared from the dilute reaction (dots) and absent from those of the amorphous material. In addition, the weak high angle reflection pattern of the "dot-like" material, which was appreciably sharper than the broad high angle band in amorphous calcium phosphate and which is centered at a lower angle than this amorphous reflection, was attributable to the overlap of the 222 and 213 reflections of hydroxyapatite. Thus, from all of these observations we can conclude that the "dot-like" material is a poorly crystalline hydroxyapatite.

The fact that all solids precipitated in this experiment including the initial precipitate are apatitic in nature is further confirmed by the chemical analysis of the reaction solution. Table III shows that $\Delta\text{Ca}/\Delta\text{PO}_4$ does not vary significantly from the mean value of 1.67 throughout the time of the experiment. These values are defined as follows: ΔCa is the difference between the initial Ca concentration and the Ca concentration at time *t*; ΔPO_4 is the difference between the initial PO_4 concentration and the PO_4 concentration at time *t*. The data in this table are based on all experiments performed at ionic strength of 0.15 *M*, and includes observations from solutions containing different initial amounts of calcium and phosphate. Each individual experimental result was based on at least five solution analyses, and the average includes at least five individual experi-

TABLE III: Changes in Solution Calcium and Phosphate and Hydroxyl Concentrations during Crystal Growth at Low Supersaturations

Cor time, ^a min	Typical concn, ^b mM			Mean $\Delta\text{Ca}/\Delta\text{PO}_4$ molar ratio ^c
	Ca	PO_4	OH	
0	1.333	1.130	0	
5				1.67 ± 0.06
15	1.160	1.028	0.025	1.69 ± 0.05
60				1.69 ± 0.04
120	1.140	1.013	0.050	1.67 ± 0.06
180	1.115	0.997	0.061	1.59 ± 0.08
300	1.090	0.892	0.077	1.73 ± 0.07
360	1.040	0.825	0.086	1.69 ± 0.05
1440	0.338	0.565	0.200	1.61 ± 0.06
1800				1.69 ± 0.08
2800				1.60 ± 0.08
3240	0.265	0.459	0.228	1.70 ± 0.06
10080				1.66 ± 0.05

^a Time after conclusion of induction period. ^b Concentrations measured in experiment no. 307, ionic strength 0.156 *M*. ^c $\Delta[\text{Ca}] = [\text{Ca}]_{\text{initial}} - [\text{Ca}]_t$, $\Delta[\text{PO}_4] = [\text{total PO}_4]_{\text{initial}} - [\text{total PO}_4]_t$. Mean values for all experiments at ionic strength 0.156 *M*.

ments. The lack of systematic deviation of $\Delta\text{Ca}/\Delta\text{PO}_4$ from 1.67, the expected ratio for hydroxyapatite, during the course of the experiment indicates that only one phase is being formed and that the precipitated phase has the Ca/ PO_4 ratio expected for hydroxyapatite. No direct chemical analysis of the initial material was possible due to the low concentration of product. However, material obtained at the conclusion of the experiments has a Ca/ PO_4 molar ratio of 1.65 ± 0.05 . Calcium and phosphate concentrations and OH uptake measured during a typical experiment at $S_{\text{CaP}} = 10^9$ are also shown in this table. Throughout the entire reaction 1 mol of hydroxyl is added to the solution relative to every 5 mol of calcium and 3 mol of phosphate consumed. Although the observed hydroxyl uptake is less than that predicted (on the basis of phosphate equilibria) for the formation of hydroxyapatite, the invariant average $\Delta\text{Ca}/\Delta\text{PO}_4$ values, combined with the diffraction data, are convincing proof that the "dot-like" material is hydroxyapatite. However, due to the complexity of the precipitation process and the multiple equilibria involved the analytical data cannot stand alone.

It can be seen from the micrographs in Figure 1 that the initially "dot-like" hydroxyapatite grows essentially in only one dimension as a function of time. The axis along which growth was occurring was shown by a combination of dark field and diffraction analyses to correspond to the hydroxyapatite *c* axis. A compilation of the change in average

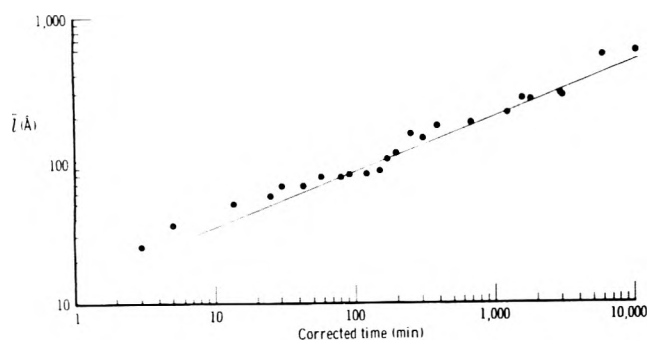


Figure 2. A log-log plot of average hydroxyapatite particle size, \bar{l} , vs. corrected time, t , for all data obtained at $S_{CaP} = 10^8$, 26°C , and pH 7.4.

length with time for 37 independent experiments performed at $\mu = 0.15$ and $S_{CaP} = 10^8$ is shown in Figure 2. Time zero for each experiment was defined as the time of conclusion of the induction period. That is, the time of initial hydroxyl uptake is coincident with the time of the first measurable drop in solution calcium activity measured by the Ca electrode. The straight line shown in this figure was calculated by the method of least squares to be $\bar{l} = 13.7 \times 10^{-8} t^{0.37}$ (cm), where \bar{l} is the average length in the c axis direction, and t is the time corrected for the induction period (hereafter referred to as corrected time).

The number of individual hydroxyapatite particles present at any given time was estimated from the change in solution calcium concentration and the average particle size at that time. Typical values for an experiment with the initial $\text{Ca} = 1.33 \text{ mM}$, initial $\text{PO}_4 = 1.0 \text{ mM}$, are given in Figure 3. From the figure it can be seen that after the first 1.5 hr beyond the completion of the induction period no new particles are formed and the process is one of growth by ripening. From the data in this figure and the solution chemistry it can be predicted that no nucleation will take place below a supersaturation S_{CaP} of ca. 10^2 .

The rate of the crystal proliferation reaction was a function only of the ionic strength, pH, temperature, and degree at supersaturation in the reaction medium and did not depend on the method in which the reactants were added or their order of addition. However, the observed induction times (i.e., the time required for the onset of nuclei formation) did depend upon the method of addition of reactants. The induction times in those experiments where large volumes of dilute calcium and dilute phosphate solutions were mixed together were appreciably longer (23–28 hr) than the induction times in experiments where, due to the configuration of the pH stat, more concentrated calcium (or phosphate) solutions had to be added to dilute phosphate (or calcium) solutions (23–35 min at $S = 10^9$). In the latter experiments the shorter induction periods are probably attributable to the formation of large ion clusters because of concentration gradients during the addition of the more concentrated reagents. In all experiments at the same degree of supersaturation, regardless of the induction time, once the induction period was completed the rate of disappearance of calcium and phosphate did not vary outside the limits of experimental error. Furthermore, similar sizes, morphology, and selected area diffraction patterns were observed for the first solid seen by electron microscopy at the completion of both the long and short induction periods. The kinetic analyses were performed on the pH-Stat experiments with shorter induction periods.

TABLE IV: Effect of Ionic Strength on Rate of Hydroxyl Ion Uptake at Low Supersaturations

Ionic strength, M	Salt	Av half-life, min
5.0	NaCl	30 ± 5
5.0	KCl	35 ± 5
2.0	NaCl	205 ± 7
2.0	KCl	200 ± 10
1.0	NaCl	265 ± 15
1.0	KCl	320 ± 15
0.5	NaCl	285 ± 5
0.5	KCl	285 ± 5
0.15	NaCl	355 ± 18
0.15	KCl	350 ± 15
0.05 ^a	NaCl	350 ± 5
0.02 ^a	NaCl	325 ± 7
0.001 ^a	TEA ^b	330 ± 5
0.001 ^a	NaCl	340 ± 10
0.005 ^a	TEA	335 ± 10

^a Corrected for the concentrations of Ca, PO_4 , and titrants added before start of experiment. ^b Triethanolamine-HCl.

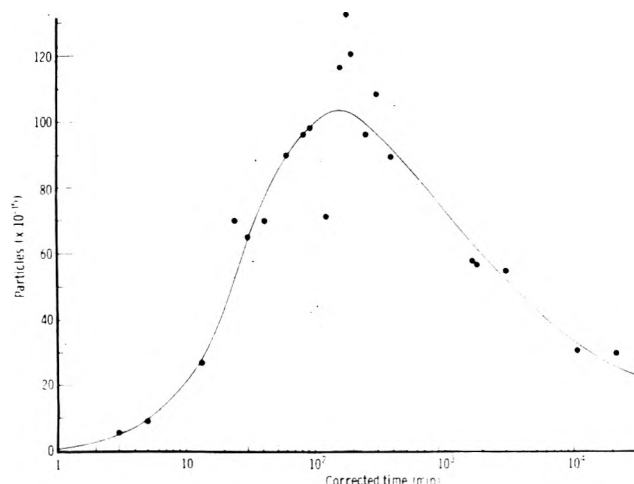


Figure 3. A plot of the calculated number of particles of hydroxyapatite as a function of corrected time, t ; $S_{CaP} = 10^8$, pH = 7.4, 26°C . These data, obtained from a single run, are typical of all of the experiments.

The effect of ionic strength on the course of the reaction was evaluated by assessing the half-life, measured in terms of the time required to consume one-half the total number of hydroxyl ions, for the reaction carried out with the same initial concentration of calcium and phosphate but at differing ionic strengths and in the presence of differing ionic species. Typical half lives at different ionic strengths are listed in Table IV. From this table it can be seen that with decreasing ionic strengths the half-life levels off and becomes constant so that below $\mu = 10^{-1} M$ the reaction rate is essentially independent of ionic strength and certain extraneous ions.

An analysis of the change in Ca, total PO_4 , and hydroxyl concentrations with time, for $\mu = 0.15 M$, showed the total reaction (nucleation and growth) to be first order in Ca^{2+} and OH^- and of order 1.25 in total phosphate. The reaction orders were determined by a variety of standard kinetics methods as shown in Table V. The validity of the reaction orders is emphasized by the agreement among the different independent methods. It should be noted that the reaction order for Ca and PO_4 were found to be the same by Mohan and Nancollas¹⁶ in their study of hydroxyapatite crystal growth.

TABLE V: Rate Constants Calculated for the Formation of Hydroxyapatite at Low Supersaturation, pH 7.40, and 26°C

Method of calculation	k_{Ca} , ^a min ⁻¹	k_{PO_4} , ^a mol ^{-1/4} min ⁻¹	k_{OH} , ^a min ⁻¹
Half-life dependence ^b	9×10^{-3}	4×10^{-4}	2×10^{-3}
Powell's dimensionless method ^c	9×10^{-3}	2×10^{-4}	1.6×10^{-3}
van't Hoff Differential method ^c	9.5×10^{-3}	1.3×10^{-4}	1.5×10^{-3}
Least-squares analysis of integrated rate equation ^c	9.46×10^{-3}	1.36×10^{-4}	1.12×10^{-3}

^a Order determined: Ca, $n = 1$; PO₄, $n = 1.25$; OH, $n = 1$. ^b Reference 25. ^c Reference 26.

Conclusions

Our experiments show that it is possible to precipitate hydroxyapatite without forming an amorphous precursor phase if the solution is sufficiently dilute. The fact that amorphous calcium phosphate is not observed to be a precursor to hydroxyapatite at these low supersaturations is not surprising since our approximations (Table I) suggest that the system is undersaturated with respect to amorphous calcium phosphate. Nancollas and Tomazic¹² working at similar supersaturations in the presence of large hydroxyapatite seeds concluded from solution analysis that hydroxyapatite was formed directly if S_{CaP} was low (10^7) and that at higher supersaturations (10^{11}) amorphous calcium phosphate formed on the hydroxyapatite surface. Our experiments, performed in the absence of large hydroxyapatite seeds, confirm the fact that hydroxyapatite can be formed without an amorphous calcium phosphate precursor at low supersaturations.

The observation that hydroxyapatite can be formed from very dilute solutions without the intermediate precipitation of amorphous calcium phosphate initially appears to contradict the findings of Termine et al.¹⁷ and Eanes,³ who concluded that amorphous calcium phosphate was an obligatory precursor to hydroxyapatite. However, the most dilute solutions used by these workers had $Ca \times PO_4$ mM² products of 7.1 (at pH 7.4) and 4.5 mM² (at pH 10), respectively. The degrees of supersaturation in these solutions, calculated as described in the text, would correspond to 10^{12} and 10^{14} (S_{CaP} , relative to hydroxyapatite) and approximately 1 (S_{Ca}) relative to amorphous calcium phosphate. Thus, not only were these solutions much more concentrated than those used in our experiments, but, in addition, based on the calculation of S_{Ca} , one would have a priori predicted amorphous calcium phosphate precipitation. It is interesting to speculate that had the earlier work been carried out in more dilute solutions an "obligatory" precursor might not have been proposed. Furthermore, it is apparent from our work and that of others^{3,12,18-20} that the pH, and specific concentrations of calcium and inorganic phosphate, as well as the ionic strength, temperature, and presence of heteronuclei, rather than calcium phosphate millimolar products alone, are critical in determining the initial phase precipitated in the course of hydroxyapatite formation.

In the dilute solutions where only one phase is seen, the growth of hydroxyapatite appears to occur by a ripening process after a brief period during which nucleation and growth probably take place simultaneously. The equation of crystal growth calculated from experimental data is comparable to the theoretical calculation by Nielsen²¹ for Ostwald ripening. In addition, in our system it is seen that the number of particles decrease as a function of time suggesting that the smaller more soluble particles dissolve and

redeposit on the larger particles. Again, this reinforces the view that a ripening process is taking place.

Finally, since amorphous calcium phosphate has recently been shown by electron diffraction to be a part of embryonic bone²² and since radial distribution analysis has shown that the mitochondria of calcifying cells contain large amounts of this amorphous material,²³ one can infer from our experiments that the concentrations at the sites of mineralization are appreciably higher than those used in our experiments. It is interesting to note, however, that the mineral observed in fetal bone has a morphology and size comparable to the "dot-like" solutions.²⁴ Since biological calcification occurs in a far more complex environment than that described in this paper, the exact mechanism of mineralization remains to be determined.

Acknowledgment. This is publication No. 101, from the Laboratory of Ultrastructural Biochemistry and supported by Grant No. DE-04141 and AM 05414 of the National Institutes of Health. We wish to thank Dr. Foster Betts for his helpful discussions, and Ms. Zoraida Navarro for her technical assistance.

References and Notes

- See, for example, the following reviews: (a) H. Fleisch, *Clin. Orthop.*, **52**, 170 (1964); (b) J. C. Elliot, *Calcif. Tissue Res.*, **3**, 293 (1969); (c) J. D. Termine, *Clin. Orthop.*, **85**, 207 (1972); (d) G. L. Meyer, J. D. Erick, G. H. Nancollas, and J. N. Johnson, *Calcif. Tissue Res.*, **10**, 91 (1972); (e) A. S. Posner, *Fed. Proc.*, *Fed. Am. Soc. Exp. Biol.*, **32**, 1933 (1973).
- A. L. Boskey and A. S. Posner, *J. Phys. Chem.*, **77**, 2313 (1973).
- E. D. Eanes, *Calcif. Tissue Res.*, **5**, 133 (1970).
- F. Betts and A. S. Posner, *Trans. Am. Crystallog. Assoc.*, **10**, 73 (1973).
- J. B. Willis, *Spectrochim. Acta*, **16**, 259 (1960).
- S. R. Crouch and H. V. Malmstadt, *Anal. Chem.*, **39**, 1034 (1967).
- C. E. Vanderzee and A. S. Quist, *J. Phys. Chem.*, **65**, 118 (1961).
- A. Chughtai, R. Marshall, and G. H. Nancollas, *J. Phys. Chem.*, **72**, 208 (1968).
- E. A. Moelwyn-Hughes, "Physical Chemistry", 2nd ed, Pergamon Press, New York, N.Y., 1961, Chapter XVIII.
- K. A. Selvig, *J. Ultrastruct. Res.*, **41**, 369 (1972).
- D. S. Howell, J. C. Pita, J. F. Marquez, and J. E. Madruga, *J. Clin. Invest.*, **47**, 112 (1968).
- G. H. Nancollas and E. Tomazic, *J. Phys. Chem.*, **78**, 2218 (1974).
- J. S. Clark, *Can. J. Chem.*, **33**, 1696 (1955).
- A. G. Walton, "The Formation and Properties of Precipitates", Interscience, New York, N.Y., 1967, Chapter 4.
- ASTM Stand.* **9**, 432 (1960).
- G. H. Nancollas and M. S. Mohan, *Arch. Oral Biol.*, **15**, 731 (1970).
- J. D. Termine and A. S. Posner, *Arch. Biochem. Biophys.*, **140**, 307 (1970).
- H. Newesely, *Monat. Chem.*, **97**, 468 (1966).
- Lj. Brecevic and H. Furedi-Milhofer, *Calcif. Tissue Res.*, **10**, 82 (1972).
- H. Furedi-Milhofer, B. Purgaric, Lj. Brecevic, and N. Pavkovic, *Calcif. Tissue Res.*, **8**, 142 (1971).
- A. E. Nielsen, "Kinetics of Precipitation", MacMillan, New York, N.Y., 1964, p 115.
- W. J. Landis, B. T. Hauschka, and M. C. Paine, Orthopaedic Research Society, San Francisco, Calif., Feb-Mar 1975, Abstract No. 43.
- F. Betts, N. C. Blumenthal, A. S. Posner, G. L. Becker, and A. L. Lehninger, *Proc. Nat. Acad. Sci. U.S.A.*, **72**, 2088 (1975).
- H. J. Hohling and H. Schopfer, *Naturwissenschaften*, **55**, 545 (1968).
- K. J. Laidler, "Chemical Kinetics", 2nd ed, McGraw-Hill, New York, N.Y., 1961, Chapter 1.
- A. S. Frost and R. G. Pearson, "Kinetics and Mechanism", Wiley, New York, N.Y., 1961, pp 14-15.

Kinetics of Radical Decay in Crystalline Amino Acids. II. High-Temperature Study

Avinash Joshi and Russell H. Johnsen*

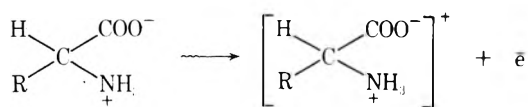
Department of Chemistry, Florida State University, Tallahassee, Florida 32306 (Received June 20, 1975)

Publication costs assisted by the Energy Research and Development Administration

Radical decay in x-irradiated L-leucine, and DL-valine, L- and DL-alanine, and L-arginine hydrochloride was studied between 300 and 430 K. Free radical decay was observed to take place with two distinct rates: an initial short duration process having an activation energy of 18 kcal/mol and a second, slower process. In most cases, the fraction of radicals decaying by the faster process is the same as the very slow room-temperature decay previously observed.¹⁴ The major process has a 3–6-kcal/mol higher activation energy. There is no evidence of radical conversion in either the initial or the slower process. However, in at least two cases residual peroxy radicals were observed at the termination of the slower process. Both decays obey second-order rate laws. The peroxy radical in at least one case decayed by a second-order law also. Vacancy controlled bulk diffusion is proposed for the major process, and the initial process is thought to be a conformationally aided bulk diffusion. It was observed that at any given temperature the spin concentration reaches a constant value. Increasing the temperature results in a second decay to a new constant value in a stepwise fashion. In the case of hydrated L-arginine hydrochloride and its partially deuterated derivative, the decay was found to be related to the dehydration process: A rapidly propagating radical transfer mechanism involving hydrogen abstraction is postulated for this decay process.

Introduction

The free radicals produced by ionizing radiation in many amino acids have been identified by ESR, ENDOR, and ELDOR techniques.^{1–8} In all this work it has been realized that, in general, the initially produced free radicals are not stable at room temperature. They undergo series of conversions before a radical, relatively stable at room temperature, is produced. Many of these conversions have been studied. It is well known that organic compounds are ionized, when irradiated, into electrons and positively charged molecules. These electrons are seen⁹ to be trapped in some frozen glasses. Thus the initial process in case of amino acids is thought to be

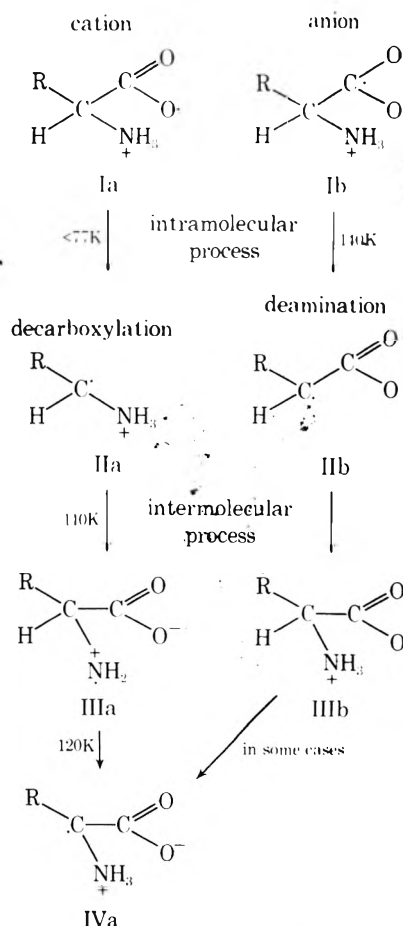


This is then followed by the sequence of events described by Saxebol¹⁰ as shown in Scheme I.

The rates of radical conversions have been studied by many,^{10–12} and are, in most cases, found to fit first-order kinetics. The activation energies range from 5 to 15 kcal/mol. A first-order rate process is not surprising since the radicals either decompose, which is a true first-order process, or the radicals undergo a reaction with the parent nonradical molecules which are in abundance. The latter reaction is then pseudo first order.

The free radicals observed at room temperature (IVa, IIIb) were once considered to be completely stable¹³ at this temperature. However, recently it was shown that these so-called stable free radicals do, in fact, decay¹⁴ spontaneously at room temperature. The decay was shown to be second order, and a vacancy controlled bulk diffusion mechanism was proposed. In this study it was also noted that, after initial decay, there is frequently a spin concentration which is relatively more stable at room temperature. This leads to the observation of "stepwise" decay.

Scheme I



Mikhailov, Lebedev, and Buben^{15,16} studied the decay kinetics of irradiated glycine and a number of other compounds and discovered that the decay took place stepwise, without a change in the type of radical, and that the value

of the radical concentration stable at a given temperature was a function of the final temperature and not the rate of heating. Three models were proposed: (1) the radicals are localized in zones with different softening temperatures (varying rigidity); (2) the radicals are fixed in traps with different stabilization energies; and (3) the probability of recombination of pairs depends on the distance between the radical sites.

Horan and coworkers¹⁷ reported that radiation-induced organic free radicals stable at room temperature decay by a first-order process and that the temperature dependence of the decay was equivalent to the temperature dependence for electrical conductivity in crystals of this type. It may be noted that of the many compounds studied by this group, only one compound was common in the comparison of the two processes. In this mechanism the unpaired electron of the free radical is either carried by the parent nonradical molecules until it encounters an acceptor site or, in the alternate case, heating causes matrix molecules to ionize. The negative ions thus formed transport the electrons to the radical by conducting them through the medium. However, as mentioned earlier,¹⁰ the ionized species appear to be very unstable and undergo radical conversions even at temperatures as low as 77 K. Thus formation of ionic species by heat would aid in the formation rather than destruction of free radicals. Also the electron-hopping mechanism does not explain the steplike nature observed by others, unless it is assumed that these unpaired electrons are distributed in the system in traps of different depths, which is very difficult to explain if the electrons are as mobile as postulated.

The correlation between the decay process at room temperature reported earlier from this laboratory and those at higher temperature reported by Horan was not obvious. The present work was done in order to resolve the discrepancy in the two reports.

Experimental Section

Polycrystalline as well as single crystal samples were prepared. Polycrystalline DL-valine, L-leucine, and L-alanine were from International Chemical and Nuclear Corp. of ICN grade, and were used without further purification. DL-alanine was from Eastman Organic Chemicals, and L-arginine HCl was from Calbiochem. The single crystals were grown from aqueous solutions by slow evaporation. The samples were enclosed in Suprasil quartz tubes, which were initially evacuated to 10^{-5} – 10^{-6} Torr, and then filled with 1 atm of argon. Argon was used as a conducting medium for quick heating¹⁸ and was preferred over helium for its lower diffusivity.

The ESR spectra were recorded with a Varian E-12 spectrometer, operated in the X-band frequency mode (9.5 GHz). The single crystals were oriented in the cavity as in the earlier experiments.¹⁴ The second integral was obtained using a Varian 620/i minicomputer with the Varian Program E-LINE EPR/TTY SYSTEM 994002-00A. First integral (overall and peakwise) and stick plot could be obtained using the same program. The absolute spin value was obtained by using strong pitch as a standard.

Samples were heated to the specified temperature for specified periods of time and then cooled to room temperature for examination of the EPR spectra. The heating was usually done in a separate oven, where the temperatures could be controlled with an accuracy of $\pm 0.1^\circ\text{C}$. Heating and cooling times were of the order of 5 min. This time was small compared to average heating interval of 1500 min.

In some cases where radicals were short lived, the Varian variable-temperature accessory was used, where the temperature of the sample could be controlled to $\pm 2^\circ\text{C}$. The time required to reach the desired temperature was of the order of 5–8 min.

The free radicals were produced by x rays generated by a 3-MeV Van de Graaff accelerator. The average dose received by the samples was of the order of 1 Mrad. In selected cases, doses were varied by a factor of 2 in order to test the effect of concentration on the rate.

Results and Discussion

L-Leucine. Figure 1 shows a series of spectra taken over a period of time showing the decay of L-leucine (polycrystalline) radical at an elevated temperature. It can be noted that the decay is uniform and that there is no apparent free radical conversion during the decay process.

Figures 2 and 3 show the first- and second-order plots of the radical decay at 70°C . It can be seen that the second-order rate law fits much better than the first-order. In the second-order plot, the slope of the initial decay is different from that of the rest of the decay. At higher temperatures the duration of this initial decay is either very small or it is not seen at all. It has frequently been missed in other studies.

Figures 4a and 4b indicate that when L-leucine is allowed to decay at room temperature to constant spin concentration and then the temperature increased to some higher value, further decay occurs. In this case, however, there is a different radical involved, since the spectrum changes considerably as shown in Figure 5. This is essentially a singlet with some side structure, probably produced by a residual concentration of the initial radical. It has been shown¹⁹ that a singlet is produced by peroxy radicals formed by the reaction of atmospheric oxygen with the trapped radicals. Both the decays of Figure 4 are second order as shown by Figures 6a and 6b. It is interesting to note that in the latter case there is no separate initial decay. In each case, the last point does not fit the curve, presumably owing to the presence of still another stable radical population.

Figures 7 and 8 give activation energy plots for the two processes. The activation energies calculated for initial and major process are 19.4 and 22.9 kcal/mol, respectively (Table I).

DL-Valine. Figure 9 shows that the DL-valine (polycrystalline) radical is of the type that decays to the point of producing a stable radical population at each temperature; that is, stepwise decay is observed. As in the case of L-leucine, there is an initial process and a major process, each of which fits a separate second-order rate law. The initial process is better observable at lower temperatures and was studied earlier.¹⁴ Figure 10 shows a short initial process and then a major process, which is followed by steady concentration at this temperature. Any attempt to fit these to a first-order rate law is futile. There is, furthermore, no evidence of change in the overall appearance of the spectrum during the course of the entire decay. The activation energies calculated (Table I) from Figures 11 and 12 are 17.3 and 23.7 kcal/mol for initial and major processes, respectively.

DL-Valine (single crystal) shows similar behavior (Figure 13). Over long periods of time after the major process is complete, the spectrum is seen to change into a singlet, probably indicating the presence of a peroxy radical.

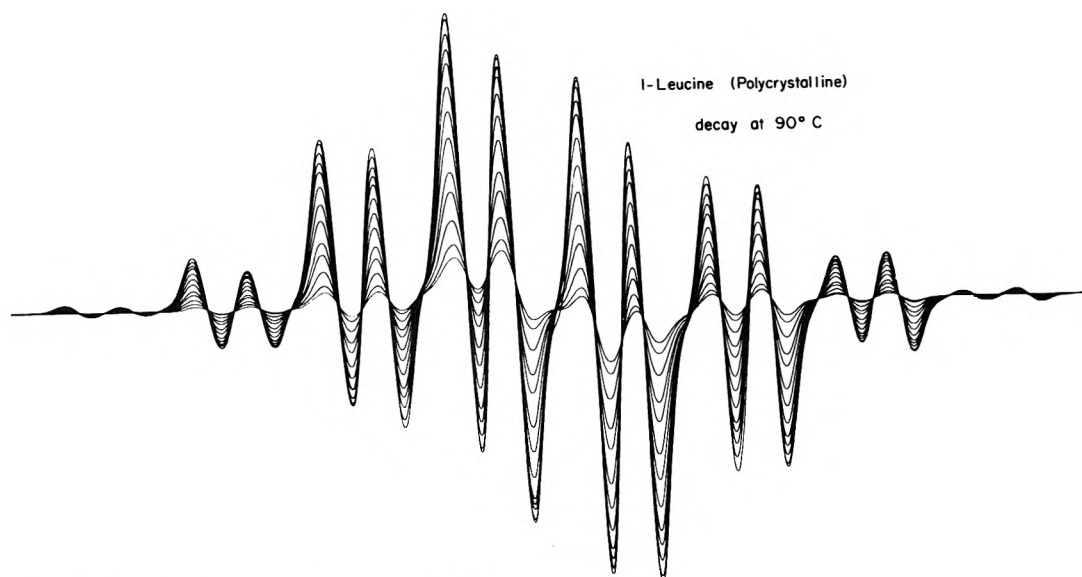


Figure 1. Successive ESR spectra of L-leucine decaying at 90°C.

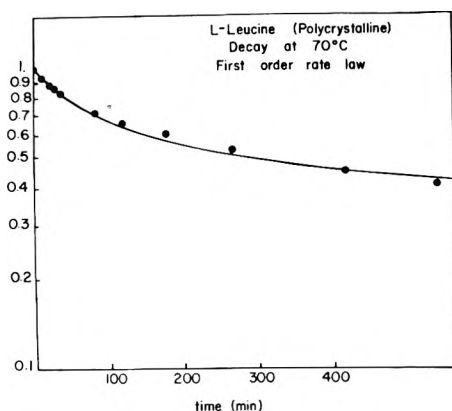


Figure 2. A first-order plot of the radical decay in polycrystalline L-leucine at 70°C.

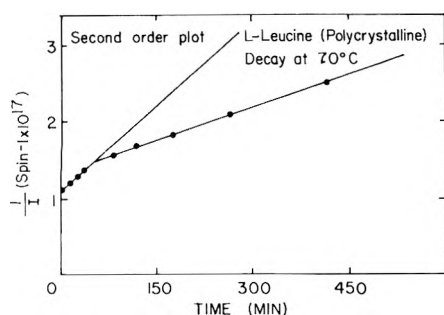


Figure 3. A second-order plot of the radical decay in polycrystalline L-leucine at 70°C.

L-Valine behaves similarly, exhibiting a faster initial process and then a slower major process.

Alanine. DL-Alanine (polycrystalline) showed a second-order decay similar in nature to the case of DL-valine. At the end of the major process the spin concentration again reaches a constant value.

L-Alanine (single crystal) behaves in exactly the same manner. The rate constants for the decay in the two substances are, however, quite different (see Table I).

L-Arginine Hydrochloride. This material irradiated as

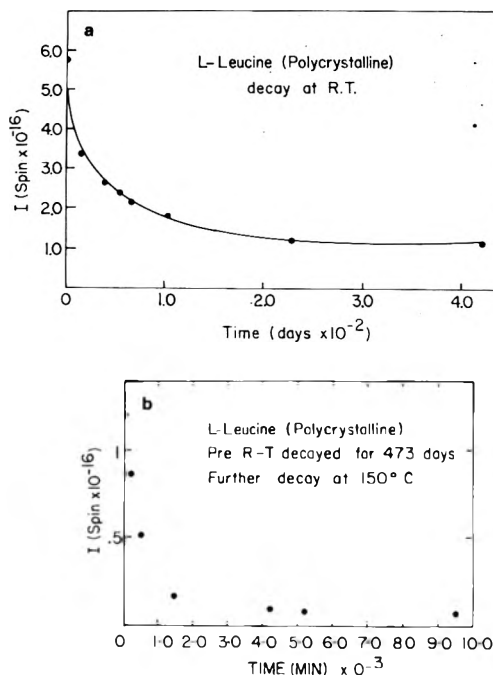


Figure 4. (a) The room-temperature decay of polycrystalline L-leucine (473 days). (b) Subsequent decay of the same sample at 150°C.

I-Leucine (Polycrystalline)
Decay at R.T. for 473 days
and at 150°C for 6 days

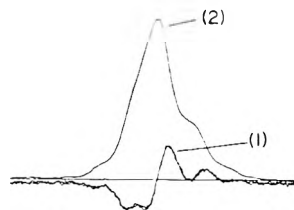


Figure 5. (1) ESR derivative spectrum of the residual radical in L-leucine. (2) Absorption spectrum of the radical.

TABLE I

Compound	k_2 , mol spin ⁻¹ min ⁻¹	E_a , kcal/mol	Diffusion coeff, cm ² sec ⁻¹ , D_2 , at 428 K
DL-Valine (polycrystalline)	Major process at 428 K 1.9×10^{-23}	23.7	1.28×10^{-14}
	Initial process at 428 K 1.36×10^{-22}	17.3	2.51×10^{-11}
L-Leucine (polycrystalline)	Major process at 383 K 4.32×10^{-22}	22.9	2.1×10^{-14} (1.56×10^{-15} at 383 K)
	Initial process at 383 K 0.93×10^{-21}	19.4	2.15×10^{-12} (1.5×10^{-13} at 383 K)
DL-Alanine (polycrystalline)	Major process at 430 K 1.77×10^{-23}	~20	at 383 K)
L-Valine (polycrystalline)	Major process at 363 K 1.23×10^{-24}		
L-Arginine Hydrochloride (polycrystalline)	Major process at 430 K 2.31×10^{-24}		
DL-Valine (single crystal)	Major process at 430 K 2.65×10^{-24}		
L-Alanine (single crystal)	Major process at 430 K 1.04×10^{-24}		

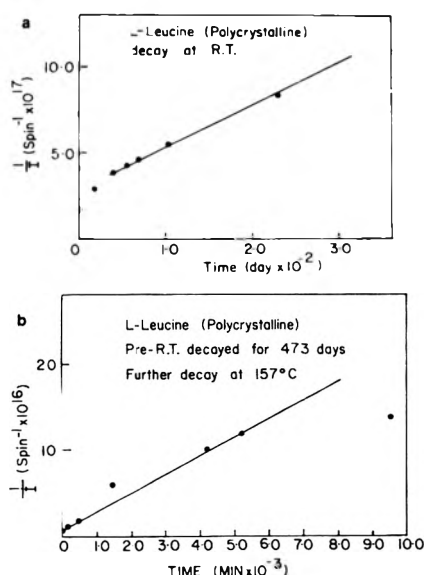


Figure 6. (a) Second-order plot of room temperature decay in L-leucine. (b) Second-order plot of the subsequent high-temperature (157°) decay in L-leucine.

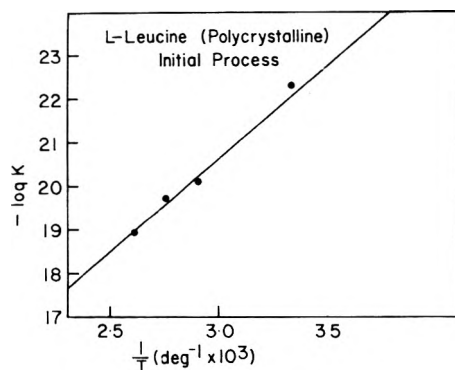


Figure 7. Arrhenius plot for the initial process in L-leucine.

taken from the bottle showed a second-order decay at 157°C, with rate constant 2.31×10^{-24} mol spin⁻¹ min⁻¹. The initial fast process is observed but is of too short duration to obtain any worthwhile information.

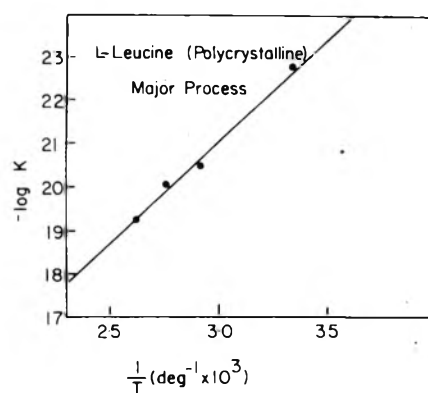


Figure 8. Arrhenius plot for the major process in L-leucine.

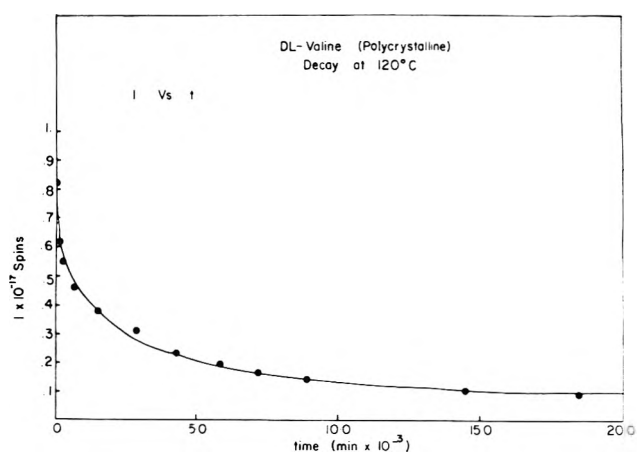


Figure 9. Decay curve for DL-valine at 120°C.

When an aqueous solution of L-arginine hydrochloride was cooled suddenly to 77 K, a precipitate was formed. Drying this at room temperature gave a different spectrum on irradiation.²⁰ This spectrum has an enhanced central line which looks like an overlap due to a second radical. The radical(s) appears to decay by a process that is mixed first and second order.

L-Arginine Hydrochloride Monohydrate. Single crystals

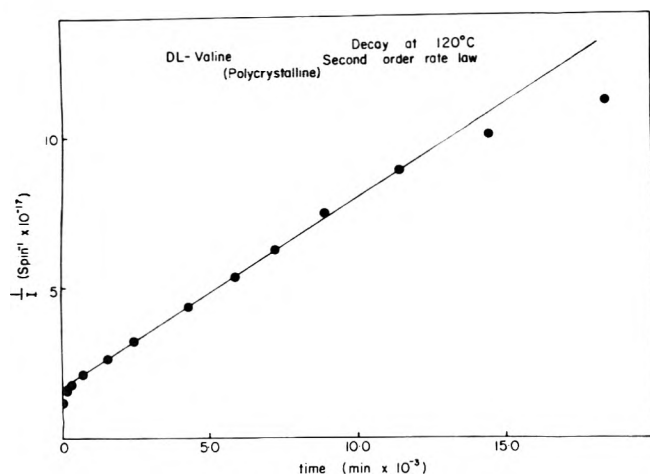


Figure 10. Second-order plot for DL-valine.

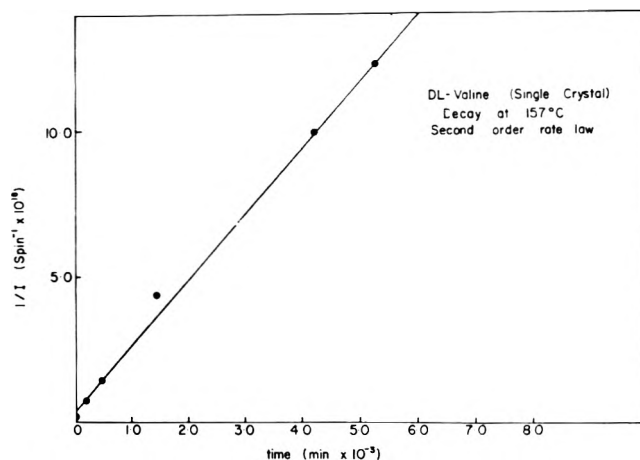


Figure 13. Second-order plot of decay in a single crystal of DL-valine at 157°C.

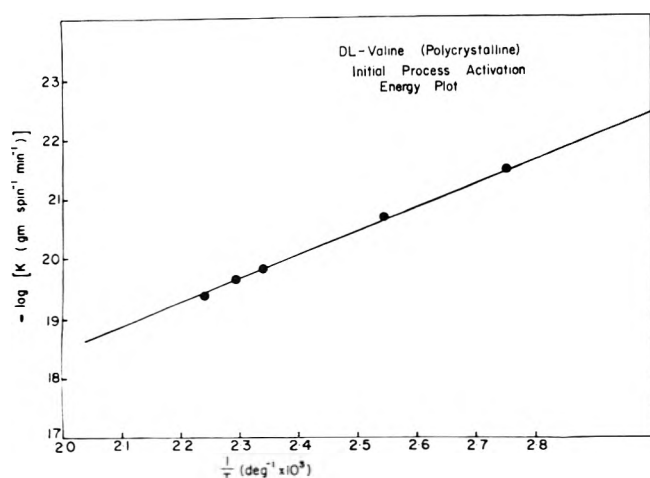


Figure 11. Arrhenius plot for DL-valine, initial process.

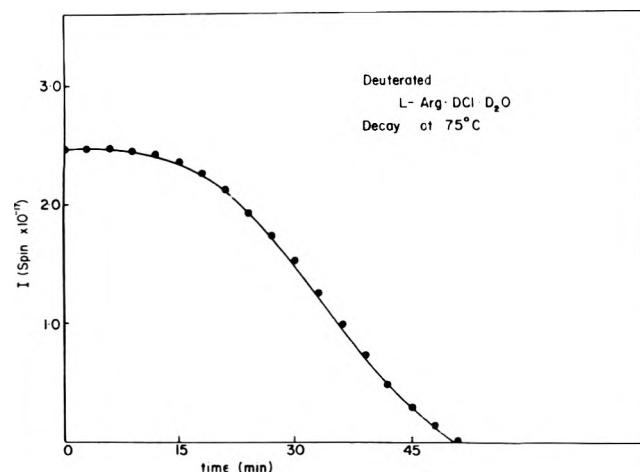


Figure 14. Decay curve for L-arginine hydrochloride monohydrate.

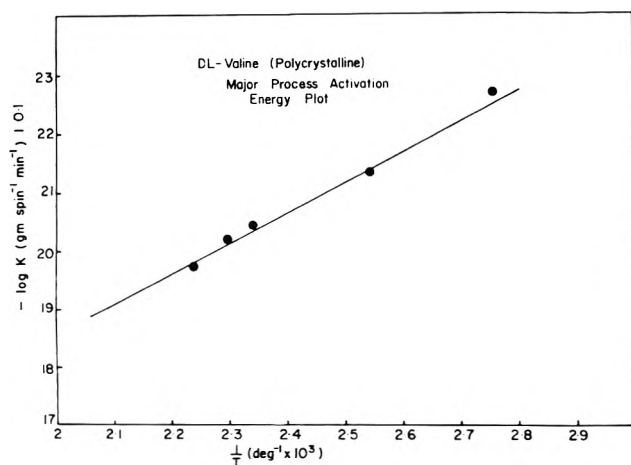


Figure 12. Arrhenius plot for DL-valine, major process.

obtained from aqueous solution were shown²⁰ to be L-Arg-HCl·H₂O, and those grown from D₂O were presumably L-Arg-DCl·D₂O with all active hydrogen replaced by deuterium. These single crystals gave radicals that were as stable as other amino acid radicals at room temperature. However, a slight rise in the temperature caused the crystals to turn opaque with a simultaneous rapid decrease in spin

concentration. At 90°C, both protonated and deuterated samples decay completely within a few minutes, with the deuterated radical seeming to be slightly longer lived. At 75°C, the deuterated crystal, after the initial heating period, decayed over the major concentration range at an almost constant rate (Figure 14).

Conclusions

From an examination of the above data, it can be seen that the decay of the free radicals in irradiated amino acids appears to involve two distinct processes: an initial faster process and then a slower decay for the major portion of the radicals. Both of these processes appear to obey second-order kinetics. This is substantiated by the fact that, if the initial concentration is increased, the rate is increased when fractional decay is compared. The activation energies calculated from these second-order rate processes are very close to those reported earlier using first-order kinetics.¹⁷

The subdivision into two processes has been postulated earlier²¹ in the case of radical recombination in anthracene crystals. In this case it was attributed to a fast radical combination in spurs followed by a slower bulk diffusion process.

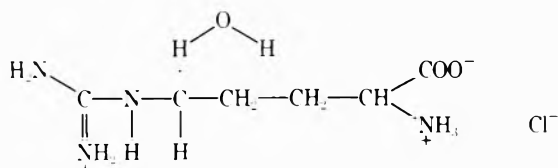
Also, in accordance with the study of Mikhailov and co-workers,¹⁵ it is noted that at each annealing temperature the decay curve essentially levels out, thus causing the last

few points in the second-order plots to have lower spin^{-1} values than predicted by the rate law. These radicals are presumably nearly stable at this temperature and are destabilized only at a higher temperature.

It seems very likely that vacancy controlled bulk diffusion is mainly responsible for the major decay. The initial faster decay must also be a diffusion process since it obeys a rate law. This conclusion arises out of the fact that, although the diffusion rate of all the molecules in the crystal must be more or less the same, the decay occurs only when the radical sites encounter each other. To account for the faster second-order decay of this initial process, it is assumed that those radicals which are formed within a few molecular diameters of one another at the end of the electron tracks form a separate population. These undergo more rapid decay due to their favored orientation and also perhaps as a result of nonrandom diffusion resulting from lattice strain. There is a difference between this and combination in spurs. The latter case is not expected to be a rate process since it is concentration independent.

Diffusion coefficients have been calculated with the assumption that the activation energy for the decay process is also the activation energy for the diffusion if these two processes are correlated (Table I). These values seem to be slightly lower than the self-diffusion coefficient values observed in the case of solid isobutylene²² at 77 K. This is not very surprising since the mobility in amino acid crystals is greatly hindered by the extensive hydrogen bonding. The simpler diffusion model of Smoluchuski²⁵ and the more elaborate one of Waites²⁶ have both been examined. Neither appear to fit the data in *both* decay regimens.

Finally, it may be noted that this mechanism does not apply to the case of L-Arg·HCl·H₂O. This decay appears to be controlled by the dehydration process. The proposed²⁰ radical is



From the crystal structure,²³ it can be seen that the water molecule is located in close proximity to the proposed radical site. Thus a hydrogen bond is formed between one of the hydrogen atoms in the water molecules and the unpaired electron of the free radical. When the water molecule leaves the crystal by evaporation, the unpaired electron abstracts the hydrogen atom in the equivalent position in the neighboring molecule generating a new radical. The distance between these equivalent sites is 5.6 Å; hence the hydrogen atom that is in between is quite accessible to both the carbons. In this fashion the unpaired electron migrates rapidly until it encounters another of its kind. It may be noted that in the case of L-Arg·HCl, where a water

molecule is not involved, the decay is by the much slower second-order process.

In cases where the samples were allowed to decay over a long period of time, a singlet due to peroxy radical was noted. However, the concentration of these radicals was very low. The rate of decay is lower than the major process. These radicals have been noted earlier.^{17,24} In the present case they are probably formed when a sufficient amount of atmospheric oxygen has diffused into the sample tube.

It is also noted that in most cases the initial process is responsible for the decay of 25–30% of the total radical concentration. At room temperature, in many cases, this is the total decay observed. This substantiates the claim of the separate initial process. This process, as mentioned earlier, is clearly a rate process obeying a second-order rate law.

Acknowledgments. The authors wish to acknowledge the assistance of Dr. W. Gulick for valuable advice and assistance with the ESR measurement, and Mr. Dempsey Lott for assistance with the irradiation. The financial assistance of the U.S. Atomic Energy Commission is also gratefully acknowledged. This is ORO Document ORO-2001-31.

References and Notes

- (1) M. A. Collins and D. H. Whiffen, *Mol. Phys.*, **10**, 317 (1966).
- (2) H. Shields, P. Hamrick, and D. Delaigle, *J. Chem. Phys.*, **46**, 3649 (1967).
- (3) B. W. Castleman and G. C. Moulton, *J. Chem. Phys.*, **57**, 2762 (1972).
- (4) H. Swenson and G. C. Moulton, *Radiat. Res.*, **53**, 366 (1973).
- (5) R. B. Lyons, D. M. Close, and R. S. Anderson, *Chem. Phys. Lett.*, **20**, 442 (1973).
- (6) M. F. Deigen, V. G. Krivenko, M. K. Pulatova, M. A. Ruban, V. V. Teslenko, and L. P. Kayuslin, *Biofizika*, **18**, 235 (1973).
- (7) F. Quac-hai Ngo, E. E. Budzinski, and H. C. Box, *J. Chem. Phys.*, **60**, 3373 (1974).
- (8) L. D. Kispert, K. Chang, and C. M. Bogan, *J. Chem. Phys.*, **58**, 2164 (1973).
- (9) J. Zimbrick and L. Kevan, *J. Chem. Phys.*, **47**, 2364 (1967).
- (10) G. Saxebol, *Int. J. Radiat. Biol.*, **24**, 475 (1973).
- (11) P. K. Horan, T. Henniksen, and W. Snipes, *J. Chem. Phys.*, **52**, 4324 (1970).
- (12) H. Shields, P. J. Hamrick, Jr., C. Smith, and Y. Haven, *J. Chem. Phys.*, **58**, 3420 (1973).
- (13) W. Snipes and P. K. Horan, *Radiat. Res.*, **30**, 307 (1967).
- (14) F. B. Stenz, E. D. Taylor, and R. H. Johnsen, *Radiat. Res.*, **49**, 124 (1972).
- (15) A. I. Mikhailov, Ya. S. Lebedev, and N. Ya. Buben, *Kinet. Katal.*, **5**, 1020 (1964).
- (16) A. I. Mikhailov, Ya. S. Lebedev, and N. Ya. Buben, *Kinet. Katal.*, **6**, 48 (1965).
- (17) P. K. Horan, W. D. Taylor, G. K. Stother, and W. Snipes, *Biophys. J.*, **8**, 164 (1968).
- (18) A. K. E. Hagopian and R. H. Johnsen, *J. Chem. Soc., Chem. Commun.*, 838 (1974).
- (19) G. Alder, *Mol. Cryst. Liq. Cryst.*, **9**, 297 (1969).
- (20) A. Joshi, G. C. Moulton, and R. H. Johnsen, to be submitted for publication.
- (21) A. R. McGhie, H. Blum, and M. M. Labes, *Mol. Cryst.*, **5**, 245 (1969).
- (22) T. S. Hutchinson and D. C. Baird, "The Physics of Engineering Solids", Wiley New York, N.Y., 1963.
- (23) G. C. Rappe, R. C. Reid, and M. W. Strandberg, *J. Phys. Chem.*, **74**, 3176 (1970).
- (24) J. Dow, L. H. Jensen, S. K. Mazundar, R. Srinivasan, and G. N. Ramachandran, *Acta Crystallogr. Sect. B*, **26**, 1662 (1970).
- (25) M. V. Smoluchuski, *Z. Phys. Chem. A*, **92**, 192 (1917).
- (26) T. R. Waites, *Phys. Rev.*, **107**, 463 (1957).

Lattice Energies and Heats of Sublimation at 0 K for *n*-Pentane, *n*-Hexane, *n*-Octane, and Ammonia¹

Lester L. Shipman,² Antony W. Burgess,³ and Harold A. Scheraga*⁴

Department of Chemistry, Cornell University, Ithaca, New York 14853 (Received August 14, 1975)

The lattice energies of *n*-pentane, *n*-hexane, *n*-octane, and ammonia have been calculated to be -11.1, -13.2, -17.3, and -8.7 kcal/mol, respectively. These values have been compared to previously calculated values, where available. A general discussion of the calculation of lattice energies and heats of sublimation at absolute zero temperature is presented.

I. Introduction

The lattice energies of crystals are of major importance as input data to the derivation of empirical potentials for the calculation of low-energy conformations and low-energy orientations within aggregates of molecules. An example of such a potential energy function is EPEN⁵ (empirical potential using electrons and nuclei), an approach to empirical intermolecular and conformational potential energy functions in which electrons and nuclei are treated explicitly. In EPEN, a molecule is divided up into heavy atom (nonhydrogen) fragments, each with a characteristic set of potential parameters, and the total interaction potential is the sum of the pairwise interactions between heavy atom fragments. Coulombic interactions, overlap repulsions, and R^{-6} attraction terms are included in EPEN. The parameters of EPEN were obtained⁵ by fitting to experimental data such as molecular geometries, dipole moments, rotational energy barriers, conformer energy differences, crystal lattice constants, and crystal lattice energies. The crystal lattice energies of *n*-pentane, *n*-hexane, *n*-octane, and ammonia constituted part of the set of data that was used to parameterize EPEN. For that purpose, it was necessary to recalculate these lattice energies because there was considerable discrepancy in the literature as to their numerical values (in the case of ammonia, we were unable to find an estimate of the lattice energy in the literature). The resolution of these discrepancies is of general interest, and we therefore present the procedure and results here.

The lattice energy of a crystal is defined as the negative of the potential energy required to take molecules with motionless nuclei out of a crystal lattice at 0 K and separate them by an infinite distance (keeping them motionless), without changing the bond angles, bond lengths, or dihedral angles of the molecules. Thus, the lattice energy arises *only* from the intermolecular interactions in a crystal. It is impossible to measure the lattice energy directly because the molecules are vibrating in the crystal, even at absolute zero temperature. However, the lattice energy is the quantity calculated in crystal packing studies. It should be noted that the heat of sublimation at 0 K and the lattice energy are *not* identical quantities. The heat of sublimation at 0 K is defined as the energy required to take molecules in the lowest vibrational state in the crystal and to separate them by an infinite distance, allowing the isolated molecules to occupy their ground intramolecular vibrational state in the lowest-energy conformation, with relaxation of their equilibrium bond lengths and bond angles to their expectation values in the ground vibrational state of the isolated molecule.

In general, lattice energies are calculated from the sum of (i) the negative of the heat of sublimation of 0 K, (ii) the negative of the vibrational zero point energy in the crystal, (iii) the vibrational zero point energy in the lowest energy conformation of the isolated molecule, and (iv) the difference between the geometrical and conformational potential energy of the crystal conformation and the lowest energy conformation of the isolated molecule.

The heat of sublimation at 0 K may be calculated only by using a full thermodynamic cycle for which there are experimental data available at each step in the cycle. For example, the terms to be considered in the calculation of a heat of sublimation at 0 K for a crystal with, e.g., two forms between 0 K and its melting point are: (i) the enthalpy change as crystal form 1 is heated from 0 K to the transition temperature, (ii) the heat of transition between crystal form 1 and crystal form 2, (iii) the enthalpy change as crystal form 2 is heated from the transition temperature to the melting point, (iv) the heat of fusion, (v) the enthalpy change as the liquid is heated from the melting point to the normal boiling point, (vi) the heat of vaporization at the normal boiling point, (vii) the enthalpy change as the gas is expanded from 1 atm pressure at the normal boiling point to 0 atm pressure (ideal gas correction), and (viii) the enthalpy change as the ideal gas is cooled from the normal boiling point of the liquid to 0 K.

The vibrational zero point energy of the crystal arises from a sum of the zero point vibrational energies over the $3N$ vibrational modes per molecule, where N is the number of atoms in the molecule. It is usually not possible to separate the intramolecular from the intermolecular vibrational modes rigorously. The vibrational zero point energy of the isolated molecule in its lowest energy conformation is the sum of the zero point vibrational energies over the $3N - 6$ intramolecular vibrations. The geometry and conformation of the molecule in the crystal and in its lowest energy conformation as an isolated molecule need not be identical; there is a potential energy change associated with changing the bond angles, bond lengths, and dihedral angles from their values in the crystal conformation to their values in the lowest energy conformation of the isolated molecule.

II. Lattice Energies of *n*-Pentane, *n*-Hexane, and *n*-Octane

The calculation of the experimental lattice energies of *n*-pentane, *n*-hexane, and *n*-octane is summarized in Table I; the calculated values are -11.1, -13.2, and -17.3 kcal/mol, respectively. From the data^{6,7} given in Table I, the corresponding heats of sublimation at 0 K were calculated

TABLE I: Calculation of the Lattice Energies of *n*-Pentane, *n*-Hexane, and *n*-Octane from Experimental Data

	Energy, kcal/mol		
	<i>n</i> -Pentane	<i>n</i> -Hexane	<i>n</i> -Octane
Heat content of condensed phase at 298.15 K	9.342 ^a	11.215 ^a	14.695 ^a
Heat of vaporization at 298.15 K	6.316 ^b	7.540 ^b	9.915 ^b
Ideal gas correction	0.058 ^c	0.024 ^c	0.004 ^c
-(Heat content of ideal gas at 298.15 K)	-5.668 ^b	-6.691 ^b	-8.736 ^b
Z _{inter} (cryst)	0.67 ^d	0.64 ^d	0.64 ^d
Z _{intra} (cryst) - Z _{intra} (gas)	0.4 ^d	0.5 ^d	0.8 ^d
-Lattice energy	11.1	13.2	17.3

^aReference 6. ^bReference 7. ^cThis quantity is the enthalpy associated with the expansion of the real gas at saturation pressure and 298.15 K to 0 atm pressure. See the text for a discussion of the calculation of this quantity. ^dSee text.

to be 10.05, 12.09, and 15.88 kcal/mol. It should be noted that we have not explicitly included (in Table I) the potential energy difference associated with the difference in conformation between the crystal conformation and the lowest energy isolated molecule conformation. For the three molecules considered here, these two conformations are essentially the same (fully extended), and so the potential energy difference between the two would be expected to be negligible.

Several of the steps in Table I require further explanation. The ideal gas correction was calculated using the equation

$$H_{\text{ideal}} - H_{\text{real}} = \left[\frac{9RT_c}{(128P_c)} \right] \left[\frac{(18T_c^2)}{(298.15)^2} - 1 \right] P_v \quad (1)$$

where T_c is the critical temperature, P_c is the critical pressure, R is the universal gas constant, and P_v is the vapor pressure of the liquid at 298.15 K. Experimental values for T_c , P_c , and P_v are available.⁷ Equation 1 was derived from an equation reported previously,⁸ viz.

$$H_{\text{ideal}} - H_{\text{real}} = RT - PV + \int_V^\infty [T(\partial P/\partial T)_V - P] dV \quad (2)$$

where V is the molar volume, using the truncated and rearranged virial equation

$$P = (RT)/(V - B) \quad (3)$$

where B is the second virial coefficient, given approximately by⁹

$$B \approx [9RT_c/128P_c] [1 - (6T_c^2)/T^2] \quad (4)$$

where T is the absolute temperature.

We turn now to the calculation of the intermolecular zero point energy; the calculation of the intramolecular zero point energy is considered in the succeeding paragraph. The intermolecular zero point energy, Z_{inter} , was calculated by reanalyzing the results of Shimonaev,¹⁰ who erroneously assumed that 15, 18, and 24 vibrational modes contribute to the low temperature heat capacities of *n*-pentane, *n*-hexane, and *n*-octane, respectively. A more realistic assumption would be that the three librations, the three hindered translations, and only a couple of intramolecular

modes have sufficiently low frequencies to contribute significantly to the low temperature heat capacity of these crystals (i.e., a total of approximately eight modes). Assuming that (i) all eight modes contribute equally to the heat capacity, and (ii) a Debye function may be used to approximate the true frequency distribution, the intermolecular vibrational zero point energies (not including the two intramolecular modes) were calculated (Table I). These values are similar to those computed from a potential energy function by Warshel and Lifson (0.5 and 0.7 kcal/mol)¹¹ for *n*-hexane and *n*-octane, respectively. Further support for these values of Z_{inter} comes from the results of a Raman spectroscopic study of the lattice vibrations of *n*-hexane and *n*-octane by Brunel and Dows,¹² who reported values of 53, 74, and 87 cm⁻¹ for the librations of *n*-hexane and the values of 47.5, 65, and 72 cm⁻¹ for the librations of *n*-octane. Under the assumption of harmonic vibrations, these sets of frequencies correspond to librational zero point energies of 0.31 and 0.26 kcal/mol, respectively. With the approximation that the three hindered translational modes and three librational modes per molecule contribute equally to the heat capacity, our calculated values of the librational zero point energy would be 0.64/2 = 0.32 kcal/mol for both *n*-hexane and *n*-octane, which agrees well with these spectroscopically determined values.

The value for $Z_{\text{intra}}(\text{cryst}) - Z_{\text{intra}}(\text{gas})$ is difficult to obtain experimentally; an experimental determination of this quantity for *n*-octane, for example, would require accurate values for a total of 144 vibrational frequencies (72 frequencies for the vibrations of the isolated molecule and 72 frequencies for the intramolecular vibrations in the crystal). For the three molecules considered here, these experimental frequencies are not all available. As an alternative, we have used Warshel and Lifson's computed values¹¹ for $Z_{\text{intra}}(\text{cryst}) - Z_{\text{intra}}(\text{gas})$ for *n*-hexane and *n*-octane. The value for *n*-pentane given in Table I (viz., 0.4 kcal/mol) was obtained by extrapolation from values for *n*-hexane and *n*-octane (0.5 and 0.8 kcal/mol, respectively) by assuming that this quantity is a linear function of the number of intramolecular vibrational modes. The heat content of the condensed phase at 298.15 K was taken from a compilation by Messerly et al.,⁶ and the heat content of the ideal gas at 298.15 K and the heat of vaporization at 298.15 K were taken from a compilation by Rossini et al.⁷

Shimonaev has calculated the lattice energies¹³ and heats of sublimation at 0 K¹⁴ for all three molecules considered here. His values for these quantities are given in Table II. The primary reason for the difference between his and our values for the lattice energies is his overestimate of the number of modes contributing to the low temperature heat capacity, which leads to an overestimate of the intermolecular zero point energies. It should be noted that the sublimation energies at 0 K do not depend upon this assumption (because Z_{intra} and Z_{inter} are not used in the calculation of the sublimation energy), but Shimonaev's values¹⁴ for this quantity are still not in good agreement with our values. Warshel and Lifson¹¹ have calculated the sublimation energies of *n*-hexane and *n*-octane at 0 K (from experimental data). These values, along with their calculated zero point energies, lead to lattice energies of -13.1 and -17.4 kcal/mol (these values were not reported by Warshel and Lifson, but may be calculated from data given in their Table IV). Bondi¹⁵ has calculated the heat of sublimation at the lowest first-order transition temperature (from experimental data); his values are given in Table II, and agree

TABLE II: Comparison of Lattice Energies and Heats of Sublimation at 0 K

	Energy, kcal/mol			
	<i>n</i> -Pentane	<i>n</i> -Hexane	<i>n</i> -Octane	Ref
Lattice energy		-13.1	-17.4	11
	-12.7	-15.6	-20.9	13
	-11.1	-13.2	-17.3	This work
Heat of sublimation at 0 K		12.14	15.88	11
	10.68	13.12	17.24	14
	10.03	12.15	16.27	15 ^a
	10.05	12.09	15.88	This work

^a These sublimation energies are at the lowest first-order transition temperature, rather than at 0 K.

TABLE III: Approximate Lattice Energy of Crystalline Ammonia

Process	Energy, kcal/mol
H _s (0 K) → H _s (195.36 K)	1.13 ^a
H _s (195.36 K) → H _l (195.36 K)	1.35 ^b
H _l (195.36 K) → H _l (239.68 K)	0.78 ^c
H _l (239.68 K) → H _g (239.68 K)	5.58 ^b
H _g (239.68 K) → H _g (0 K)	-1.91 ^d
Z _{inter}	1.75 ^e
-Lattice energy	8.68

^a This quantity was obtained from numerical integration of $\int_{0K}^{195.36K} C_p(s) dT$ where the temperature dependence of the heat capacity, $C_p(s)$, was taken from ref 18. ^b Reference 17. ^c Computed as $C_p(l)(239.68 K - 196.36 K)$ where $C_p(l)$ was taken to be 17.6 cal mol⁻¹ deg⁻¹ (see ref 17). ^d Reference 19. ^e Intermolecular zero point vibrational energy computed under the assumption of harmonic vibrations as $(3hc \cdot 129 \text{ cm}^{-1})/2$ for the hindered translational vibrations and as $(3hc \cdot 280 \text{ cm}^{-1})/2$ for the librations. The frequencies were taken from ref 16.

quite closely with our values for the sublimation energy at 0 K.

All the lattice energies and sublimation energies calculated from experimental data for the three molecules considered here have been collected in Table II for comparison. It may be concluded that the values given by Shimo-naev^{13,14} are in significant disagreement with the values reported by others, and that the values reported by others (Warshel and Lifson,¹¹ Bondi,¹⁵ and the present study) are in general agreement.

III. Lattice Energy of Ammonia

The lattice energy of ammonia has not been reported previously, but can be computed approximately from published experimental data¹⁶⁻¹⁹ in the manner shown in Table III; the calculated value is -8.7 kcal/mol. A more accurate value for the lattice energy requires more experimental data than are yet available, and several terms had to be neglected in our approximate calculation. The terms that are not available are: (i) the change in the potential energy corresponding to the difference in nuclear geometry between the gas structure and the crystal structure, (ii) the difference in intramolecular zero point energy between the gas and the crystal, (iii) the enthalpy for the expansion of the real gas at 1 atm and 239.68 K to zero pressure at the

same temperature, and (iv) the contribution of intramolecular vibrational modes to the ideal gas enthalpy at 239.68 K. An approximate heat of sublimation at 0 K (6.9 kcal/mol) can be calculated from the quantities in Table III.

IV. Summary and Conclusions

The lattice energies of *n*-pentane, *n*-hexane, *n*-octane, and ammonia were calculated to be -11.1, -13.2, -17.3, and -8.7 kcal/mol, respectively. The hydrocarbon lattice energies should be accurate to 0.1 kcal/mol. While the ammonia lattice energy is approximate, the error is not likely to be as much as 1 kcal/mol; as the missing pieces of experimental data become available, a more accurate calculation of the lattice energy of ammonia will be possible. This uncertainty in the value of the ammonia lattice energy would be expected to carry over as an uncertainty in the values of empirical potential energy function parameters derived using this quantity (e.g., the EPEN⁵ nitrogen parameters). There is general agreement among the hydrocarbon lattice energies and sublimation energies calculated by Warshel and Lifson,¹¹ Bondi,¹⁵ and the values calculated in the present study; however, the values calculated by Shimo-naev^{13,14} are in considerable disagreement with the rest.

References and Notes

- (1) This work was supported by research grants from the National Institute of General Medical Sciences of the National Institutes of Health, U.S. Public Health Service (GM-14312), from the National Science Foundation (BMS71-00872 A04), and from Walter and George Todd.
- (2) N.I.H. Postdoctoral Fellow, 1972-1974.
- (3) Fulbright-Hays Fellow, 1972-1974.
- (4) To whom requests for reprints should be addressed.
- (5) L. L. Shipman, A. W. Burgess, and H. A. Scheraga, *Proc. Natl. Acad. Sci. U.S.A.*, **72**, 543 (1975).
- (6) J. F. Messerly, G. B. Guthrie, S. S. Todd, and H. L. Finke, *J. Chem. Eng. Data*, **12**, 338 (1967).
- (7) F. D. Rossini, K. S. Pitzer, R. L. Arnett, R. M. Braun, and G. C. Pimentel in "Selected Values of Physical and Thermodynamic Properties of Hydrocarbons and Related Compounds", Carnegie Press, Pittsburgh, Pa., 1953, pp 326, 339, 340, 342, 484, 485, 487, 583, 584, 586.
- (8) J. O. Hirschfelder, C. F. Curtiss, and R. B. Bird in "Molecular Theory of Gases and Liquids", Wiley, New York, N.Y., 1954, p 230.
- (9) J. O. Hirschfelder, C. F. Curtiss, and R. B. Bird, ref 8, p 252.
- (10) G. S. Shimo-naev, *Russ. J. Phys. Chem.*, **41**, 138 (1967).
- (11) A. Warshel and S. Lifson, *J. Chem. Phys.*, **53**, 582 (1970).
- (12) L. C. Brunel and D. A. Dows, *Spectrochim. Acta, Part A*, **30**, 929 (1974).
- (13) G. S. Shimo-naev, *Russ. J. Phys. Chem.*, **41**, 182 (1967).
- (14) G. S. Shimo-naev, *Russ. J. Phys. Chem.*, **39**, 1347 (1967).
- (15) A. Bondi, *J. Chem. Eng. Data*, **8**, 371 (1963).
- (16) P. S. Goyal, B. A. Dassannacharya, C. L. Thaper, and P. K. Iyengar, *Nucl. Phys. Solid State Symp.*, **3**, 457 (1970).
- (17) R. Overstreet and W. F. Giaouque, *J. Am. Chem. Soc.*, **59**, 254 (1937).
- (18) V. A. Popov, V. G. Manzhelli, and M. I. Bagatskii, *J. Low Temp. Phys.*, **5**, 427 (1971).
- (19) L. Haar, *Natl. Stand. Ref. Data Ser., Natl. Bur. Stand.*, **No. 19** (1968).

Dielectric Properties of Sephadex and Its Water of Hydration

G. T. Koide*¹ and E. L. Carstensen

*Department of Electrical Engineering, College of Engineering and Applied Science, University of Rochester, Rochester, New York 14627
(Received December 14, 1972; Revised Manuscript Received July 16, 1975)*

Publication costs assisted by the University of Rochester

Sephadex in the nonpolar solvent dioxane shows a uhf dielectric relaxation. If Sephadex is first brought to equilibrium with water and then washed repeatedly with dioxane, it retains about 0.16 g of water/g of Sephadex. This hydration does not appear to change the dielectric properties of Sephadex itself. With that assumption, the measurements indicate that the bound water relaxes at frequencies of the order of 4 GHz.

Introduction

The dielectric properties of protein solutions are characterized by dispersions throughout the frequency range from below 1 MHz to beyond 20 GHz.²⁻⁸ There is little reason to doubt that the relaxation below 10 MHz is related to rotation of the entire protein molecule. Also, there is general agreement that the dispersion above 10 GHz is dominated by relaxation of free water. In the uhf region, however, it is much more difficult to elucidate the mechanism of the dielectric dispersion. Because of the complex nature of the interaction of protein and water, it is difficult to design experiments which demonstrate clearly whether the dispersion arises from movement of a subunit of the macromolecule or whether forces exerted by the macromolecules have shifted the relaxation frequency of a part of the water to the uhf region. Pennock and Schwan³ conjecture that side chains of hemoglobin relax at frequencies in the order of 100 MHz or less and attribute the dispersion which they observe above 100 MHz to bound water.

There is a firm basis for the belief that bound or crystalline water has a lower relaxation frequency than free water. Pure, hexagonal ice relaxes near 10 kHz.^{9,10} Gas hydrates and certain high pressure ices have relaxation frequencies between 0.1 and 1 MHz.¹¹⁻¹⁷ In aqueous solutions of macromolecules, the conductivity near the relaxation frequency of free water is less than would be expected from the total amount of water present in the sample.⁵ In some cases this can be used as a measure of the amount of bound water in the solution. Although it is clear that the relaxation frequency of the bound water is lower than that of free water, we can say little more than this with certainty. The lower the frequency, the more reasonable it is to expect contributions to the dispersion from the solute. In fact, it has not been possible up to the present time to find a clear cut example of water which relaxes in the uhf part of the spectrum.

Partially hydrated, powdered proteins have provided a somewhat different approach to this problem.¹⁸⁻²⁰ Rosen¹⁸ showed that dry bovine serum albumin had a dielectric constant of about 1.5 or less at 1 MHz and the first 0.2 g of water/g of protein added to the powder had almost no effect on the dielectric constant, as though the first water added was irrotational. As the water content increased above 0.2 g of water/g of protein, there was a steady in-

crease in the dielectric constant of the sample. Harvey and Hoekstra²⁰ found a dielectric relaxation at 250 MHz in lysozyme samples containing slightly more than a monolayer of water. It is tempting to attribute these effects directly to the water. However, the present study shows that we cannot rule out the possibility that the added solvent is simply mobilizing some part of the protein molecules.

A preparation called Sephadex (Pharmacia, Uppsala, Sweden) has a number of properties which are very useful in the investigation of this problem. Sephadex consists of small, porous, spherical beads of cross-linked dextran molecules. Since the dextran molecules are uncharged, dielectric measurements need not be complicated or masked by ionic conductivity. Dielectric dispersion in Sephadex presumably arises from rotation of polar groups in the dextran molecules. The particles can be suspended in dioxane and dioxane-water mixtures. Fortunately, the dielectric properties of Sephadex alone appear to be the same both in dioxane and water. A technique, based on reasonable assumptions, has permitted us to obtain direct measurements of the amount of water which is tightly bound to the Sephadex. Finally, it has been possible to obtain some indication of the dielectric properties of the tightly bound water.

Methods and Materials

Sephadex G10 is supplied by Pharmacia Fine Chemicals (Uppsala, Sweden) in the form of spherical beads 10-40 μ in diameter. When suspended in water, pores in the material will admit molecules with molecular weight up to 700. Deionized water and reagent grade nonaqueous solvents were used in the experiments. The Sephadex was allowed to equilibrate with water for at least 4 hr and in alcohols and dioxane for 24 hr before using. This procedure was repeated several times with no appreciable change, which indicated that the Sephadex was stable with respect to the suspending medium.

Liquid Determination. Total liquid concentrations in samples were determined from dry weight measurements. Water content was determined by the Karl Fischer potentiometric back-titration technique.²¹ For samples in which the only solvent was water, the two methods, dry weight and Karl Fischer measurements, agree within 5%.

Volume Fraction and Bound Water Determinations. Estimates of the amount of water intimately associated with a solute (bound water) can be obtained in cases where solute can be separated mechanically from the environmental liquid (supernatant). For clarity, the application of the tech-

* Address correspondence to this author at the Department of Electrical Engineering, Rochester Institute of Technology, Rochester, N.Y. 14623.

nique to the cross-linked dextran particle, Sephadex, will be described. The broader applicability of the technique will be apparent.

Let us assume that a sample of Sephadex has been allowed to come to equilibrium with water. The particles are allowed to settle and all excess water is removed. Another liquid which will mix freely with liquid water but does not associate with Sephadex or bound water is chosen. Let us assume that dioxane has these properties. The true meaning of these assumptions will be apparent from the description of the method. A quantity of dioxane is added to the sample of Sephadex, mixed thoroughly, and allowed to come to equilibrium. Again Sephadex is permitted to settle and later the excess liquid is removed. This becomes the sample. By repeating the dioxane washing procedure more water can be removed from the sample.

All weights are given relative to the weight of the sample, e.g., the sample will contain W_w , W_a , and W_s weight fractions of water, dioxane, and Sephadex respectively so that

$$W_w + W_a + W_s = 1 \quad (1)$$

From a dry weight measurement on the sample we can determine W_s and the total liquid weight fraction W_l of the sample.

$$W_l = 1 - W_s = W_w + W_a \quad (2)$$

Part of the water is bound to the Sephadex while the rest mixes freely with dioxane. The water-dioxane mixture pervades all of the sample not occupied by the solute, Sephadex, and the water bound to it. The ratio of water to dioxane in this region will be the same as that in the supernatant from the sample. This ratio W_{ws}/W_{as} can be determined by the Karl Fischer technique. W_{ws} and W_{as} are the weight fractions of water and dioxane of the supernatant, respectively. Knowing the total water W_w in the sample (by Karl Fischer technique) the total dioxane W_a in the sample is obtained by use of eq 1. Knowing the total dioxane W_a in the sample gives the total free water W_{fw} in the sample.

$$W_{fw} = W_a(W_{ws}/W_{as}) \quad (3)$$

Hence, the remaining water in the sample must be bound.

$$W_{bw} = W_w - W_{fw} \quad (4)$$

From this description it is apparent that the measurement defines bound water W_{bw} as the fraction of the water which at a particular concentration of dioxane is associated with Sephadex and does not mix with dioxane. It is also implicit that association of dioxane with Sephadex is negligible. If this is not true, then W_{bw} is a measure of the preference of Sephadex for water over dioxane.

The volume fractions of Sephadex in the sample can be obtained from these measurements.²²

$$V_s = 1 - \rho_t \left(\frac{W_{fw}}{\rho_{fw}} + \frac{W_{bw}}{\rho_{bw}} + \frac{W_a}{\rho_a} \right) \quad (5)$$

where ρ_t , ρ_{fw} , ρ_{bw} , and ρ_a are densities of the whole sample, the free water, the bound water, and the interstitial fluid, respectively. When the Sephadex is suspended in either water or dioxane alone this simplifies to

$$V_s = 1 - (1 - W_s) \frac{\rho_t}{\rho_1} \quad (6)$$

where W_s is the dry weight of the sample and ρ_1 is the density of the suspending fluid. In these calculations we have

used 1.00 g/ml for the density of both free and bound water²³ and 1.03 g/ml for the density of dioxane.

Dielectric Measurements. Measurements in the frequency range from 0.5 to 200 MHz were performed with an RX Meter, Type 250A (Boonton Radio Corp., Boonton, N.J.). Measuring cells and calibration procedures were similar to those of Pauly and Schwan.²⁴

Measurements from 300 to 1600 MHz were made with a Rohde and Schwarz (München, West Germany) BN3926/50 coaxial slotted line and NB31319 sample holder. Voltage standing wave ratios were determined either by directly measuring the maximum and minimum of the electric field in the standing wave pattern or by using a 3-dB technique. An iterative method was used to calculate the complex propagation constant from which the complex dielectric constant can be obtained.²²

Although the dielectric data yield some qualitative information directly, it would be desirable to eliminate the contributions of the suspending medium from the observations. There is no rigorous way of doing this but we can make rough estimates of the properties of the suspended phase alone. It is important, however, to recognize that several assumptions are made in the process. The Sephadex samples used in the dielectric measurements are obviously inhomogeneous. Since it is impossible to characterize the shape of the suspended phase, we have simply used the Maxwell-Wagner mixture equation to estimate its effective complex dielectric constant κ_e^+ .^{25,26}

$$\frac{\kappa^+ - \kappa_s^+}{\kappa^+ + 2\kappa_s^+} = V \frac{\kappa_e^+ - \kappa_s^+}{\kappa_e^+ + 2\kappa_s^+} \quad (7)$$

κ^+ and κ_s^+ are the measured complex dielectric constants of the suspension and suspending fluid and V is the volume fraction of the suspended phase (Sephadex or Sephadex plus bound water). In so doing we assume that the particles in suspension are spheres. It should be noted that the volume V used in the calculations is that of the solute plus bound water and not that of the porous Sephadex beads. Thus the suspended "particles" are the dextrans plus their shell of bound water.

The bound water presumably forms a shell around the cross-linked macromolecules which make up the Sephadex particles. To compute the complex dielectric constant κ_1^+ of the bound water we again assume that the solute is in the form of a sphere with a spherical shell of bound water around it. Then^{25,26}

$$\frac{\kappa_e^+ - \kappa_1^+}{\kappa_e^+ + 2\kappa_1^+} = p \frac{\kappa_2^+ - \kappa_1^+}{\kappa_2^+ + 2\kappa_1^+} \quad (8)$$

where κ_2^+ is the complex dielectric constant of the Sephadex and p is the volume of Sephadex per unit of Sephadex-bound water complex. Although the shape of the material may not be spherical, this shelled model should at least give us a rough estimate of the properties of the bound water.

Experimental Observations

Bound Water Measurements. Both dry and hydrated Sephadex have been included in the present study. In the first case Sephadex G10 was suspended in dioxane or other organic solvents for dielectric measurements. In the second case, the Sephadex was first allowed to come to equilibrium in an excess of water and then washed at least three times in dioxane until a new equilibrium water content for the Sephadex preparation was reached. Sephadex which has

TABLE I: Water Associated with Sephadex in a Dioxane-Water Environment Containing about 5% Water by Weight

Sample	g of water/ g environment	g water/ g Sephadex
1	0.056	0.153
2	0.069	0.170
3	0.046	0.153
4	0.069	0.174

TABLE II: Relative Dielectric Constant of Sephadex G10 in the Presence of Various Solvents

Rel dielectric constant of Sephadex G10	Solvent
15 ± 2	Water
15 ± 2	Dioxane
14 ± 2	Methanol
8 ± 2	Ethanol
3.3 ± 1	1-Butanol
2.3 ± 1	Carbon tetrachloride
2.3 ± 1	Ethylene dichloride

been exposed to water and then washed in an organic solvent such as dioxane or ethanol retains a certain amount of water even at a considerable concentration gradient with the environment. It was found that 0.16 ± 0.02 g of water was associated with each gram of Sephadex when the environment contained about 5 wt % water (see Table I).

Low-Frequency Dielectric Constant. If dry Sephadex is measured in air it does not appear to be polar. However, in certain organic solvents it appears to have the same effective dielectric constant that it has when suspended in water. This is shown in Table II. To obtain these data, Sephadex G10 was allowed to come to equilibrium with the indicated solvent, placed in the measuring cell for the RX Meter, and the beads of Sephadex were allowed to settle around the electrodes. Thus, as with all Sephadex studies, the measurements were made on a bed or pellet of the material. Because the particles are nonionic, shorting problems arising from contact of one bead with another are much less severe than would be found with materials such as ion-exchange resins. The volume fraction of Sephadex in these pellets was determined from a density measurement and a dry weight measurement as described in the Methods section. The effective dielectric constant of the Sephadex itself is calculated from dielectric measurements of the pellet and its suspending fluid using Maxwell's mixture equation (eq 7). Fortunately for these experiments, it was found that Sephadex has essentially the same effective polarization in the nonpolar solvent dioxane as in water. It also has a high effective dielectric constant in methanol although it appears to be essentially nonpolar in carbon tetrachloride and ethylene dichloride.

Uhf Measurements. Measurements in nonpolar dioxane give the dielectric properties of the Sephadex itself in the unhydrated or "dry" form. Dielectric constants and conductivities of a sample of Sephadex in pure dioxane are shown in Figure 1. Knowing the dielectric constant of the suspending medium (dioxane, $\kappa = 2.2$) and volume fraction of suspended material, Maxwell's mixture equation (eq 7) can be used to determine the dielectric properties of Sephadex. The results of these calculations are presented in Figure 2.

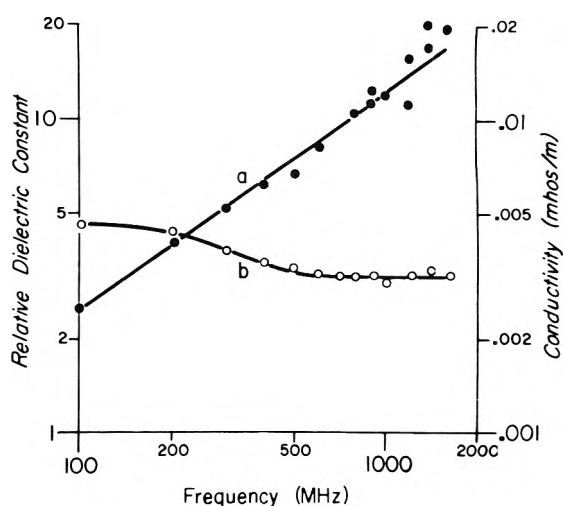


Figure 1. Relative dielectric constant (a) and conductivity (b) of a sample of Sephadex G10 in dioxane vs. frequency. Volume fraction of Sephadex is 0.41. $T = 25^\circ\text{C}$.

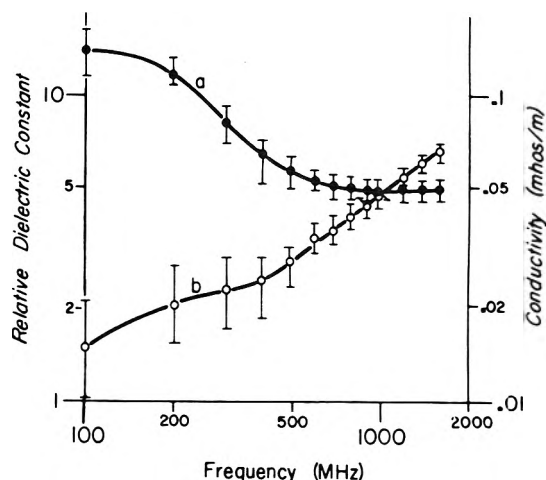


Figure 2. Effective homogeneous relative dielectric constant (a) and conductivity (b) of the Sephadex G10 in dioxane of Figure 1 vs. frequency. $T = 25^\circ\text{C}$.

phadex. The results of these calculations are presented in Figure 2.

Similar measurements were carried out on "hydrated" Sephadex, i.e., Sephadex which had been allowed to come to equilibrium in water and washed in dioxane. Although the suspending medium contained only 5 wt % water in dioxane, the final sample contained 0.16 g of bound water/g of Sephadex. Thus most of the water in the sample must be rather tightly bound to Sephadex. (This can be compared with values of the order of 0.3 g of bound water/g of solute which is frequently assumed to be associated with proteins in aqueous solution.) From dry weight and Karl Fischer measurements, the volume fraction of the Sephadex-bound water complex in the sample was determined (see Methods section). Figure 3 shows the dielectric constant and conductivity of the sample of hydrated Sephadex G10 in the presence of water and dioxane. The volume fraction of Sephadex plus its water of hydration in this sample was 0.41. The complex dielectric constant of the dioxane-water suspending medium is shown in Figure 4. Using these data, the equivalent dielectric constants and conductivities of the Sephadex-bound water complex were calculated with Maxwell's mixture equation (eq 7) and are presented in Figure 5.

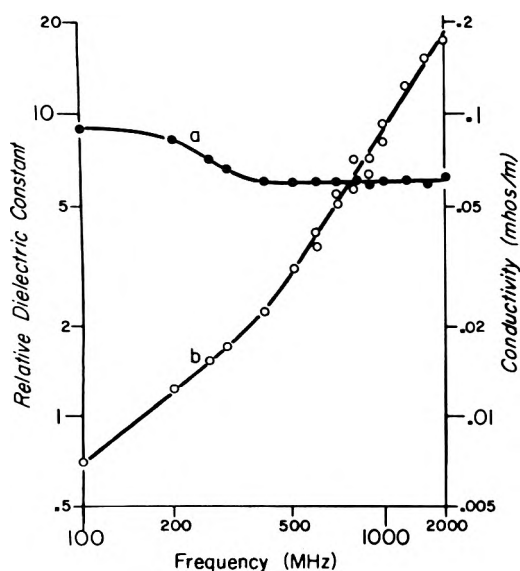


Figure 3. Relative dielectric constant (a) and conductivity (b) of a sample of Sephadex G10 with 0.16 g of bound water/g of Sephadex. Volume fraction of Sephadex-bound water complex is 0.41. $T = 25^\circ\text{C}$.

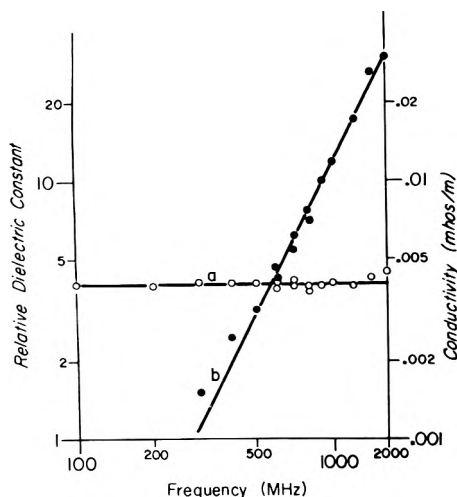


Figure 4. Relative dielectric constant (a) and conductivity (b) of suspending fluid for the sample of Figure 3 (water-dioxane mixture with 0.07 g of water/g of supernatant) vs. frequency. $T = 25^\circ\text{C}$.

Estimates of the standard errors for the calculated effective, homogeneous dielectric constants and conductivities have been estimated by a procedure described by Carstensen and Smearing²⁷ and are indicated by vertical bars in Figures 2 and 5. The original dielectric data as well as the volume fraction determinations are accurate to within $\pm 5\%$. Errors in the effective conductivity increase very significantly at low frequencies so that for "hydrated" Sephadex, the effective conductivities below 300 MHz are omitted.

Discussion

Almost all biological materials exhibit dielectric relaxation in the uhf region. This dispersion has been ascribed to the water which is closely associated with macromolecular solutes.^{8,20} These conclusions are very likely correct. However, they must be made under the assumption that the solutes are not relaxing at these frequencies. In fact, there are examples of pure liquid polymers which relax at uhf

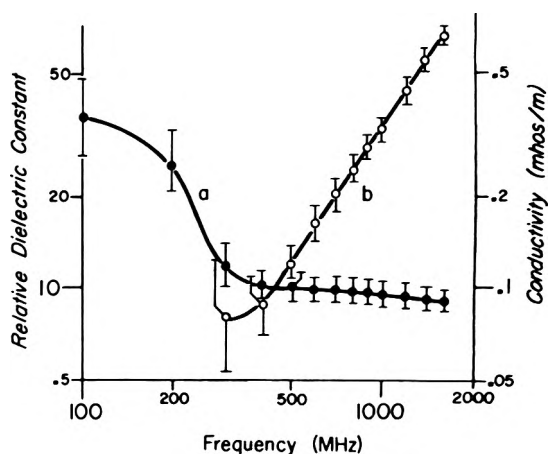


Figure 5. Effective homogeneous dielectric constant (a) and conductivity (b) of hydrated Sephadex G10 of Figure 3. $T = 25^\circ\text{C}$.

frequencies.^{22,28-30} There seems to be no way to determine the dielectric properties of most biological solutes alone. It is clear that hemoglobin changes dramatically when it is dehydrated.¹⁸ On the other hand, there is at present no clear example of water which relaxes at uhf frequencies. Actually the present investigation is a part of an unfruitful search for this kind of water.

The studies of Sephadex are relatively easy to interpret. First from the measurements of Sephadex in the nonpolar solvent dioxane it is clear that the macromolecular structure itself relaxes in the uhf region (Figure 2). It will be noted from Table II that the environment is important in mobilizing the polar structures. Water, dioxane, and methanol all facilitate the polarization but Sephadex appears essentially nonpolar in carbon tetrachloride and ethylene dichloride. Thus if we had started with dry Sephadex and gradually hydrated it, we might have been tempted to attribute the increase in polarization to the water.^{8,20} However, because of the dioxane-Sephadex measurements we see that Sephadex itself can have a high effective dielectric constant and furthermore that it relaxes in the uhf range.

In the partially hydrated state, the magnitude and frequency of the dispersion remains the same. For convenient comparison, the effective homogeneous dielectric constant and conductivity of (1) "dry" Sephadex (i.e., Sephadex in dioxane) and (2) the Sephadex-bound water complex are shown together in Figure 6. Because two polar components are present, an assumption is required. However, by far the simplest explanation for this behavior is that the dielectric properties of the Sephadex itself are unchanged by hydration and that the additional polarization of the complex is contributed by the bound water. The conductivity of the Sephadex-bound water complex is much higher than Sephadex alone particularly at high frequencies. All forms of water have been found to have conductivities which are given by⁵

$$\sigma = \frac{(\epsilon_s - \epsilon_\infty)\omega^2/\omega_0}{1 + \omega^2/\omega_0^2} \quad (9)$$

where ϵ_s and ϵ_∞ are low- and high-frequency limits of the permittivity, ω is the angular frequency, and ω_0 is the angular relaxation frequency. If all of the water in the complex had the dielectric properties of free water, the contribution of the water to the conductivity would be that shown by the dashed line in Figure 6. However, since $\omega^2/\omega_0^2 \ll 1$, a de-

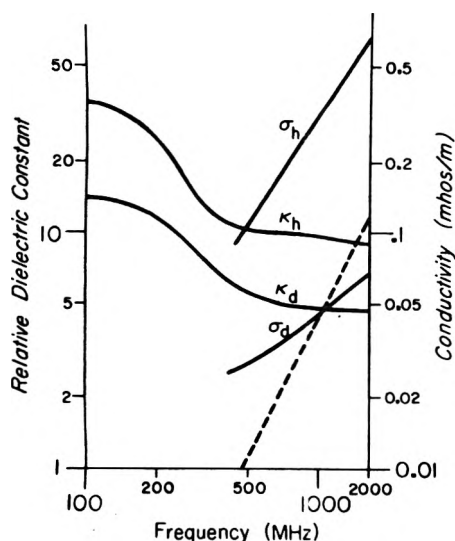


Figure 6. Effective dielectric constant (a) and conductivity (b) of "dry" Sephadex (κ_d and σ_d) and Sephadex-bound water complex (κ_h and σ_h) from Figures 2 and 5. The dashed line is the conductivity which would be expected if the water in the Sephadex-bound water complex had the dielectric properties of free water.

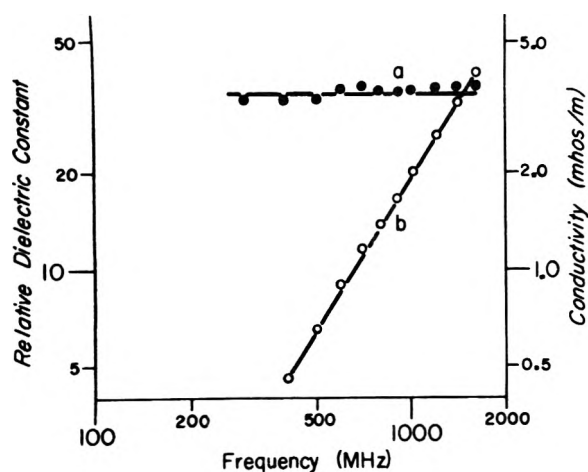


Figure 7. Relative dielectric constant (a) and conductivity (b) of bound water in the presence of Sephadex G10 as a function of frequency. Note the slope of the curve of log conductivity vs. log frequency is significantly less than two. $T = 25^\circ\text{C}$.

crease in ω_0 causes an increase in the conductivity. Thus, it appears that the tightly bound water associated with the Sephadex must relax at frequencies somewhat lower than that characteristic of free water. A crude estimate of the properties of the bound water can be obtained by assuming that the 0.16 g of water/g of Sephadex forms a shell around the dextran molecules which make up the Sephadex particles. Then the dielectric properties of the shell can be calculated from the effective homogeneous dielectric constant and the conductivity of the Sephadex-bound water complex (eq 12) if one assumes that the Sephadex itself remains unchanged by the hydration. The results of these calculations are given in Figure 7. It is granted that these calculations could not be carried out without major as-

sumptions about the geometry and properties of the Sephadex. However, it appears that the bound water has a lower dielectric constant and relaxation frequency than that of free water. On the other hand, the relaxation frequency is clearly above the uhf range, perhaps in the order of 4 GHz.

Summary

Sephadex provides us with important information about the uhf dielectric behavior of complex, crosslinked macromolecular solutes and bound water. First, it is clear that Sephadex itself has uhf relaxation. Thus, it is reasonable to expect that complex biological structures might exhibit a similar behavior. If Sephadex is first brought to equilibrium with water and then washed repeatedly with dioxane, it retains 0.16 g of water/g of Sephadex. It appears that the Sephadex itself is unchanged by this hydration. With that assumption it appears that the bound water relaxes above 1000 MHz but at lower frequencies than free water.

Acknowledgments. The authors are indebted to Mrs. Sally Child for assistance in the measurements.

This work was supported in part by USPHS Grant No. GM09933.

References and Notes

- (1) Author to whom correspondence should be addressed.
- (2) J. L. Oncley, *Chem. Rev.*, **30**, 433 (1942).
- (3) H. F. Cook, *Nature (London)*, **168**, 247 (1951).
- (4) H. P. Schwan, "Electrical Properties of Tissue and Cell Suspensions" in "Advances in Biological and Medical Physics", Vol. V, Tobias and Lawrence, Ed., Academic Press, New York, N.Y., 1957.
- (5) H. P. Schwan, *Ann. N.Y. Acad. Sci.*, No. 125, **2**, 344 (1965).
- (6) E. H. Grant, *Phys. Med. Biol.*, **167**, 607 (1957).
- (7) M. W. Aaron, E. H. Grant, and S. E. Young, *Chem. Soc. Spec. Publ.*, **20**, 77 (1966).
- (8) B. E. Pennock and H. P. Schwan, *J. Phys. Chem.*, **73**, 2600 (1969).
- (9) C. P. Smyth and C. S. Hitchcock, *J. Am. Chem. Soc.*, **54**, 4631 (1932).
- (10) R. P. Auty and R. H. Cole, *J. Chem. Phys.*, **20**, 1309 (1952).
- (11) D. W. Davidson and G. J. Wilson, *Can. J. Chem.*, **41**, 1424 (1963).
- (12) G. J. Wilson and D. W. Davidson, *Can. J. Chem.*, **41**, 264 (1963).
- (13) A. D. Potts and D. W. Davidson, *J. Phys. Chem.*, **69**, 596 (1965).
- (14) G. J. Wilson, P. K. Chan, D. W. Davidson, and E. Whalley, *J. Chem. Phys.*, **43**, 2384 (1965).
- (15) R. E. Hawkins and D. W. Davidson, *J. Phys. Chem.*, **70**, 1889 (1966).
- (16) E. Whalley, D. W. Davidson, and J. B. R. Heath, *J. Chem. Phys.*, **45**, 3976 (1966).
- (17) A. Venkateswaran, J. R. Easterfield, and D. W. Davidson, *Can. J. Chem.*, **45**, 884 (1967).
- (18) D. Rosen, *Trans. Faraday Soc.*, **59**, 2178 (1963).
- (19) S. Takashima and H. P. Schwan, *J. Phys. Chem.*, **69**, 4176 (1965).
- (20) S. C. Harvey and P. Hoekstra, *J. Phys. Chem.*, **76**, 2995 (1972).
- (21) J. Mitchell, Jr., and D. M. Smith in "Aquametry", Interscience, New York, N.Y., 1948.
- (22) These and other methods are described in greater detail in an internal report (G. T. Koide and E. L. Carstensen, Electrical Engineering Technical Report No. GM09933-16) which may be made available to the interested reader. This is also available from University Microfilms, Ann Arbor, Mich., order no. 70-2884.
- (23) T. K. McMeekin, M. L. Graves, and N. J. Hipp, *J. Polym. Sci.*, **12**, 309 (1954).
- (24) H. Pauly and H. P. Schwan, *Biophys. J.*, **6**, 621 (1966).
- (25) J. C. Maxwell in "A Treatise on Electricity and Magnetism", 3rd ed, Oxford University Press, London, Art. 310-314, 1892.
- (26) K. W. Wagner, *Ann. Physik. (Leipzig)*, **40**, 817 (1913).
- (27) E. L. Carstensen and R. W. Smearing, *IEEE Trans. BioMed. Eng.*, **14**, 216 (1967).
- (28) N. Koizumi, *J. Chem. Phys.*, **27**, 625 (1957).
- (29) M. Davies, G. Williams, and G. D. Loveluck, *Z. Electrochem.*, **64**, 575 (1960).
- (30) S. K. Garg and C. P. Smyth, *J. Chem. Phys.*, **43**, 2959 (1965).

Hydrophobic Properties of Zeolites

N. Y. Chen

Mobil Research and Development Corporation, Central Research Division, Princeton, New Jersey 08540 (Received May 30, 1974)

Publication costs assisted by the Mobil Research and Development Corporation

Although porous, amorphous, or crystalline silicates are generally considered to be excellent sorbents for water vapor, experimental evidence on a series of mordenites of varying aluminum concentrations supports the view that a $\equiv\text{Si}-\text{O}-\text{Si}\equiv$ surface is truly hydrophobic or nonpolar. Experimental data are presented to show that the adsorption of water molecules in zeolites involves the specific interaction between the water molecule and the hydrophilic centers, which may be a silanol group or a cation associated with the tetrahedrally coordinated aluminum. A definite stoichiometric ratio, namely, four water molecules to each hydrophilic center associated with the framework aluminum, was found in mordenites with $\text{SiO}_2/\text{Al}_2\text{O}_3$ ratio above 10. It is suggested that for zeolites of lower $\text{SiO}_2/\text{Al}_2\text{O}_3$ ratio, the aluminum concentration is high enough such that the available crystalline void volume is less than the volume of the stoichiometrically associable water. Therefore, the stoichiometric relationship for water sorption eludes detection unless the experimenter explores the region of unusually low aluminum concentration, i.e., silica-alumina ($\text{SiO}_2/\text{Al}_2\text{O}_3$) ratios greater than 10.

Introduction

It is generally acknowledged¹ that the surface of most porous, amorphous, or crystalline silicates contains both silanol groups ($\equiv\text{SiOH}$) and $\equiv\text{Si}-\text{O}-\text{Si}\equiv$ bonds. Young, in studying the interaction of water vapor with amorphous silica surfaces, suggested that water vapor physically adsorbs only on the silanol sites and that the $\equiv\text{Si}-\text{O}-\text{Si}\equiv$ bonds similar to those of the bulk structure are nearly homopolar and hydrophobic.² In the case of crystalline aluminosilicate zeolites, the silica and alumina tetrahedra are arranged in a rigid three-dimensional framework which, in effect, is porous. Unlike the external surface, such as that of a conventional high surface area amorphous silica, the atoms of the intracrystalline "surfaces" are actually made up of atoms and bonds of the bulk structure. Thus, one would expect that the $\equiv\text{Si}-\text{O}-\text{Si}\equiv$ bonds of this surface should be hydrophobic. On the other hand, all the commonly known zeolites, both natural and synthetic, show strong affinity for water and are excellent drying agents even at extremely low partial pressure of water.

We have now demonstrated a direct relationship of the water sorption behavior in crystalline aluminosilicate zeolites to the presence in these silicates of tetrahedrally coordinated aluminum and its associated cations. Recent work in this laboratory and elsewhere^{4,5} showed that tetrahedrally coordinated aluminum may be removed from the framework structure of zeolites. For example, the aluminum in synthetic mordenite (Norton's Zeolon) may be removed to extinction without collapsing the crystalline structure.⁶⁻⁸ With this capability available we have measured the changes in the sorption capacity for water and hydrocarbon molecules as the zeolite is progressively dealuminized, and studied the nature of the interaction of water vapor with the zeolite.

Experimental Section

1. *Zeolite.* Two batches of synthetic mordenite (Zeolon) in their hydrogen form, obtained from the Norton Company, were used. The as received samples have a silica-alumina ratio of 11.0 (Lot No. BG-10) and 14.6 (Lot No. AG-5),

respectively. These samples were dealuminized by two methods: (a) by acid extraction by refluxing in 2 N HCl solution or (b) by repeated alternate treatments, with the HCl solution for 4 hr followed by treating with 1 atm of steam at 538°C for 2 hr, as described in ref 6. The ease of dealuminization appears to depend on the nature of the mordenite as synthesized. Dubinin et al.⁷ reported a 70:1 silica to alumina mole ratio mordenite by acid leaching alone. The samples used in this study (Norton Lot No. BG-10 and AG-5), when leached repeatedly with method a, gave a maximum silica to alumina ratio of about 30, while method b produced samples with silica to alumina ratio greater than 100. Figure 1 shows the typical range of silica to alumina ratio obtainable by method b on two batches of samples.

The drop in silica-alumina ratio on the third cycle is reproducible. It could be explained by a simultaneous loss of alumina and silica from the crystal. X-ray diffraction data showed that the crystallinity of all samples was within $\pm 10\%$ of the starting material. Coincidental to the reversal in silica-alumina ratio on the third cycle, the diffraction pattern of samples after the third cycle showed the peaks shifted to larger angles indicating a shrinkage of the unit cell. Similar observation was made by Dubinin et al.⁷ and Eberly et al.⁹ on their aluminum deficient mordenite samples.

2. *Measurement of Sorption Capacity.* The sorption determinations were made gravimetrically at 25°C with a quartz spring similar to that of a McBain balance. The sample weighing about 1 g placed in a Vycor basket was first heated in vacuo to 500°C to constant weight and cooled to room temperature before the sorbate was admitted. The sorption capacity was determined by the weight gain at a given partial pressure of the sorbate and converted to milliliters of sorbate per gram sorbent assuming normal liquid densities.

For water sorption, the sorption capacity at 1 (p/P = 0.05) and 12 mmHg (p/P⁰ = 0.6) was determined on all samples. Sorption of cyclohexane was measured at p/P⁰ = 0.2 (20 mmHg). After equilibration, the system was evacuated to less than 1 mmHg pressure and the sample allowed

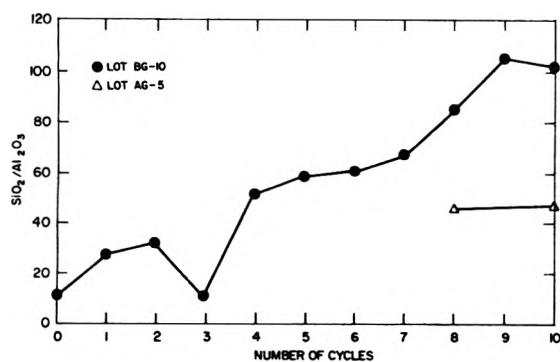


Figure 1. Increasing the silica/alumina ratio of a mordenite by alternating cycles of high temperature hydrolysis and acid extraction.

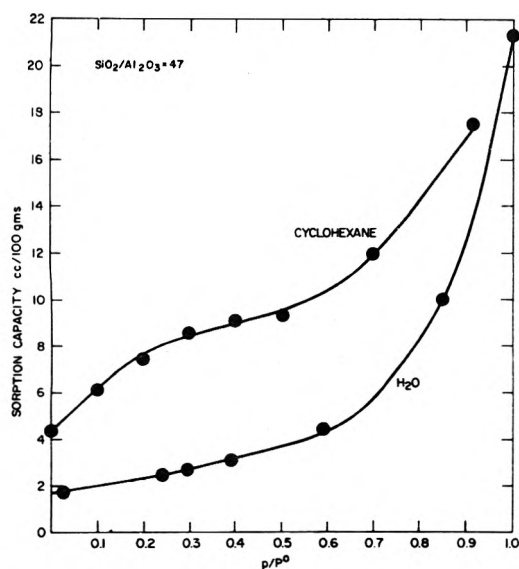


Figure 2. Adsorption isotherm at 25°C.

to reequilibrate at pressures corresponding to a p/P^0 value of about 0.01. Equilibration at low p/P^0 values was obtained in much less time by this method than by equilibrating a fully dehydrated sample with the sorbate maintained at a constant low p/P^0 value. Complete sorption isotherms for water and cyclohexane were determined on only one of the dealuminized mordenite samples ($\text{SiO}_2/\text{Al}_2\text{O}_3 = 47$).

Results

1. *Adsorption Isotherms at 25°C.* The isotherms for water and cyclohexane of a 47 $\text{SiO}_2/\text{Al}_2\text{O}_3$ dealuminized mordenite sample are shown in Figure 2. Both sorbates give type II¹⁰ or S-shaped isotherms. The finite sorption capacity at p/P^0 less than 0.1 typifies the sorption characteristics of zeolites. Both isotherms are concave upward at relative pressures above about 0.6 p/P^0 signalling the commencement of interparticle capillary condensation. It is significant to note that unlike zeolites A or X,³ the isotherms for cyclohexane lie consistently above that for water.

2. *Cyclohexane Sorption.* The change in sorption capacity as a function of the $\text{SiO}_2/\text{Al}_2\text{O}_3$ of the sample is presented in Figure 3. The top curve represents the sorption capacity for cyclohexane at 20 mmHg ($p/P^0 = 0.2$). The sorption capacity at below 1 mmHg ($p/P^0 = 0.05$) is shown as the lower curve. The adsorbed molecules represented by the lower curve are strongly held by the zeolite and could be desorbed with ease only at elevated temperatures. The

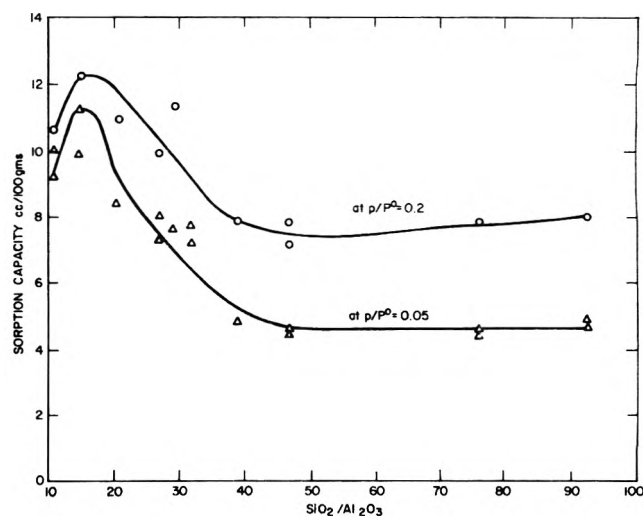


Figure 3. Cyclohexane sorption at 25°C.

incremental capacity between the lower curve and the upper curve, on the other hand, are not strongly held by the zeolite, and could be reversibly sorbed and desorbed at 25°C. The strongly held portion of the sorption capacity is no doubt sorbed in the intracrystalline pores of the zeolite; the less tightly held portion sorbed at $p/P = 0.2$ increased from 1% to nearly 3% with increasing severity of dealumination. Since these samples were highly crystalline, we are led to believe that a portion of the less tightly held sorption capacity may be held on the "external" surface which increased during the dealumination process by the possible creation of fissures or imperfections in the crystal.

3. *Water Sorption.* The sorption capacity for water decreased as aluminum was removed from the zeolite structure. The equilibrium sorption capacity at a given relative pressure of water vapor appears to bear a linear relationship with the concentration of aluminum in the zeolite.

The experimental results at 1 and 12 mmHg H₂O are presented in Figure 4. The slope of these straight lines corresponds to four water molecules per aluminum atom in the zeolite.

Discussions

1. *Zeolite Structure Changes as Reflected by Cyclohexane Sorption.* Parallel to the reaction of zeolite Y with ethylenediaminetetraacetic acid,⁴ the reaction of mordenite with hydrochloric acid effects the removal of tetrahedrally coordinated aluminum from the zeolite framework via hydrolysis. Removal of the first 30% of the aluminum led to an increase in cyclohexane sorption capacity by about 15%.

Increase in sorption capacity after aluminum removal was also reported by other investigators on a number of zeolites including zeolite Y,⁴ erionite,¹¹ and mordenite.^{7,12} Kerr⁴ found that as aluminum was extracted from the zeolite, there was a decrease in the density of the zeolite and the sorption capacity per gram of SiO₂ in the zeolite remains nearly constant. However, the percentage of increase in sorption capacity of dealuminized mordenite found in the present study is higher than could be accounted for by the above mechanism. We are thus inclined to agree with Eberly et al.¹² that the increased capacity results from the removal of extraneous materials from the mordenite channels.

As shown in Figure 3, the sorption capacity passes through a maximum at a $\text{SiO}_2/\text{Al}_2\text{O}_3$ ratio between 10 and

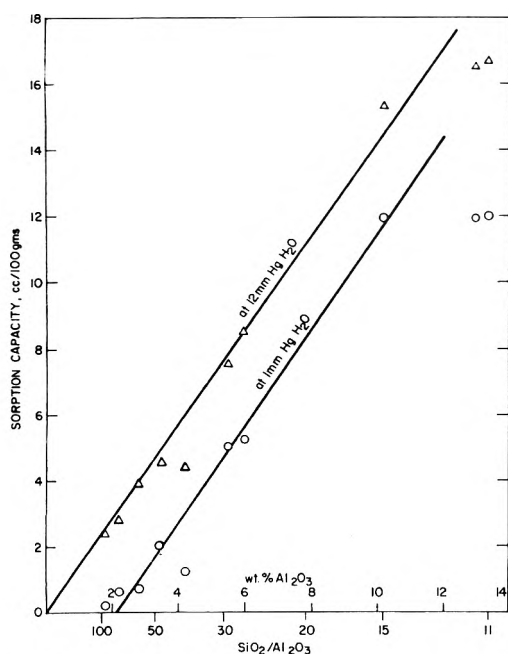


Figure 4. Water sorption at 25°C.

20 μ m and then decreased to a constant value above a $\text{SiO}_2/\text{Al}_2\text{O}_3$ ratio of 40. These higher silica-alumina samples were prepared after repeated exposure to steam at elevated temperature and extractions with hydrochloric acid. A fresh sample after three cycles of these treatments showed a reversal of $\text{SiO}_2/\text{Al}_2\text{O}_3$ ratio together with an indication of unit cell shrinkage. The observed loss of sorption capacity is believed to be related to these structural changes. The "shrunk" mordenite appears to have only about 50% of the original intracrystalline sorption capacity. A similar decrease in sorption capacity for cumene was noted by Dubinin and his coworkers in their earlier work,⁷ however, they attributed the loss of sorption capacity to the partial amorphization of the crystal structure.

2. Hydrophobicity of Silica Surface. The suggestion made by Young² that the $\equiv\text{Si}-\text{O}-\text{Si}\equiv$ bond is hydrophobic was largely based on the observation that the sorption capacity of different preparations of amorphous silicas for water vapor varies significantly from expectation based on their available surface areas. Crystalline aluminosilicate zeolites differ from amorphous silicas by having a porous bulk structure constituted solely of $\equiv\text{Si}(\text{Al})-\text{O}-\text{Si}(\text{Al})\equiv$ bonds. Our sorption data showed that, before aluminum removal, the sorption capacity of synthetic mordenite is nearly the same for water and hydrocarbons. This is also true for all the commonly known zeolites indicating that the available intracrystalline void space is completely filled by all the sorbates. Thus, at first glance, the supposition that the $\equiv\text{Si}-\text{O}-\text{Si}\equiv$ surface is hydrophobic finds no confirmation with zeolites. However, we note from the data shown in Figure 5 that, as the aluminum is progressively removed from the zeolite, the hydrocarbon molecules continue to fill the pores at low relative pressures; water molecules, on the other hand, are no longer filling the pores of the more siliceous samples. In fact, dealuminized mordenites with $\text{SiO}_2/\text{Al}_2\text{O}_3 > 80$ adsorb little or no water at these pressures. Thus these highly siliceous zeolites are truly hydrophobic.

The structural change of mordenite accompanying alu-

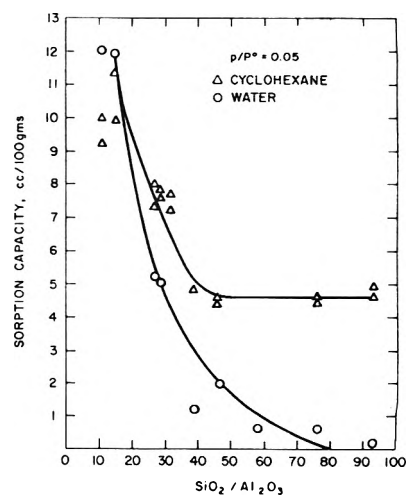
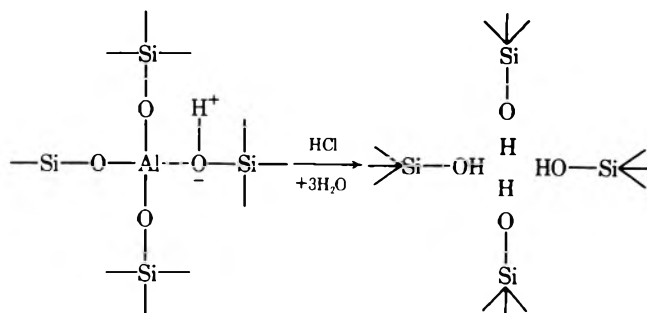


Figure 5. Intracrystalline sorption at 25°C.

minum removal was proposed earlier by Barrer and Peterson¹³ to involve the expulsion of aluminum in a soluble form, and its replacement by a nest of four hydroxyl groups as follows:



This mechanism has been accepted for the removal of aluminum from other zeolites such as zeolite Y.¹⁴ However, the disposition of these hydroxyl groups upon heating or steaming at high temperatures has not been definitively resolved. Kerr¹⁴ based on the finding that the unit cell of a stabilized Y is smaller than that of a hydrogen Y suggested that, in the case of zeolite Y, these four hydroxyl groups are probably lost as water, resulting in some type of $\text{Si}-\text{O}-\text{Si}$ bonding. Eberly et al.,^{12,15} based on x-ray and infrared examination of their dealuminized mordenite, speculated that perhaps the crystal lattice has re-formed, so that the original alumina tetrahedra are replaced by silica tetrahedra. Recently Rubinshtein and his coworker¹⁶⁻¹⁸ in studying the effect of heat treatment on the dealumination of mordenite concluded on the basis of infrared and thermogravimetric analysis that the cleavage of some of the $\text{Al}-\text{O}$ bonds is accompanied at least in part by a closure of the $\text{Si}-\text{O}-\text{Si}$ bond without the intermediate step of forming $-\text{OH}$ groups. Their water sorption data also suggested a decrease of hydrophilic centers with increasing $\text{SiO}_2/\text{Al}_2\text{O}_3$ ratio.

If we accept the theory that the adsorption of water molecules in zeolites involves the specific interaction between the water molecules and the hydrophilic centers, which may be a silanol group, or a cation associated with the tetrahedrally coordinated aluminum, then the degree of structural re-formation, which may depend on the method of preparation, would determine the concentration of hy-

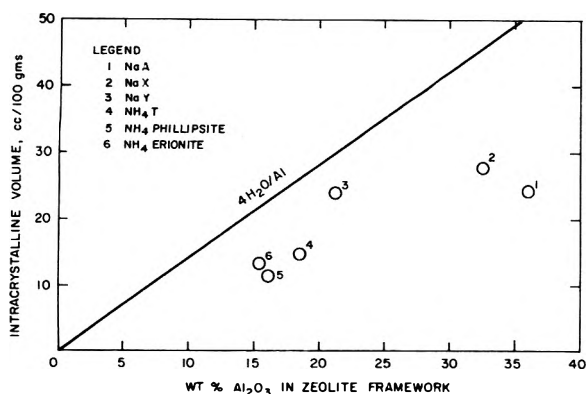


Figure 6. Intracrystalline volume of some known zeolites.

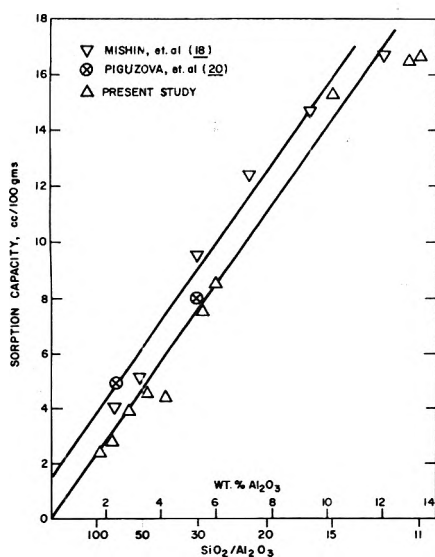


Figure 7. Water sorption at 25°C and 12 mmHg of water.

drophilic centers of the sorption capacity for water. Those methods which lead to incomplete structural re-formation would produce dealuminized products having more hydrophilic centers than a completed re-formed structure. This theory would explain the high sorption values reported by several earlier investigators^{7,19} particularly in view of the fact that the dealumination method used by these early investigators did not involve any high temperature treatment which would be expected to accelerate the structural re-formation process.

The hydrophobic property of our dealuminized mordenites offers support to the postulate that lattice re-formation takes place during the dealumination process. In fact, the stoichiometry of water sorption, as will be discussed later, could be a useful tool in determining the degree of crystal re-formation. However, it does not rule out that the replacement of lattice aluminum by four hydroxyl groups is a possible intermediate step in the dealumination process.

3. *Stoichiometry of Water Sorption.* Our data suggest that the specific interaction between the water molecules and the cations (protons) associated with the tetrahedrally coordinated aluminum corresponds to a coordination of four water molecules for each proton associated with each tetrahedrally coordinated aluminum in the zeolite, in other words, a cluster of three water molecules around each hydronium ion ($H_3O_4^+$). A linear relationship between the

amount of water sorbed and the concentration of alumina in the sample at a constant partial pressure of water is shown in Figure 4. The slope of both straight lines corresponds to a coordination number of 4.

Not all the protons associated with the tetrahedrally coordinated aluminum sites in the zeolite are equivalent in their affinity toward water. Figure 4 shows that about 2% of them did not adsorb any water at 1 mmHg H_2O pressure and became fully coordinated only when the relative pressure was raised to $p/P^\circ = 0.6$.

Taken from published data, the intracrystalline volume of a number of natural and synthetic zeolites is plotted against the concentration of alumina in the zeolite as shown in Figure 6. Also shown is a straight line which corresponds to the necessary sorption capacity for water when each hydrophilic site associated with aluminum is coordinated with four molecules of water. The data clearly show that because of the limited available space within the zeolite pores, the stoichiometric relationship observed in the dealuminized mordenite samples could not be fulfilled in those zeolites having a SiO_2/Al_2O_3 ratio of 10 or lower. In Figure 7 published data on water sorption of dealuminized mordenites which had been heat treated are compared with the results of the present study. Except for the generally higher absolute values and the considerable scatter represented by these data, they appear to fall on a straight line parallel to our data indicating that the coordination number of four is observed.

Conclusions

By removing aluminum from the framework structure of a synthetic Zeolon and re-forming $\equiv Si-O-Si \equiv$ bonds, we have reduced the affinity of the zeolitic surface for water. The amount of water adsorbed was shown to bear a stoichiometric ratio of four molecules for each tetrahedrally coordinated aluminum site remaining in the zeolite. We conclude that the tetrahedrally coordinated silica constituting the framework of the zeolite structure is hydrophobic. The four to one stoichiometric relation between water and aluminum concentration could be observed only in those zeolites having sufficient pore volume to accommodate four water molecules for each of the tetrahedrally coordinated aluminum site and its associated cation present.

Acknowledgment. The valuable comments made during the preparation of this manuscript by Dr. P. B. Weisz of this laboratory are gratefully acknowledged. The author also wishes to thank Messrs. F. A. Smith, S. J. Lucki, and J. Bowman for their contribution to the experimental studies.

References and Notes

- (1) See, for example, R. K. Iler, "The Colloid Chemistry of Silica and Silicates", Cornell University Press, Ithaca, N. Y., 1955.
- (2) G. J. Young, *J. Colloid Sci.*, **13**, 67 (1958).
- (3) See, for example, D. W. Breck, *J. Chem. Educ.*, **41**, 678 (1964).
- (4) G. T. Kerr, *J. Phys. Chem.*, **72**, 2594 (1968).
- (5) R. M. Barrer and M. B. Makki, *Can. J. Chem.*, **42**, 14E1 (1964).
- (6) N. Y. Chen and F. A. Smith, U.S. Patent 3551353, Dec 29, 1970.
- (7) M. M. Dubinin, G. M. Fedorova, D. M. Plavnik, L. I. Pliguzova, and E. N. Prokofeva, *Izv. Akad. Nauk. SSSR, Ser. Khim.*, 2429 (1968).
- (8) W. L. Kranich, Y. H. Ma, L. B. Sand, A. H. Weiss, and I. Zwiebel, *Adv. Chem. Ser.*, **101**, 502 (1970).
- (9) P. E. Eberly, Jr., and C. N. Kimberlin, Jr., *Adv. Chem. Ser.*, No. **109**, 506 (1972).
- (10) S. Brunauer, L. S. Deming, W. E. Deming, and E. Teller, *J. Am. Chem. Soc.*, **82**, 1723 (1940).
- (11) S. P. Zhdanov and B. G. Novikov, *Dokl. Akad. Nauk. SSSR*, **18**, 1107 (1966).
- (12) P. E. Eberly, Jr., and C. N. Kimberlin, Jr., *Ind. Eng. Chem., Prod. Res. Dev.*, **9**, 335 (1970).

- (13) R. M. Barrer and D. L. Peterson, *Proc. R. Soc. London, Ser. A*, **280**, 466 (1964).
- (14) G. T. Kerr, *J. Phys. Chem.*, **71**, 4155 (1967).
- (15) P. E. Eberly, Jr., C. N. Kimberlin, Jr., and A. Voorhies, Jr., *J. Catal.*, **22**, 419 (1971).
- (16) B. I. Mikunov, V. I. Yakerson, L. I. Lafer, and A. M. Rubinshtein, *Izv. Akad. Nauk. SSSR, Ser. Khim.*, 449 (1973).
- (17) I. V. Mishin, A. L. Klyachko-Gurvich, and A. M. Rubinshtein, *Izv. Akad. Nauk. SSSR, Ser. Khim.*, 445 (1973).
- (18) I. V. Mishin, G. A. Piloyan, A. L. Klyachko-Gurvich, and A. M. Rubinshtein, *Izv. Akad. Nauk. SSSR, Ser. Khim.*, 1343 (1973).
- (19) R. M. Barrer and E. V. T. Murphy, *J. Chem. Soc. A*, 2506 (1970).
- (20) L. I. Piguzova, E. N. Prokofeva, M. M. Dubinin, N. R. Bursian, and Y. A. Shavandin, *Kinet. Katal.*, **10**, 315 (1969).

Spectroscopic Studies of Surfactant Solubility. I. Formation of Hydrogen Bonding between Surfactants and Chloroform

Mitsuyo Okazaki, Ichiro Hara,

Laboratory of Chemistry, The Department of General Education, Tokyo Medical and Dental University, Ichikawa, Japan

and Tsunetake Fujiyama*

Department of Chemistry, Faculty of Science, Tokyo Metropolitan University, Setagaya, Tokyo, Japan (Received July 28, 1975)

Water soluble surfactants which have high solubilities in chloroform are verified to form hydrogen bonds to chloroform by the analysis of infrared absorption spectra. The quantitative analysis of the C–D stretching vibration bands shows that these molecules dissolve in chloroform by forming a complex consisting of several solvent molecules and one solute molecule. A detailed method of determining the composition of the complex in solution is described. The molecules studied are trimethyl- and dodecyldimethylamine oxide, decyltrimethyl-, cetyltrimethyl-, tetraethyl-, and tetra-*n*-butylammonium chloride, decyl- and octadecylphosphorylcholine, and cetylpyridinium chloride. Pyridine, pyridine 1-oxide, and *n*-octylamine are also studied as references.

Introduction

Solubilities of surfactants in organic solvents have been studied by many authors.^{1–11} The present report concerns the study of the solubilities of some surfactants in chloroform by infrared spectra. Hydrogen bonding of chloroform to proton acceptor molecules has been well established, and various systems have been studied by infrared and NMR spectra of chloroform and chloroform-*d* complexes.^{13–38} Most of the spectroscopic studies were based upon the assumption of 1:1 complex formation between solvent and solute molecules. In this study, we determine the number of chloroform-*d* molecules bonded to a proton acceptor by quantitative analysis of the C–D stretching vibration band at the dissociation equilibrium between free and bonded chloroform-*d* molecules.

Experimental Section

Materials. Chloroform-*d* was purchased from Merck and Co., Ltd. and was used without further purification.

Decyl- and octadecylphosphorylcholines were synthesized by the authors. An aqueous solution of decyldimethylamine oxide was supplied from Kao Atras Co., Ltd. and was used after a crystallization from acetone. Cetyl- and decyltrimethylammonium chlorides and cetylpyridinium chloride were purchased from Tokyo Kasei Co., Ltd. and purified by recrystallization from acetone. The purities of these samples were checked by thin layer chromatography.

Trimethylamine oxide, tetraethylammonium chloride, tetra-*n*-butylammonium chloride, *n*-octylamine, pyridine,

and pyridine 1-oxide were purchased from Tokyo Kasei Co., Ltd. and were used without further purification.

Absorption Measurements. The absorption spectra were recorded with JASCO IR-G grating spectrometer at a resolution of 1 cm⁻¹. The spectra of chloroform-*d* solutions containing the acceptor in the concentration range from 0 to 0.5 *M* were measured with a KBr cell having a thickness of 0.1 mm. The thickness of the sample cell was checked by the interference fringe method.

Sample solutions containing various amounts of the solute molecule were prepared just before measurement by weighing the solute and chloroform-*d* in the sample flask. Since all of the solutes are very hygroscopic, they were dried thoroughly to an anhydrous condition before each measurement. The elimination of water from the sample solution was confirmed by observing the infrared spectra in the region of 4000–2000 cm⁻¹.

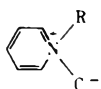
The refractive index n_D^{20} and the specific gravity of the solution were measured with an Abbe refractometer and a pycnometer, respectively, at the same time as the absorption measurements.

All the measurements were done at 20 ± 2°C and the absorption spectra of the C–D stretching vibration for the frequency region of 2500–2000 cm⁻¹ were measured with a resolution of 1 cm⁻¹ and scanning speed of 33.3 cm⁻¹/min.

Results and Discussion

Infrared Spectra of Chloroform-*d* Solution. Table I shows the structures of the molecules studied in the

TABLE I: Molecules Studied and Spectral Characteristics for C-D Stretching Vibration of Chloroform-*d*

	Acceptor ^a R		$\nu - \nu^0$, cm^{-1}	$\Delta\nu_{1,2,3}$, cm^{-1}
$\begin{array}{c} \text{CH}_3 \\ \\ \text{R}-\text{N}^+-\text{O}^- \\ \\ \text{CH}_3 \end{array}$	CH ₃	Trimethylamine oxide	-77	68
	C ₁₂ H ₂₅	Dodecyl-dimethyl-amine oxide	-82	68
$\begin{array}{c} \text{CH}_3 \\ \\ \text{R}-\text{N}^+-\text{CH}_3 \cdot \text{Cl}^- \\ \\ \text{CH}_3 \end{array}$	C ₁₀ H ₂₁	Decyltrimethyl-ammonium chloride	-59	42.5
	C ₁₆ H ₃₃	Cetyltrimethyl-ammonium chloride	-59	43.5
$\begin{array}{c} \text{R} \\ \\ \text{R}-\text{N}^+-\text{R} \cdot \text{Cl}^- \\ \\ \text{R} \end{array}$	C ₂ H ₅	Tetraethyl-ammonium chloride	-62	43.5
	C ₄ H ₉	Tetra- <i>n</i> -butyl-ammonium chloride	-68	49.5
$\begin{array}{c} \text{O} \\ \\ \text{ROPO}^- \\ \\ \text{OCH}_2\text{CH}_2 \\ \\ \text{CH}_3-\text{N}^+-\text{CH}_3 \\ \\ \text{CH}_3 \end{array}$	C ₁₀ H ₂₁	Decylphosphorylcholine	-46.5	44.5
	C ₁₈ H ₃₇	Octadecyl-phosphorylcholine	-45.5	44
	C ₁₆ H ₃₃	Cetylpyridinium Chloride	-56	40

^a The acceptor concentration is 0.45 M.

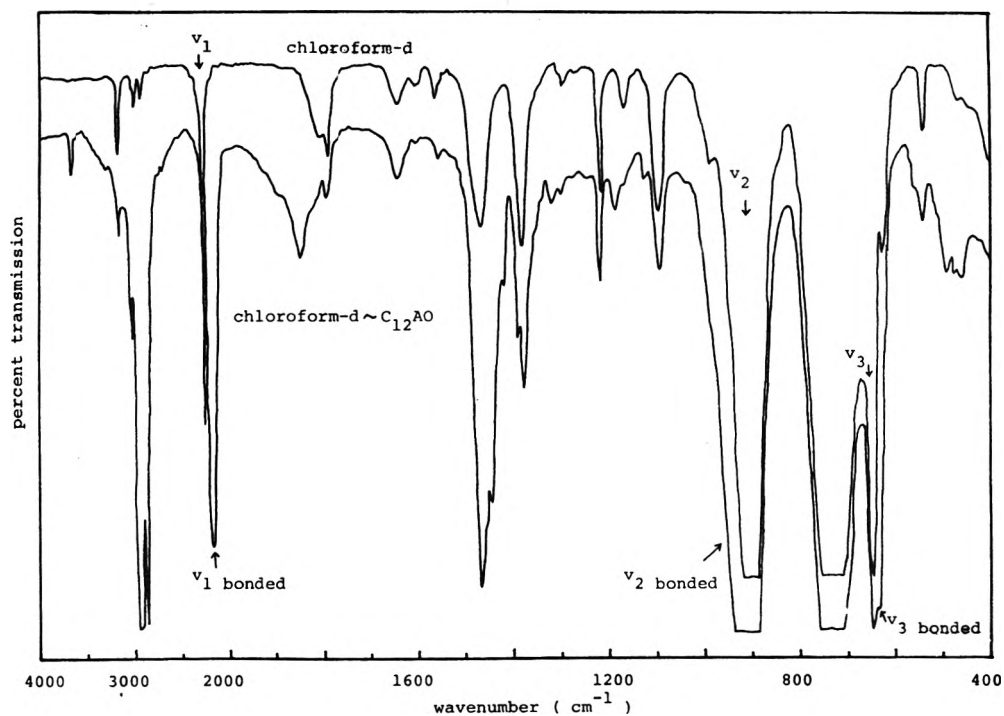


Figure 1. Infrared spectra for the chloroform-*d*-C₁₂AO system. C₁₂AO concentration is 0.70 M.

present work. All the molecules have the $\text{-N}^+\text{-}$ structure with zwitterionic or ammonium salt form and show high solubilities in both water and chloroform. As these substances are hardly soluble in nonpolar solvents and slightly soluble in non-hydrogen-bonding polar solvents, the solubilities in chloroform suggest the existence of some intermolecular interactions between the solute and solvent mol-

ecules. Actually, the infrared spectra of chloroform-*d* show remarkable changes in the fundamental bands of chloroform-*d*; the C-D stretching, the C-D bending, and the C-Cl₃ symmetric stretching vibrations. The ν_1 vibration changes its frequency about -45 to -82 cm^{-1} from that of pure liquid chloroform-*d*, while the ν_2 and ν_3 vibrations shift about 20 and -15 cm^{-1} , respectively. These observa-

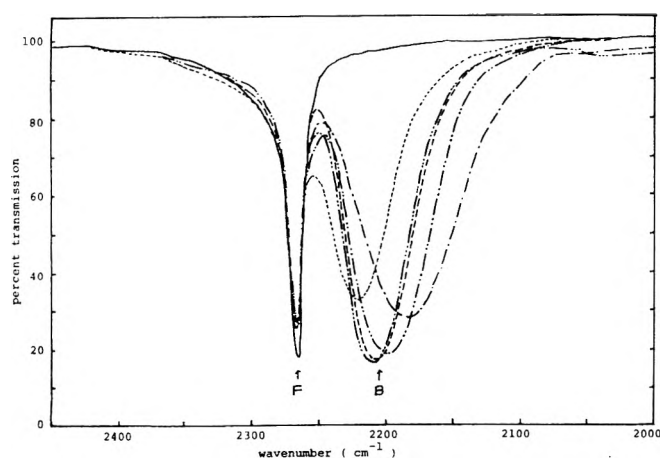


Figure 2. Infrared spectra for chloroform-*d* solutions in the C-D stretching region (F. free; B. bonded): — chloroform-*d* (pure), — · · · C₁₂AO, - - - octadecylphosphorylcholine, - - - - cetyltrimethylammonium chloride, - · · · · cetylpyridinium chloride, - · · · · · tetra-*n*-butylammonium chloride.

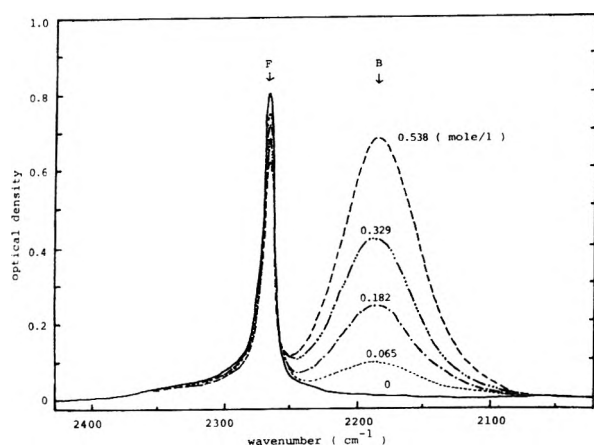


Figure 3. Concentration dependence of the C-D stretching vibration of chloroform-*d* for C₁₂AO solution.

tions indicate the formation of hydrogen bonding between the solute molecule and chloroform-*d*. As an example, the infrared spectra for the chloroform-*d* solution of dodecyl-dimethylamine oxide (C₁₂AO) are shown in Figure 1.

Intensity Measurements of ν_1 Bands. The absorption spectra for the chloroform-*d* solutions in the frequency region from 2500 to 2000 cm⁻¹ are shown in Figure 2. Bands of the C-D stretching vibration corresponding to the free and the bonded states are observed separately. All of the bonded bands for various solutes show large frequency changes to the low-frequency side and increased band width or absorption intensity. The half-band width, $\Delta\nu_{1/2}$, and the frequency shift, $\nu - \nu^0$, are listed in Table I, where the concentration of the solute is 0.45 M and ν^0 is the maximum absorption frequency of the C-D stretching vibration of pure liquid chloroform-*d* ($\nu^0 = 2254$ cm⁻¹). The values of $\nu - \nu^0$ and $\Delta\nu_{1/2}$ of Table I are much larger than those observed for diethyl ether, acetone, and pyridine solutions,¹³ which may indicate the formation of stronger hydrogen bonding in the present systems. The absorption spectra for the C-D stretching vibration of chloroform-*d* containing various amounts of the solute molecule were measured in each system. The spectra obtained for chloroform-*d*-C₁₂AO system are shown in Figure 3. As the concentration

TABLE II: Relative Intensities of the C-D Stretching Vibration for the Chloroform-*d*-C₁₂AO System

Sample no.	Wt % C ₁₂ AO	n_D^a	d	I_b^*	I_f^*
0	0	1.4470	1.48	0	1.302
1	0.2569	1.4471	1.478	0.186	1.279
2	1.0106	1.4472	1.472	0.629	1.262
3	1.4062	1.4473	1.469	0.886	1.252
4	1.7816	1.4474	1.465	1.064	1.216
5	2.8574	1.4476	1.457	1.709	1.209
6	2.8608	1.4476	1.457	1.647	1.189
7	5.2304	1.4481	1.438	2.943	1.120
8	6.4981	1.4486	1.428	3.610	1.068
9	8.7316	1.4488	1.411	5.029	1.010

^a n_D is refractive index and d is specific gravity for the solution. I_b^* and I_f^* are relative intensities defined by the eq 2. (See text.)

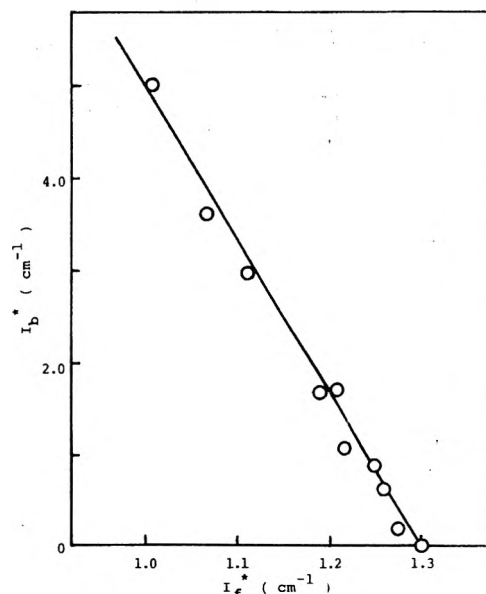


Figure 4. I_b^* vs. I_f^* plot for the chloroform-*d*-C₁₂AO system (see Table II).

of the acceptor molecule increases, intensities of bonded bands increase remarkably, while those of free bands decrease. One of the results is listed in Table II (chloroform-*d*-C₁₂AO system).

Analysis of Intensity Data. The relative intensities of the free and the bonded bands are defined, respectively, as

$$I_f = \frac{1}{l} \int_{\text{band}} \ln \left(\frac{I_0}{I} \right) d(\ln \nu)$$

and

$$I_b = \frac{1}{l} \int_{\text{band}} \ln \left(\frac{I_0}{I} \right) d(\ln \nu) \quad (1)$$

in cm⁻¹, where l is the thickness of the sample, I_0 the energy of incident light, I the energy of transmitted light, and ν the frequency of light. Hereafter, the subscripts b and f refer to the bonded and free states, respectively.

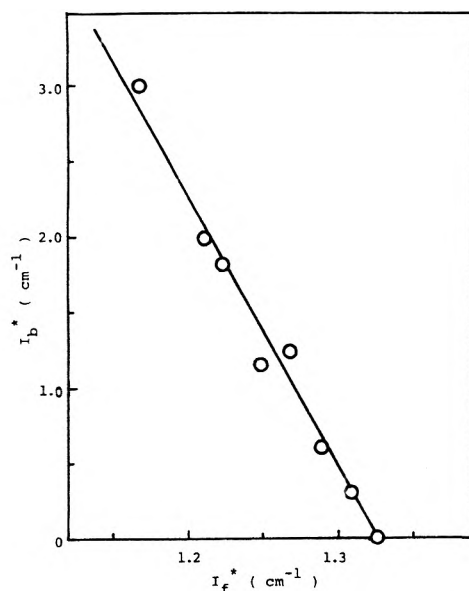
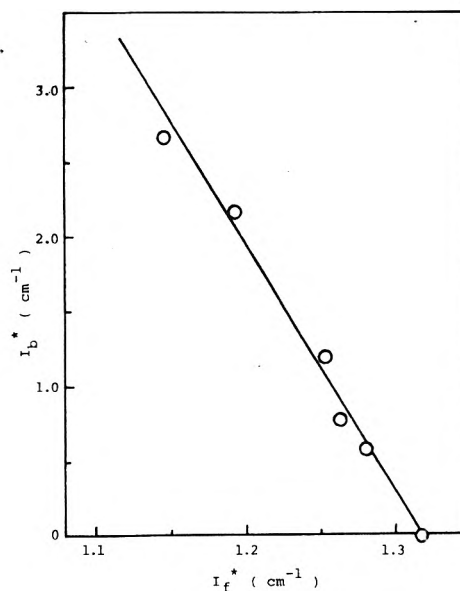
The molar concentration of chloroform-*d* in the solution

$$C_{\text{CDCl}_3} = C_f + C_b$$

was determined from the observed weight concentration and density of the solution. After being corrected for the local field effect,¹² the relative intensities, I_b and I_f , are re-

TABLE III: Final Results for Intensity Data

Acceptor	Γ_b , cm ² /mol	Γ_f , cm ² /mol	Intensity ratio, Γ_b/Γ_f	Solvation no., n	$(\Gamma_b/\Gamma_f)n$
Trimethylamine oxide	3177	106	30	2.5	75
Dodecylmethyl- amine oxide	1726	106	16	5	80
Decylphosphoryl- choline	1944	108	18	3-3.5	54-63
Octadecyl- phosphorylcholine	1460	104	14	4-5	56-70
Decyltrimethyl- ammonium chloride	1906	106	18	4-4.5	72-81
Cetyltrimethyl- ammonium chloride	1930	106	18	4-5	72-90
Tetraethyl- ammonium chloride	4468	114	39	2-2.5	78-98
Tetra- <i>n</i> -butyl- ammonium chloride	5483	112	49	2	98
Cetylpyridinium chloride	2310	105	22	3-4	66-88
<i>n</i> -Octylamine	1824	103	18	1	18
Pyridine	1780	107	17	1	17
Pyridine 1-oxide	1850	106	17.4	2	35

Figure 5. I_b^* vs. I_f^* plot for the chloroform-*d*-decylphosphorylcholine system.Figure 6. I_b^* vs. I_f^* plot for the chloroform-*d*-pyridine system.

duced to the values at the molar concentration of pure liquid chloroform-*d*, $C_{\text{CDCl}_3}^0 = 12.30 \text{ M}$, thus

$$I_f^* = f_d f_c I_f \quad (2)$$

$$I_b^* = f_d f_c I_b$$

and

$$f_c = 12.30/C_{\text{CDCl}_3} \quad (3)$$

$$f_d = 9nD/(nD^2 + 2)^2$$

where nD is the refractive index of the solution and $C_{\text{CDCl}_3}^0$ is the molar concentration of chloroform-*d*.

Now, the absolute intensities, Γ_f and Γ_b , are defined as

$$C_b^* \Gamma_b = I_b^* \quad (4)$$

$$C_f^* \Gamma_f = I_f^*$$

and

$$(C_b^* + C_f^*) = f_c(C_b + C_f) = C_{\text{CDCl}_3}^0 \quad (5)$$

Equations 4 and eq 5 give the relation

$$\frac{I_b^*}{\Gamma_b} + \frac{I_f^*}{\Gamma_f} = C_{\text{CDCl}_3}^0$$

or

$$I_b^* = -(\Gamma_b/\Gamma_f)I_f^* + \Gamma_b C_{\text{CDCl}_3}^0 \quad (6)$$

By plotting I_b^* against I_f^* at a series of concentrations, a straight line with a slope of $-(\Gamma_b/\Gamma_f)$ is generated so far as the absolute intensities, Γ_f and Γ_b , are constant over the concentration range employed. The extrapolated I_f^* value at $I_b^* = 0$ corresponds to the Γ_f value of pure liquid chloroform-*d*, and may be compared with the Γ_f value directly observed for pure liquid chloroform-*d*.

TABLE IV: Calculation of Solvation Number, n , for the Chloroform- d - C_{12} AO System

Sample no.	$10^3 \times C_b$, mol/cm ³	$10^3 \times C_s$, mol/cm ³	Solvation no., n
1	0.108	0.017	6.47
2	0.364	0.066	5.52
3	0.513	0.092	5.56
4	0.616	0.117	5.25
5	0.990	0.190	5.21
6	0.954	0.190	5.01
7	1.705	0.357	4.78
8	2.092	0.449	4.66
9	2.914	0.619	4.71

^a C_b is I_b/Γ_b , C_s is the concentration of the acceptor molecule. Solvation number, n , is C_b/C_s . (See text.)

In Figures 4–6, plots of I_b^* vs. I_f^* for chloroform- d - C_{12} AO, chloroform- d -decylphosphorylcholine, and chloroform- d -pyridine systems are shown. It can be seen from these figures that linear relationships exist between I_b^* and I_f^* . Consequently, the validity of Lambert–Beer's law was verified in these concentration ranges. It is also seen from the figures that the extrapolated I_f^* values at $I_b^* = 0$ are almost same for those systems. For the chloroform- d - C_{12} AO system the Γ_f and Γ_b were 106 and 1726 cm²/mol, respectively. The observed absolute intensities by this method are summarized in Table III. The values of Γ_f are fairly identical for all systems. Γ_b values are approximately equal for all acceptors except tetraethyl and tetra- n -butylammonium chloride, and trimethylamine oxide.

Determination of Solvation Number. At a low concentration of the proton acceptor, all acceptor molecules are considered to be bonding to chloroform- d molecules.¹⁹ Therefore, the ratio of the concentration, C_b , of the bonded chloroform- d to the concentration, C_s , of the solute, C_b/C_s , corresponds to the number of chloroform- d molecules attached to an acceptor molecule. Using the observed Γ_b value, C_b is determined as

$$C_b = f d I_b / \Gamma_b \quad (7)$$

As C_s is known, the ratio, C_b/C_s , is easily determined. We call the ratio solvation number, n . The calculated results for n are summarized in Table III. As an example, the detailed data for C_{12} AO system are shown in Table IV. The solvation number obtained in this case is 4.71–6.47. Therefore, it is concluded that about five chloroform- d molecules and one C_{12} AO molecule form a complex molecule in solution.

Spectroscopic Information and Solubility. Table III shows the absolute intensities and the solvation numbers observed for various acceptors. It is seen from Table III that a complex consisting of several solvent molecules and one acceptor molecule is formed in the solution. Only when an acceptor is pyridine or n -octylamine is the existence of a 1:1 complex verified. The solvation number is largest in the octadecylphosphorylcholine system and smallest in the tetra- n -butylammonium chloride system.

The absolute intensity of the hydrogen bonded chloroform- d , on the other hand, is largest for the tetra- n -butylammonium chloride system. If the intensity ratio, Γ_b/Γ_f , can represent the strength of hydrogen bonding between

chloroform- d and the acceptor molecule, the product of the ratio, Γ_b/Γ_f , and the solvation number, n , is an appropriate estimate of the stabilization energy of one acceptor molecule through hydrogen bond formation in solution. In other words, the product is a good way to estimate the solubility of an acceptor in the solvent.

The last column of Table III shows the calculated $n(\Gamma_b/\Gamma_f)$ products. The results indicate that the product takes almost similar values for all the surfactants studied. This may correspond to the fact that the stabilization energy necessary for the acceptor to be dissolved in chloroform- d is almost the same. In case weak hydrogen bonding is formed, e.g., octadecylphosphorylcholine, a large number of solvent molecules are necessary to dissolve the acceptor. In case strong hydrogen bonding is formed, e.g., tetra- n -butylammonium chloride, only a few solvent molecules are necessary to form a stable complex in solution.

References and Notes

- (1) R. A. Reck, H. L. Harwood, and A. W. Ralston, *J. Org. Chem.*, **12**, 517 (1947).
- (2) R. S. Sedgwick, C. W. Hoerr, and A. W. Ralston, *J. Org. Chem.*, **10**, 498 (1945).
- (3) H. J. Harwood, A. W. Ralston, and W. M. Selby, *J. Am. Chem. Soc.*, **63**, 1916 (1941).
- (4) C. W. Hoerr, H. J. Harwood, and A. W. Ralston, *J. Org. Chem.*, **9**, 201 (1944).
- (5) A. W. Ralston, C. W. Hoerr, W. O. Pool, and H. J. Harwood, *J. Org. Chem.*, **9**, 102 (1944).
- (6) A. W. Ralston, H. J. Harwood, and E. L. DuErow, *J. Org. Chem.*, **9**, 239 (1944).
- (7) S. H. Shapiro, "Fatty Acids and Their Industrial Applications", E. S. Patison, Ed., New York, N.Y., 1968, pp 109–119.
- (8) C. C. Addison and C. R. L. Furnidge, *J. Chem. Soc.*, 3229 (1956).
- (9) J. H. Hildbrand and R. L. Scott, "Solubility of Non-electrolytes", Reinhold, New York, N.Y., 1950.
- (10) F. K. Brown and H. J. Harwood, *J. Am. Chem. Soc.*, **72**, 3257 (1950).
- (11) C. W. Hoerr and H. J. Harwood, *J. Am. Chem. Soc.*, **74**, 4290 (1952).
- (12) S. R. Polo and M. K. Wilson, *J. Chem. Phys.*, **23**, 2376 (1955).
- (13) R. C. Lord, B. Nolin, and H. D. Stidham, *J. Am. Chem. Soc.*, **77**, 1365 (1955).
- (14) C. M. Huggins and G. C. Pimentel, *J. Chem. Phys.*, **23**, 896 (1955).
- (15) C. M. Barrow and E. A. Yenger, *J. Am. Chem. Soc.*, **78**, 5247 (1956).
- (16) R. E. Glick, *Chem. Ind.*, 413 (1956).
- (17) C. M. Huggins and G. C. Pimentel, *J. Chem. Phys.*, **23**, 1244 (1955).
- (18) G. J. Korinek and W. G. Schneider, *Can. J. Chem.*, **35**, 1157 (1957).
- (19) L. W. Reeves and W. G. Schneider, *Can. J. Chem.*, **35**, 251 (1957).
- (20) M. F. Rettig and R. S. Drago, *J. Am. Chem. Soc.*, **88**, 2966 (1966).
- (21) M. W. Hanson and J. B. Bouck, *J. Am. Chem. Soc.*, **79**, 5631 (1957).
- (22) E. Halpern, J. Bouck, H. Finegold, and J. Goldenson, *J. Am. Chem. Soc.*, **77**, 4472 (1955).
- (23) B. N. Khore, S. S. Mitra, and G. Lengyel, *J. Chem. Phys.*, **47**, 5173 (1967).
- (24) P. J. Berkeley, Jr., and M. W. Hanna, *J. Chem. Phys.*, **41**, 2530 (1964).
- (25) P. J. Berkeley, Jr., and M. W. Hanna, *J. Phys. Chem.*, **67**, 846 (1963).
- (26) A. L. McClellan, S. W. Nicksic, and J. C. Guffy, *J. Mol. Spectrosc.*, **11**, 340 (1963).
- (27) J. Devaure, G. Turrell, P. Van Huong, and J. Lascombe, *J. Chim. Phys. Physicochim. Biol.*, **65**, 1064 (1968).
- (28) P. Bachelon, J. Corset, and C. De Loze, *J. Chim. Physicochim. Biol.*, **70**, 1145 (1973).
- (29) R. Mierzecki, *Rocz. Chem.*, **46**, 1375 (1972).
- (30) W. E. Thompson and G. C. Pimentel, *Z. Elektrochem.*, **84**, 748 (1960).
- (31) L. Segal, *J. Phys. Chem.*, **65**, 697 (1961).
- (32) K. Szczepaniak, *Bull. Acad. Pol. Sci. Ser. Sci. Math., Astron. Phys.*, **12**, 189 (1964).
- (33) K. Szczepaniak and A. Tramer, *Bull. Acad. Pol. Sci. Ser. Sci. Math., Astron. Phys.*, **13**, 79 (1965).
- (34) W. G. Paterson and D. M. Cameron, *Can. J. Chem.*, **41**, 198 (1963).
- (35) R. Kaiser, *Can. J. Chem.*, **41**, 430 (1963).
- (36) V. V. Bhujle and M. R. Padhye, *Indian J. Pure Appl. Phys.*, **10**, 867 (1972).
- (37) J. R. Baker, I. D. Watson, and A. G. Williamson, *Aust. J. Chem.*, **24**, 2047 (1971).
- (38) Wei-chuan Lin and Shyr-jin Tsay, *J. Phys. Chem.*, **74**, 1037 (1970).
- (39) It is ascertained that the C–D stretching band corresponding to the free state completely disappears at saturation.

Rates of Ion Pair Formation and Dissociation and of Electron Exchange between Free Ion and Neutral Molecule in Hexamethylphosphoramide

Gerald R. Stevenson* and Antonio E. Alegría

Department of Chemistry, University of Puerto Rico, Rio Piedras, Puerto Rico 00931 (Received May 20, 1975)

Publication costs assisted by the University of Puerto Rico

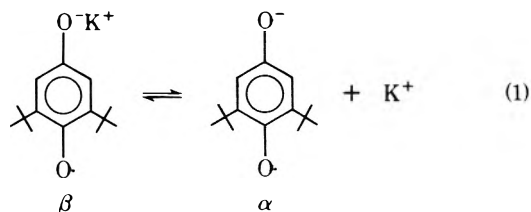
ESR line amplitudes have been substituted into the solutions to the Bloch equations in place of the first-derivative line breadth so that the rate constant of electron exchange (k_{ex}) between the 2,6-di-*tert*-butylbenzoquinone (DBQ) anion radical and neutral molecule, and rate constant for ion pair dissociation (k_1), and ion pair formation (k_2) could be calculated from the relative line heights of the three-line ESR spectrum. Since k_2 was found to be slightly larger than k_{ex} , it is concluded that the rate of ion pair formation is encounter controlled. The activation parameters indicate that the activated complex between free ion and ion pair closely resembles the free solvated ions, and the solvation sheath of the solvated cation is still intact in the activated complex. However, the solvation structure of the ion pair is very different from that for the activated complex or free solvated ions as evidenced by comparison of the activation parameters with the thermodynamic parameters controlling the equilibrium constant of ion pair dissociation.

Since the very first ESR investigations of ion pairing by Adam and Weissman¹ and Atherton and Weissman,² a wealth of information has appeared in the literature concerning the actual structures of ion pairs, the thermodynamic parameters controlling ion pair dissociations, and their parameters controlling interconversions between types of ion pairs. The bulk of this work has been carried out utilizing ESR, conductivities, visible spectroscopy, and NMR. Despite the fact that the thermodynamic parameters for ion pair dissociation can be attacked by a variety of techniques, the kinetic parameters are not so accessible. Over the years only a scattering of reports have appeared of actual rate constants of ion pair dissociation to form solvent separated ion pairs, and no reports of ion pair dissociation to free ion kinetic parameters have appeared. Kinetic and activation parameters for ion pair dissociation to free anion and solvated cation are vital to the understanding of the mechanism of ion pair formation and dissociation.

Such a study would have to be carried out in a solvent where anions can be generated in the fully dissociated state. Hexamethylphosphoramide (HMPA) is the solvent of choice. It is well documented that, in this solvent, many anion radicals are fully dissociated.³ However, the addition of alkali metal salts to these solutions often results in the formation of ion pairs.⁴ The appearance of the ion pair may manifest itself in two ways upon ESR analysis. The spectra of the free ion and ion pair may be superimposed upon each other (simultaneous observation), or the time between ion association-dissociation events may be small on the ESR time scale and only the time-averaged spectrum observed.^{5,6} The determination of rate constants of ion pair dissociation by the use of spin relaxation techniques can be carried out only for the latter case. Further, before a kinetic study can be initiated, the thermodynamic parameters of ion pair dissociation must be known.

The anion radical of 2,6-di-*tert*-butylbenzoquinone (DBQ) in HMPA fulfills all of the above requirements for a kinetic study of the ion pair dissociation. The free anion radical can be generated in HMPA, addition of potassium iodide results in the formation of the ion pair, the ion pair

is in rapid (on the ESR time scale) equilibrium with the free ion, and the thermodynamic parameters of ion pair dissociation (eq 1) are known.^{6,7}



Here we wish to report the kinetic and activation parameters for the formation and dissociation of the DBQ ion pair to form the free ion, and utilize these data to gain insight into the mechanism of ion pair dissociation and formation.

The study is carried out by making use of the relaxation theory (in modified form) as applied to the two site model, which has been derived in detail by Fraenkel.⁸ Since the two forms of the anion radical (α and β) are rapidly interchanging, the observed hyperfine coupling constant is given by

$$\bar{A} = P_\alpha A^\circ + P_\beta A' \quad (2)$$

where P_α and P_β are the probabilities of finding the anion radical in the form of the free ion (α) or ion pair (β), respectively, and A° and A' are the coupling constants for α and β , respectively. Equation 2 shows how the observed coupling constant is affected by the equilibrium mixture, but the rates of ion pair formation and dissociation are defined by the line widths. From the Bloch equations, the line widths are^{8,9}

$$T_2^{-1}(m) = \gamma_e^2 \tau P_\alpha P_\beta (A^\circ - A')^2 m^2 + T_{2,0}^{-1} \quad (3)$$

where

$$\tau = \tau_\alpha \tau_\beta / (\tau_\alpha + \tau_\beta) \quad (4)$$

and $T_{2,0}^{-1}$, the contribution to the line widths from other line broadening mechanisms, is assumed to be independent of m . The quantity $T_2(m)$ is the transverse relaxation time

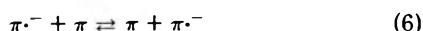
for the line corresponding to spin quantum number m (either -1 , 0 , or $+1$ for the case studied here).

From eq 1 the forward rate constant (k_1) is first order and the reverse rate constant (k_2) is second order, thus $k_1 = 1/\tau_\beta$ and $k_2 = 1/\tau_\alpha(K^+)$. Putting the line widths (δ_m) in terms of gauss, $\delta_m = 2/\sqrt{3}|\gamma_d|T_2(m)$, and solving for δ_m yields

$$\delta_m = 2\tau X_m/\sqrt{3}|\gamma_d| + \delta^\circ \quad (5)$$

where $X_m = P_\alpha\{\omega_\alpha(m) - \bar{\omega}(m)\}^2 + P_\beta\{\omega_\beta(m) - \bar{\omega}(m)\}^2$, and $\omega_\alpha(m)$, $\omega_\beta(m)$, and $\bar{\omega}(m)$ are the positions of the m th line for the free ion, ion pair, and time-averaged species, respectively. These values can be easily calculated for the known g values and coupling constants.⁷

For first derivative Lorentzian ESR lines, the line width (δ_m) is inversely proportional to the square root of the peak-to-peak line height (h_m). For this reason, more precise relative relaxation times can be obtained from measurements of changes in h than in direct measurements of δ_m . For radicals that are involved in rapid equilibria that limits the lifetime of a particular spin state, not all of the hyperfine lines are broadened to the same degree. For this reason, Zandstra and Weissman¹⁰ added a correction factor to the expression for the rate constant (k_{ex}) of electron exchange from the anion radical to the neutral molecule



This correction factor accounts for the difference between the lifetime of a particular anion radical and the residence time in a particular nuclear spin arrangement. This correction factor is $(1 - g_m/N)^{-1}$ where g_m is the statistical intensity of the m th line and N is the sum of the intensities of all of the lines in the absence of exchange

$$k_{ex} = \sqrt{3} \pi (2.8 \times 10^6) \{\delta_m - \delta^\circ\} / \{1 - g_m N^{-1}\} (\pi) \quad (7)$$

Thus for both the electron exchange reaction (eq 6) and the ion pair formation and dissociation reaction (eq 1), the individual hyperfine lines are not broadened to the same extent. For the case of the electron exchange, the $m = +1$ and $m = -1$ lines are broadened more rapidly than the $m = 0$ line as the rate of electron transfer from the DBQ anion radical to the neutral molecule increases. For the case of the ion pair association-dissociation all of the lines are broadened at different rates, since the g values for α and β are different.⁷ Since the heights are more convenient to measure than the line widths, we wish to detail the use of line height changes for the determination of ion pair dissociation and electron exchange kinetics.

Results

Electron Exchange. In order to find the rate constant (k_{ex}) for electron transfer (eq 6) by the use of line heights, it is first necessary to change eq 7 into a function of line heights. Remembering that the ratio of line intensities ($I_m = h_m \delta_m^2$) is always 1:2:1, eq 7 can be rearranged to yield

$$\{\sqrt{3} \pi (2.8 \times 10^6) \delta^\circ\}^{-1} (\text{DBQ}) k_{ex} + \frac{4}{3} = \{\sqrt{2} (h_1/h_0)^{1/2} \frac{9}{4} - \frac{3}{2}\}^{-1} \quad (8)$$

From this expression, a simple plot of the concentration of neutral DBQ added to the anion radical solution in HMPA vs. the reciprocal of $\sqrt{2} (h_1/h_0)^{1/2} \frac{9}{4} - \frac{3}{2}$ should be linear with an intercept of $\frac{4}{3}$ and a slope that is proportional to k_{ex} .

The addition of neutral DBQ to the free anion radical of

DBQ in HMPA does result in greater line broadening of the two outer lines than it does for the central line, Figure 1. Plotting the data as described above yields a rate constant for electron exchange of $2.09 \pm 0.09 \times 10^8 M^{-1} \text{sec}^{-1}$. The intercept obtained from this plot is 1.31 ± 0.04 .¹¹ This is in good agreement with the expected intercept of $\frac{4}{3}$. The plot shown in Figure 2 consists of points taken from several different anion radical solutions. The average value for δ° is 0.198 ± 0.006 G. This value was measured from the ESR spectra before the addition of any neutral molecule to the solution. δ° is relatively large due to the unresolved γ proton splittings.

Now that it has been demonstrated that the use of line heights can be utilized to obtain accurate rate constants for reactions limiting the lifetime of the spin state, the technique can be applied to the more complicated kinetics of ion pair dissociation.

Ion Pair Dissociation. First it is necessary to rearrange eq 5 so that τ can be determined from the line heights. Since

$$I_{-1}/I_1 = h_{-1}\delta_{-1}^2/h_1\delta_1^2 = 1 \quad (9)$$

then

$$(h_1/h_{-1})^{1/2} = (\alpha_{-1}\tau + \delta^\circ)/(\alpha_1\tau + \delta^\circ) \quad (10)$$

where

$$\alpha_m = 2X_m/\sqrt{3}|\gamma_d| \quad (11)$$

Equation 10 can now be solved for τ giving

$$\tau = \delta^\circ \{1 - (h_1/h_{-1})^{1/2}\} \sqrt{3}|\gamma_d| / 2\{X_1(h_1/h_{-1})^{1/2} - X_{-1}\} \quad (12)$$

The equilibrium constant for the ion pair dissociation (eq 1) has been determined by the use of time-averaged coupling constants^{5,6} and g values⁷ by measuring these values after the addition of quantities of KI to the anion radical solution. At 25° the value for K_{eq} is 0.089. This value is an average of that obtained from the g value and coupling constant experiments, but is subject to a small correction due to the fact that there is some ion association between the I^- ions and K^+ ions of the added KI.¹²

Knowing this value for K_{eq} , k_1 and k_2 can now be determined from τ , which is calculated from the experimental line heights and eq 12. The rate constants are related to K_{eq} and τ in the following manner:

$$K_{eq} = (\alpha)(K^+)/(\beta) = \tau_\alpha/\tau_\beta = k_1/k_2 \quad (13)$$

and thus

$$k_1 = \tau^{-1}/\{1 + (K^+)K_{eq}^{-1}\} \quad (14)$$

and

$$k_2 = \tau^{-1}\{K_{eq} + (K^+)\}^{-1} \quad (15)$$

Successive additions of potassium iodide to the free anion radical in HMPA result in the expected line width and line height fluctuations. Utilizing the known coupling constants^{5,6} and g values⁷ for the ion pair and free ion and the previously determined equilibrium constant, the observed rate constant for ion pair formation ($k_{2,obsd}$) was calculated from the measured line heights, Table I.

It is immediately noted from Table I that $k_{2,obsd}$ decreases with increasing concentration of added KI. This is the expected result, since the viscosity of the solution increases with increasing salt concentration and K_{eq} used in

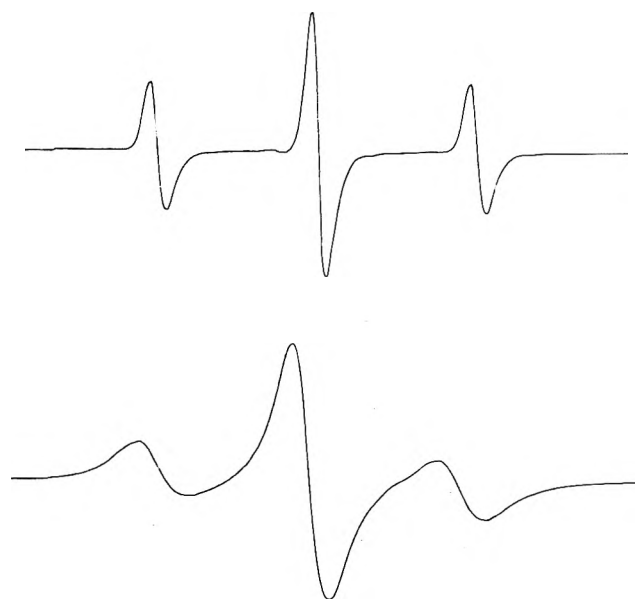


Figure 1. ESR spectra of the anion radical of DBQ in HMPA at 25°. The lower spectrum was recorded for a solution containing 0.3 M neutral molecule.

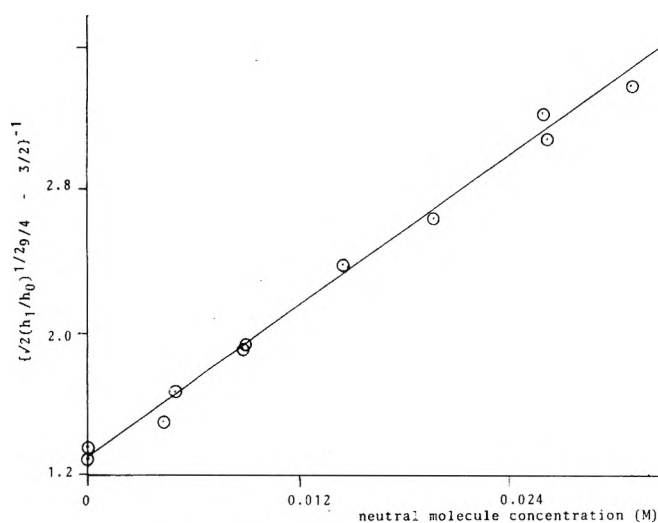


Figure 2. Plot of $\{\sqrt{2} (h_1/h_0)^{1/2} g/4 - 3/2\}^{-1}$ vs. the concentration of neutral molecule at 25°.

the calculations has not been corrected for possible association between the K^+ and I^- ions. The rate constant for ion pair formation can now be determined from an extrapolation of $k_{2,obsd}$ to zero KI concentration, Figure 3. The data given in Table I represents just one experiment. The entire process was carried out four times with different solutions, and an average k_2 was found to be $(4.28 \pm 0.48) \times 10^8 M^{-1} sec^{-1}$. From this value and K_{eq} , $k_1 = (3.81 \pm 0.43) \times 10^7 sec^{-1}$. Extrapolating the data to a zero concentration of added KI eliminates the error due to increased viscosity and due to possible association of the KI itself.

Since δ° is not controlled by either electron transfer or the ion pair formation dissociation process, the viscosity of the solvent media probably has only a very slight effect upon $T_{2,0}$ while clearly having a large effect upon the observed rate constant for ion pair formation. However, the extrapolated rate constants are valid even if $T_{2,0}$ is more severely affected by viscosity changes due to salt addition.

TABLE I: ESR Parameters and Observed Rate Constant for Ion Pair Formation for a Representative Anion Radical Solution with Added Potassium Iodide

(KI), M	\bar{A} , G ^a	\bar{g}	$\tau \times 10^8$, sec	$k_{2,obsd}$, $\times 10^{-8}$, $M^{-1} sec^{-1}$
0	2.346	2.004814	2.74	
0.018	2.298	2.004801	2.64	3.55
0.034	2.267	2.004793	2.45	3.32
0.050	2.243	2.004786	2.41	2.99
0.067	2.223	2.004781	2.37	2.70
0.0835	2.208	2.004776	2.41	2.40
0.101	2.194	2.004773	2.58	2.04

^a These weighted average coupling constants and g values have been accurately determined previously.^{5-7,12}

This is true, since the data are extrapolated to zero salt concentration where $T_{2,0}$ is responsible for the entire line width (δ°).

In order to obtain the activation parameters for ion pair formation and dissociation, it is necessary to obtain k_1 or k_2 at another temperature. Carrying out a similar set of experiments at another temperature would not be advantageous, since the relatively large error in k_1 and k_2 would lead to serious error in E_{a1} and E_{a2} . This difficulty can be avoided by determining k_2 for a set of samples from the same solution (an example of the data obtained from the same initial solution is given in Table II) at 25° and 0°. The energy of activation can then be calculated from the Arrhenius equation and the two experimental rate constants. Even though the values for k_2 from this experiment may not be equal to the statistical average of k_2 for many determinations, the difference in k_2 at 0 and 25° accurately reflects the true energy of activation. E_{a2} was determined in this manner three times yielding values of 4.95, 4.57, and 4.64 kcal/mol. The data obtained at 0° were extrapolated in the same manner as it was at 25°. Since the thermodynamic parameters are known, the activation parameters can be determined.

Conclusions

The strong affinity of the HMPA for solvating cations¹³ is reflected by the negative entropy and enthalpy of ion pair dissociation. The entropy of activation for this dissociation is -15.1 eu, indicating that the activated complex more closely resembles the solvated ions than it does the ion pair. The negative value for ΔS^\ddagger_2 is somewhat surprising and shows that there is more order in the activated complex than there is in the solvated ions. This means that the solvation sheaths around the cation must be still intact in the activated complex, but there is still some Coulombic attraction between the cation and anion, which lowers the entropy of activation. This supports the previous statement that the activated complex closely resembles the solvated ions (with respect to solvation structure).

The kinetic parameters for ion pair formation (k_2 and ΔH^\ddagger_2) are of a magnitude that would be expected for an encounter controlled reaction. It is known that rates of electron transfer are generally encounter controlled.¹⁴ Since k_2 is slightly larger than k_{ex} , it too is encounter controlled. The larger value for k_2 reflects the Coulombic attraction between the K^+ and anion radical as opposed to the very weak attraction between the anion radical and neutral molecule that come together in the electron exchange.

Since k_2 is encounter controlled, it should not vary ap-

TABLE II: Thermodynamic and Kinetic Parameters Controlling the Ion Pair Formation and Dissociation of 2,6-Di-*tert*-butylsemiquinone in HMPA

Reaction	k at 25° ^a	E_a	ΔH^\ddagger	ΔH°	ΔS^\ddagger , eu	ΔS° , eu
Ion pair formation	4.3×10^8	4.7 ± 0.2	4.1^b	1.52	-5.1	10.2
Ion pair dissociation	3.8×10^7	3.2 ± 0.2	2.6	-1.52	-15.1	-10.2

^a The units on the rate constant for ion pair formation (k_2) are $M^{-1} \text{sec}^{-1}$ and those for k_1 are sec^{-1} . ^b The enthalpies and energies of activation are given in kcal/mol.

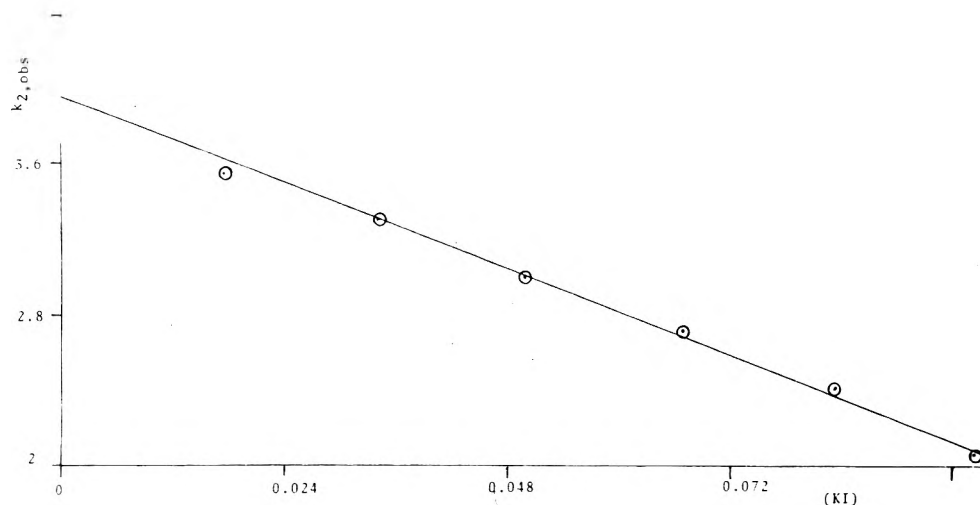


Figure 3. This is one example of a plot of $k_{2, \text{obsd}}$ vs. the concentration of KI added to the anion radical solution. All of the points on this graph were taken from one anion radical solution. Several of these plots were made to obtain an average k_2 .

precipably when DBQ^- is substituted for another semiquinone. Thus, k_1 should be proportional to K_{eq} . The ion pair dissociation equilibrium constant for the benzoquinone anion radical in HMPA with potassium is 0.036 and can now be utilized to estimate k_1 for this system. On this basis, k_1 for the benzosemiquinone system is predicted to be about $1.5 \times 10^7 \text{sec}^{-1}$. The fact that k_1 is smaller for the benzosemiquinone system than it is for the DBQ^- system is supported by the observation of the rate of ion pair formation and dissociation being slow on the ESR time scale for this system. Although it must be remembered that whether the ESR spectrum is in the fast or slow exchange limit depends not only upon the rates but also on the differences in the ESR parameters (proton and alkali metal coupling constants and g values) of the free ion and ion pair.

The three major obstacles to a study carried out by successive additions of salt (ion association of the added salt, increase in viscosity due to the presence of the salt, and changes in the ionic strength) have been eliminated by extrapolation of the determined rate constants to zero salt concentration.

Finally, it should be noted that errors can originate from two sources yet to be discussed: (1) there has been much difficulty in the past in extracting accurate activation energies from magnetic resonance line shapes,¹⁶ leaving the energy of activations obtained here from only two temperatures with possible large errors; (2) even though the ESR lines shapes are Lorentzian at the higher salt concentrations used here, they may not be at zero or very low concentrations where the line width is controlled by the unresolved splitting. This latter effect should result in more error in data taken from the lower salt concentrations but, since the value for k_2 obtained by extrapolation is the same

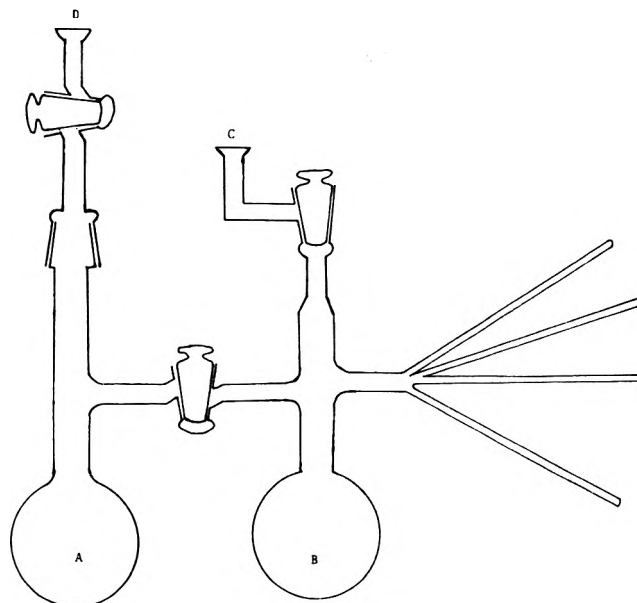


Figure 4. Apparatus used for the experimental determination of k_1 and k_2 .

whether only the higher or lower salt concentrations are considered, this error is probably small.

Experimental Section

The DBQ was purchased from Aldrich Chemical Co. and was recrystallized before use. The potassium iodide was purchased from Alpha Inorganics and was stored in a vacuum oven for 48 hr at 100° prior to use. The purification of the HMPA has been previously described.¹⁵

ESR measurements were carried out with a Varian E-9 ESR spectrometer with a dual cavity. The temperature was controlled with a Varian temperature controller calibrated with an iron constantan thermocouple.

The rate constants (k_1 and k_2) were determined by use of the apparatus shown in Figure 4. The clean dry apparatus was first weighed and about 50 ml of purified HMPA was placed in bulb A with a small piece of potassium metal. A few milligrams of DBQ were placed in bulb B and the entire system evacuated by connection with the vacuum line at joint C. The HMPA was then distilled from bulb A to bulb B. With all of the stopcocks closed, the apparatus was removed from the vacuum line, bulb A cleaned, a small piece of K metal added to bulb A, and the bulb reevacuated through D. The HMPA solution was then passed into bulb A where it was stirred until the anion radical was formed. The entire anion radical solution was then poured back into bulb B and an ESR sample taken. Bulb A was cleaned again and charged with a known quantity of potassium iodide and reevacuated. At this point the apparatus containing the solution was weighed. The anion radical solution was then placed back into bulb A and left stirring until the salt was completely dissolved. This solution was then passed back and forth between the two bulbs until the solution was uniform. Finally, it was placed in bulb B and another ESR sample taken. The apparatus was weighed again. Now, bulb A could be recharged with salt and the entire procedure repeated several times so that a series of samples with different concentrations of added salt could be taken from the same initial anion radical solution. The

ESR tubes were calibrated volumetrically to account for the loss of solution due to the taking of samples.

Acknowledgment. We are grateful to the National Institute of Health for support of this work. The NIH support was from Grant No. RR-8102 of the Division of Research Resources.

References and Notes

- (1) F. C. Adam and S. I. Weissman, *J. Am. Chem. Soc.*, **80**, 1518 (1958).
- (2) N. M. Atherton and S. I. Weissman, *J. Am. Chem. Soc.*, **83**, 1330 (1961).
- (3) J. Chaudhuri, S. Kume, J. Jagur-Grodzinski, and M. Szwarc, *J. Am. Chem. Soc.*, **90**, 6421 (1968); A. Cserhegyi, J. Jugar-Grodzinsky, and M. Szwarc, *ibid.*, **91**, 1892 (1969); A. Cserhegyi, J. Chaudhuri, E. Franta, J. Jugar-Grodzinsky, and M. Szwarc, *ibid.*, **89**, 7129 (1967); G. Levin, J. Jugar-Grodzinsky, and M. Szwarc, *ibid.*, **92**, 2268 (1970).
- (4) L. Echevoyen, H. Hidalgo, and G. R. Stevenson, *J. Phys. Chem.*, **77**, 2649 (1973); G. R. Stevenson and A. E. Alegria, *ibid.*, **77**, 3100 (1973).
- (5) G. R. Stevenson and A. E. Alegria, *J. Phys. Chem.*, **78**, 1771 (1974).
- (6) A. E. Alegria, R. Concepcion, and G. R. Stevenson, *J. Phys. Chem.*, **79**, 361 (1975).
- (7) A. E. Alegria and G. R. Stevenson, *J. Phys. Chem.*, **79**, 1042 (1975).
- (8) G. K. Fraenkel, *J. Phys. Chem.*, **71**, 139 (1967).
- (9) J. H. Freed and G. K. Fraenkel, *J. Chem. Phys.*, **39**, 326 (1963).
- (10) P. J. Zandstra and S. I. Weissman, *J. Chem. Phys.*, **35**, 757 (1961).
- (11) All of the reported errors are standard deviations. Errors in line slopes and intercepts are taken from a least-squares analysis.
- (12) G. R. Stevenson and A. E. Alegria, *J. Am. Chem. Soc.*, **97**, 3869 (1975).
- (13) H. Normant, *Angew. Chem., Int. Ed. Engl.*, **6**, 1046 (1967).
- (14) For a recent example see A. C. Wahl and M. A. Komarynsky, *J. Phys. Chem.*, **79**, 695 (1975).
- (15) G. R. Stevenson, L. Echevoyen, and L. R. Lizardi, *J. Phys. Chem.*, **76**, 1439 (1972).
- (16) F. A. L. Anet and R. Anet in "Determination of Organic Structures by Physical Methods", F. C. Nachod and J. J. Zuckerman, Ed., Academic Press, New York, N.Y., 1971, Chapter 7.

Gas Phase Molecular Structure of Perfluoro-*tert*-butyl Iodide by Electron Diffraction

A. Yokozeki and S. H. Bauer*

Department of Chemistry, Cornell University, Ithaca, New York 14853 (Received June 16, 1975)

The structural parameters of $(CF_3)_3CI$ [gas phase] were determined by a least-squares reduction of electron diffraction intensities: $r_g(C-C) = 1.544 \pm 0.015 \text{ \AA}$, $r_g(C-F) = 1.333 \pm 0.004 \text{ \AA}$, $r_g(C-I) = 2.16 \pm 0.03 \text{ \AA}$, $\angle CCF = 111.0 \pm 0.6^\circ$, $\angle CCC = 111.5 \pm 1.7^\circ$, and $\angle CCI = 107.3 \pm 1.0^\circ$, where the uncertainties were set at 2.5σ (σ is the least-squares standard deviation) plus estimated systematic errors due to inaccuracies in the nozzle-to-plate distances and accelerating voltage. These parameters are compared with values reported for the series, $(CF_3)_nCF_{n-3}I$ ($n = 0, 1, 2, 3$). It appears that the $\angle CCI$ decreases linearly with increasing n ($n = 1 \rightarrow 3$). This systematic change in the bond angle is consistent with the trend observed in $(CH_3)_nCH_{n-3}X$ ($X = F, Cl, CH_3$).

Introduction

Perfluoro-*tert*-butyl iodide, $(CF_3)_3CI$, was investigated as part of a broad program of study of F for H and CF_3 for CH_3 substitution effects on molecular geometries.¹ The structural parameters for perfluoromethyl, perfluoroethyl, and perfluoroisopropyl iodides have been reported by Andreassen and Bauer.^{2,3} The present study completes the series $(CF_3)_nCF_{n-3}I$ ($n = 0, 1, 2, 3$). As has been demonstrated for $(CF_3)_3COH$,⁴ "large amplitude motions" are an-

anticipated in the perfluoro-*tert*-butyl group. However, here our objective was to determine the structural parameters. With respect to the intramolecular motions, rather than undertaking a parallel detailed analysis, our knowledge of $(CF_3)_3COH$ was used; the three CF_3 rotors are regarded as a single effective rotor which describes reasonably well the coupled motions. Such a simplification does not seriously perturb the determination of other geometrical parameters for this molecule.

Experimental Section

The sample of $(CF_3)_3CI$ was supplied by Dr. D. C. England of E. I. duPont de Nemours and Co. Diffraction photographs were taken with the Cornell instrument on Kodak electron image plates. The accelerating voltage was 60 kV (λ 0.04854 Å); nozzle-to-plate distances of 128.76 ± 0.16 (HVS) and 286.65 ± 0.29 mm (HVL) were determined from MgO diffraction patterns taken concurrently with the gas photographs. Exposure times were about 7 (HVS) and 3 sec (HVL) using a beam current of 0.5 μ A. To calibrate the estimated nozzle-to-plate distances and the apparent increase in the mean amplitudes due to the extraneous scattering,⁴ diffraction patterns of CO_2 were also recorded concurrently with the sample. A least-squares analysis of CO_2 intensities gave the scale factors of -0.15% for interatomic distances and -4.9% for the root-mean-square amplitudes. The total scattering intensities are shown in Figure 1. Numerical values for the intensities at integral q 's [$= (40/\lambda) \sin \theta/2$], the error and correlation matrices are listed in the microfilm edition of the journal. (See paragraph at end of text regarding Supplementary Material.)

Analysis

Reduced Molecular Intensity Function. The molecular intensity, $qM(q)$, was calculated from $q(I_T - I_B)/I_B$, where I_T and I_B are the observed total scattered intensity and the smooth background, respectively. The initial background, drawn through the I_T curve, was refined via the proposals of Bonham and Bartell.⁵ Then the nonnuclear scattering correction $\Delta[qM(q)]$ was calculated according to the procedure of Konaka and Kimura;⁶ indeed, we closely followed their method for data reduction, and used the symbols as defined by them.

$$\Delta[qM(q)] = k \sum_{i,j} A_{ij} (g_{ij} - \mu_{ij} \cos \Delta\eta_{ij}) \sin \left(\frac{\pi}{10} q r_{aij} \right) \times \exp \left\{ -\frac{1}{2} \left(\frac{\pi}{10} q \right)^2 l_{ij}^2 \right\}$$

$g_{FF} = 1.20 + 0.5 \exp(-2 \times 10^{-4} q^2)$; $g_{CC} = 1.35 \exp(-2 \times 10^{-3} q^2) + 1.55 \exp(-10^{-5} q^2)$; $g_{CF} = 1.24 + 0.4 \exp(-10^{-3} q^2) + 0.4 \exp(-2 \times 10^{-4} q^2)$; $g_{CI} = 1.10$; $g_{IF} = 1.10$. The g functions are empirical, and were chosen on the sole criterion that $\Delta[qM(q)]$ be small compared with $qM(q)_{\text{obsd}}$. Indeed, the above choice of g functions reduced the size of the correction term to magnitudes comparable to the random noise in $qM(q)_{\text{obsd}}$. In contrast, when the g functions were set to unity the magnitudes of $\Delta[qM(q)]$ and $qM(q)_{\text{obsd}}$ were of the same order, and the correction was sensitive to the specific model inserted in the calculation. For this reason, a conventional radial distribution curve provides no useful structural information. The μ_{ij} factors were calculated from the tables of Tavard et al.⁷ [the inelastic scattering] and of Schäfer et al.⁸ [the elastic scattering and phase shifts]. Since no molecular force field was available for this molecule, its structure was refined in terms of a geometrically consistent r_a model without any corrections for shrinkage or anharmonicity. The $qM(q)_{\text{obsd}}$ and the theoretical best fit $qM(q)$ are given in Figure 2.

Structural Parameters. On the basis of a C_{3v} geometry, the following independent parameters specify the structure: three bond distances (C-C, C-F, and C-I) and two bond angles ($\angle CCF$ and $\angle CCI$). With respect to the conformation of the three CF_3 groups about their respective C-C axes, one additional parameter, φ_{eff} , adequately describes

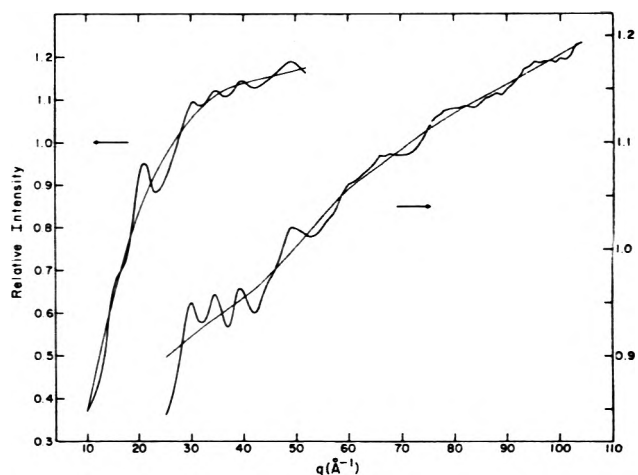


Figure 1. Photographic density for $(CF_3)_3CI$ plotted as a function of the scattering variable q . The refined background is also shown.

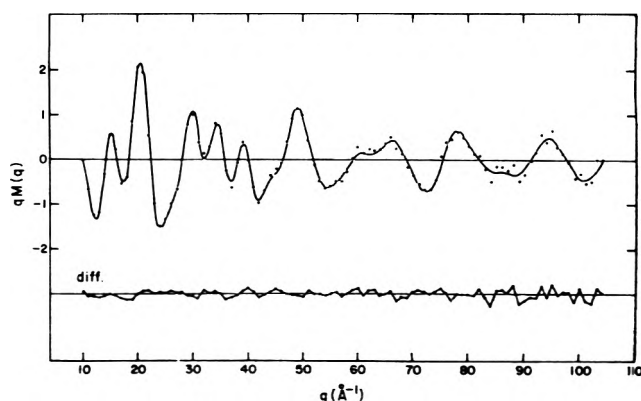


Figure 2. The reduced experimental molecular intensity (circles) and the theoretical intensity (solid curve) calculated with the structural parameters in Table I.

TABLE I: Structural Parameters for $(CF_3)_3CI$ (r_g Values)^a

$r(C-C)$, Å	1.544 (0.015)	$l(C-C; 1.54)$, Å	0.053 ^b
$r(C-F)$, Å	1.333 (0.004)	$l(C \cdots C; 2.55)$, Å	0.070
$r(C-I)$, Å	2.157 (0.030)	$l(C-I; 2.16)$, Å	0.060
$\angle CCF$, deg	111.0 (0.6)	$l(C \cdots I; 3.00)$, Å	0.085
$\angle CCC$, deg	111.5 (1.7) ^c	$l(C \cdots F; 2.81-3.04)$, Å	0.175
$\angle CCI$, deg	107.3 (1.0)	$l(C \cdots F; 3.72)$, Å	0.073
$l(C-F)$, Å	0.040 (0.007)	$l(I \cdots F; 3.10-3.34)$, Å	0.150
$l(C \cdots F)$, Å	0.072 (0.013)	$l(I \cdots F; 4.24)$, Å	0.100
$l(F \cdots F)$, Å	0.064 (0.008)	$l(F \cdots F; 2.63-2.74)$, Å	0.180
		$l(F \cdots F; 3.10-3.70)$, Å	0.210
		$l(F \cdots F; 4.10-4.20)$, Å	0.132
		$l(F \cdots F; 4.74)$, Å	0.075
	$k_1, 0.75 (0.04)^d$; $k_2, 0.88 (0.09)$		

^a $\varphi_{\text{eff}} = 10^\circ$. ^b Estimated mean amplitudes assigned for ranges in distances. ^c The $\angle CCC$ was calculated from $\angle CCI$, d k_1 and k_2 are indexes of resolution for HVL ($q = 10-28$) and for HVS ($q = 29-104$), respectively.

the thermal deviations of the CF_3 rotors from the staggered [C_{3v}] positions; this was demonstrated for the structurally similar case $(CF_3)_3COH$.⁴ φ_{eff} is defined by $\varphi_{\text{eff}} = \varphi_i$ ($i = 1$,

TABLE II: Structural Parameters for the Series $(CF_3)_nCF_{n-3}I$ [$n = 0, 1, 2, 3$]^a

	CF_3I^b	$CF_3CF_2I^b$	$(CF_3)_2CFI^b$	$(CF_3)_3CI^c$
C-I, Å	2.101 (0.009)	2.14 (0.02)	2.14 (0.02)	2.16 (0.03)
C-C, Å		1.52 (0.03)	1.55 (0.01)	1.54 (0.01)
C-F, Å	1.344 (0.004)	1.338 (0.004) ^d	1.338 (0.003)	1.333 (0.004)
$\angle CCF, ^\circ$ deg		109.9 (0.8)	111.0 (0.4)	111.1 (0.6)
$\angle CCI, ^\circ$ deg		113.4 (0.8)	109.4 (0.4)	107.3 (1.0)

^a r_g structures derived from electron diffraction. ^b Reference 2. ^c Present study. ^d All the C-F distances were assumed to be equal. ^e Bond angles in C-CF₃.

TABLE III: Comparison of C-C-X Angles

X	CH ₃ CH ₂ X	(CH ₃) ₂ CHX	(CH ₃) ₃ CX
F	109.7° (0.3) ^a	108.3° (0.4) ^b	107.9° (0.5) ^c
Cl	111.0° (0.1) ^d	109.0° ^e	107.0° (0.7) ^f
CH ₃	112.4° (1.2) ^g	110.8° (0.2) ^h	109.5°
I	113.4° (1.2) ^g	109.4° (0.4)	107.3° (1.5)

^a L. Nygaard, *Spectrochim. Acta*, **22**, 1261 (1966).
^b M. Kimura, private communication (5th Austin Symposium on Gas Phase Molecular Structure, Austin, Tex., 1974). ^c B. Haase, J. Haase, and W. Zeil, *Z. Naturforsch. A*, **22**, 1646 (1967). ^d R. H. Schwendman and G. D. Jacobs, *J. Chem. Phys.*, **36**, 1245 (1962). ^e F. L. Tobiason and R. H. Schwendman, *ibid.*, **40**, 1014 (1964). ^f R. L. Hilderbrandt and J. D. Wieser, *ibid.*, **55**, 4648 (1971). ^g T. Iijima, *Bull. Chem. Soc. Jpn.*, **45**, 21 (1972). ^h R. L. Hilderbrandt and J. D. Wieser, *J. Mol. Struct.*, **15**, 27 (1973). ⁱ Fluorocarbons, see Table II.

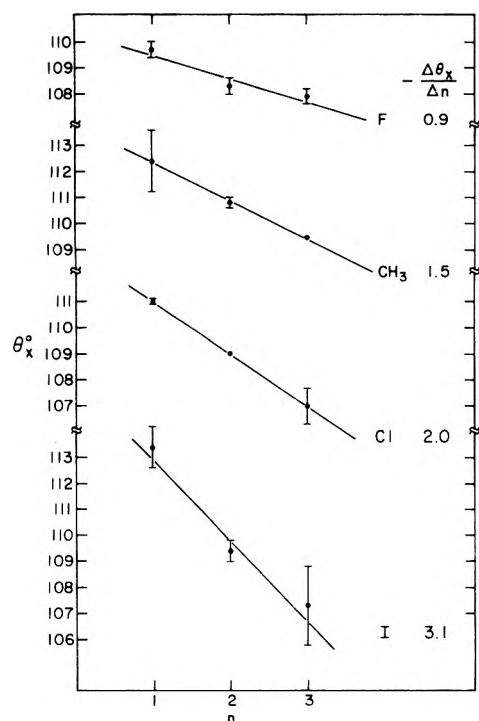


Figure 3. The change in the bond angle, [$\angle CCX = \theta_x$], in the series $(CY_3)_nCY_{3-n}X$ as a function of n . When $X = F, CH_3$, and Cl , $Y = H$; when $X = I$, $Y = F$; see Table III.

2, 3), where the φ_i 's are the dihedral angles of the $-C_iF_3$ groups, measured from the staggered position relative to C-I and the corresponding C-C_i bonds.

The above structural parameters were determined by least-squares analyses of the $qM(q)$ curve, using a starting model which was estimated from analogous molecules: $(CF_3)_3COH$,⁴ $(CF_3)_2CFI$,² and CF_3CF_2I .² The mean square

TABLE IV: Structures of *tert*-Butyl Groups^a

	$(CF_3)_3C-H^b$	$(CF_3)_3C-I^c$	$(CF_2)_3C-OH^d$
C-C, Å	1.539 (0.003)	1.544 (0.015)	1.566 (0.009)
C-F, Å	1.336 (0.002)	1.333 (0.004)	1.335 (0.004)
$\angle CCC, ^\circ$ deg	112.9 (0.2)	111.5 (1.7)	110.4 (0.8)
$\angle CCF, ^\circ$ deg	110.9 (0.2)	111.1 (0.6)	110.6 (0.4)
	$(CH_3)_3C-H^e$	$(CH_3)_3C-Cl^f$	$(CH_3)_3C-F^g$
C-C, Å	1.535 (0.001)	1.528 (0.002)	1.522 (0.008)
C-H, Å	1.113 (0.002)	1.102 (0.007)	1.097 (0.005)
$\angle CCC, ^\circ$ deg	110.8 (0.2)	111.6 (0.2)	111.0 (0.5)
$\angle CCH, ^\circ$ deg	111.4 (0.2)	110.8 (0.9)	111.6 (0.5)

^a The distances are r_g values. The r_a distances in *b* and *g* were converted to r_g . ^b R. Stolevik and E. Thom, *Acta. Chem. Scand.*, **25**, 3205 (1971). ^c Present study. ^d Reference 4. ^e R. L. Hilderbrandt and J. D. Wieser, *J. Mol. Struct.*, **15**, 27 (1973). ^f R. L. Hilderbrandt and J. D. Wieser, *J. Chem. Phys.*, **55**, 4648 (1971). ^g B. Haase, J. Haase, and W. Zeil, *Z. Naturforsch. A*, **22**, 1646 (1967).

amplitudes also were initially estimated from these molecules and then adjusted to obtain the best fit to the observed curve, by trial and error. For the φ_{eff} parameter, as was expected from the case of $(CF_3)_3COH$,⁴ an acceptable fit was obtained with models, $\varphi_{eff} = 0-17^\circ$. The best fit parameters were derived with $\varphi_{eff} \approx 10^\circ$. The results are listed in Table I. The uncertainties were estimated to be 2.5 times least-squares standard deviations plus the errors due to the scale factor corrections [0.2% for distances and 5% for mean amplitudes].

Discussion

In Table II the structural parameters of $(CF_3)_3CI$ are compared with those of members in the series. The C-I bond in $(CF_3)_3CI$ is about 0.06 Å longer than that in CF_3I . This is consistent with the general trend observed in CH_3X and $(CH_3)_3CX$ ⁴ compounds. The structure of the $-CF_3$ groups is essentially unperturbed, as discussed elsewhere.¹ The systematic change in $\angle CCI$ angle is noteworthy; the magnitude of $\angle CCI$ decreases as the number of CF_3 groups increases. This is analogous to the observed changes in $(CH_3)_nCH_{n-3}X$ [$n = 1, 2, 3$; $X = F, Cl, CH_3$] sequences; see Table III. These comparisons are further illustrated in Figure 3. The $\angle CCX$ angle (θ_x) in $(CY_3)_nCY_{n-3}X$ [$Y = H$ or F] decreases linearly with n . The gradient, $-\Delta\theta_x/\Delta n$, increases in the order $X = F, CH_3, Cl$, and I .

The structures of *tert*-butyl groups, $(CY_3)_3C-$ [$Y = F$ or H], are compared in Table IV. The $\angle CCC$ and the $\angle CCY$ angles equal 111° , within 1° except for the $\angle CCC$ angle in $(CF_3)_3CH$. The C-C distance in $(CF_3)_3C-$ seems generally longer than that in $(CH_3)_3C-$ compounds.

Supplementary Material Available: Appendices I and II contain numerical values for the intensities at integral q and error and correlation matrices (2 pages). Ordering information is given on any current masthead page.

References and Notes

- (1) A. Yokozeki and S. H. Bauer, *Top. Curr. Chem.*, **53**, 71 (1975).
 (2) A. L. Andreassen and S. H. Bauer, *J. Chem. Phys.*, **56**, 3802 (1972).

- (3) S. H. Bauer and A. L. Andreassen, *J. Phys. Chem.*, **76**, 3099 (1972).
 (4) A. Yokozeki and S. H. Bauer, *J. Phys. Chem.*, **79**, 155 (1975).
 (5) R. A. Bonham and L. S. Bartell, *J. Chem. Phys.*, **31**, 702 (1959).
 (6) S. Konaka and M. Kimura, *Bull. Chem. Soc. Jpn.*, **43**, 1693 (1970). The reader is urged to refer to this excellent paper for a thorough discussion of errors in the structure determination of molecules which incorporate atoms with large phase shift factors.
 (7) C. Tavad, D. Nicolas, and M. Rouault, *J. Chim. Phys.*, **64**, 540, 555 (1967).
 (8) L. Schafer, A. C. Yates, and R. A. Bonham, *J. Chem. Phys.*, **55**, 3055 (1971).

Nonempirical Molecular Orbital Calculations on the Electronic Structures, Preferred Geometries, and Relative Stabilities of Some $C_2H_6N^+$ Isomeric Ions

Frank Jordan

Department of Chemistry, Rutgers University, Newark, New Jersey 07102 (Received October 9, 1974; Revised Manuscript Received September 12, 1975)

Nonempirical (Gaussian ab initio) geometry optimization was performed on a number of isomeric $C_2NH_6^+$ ions. Two levels of approximation (STO-3G minimal and 4-31G extended basis set) were in agreement in support of the experimental finding that the protonated Schiff-base isomers are the most stable ones on the $C_2NH_6^+$ surface. In general, those ions possessing a resonance contribution with a filled octet were found to be the most stable ones. Barriers to CH_3^- or NH_3^- rotation were predicted to be nearly 1 kcal/mol irrespective of basis set. The results allowed estimation of the proton affinities of some C_2NH_5 isomers. The imine tautomer ($CH_3CH=NH$) was found to be slightly more basic than the enamine ($CH_2=CHNH_2$). The estimated intrinsic basicities (4-31G calculations) were similar to that of pyridine.

The sophistication of the mass spectrometrist has enabled him to determine the particular structural isomeric ion formed in a fragmentation process as well as the heat of formation of the isomer.

Quantum chemistry can be of considerable aid in delineating the geometry of the ions. In fact, one of the more severe tests of a theoretical method is its performance in predicting the electronic structure, geometry, and relative energy of a transient species. Qualitative attempts had been made in the past employing semiempirical calculations for this purpose.¹ The recent availability of rigorous, nonempirical methods and of fast computers makes it possible to study such problems quantitatively.

Ab initio methods have been employed in studies on a large number of small ions.²

This report describes nonempirical calculations of the preferred geometry and relative energies of isomeric ions with the formula $C_2NH_6^+$, a prominent peak (m/e 44) in the mass spectrum of many amines. There are two reasons for choosing this system. First, the electronic structure of Schiff-base salt structures (corresponding to some of the isomers) is of considerable biochemical interest since these are reminiscent of the intermediates found in many enzyme-catalyzed reactions. Secondly, two very recent experimental studies provide considerable insight into the rearrangement processes and relative energies of these isomeric ions.^{3,4}

Theoretical Method

The calculations were performed with the Gaussian 70 program developed by Pople and his coworkers.⁵ Two levels of approximation were used: the STO-3G minimal basis set⁶ (assigning three Gaussian functions per Slater type orbital) and the 4-31G extended basis set⁷ (assigning four Gaussians to inner-shell orbitals and three Gaussians to the inner and one Gaussian to the outer part of the valence shell orbitals such as H 1s, C and N 2s and 2p).

The wave functions were partitioned according to the Mulliken population analysis⁸ and net atomic and bond overlap populations were calculated for the energy optimized geometry of the isomeric ions.

The principal reason for employing two levels of approximation is to assure that the relative stabilities suggested remain independent of the basis set and are not an artifact of the geometry optimization procedure. While more recently Pople and coworkers suggested that polarization functions be employed to obtain isomerization energies,⁹ this laboratory at the present is not equipped to do so.

In some cases the quadratic force constants were determined with the assumption of a harmonic potential. For a variety of molecules and some diatomic ions, Newton et al.¹⁰ showed that the STO-3G approximation predicts, on the average, bond lengths within 0.035 Å, bond angles with-

in 2° , and stretching and bending force constants within 20–30% (overestimated) of experimental values.

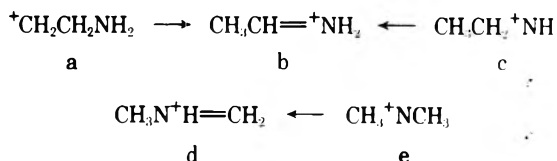
Geometry Optimization Procedure

Absolute minimization of the energy with respect to all geometric degrees of freedom was not performed since lack of symmetry in most species considered would have made it very expensive. The starting point in the geometry optimization always assumed the "standard" bond lengths and bond angles suggested by Pople and Gordon for neutral molecules.¹¹ The ethyl substituent, when present, was assumed to be totally staggered and all tetrasubstituted carbon atoms were assumed to have perfect tetrahedral angles around them (109.5°).

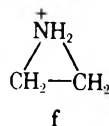
For each ion discussed sequential optimization was performed for those geometric parameters which are distinct by symmetry. The optimum values obtained by such sequential optimization were always a result of interpolation.

The interpolated values thus obtained are accurate to better than 1° in bond angles and 0.01 \AA in bond lengths. Subsequently, the interpolated optimal geometric parameters were used in a simultaneous variation of all bond angles by 2° (not dihedral ones) and all bond lengths by 0.01 \AA and the final parameters quoted are the result of these interpolated, simultaneously varied calculations. This simultaneous variation gave results always within 1° in angle and 0.01 \AA in bond length from the sequentially optimized parameters.

Levens and McLafferty established the occurrence of the isomerizations³



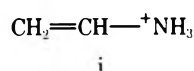
Solka and Russell published experimental heats of formation values for structures b, c, d, and e as well as for f^4 (N-protonated aziridine)



Supposedly, f could have arisen from cyclization of a. Calculations were performed on structures a–f. An attempt was made to see if structures g and h correspond to local minima on the global $C_2NH_6^+$ energy surface.



In addition, the structure of ion i (a tautomer of b) was also examined



Assuming corner protonation, no minima corresponding to cyclic structures g and h could be found (STO-3G) for a large variety of C–C and C–N distances. Rather, the calculations indicated conversion of both g and h to the acyclic analogs with no activation energy.

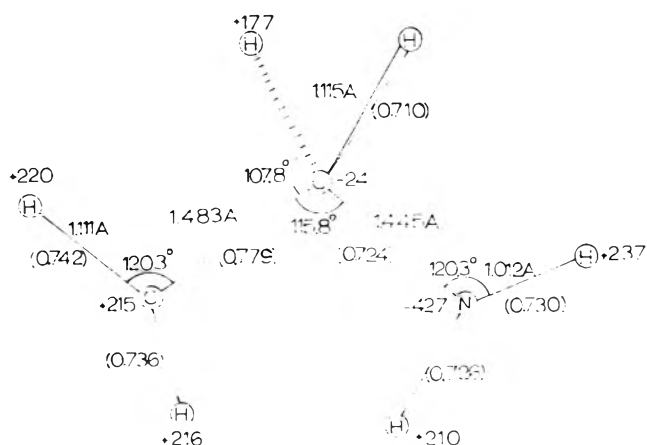


Figure 1. ${}^+\text{CH}_2\text{CH}_2\text{NH}_2$. STO-3G optimized geometrical parameters. Net atomic populations (X1000) near atoms; overlap populations in parentheses under bonds.

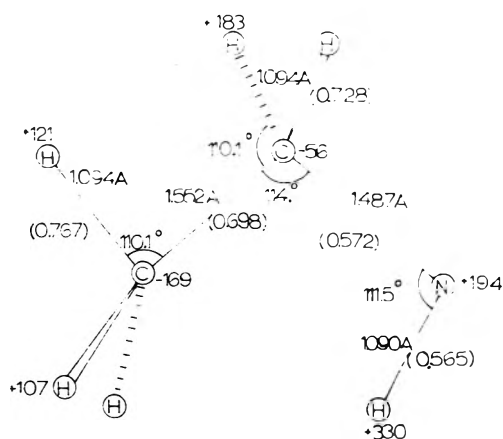


Figure 2. $\text{CH}_3\text{CH}_2\text{NH}^+$. STO-3G optimized geometrical parameters. Net atomic populations (X1000) near atoms; overlap populations in parentheses under bonds.

Results and Discussion

Optimized Geometry and Electronic Structure of Isomers. $\text{CH}_2\text{CH}_2\text{NH}_2^+$. The totally staggered conformer in Figure 1 was considered only. The optimization was performed in the sequence: N–C, C–C (reversal did not change the outcome), C_{sp^3} –H's, C_{sp^2} –H, and N–H bond lengths, angle C–C–N, angle C_{sp^2} – C_{sp^3} –H, and finally all four C_{sp^3} –H and C_{sp^3} –N–H angles simultaneously. This is the only isomer possessing an n type highest occupied molecular orbital with a relatively low (0.51 au) Koopmans' first ionization potential (negative of the energy of the highest occupied molecular orbital). As will be evident throughout this report, the bulk of the positive charge is located not at the heavy atoms rather on the hydrogens according to STO-3G (see population analysis in Figure 1). With the assumption of a harmonic potential the calculated force constant for C–N stretching is larger (7.1 mdyn/\AA) than for C–C stretching (5.2 mdyn/\AA).

$\text{CH}_3\text{CH}_2\text{NH}^+$. The totally staggered conformer shown in Figure 2 was assumed. Sequential optimization was performed on C–N, C–C, C–H (all simultaneously), and N–H bond lengths, then on angles C–N–H, C–C–N, and C–C–H (all simultaneously). The calculated quadratic force constants are 6.15 mdyn/\AA for the C–C and 4.64 mdyn/\AA for the C–N bond.

The Koopmans' theorem ionization potential (from a σ orbital) is 0.71 au, nearly identical in structures b, c, d, e, and f. The nitrogen in this structure carries only a fraction of a positive charge (Figure 2). Both the carbon atom and the hydrogens are much less positive in the methyl than in the methylene position indicating that the charge attenuation is distance dependent.

$\text{CH}_3\text{CH}_2^+\text{NH}$ is predicted to be less stable than $^+\text{CH}_2\text{CH}_2\text{NH}_2$ by nearly 10 kcal/mol. Apparently, the terminal positive charge is better accommodated on carbon than on nitrogen in accord with the greater electronegativity of the latter element.

$\text{CH}_3^+\text{NCH}_3$. Sequential optimization of the two C-N bond lengths (simultaneously) of the C-N-C angle and of the six C-H bond lengths (simultaneously) and of all N-C-H angles (simultaneously) was performed for both the totally staggered (Figure 3) and eclipsed (Figure 4) conformers.

Optimization following this order with totally staggered methyl groups led to 1.488 Å for C-N, 1.097 Å for C-H bond lengths, and 116.7° for the C-N-C angle according to STO-3G (Figure 3) and 1.419 Å for C-N, 1.085 Å for C-H bond lengths, and 121.9° for the C-N-C angle according to 4-31G. A word of caution is in order. Since absolute minimization for even such a small, symmetrical ion is nearly prohibitive in most laboratories, one should beware of the preferred geometry predictions at different levels of approximations. In addition, when comparing isomerization energies at different levels of approximation employing the same geometry, quantitative comparisons will always be subject to the same qualification, namely, that a minimum energy geometry as predicted by STO-3G may no longer be a minimum energy geometry with the extended basis set. The geometry of the ion with the two methyl groups eclipsed was also optimized at the STO-3G levels. The optimum geometry of the eclipsed conformer turned out to be identical with that of the staggered one except for a lengthening of the C-N bond (to 1.493 Å) in the eclipsed conformer (Figure 4).

Figure 3 presents the population analysis. The nitrogen is positively charged (0.2). The C-N overlap population is rather small for the bond length implying a weak bond.

$\text{CH}_3\text{CH}=\text{NH}_2^+$. Acetaldiminium ion is the N-protonated Schiff-base derived from acetaldehyde and ammonia.

The conformation shown in Figure 5 was optimized. The sequential optimization was performed on the C-N, C-C, N-H (both simultaneously), $\text{C}_{\text{sp}^2}\text{-H}$, $\text{C}_{\text{sp}^3}\text{-H}$ (all three simultaneously) bond lengths, C-C-N, N- $\text{C}_{\text{sp}^2}\text{-H}$, $\text{C}_{\text{sp}^2}\text{-C}_{\text{sp}^2}\text{-C}_{\text{sp}^3}\text{-H}$ (all three simultaneously), $\text{C}_{\text{sp}^2}\text{-N-H}$ (both simultaneously) bond angles maintaining all substituents along the C=N bond coplanar with this bond.

The population analysis is presented in Figure 5. Both the optimized C-N bond length and its overlap population imply the existence of a double bond at this position yet the nitrogen carries a negative charge suggesting the importance of the resonance contribution $\text{CH}_3\text{-}^+\text{CH-NH}_2$ in the resonance hybrid.

$\text{CH}_3^+\text{NH}=\text{CH}_2$. N-Methylformaldiminium ion is the N-protonated Schiff-base derived from N-methylamine and formaldehyde. Stepwise optimization followed the sequence: C-N, N=C, $\text{C}_{\text{sp}^2}\text{-H}$ (both simultaneously), $\text{C}_{\text{sp}^3}\text{-H}$ (all three simultaneously), N-H bond lengths, and C-N-C, H-N- C_{sp^2} , N- $\text{C}_{\text{sp}^3}\text{-H}$ (all three simultaneously), N- $\text{C}_{\text{sp}^2}\text{-H}$ (both simultaneously) angles. Table I presents some of the optimization results on this ion to illustrate two points.

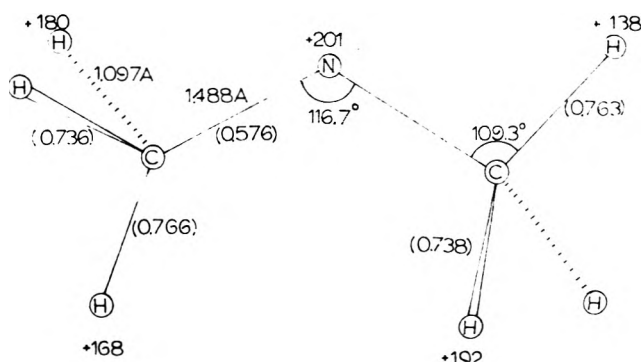


Figure 3. $\text{CH}_3^+\text{NCH}_3$, staggered. STO-3G optimized geometrical parameters. Net atomic populations (X1000) near atoms; overlap populations in parentheses under bonds.

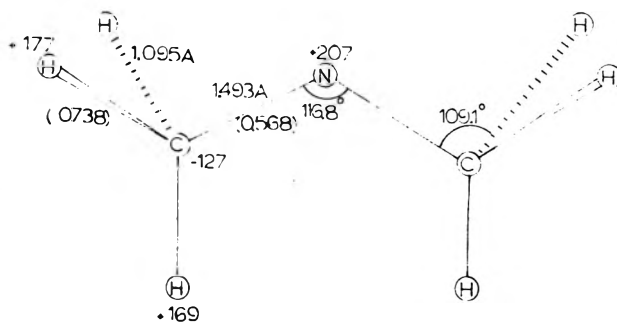


Figure 4. $\text{CH}_3^+\text{NCH}_3$, eclipsed. STO-3G optimized geometrical parameters. Net atomic populations (X1000) near atoms; overlap populations in parentheses under bonds.

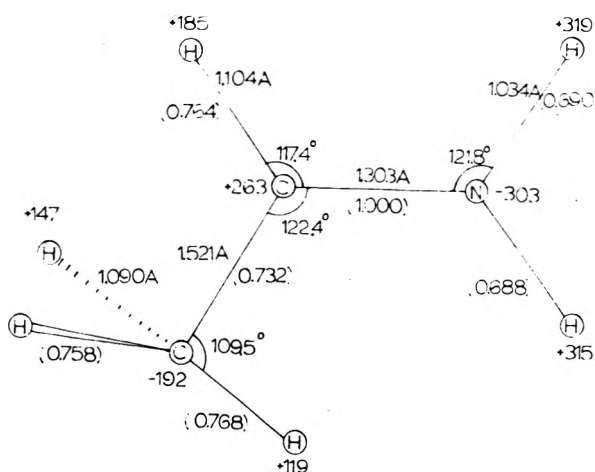


Figure 5. $\text{CH}_3\text{CHNH}_2^+$. STO-3G optimized geometrical parameters. Net atomic populations (X1000) near atoms; overlap populations in parentheses under bonds.

First, it shows that the energy variations with bond angle and bond length changes are small near the optimum geometry. Secondly, Table I provides a measure of the energy requirement for distortion of bond angles and bond length near the optimum geometry. As examples, distortion of N-H or C-H bond lengths by 0.01 Å costs less than 0.1 kcal/mol; of C-N-C angle by 2° costs less than 0.2 kcal/mol; of all bond lengths by 0.01 Å and all bond angles by 2° simultaneously less than 2 kcal/mol. These results and similar ones on the other ions not only prove the validity of the optimization but also indicate that the relative stabilities

TABLE I: STO-3G Partial Optimization Results on CH₃NHCH₂

Energy, au	Bond lengths, Å					Bond angles, deg				
	C-N	N=C	N-H	C _{sp} ² -H	C _{sp} ³ -H	C-N=C	N-C _{sp} ² -H	C _{sp} ²	N-C _{sp} ³ -H	
-131.82737	1.498	1.300	1.033	1.10	1.11	120	120	120	109.47	
-131.82825	1.498	1.300	1.033	1.10	1.11	122	120	120	109.47	
-131.82859	1.498	1.300	1.033	1.10	1.11	124	120	120	109.47	
-131.82860	1.498	1.300	1.033	1.10	1.11	124.33(opt)	120	120	109.47	
-131.82749	1.498	1.300	1.033	1.10	1.12	124.33	120	120	109.47	
-131.82924	1.498	1.300	1.033	1.10	1.10	124.33	120	120	109.47	
-131.82941	1.498	1.300	1.033	1.10	1.091(opt)	124.33	120	120	109.47	
From a slightly different starting point										
-131.82960	1.505	1.290	1.033	1.10	1.09	124.3	121.1	120	109.47	
-131.82962	1.505	1.290	1.043	1.10	1.09	124.3	121.1	120	109.47	
-131.82946	1.505	1.290	1.053	1.10	1.09	124.3	121.1	120	109.47	
-131.82964	1.505	1.290	1.039(opt)	1.10	1.09	124.3	121.1	120	109.47	
-131.82943	1.505	1.290	1.039	1.10	1.09	126.3	121.1	120	109.47	
-131.82935	1.505	1.290	1.039	1.10	1.09	122.3	121.1	120	109.47	
-131.82964	1.505	1.290	1.039	1.10	1.09	124.5(opt)	121.1	120	109.47	
-131.82949	1.505	1.290	1.039	1.11	1.09	124.5	121.1	120	109.47	
-131.82946	1.505	1.290	1.039	1.09	1.09	124.5	121.1	120	109.47	
-131.82964	1.505	1.290	1.039	1.101(opt)	1.09	124.5	121.1	120	109.47	
-131.82948	1.505	1.290	1.039	1.101	1.10	124.5	121.1	120	109.47	
-131.82928	1.505	1.290	1.039	1.10	1.08	124.5	121.1	120	109.47	
-131.82965	1.505	1.290	1.039	1.10	1.092(opt)	124.5	121.1	120	109.47	
-131.82734	1.505	1.290	1.039	1.101	1.092	124.5	121.1	120	111.47	
-131.82914	1.505	1.290	1.039	1.101	1.092	124.5	121.1	120	107.47	
-131.82976	1.505	1.290	1.039	1.101	1.092	124.5	121.1	120	108.8(opt)	
-131.82955	1.505	1.300	1.039	1.101	1.092	124.5	121.1	120	108.8	
-131.82963	1.505	1.300	1.039	1.101	1.092	124.5	121.1	120	108.8	
-131.82963	1.505	1.289	1.039	1.101	1.092	124.5	121.1	120	108.8	
Simultaneous variation of all lengths by 0.01 Å, angles by 2°										
-131.82984	1.505	1.289	1.039	1.101	1.092	124.5	121.1	120.2	108.8	
-131.82568	1.515	1.299	1.049	1.111	1.102	126.5	123.1	122.2	110.8	
-131.82710	1.495	1.279	1.029	1.091	1.082	122.5	119.1	118.2	106.8	
-131.82987	1.504	1.288	1.038	1.100	1.091	124.3	120.9	120.0	108.6	

(to be discussed below) are not significantly affected by errors in the geometry of 0.01 Å in bond lengths and 1° in bond angles.

Figure 6 presents the population analysis on this ion.

c-CH₂CH₂NH₂⁺. C_{2v} symmetry was assumed in the geometry optimization procedure. Furthermore, the H-N-H and H-C-H planes were assumed to lie at an angle bisecting the corresponding internal angles C-N-C and N-C-C, respectively. First, the ring geometry was optimized suggesting 1.50-Å C-C and 1.51-Å N-C bond lengths. Other optimized parameters were 1.08 Å C-H, 1.04 Å N-H bonds, 113° H-N-H and 117° H-C-H angles. Bond length optimization was pursued to 0.005 Å, bond angle optimization to the nearest 0.5°.

Curiously, the nitrogen is negatively charged, the carbons are nearly neutral, and the hydrogens are strongly positive (Figure 7). In addition, the C-N overlap population is very low suggesting a weak bond at this position.

CH₂=CH⁺NH₃. This ion is the N-protonated enamine (ethenylammonium) counterpart of the previously described C-protonated enamine (CH₃CHNH₂⁺) structure.

The geometric parameters were optimized in the following sequence: C-C, C-N, C-H (all three simultaneously) bond lengths, then the angles C-C-N, C-C-H, H-C-C (two simultaneously), C-N-H (all three simultaneously).

Figure 8 presents the population analysis for this ion. The nitrogen again carries a negative charge but the hydrogens attached to it are strongly positive.

c-CH₃CHNH₂⁺ and *c*-CH₃NHCH₂⁺. Corner protonation was assumed on both of these structures. The energy surface was scanned starting with nearly 1.40-Å bond lengths

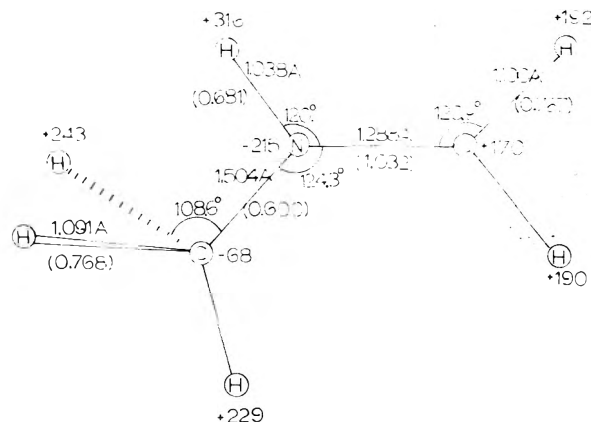


Figure 6. CH₃NHCH₂⁺. STO-3G optimized geometrical parameters. Net atomic populations (X 1000) near atoms; overlap populations in parentheses under bonds.

in the ring and varying all three bond lengths independently of each other. No minima were found for any intermediate bond lengths, scanning all the way to the acyclic analog geometries. While the interconversions drawn before undoubtedly involve some species different from the ones heretofore discussed, no attempt was made in this study to elucidate the mechanism of interconversion.

Based on the limited experience of this study, one can obtain nearly optimized energies for the ions by optimizing the bond lengths and bond angles among heavy atoms (C, N) and employing standard bond lengths and bond an-

TABLE II: Relative Stabilities of the Ions^a

Ion	STO-3G		4-31G		ΔH_f^d (expt), kcal/mol
	Energy, au	$\Delta E,^b$ kcal/mol	Energy, au	$\Delta E,^b$ kcal/mol	
CH ₃ CH ₂ NH (c)	-131.68515	98.8	-133.05740	119.5	200 ± 10
CH ₃ CH ₂ NH ₂ (a)	-131.70109	88.8		Did not converge	
c-CH ₂ CH ₂ NH ₂ (f)	-131.82320	12.3	-133.20090	29.5	173 ± 2
CH ₃ NCH ₃ (e)	-131.71860	77.8	-133.08404	102.8	
			-133.09030 ^c	98.9	206 ± 4
CH ₂ =CHNH ₃ (i)	-131.81514	17.3	-133.22214	16.2	
CH ₃ NH=CH ₂ (d)	-131.82987	8.1	-133.22940	11.7	154 ± 4
CH ₃ CH=NH ₂ (b)	-131.84277	0.0	-133.24801	0.0	154 ± 4

^a Geometry optimization according to STO-3G; the 4-31G results represent single point calculations on the geometry optimized according to STO-3G. ^b Energy of the isomer above the energy of the most stable ion, b. ^c Optimized geometry according to 4-31G. ^d From ref 4.

TABLE III: Calculated Rotational Barriers

Ion	Conformer	STO-3G		4-31G	
		Energy, au	Barrier, kcal/mol	Energy, au	Barrier, kcal/mol
CH ₃ NCH ₃ ^a	Staggered	-131.71860	0.72 ^c	-133.08404	1.29 ^c
	Eclipsed	-131.71745		-133.08199	
CH ₂ =CHNH ₃ ^b	Eclipsed	-131.81514	1.41 ^c	-133.22214	1.30 ^c
	Staggered	-131.81289		-133.22006	
CH ₃ CHNH ₂ ^b	Eclipsed	-131.84277	1.00 ^c	-133.24801	0.84 ^c
	Staggered	-131.84119		-133.24667	
CH ₃ NHCH ₂ ^b	Eclipsed	-131.82987	1.05 ^c	-133.22940	1.03 ^c
	Staggered	-131.82819		-133.22775	
CH ₃ NHCH ₂	Perpendicular	-131.68880	88.5 ^d		

^a Both staggered and eclipsed conformers were optimized. ^b Only the eclipsed conformer was geometry optimized, the staggered conformation was obtained by rotating the CH₃ or NH₃ group by 60°. The eclipsed conformation is the one in which a CH₃ or NH₃ hydrogen eclipses the double bond. ^c Barriers for single bond rotations. ^d Barrier for N=C double bond rotation.

lipes the double bond) favors the latter by nearly 1.0 kcal/mol.

Rotation of the NH₃ group in i from an H-N-C-H dihedral angle of 0 to 180° (in the latter an N-H bond eclipsing the double bond) favors the latter by 1.4 kcal/mol.

The predicted barriers at the two levels of approximation are in substantial agreement.

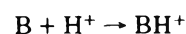
Except for ion e, the same bond angles and bond lengths were employed on the two conformers (except for the above described torsional angle) at both levels of approximation. Rotational barriers in the 1-propyl cation appear to be highly dependent on the level of approximation employed.^{2d}

Finally, the curious electron densities at N in d and b (indicative of a resonance structure placing positive charge at C not at N) raised the question as to whether the C-N double bond in these structures was normal or not. Existence of an ordinary double bond should be accompanied by a very high barrier to rotation. Indeed 90° rotation of the CH₂ group in CH₃NHCH₂ leads to a barrier of 88 kcal/mol (Table III). According to STO-3G the perpendicular structure is suggested to have N-C_{sp²} = 1.39 Å, N-C_{sp³} = 1.50 Å, C_{sp²}-H = 1.10 assuming 120° H-N-C_{sp²} and H-C_{sp²}-H angles and a tetrahedral methyl environment.

Admittedly, single determinantal wave functions may not account for rotational barriers quantitatively.¹³ Clearly, however, the conformer in which a methyl hydrogen eclipses the double bond is always favorable to the one in which it eclipses a hydrogen in all these ions, just as is the case in a neutral such as acetaldehyde.

Gas Phase Basicity of Amines

In the gas phase the energy change associated with the process



is usually defined as the proton affinity of B.¹⁴ This quantity represents the intrinsic basicity of B in the absence of solvent. Theoretically, one estimates this quantity as the difference between the total energies of BH⁺ and B. The more favorable the energy of BH⁺ compared to the energy of B, the greater is the inherent basicity of B.

Table IV lists some calculated proton affinities for C₂NH₅ → C₂NH₆⁺ processes where standard geometry 4-31G results on the neutral molecules were taken from ref 12a and 12b.

The following conclusions are apparent from Table IV.

(1) The 4-31G level of approximation predicts much smaller proton affinity than does the STO-3G level. STO-3G predicts 265 kcal/mol for the proton affinity of pyridine compared to the 4-31G value of 235 kcal/mol (unpublished from this laboratory) and the experimental value of 225¹⁴ kcal/mol. 4-31G calculations thus are capable of predicting proton affinities well within 10% of the experimental value.

(2) N-protonation for all four isomers leads to rather similar proton affinities.

(3) C-protonation is less favorable than N-protonation only when the product does not possess a resonance contribution with a filled octet. The notable exception to the N-protonation preference is the case of CH₂=CHNH₂. This

TABLE IV: Proton Affinity Estimates for $C_2NH_5 \rightarrow C_2NH_6^+$ ^a

Neutral	Process	Ion	ΔE , au	ΔE , kcal/mol, proton affinity
	STO-3G		-0.4237	-265
-131.3995		-131.8232	-0.3811	-239
-132.8198		-133.2009		
CH ₂ =NCH ₃		CH ₂ =NHCH ₃		
-132.8441		-133.2294	-0.3853	-242
CH ₂ =NCH ₃		CH ₃ NCH ₃		
-132.8441		-133.0903	-0.2462	-154
CH ₃ CH=NH		CH ₃ CH=NH ₂		
-132.8648		-133.2480	-0.3832	-240
CH ₃ CH=NH		CH ₃ CH ₂ NH		
-132.8648		-133.0574	-0.1926	-121
CH ₂ =CHNH ₂		CH ₂ =CHNH ₃		
-132.8702	-133.2221	-0.3519	-221	
CH ₂ =CHNH ₂	CH ₃ CH=NH ₂			
-132.8702	-133.2480	-0.3778	-237	

^a All results presented are based on 4-31G calculations, except where noted. 4-31G results on neutrals are from ref 12a except those on aziridine from 12b.

unusual behavior in CH₂=CHNH₂ has its origins in the much greater stability of ion b than ion i.

Finally, a few words concerning the inherent basicities of the imines and enamines are in order.

The imine tautomer (CH₃CH=NH) is intrinsically slightly more basic than the enamine (CH₂=CHNH₂). However the difference (3 kcal/mol) may be strongly basis set dependent. The intrinsic basicities of the two are definitely similar. Their predicted proton affinities are reminiscent of that of NH₃ (223 kcal/mol with 5-31G and 203 kcal/mol experimental proton affinity¹⁴) and of pyridine (235 kcal/mol with 4-31G and 225 kcal/mol experimental proton affinity¹⁴). Intrinsically, the enamine and the imine are slightly more basic than pyridine according to 4-31G. The experimental proton affinity of CH₃CH=NCH₂CH₃ is higher (228 kcal/mol) than that of pyridine (225 kcal/mol).¹⁵

Conclusions

The processes occurring in the mass spectrometer have been shown to be thermodynamically favorable. The relative stabilities of the isomers compared favorably with experimental data.

Based on the calculations one can suggest preferred sites of gas phase protonation in the corresponding neutral molecules.

A delineation of the rearrangement mechanism is of obvious interest, but the present work can only suggest the structure and properties of some stable intermediates along the reaction surface of C₂NH₆⁺ ions. While a calculation of the entire surface is needed, the force constants (static parameters) are already guides to the rearrangement processes. In the decomposition of C₂NH₆⁺ ions CH₃⁺ is very often a product.³ Significantly, in both structures b and e the bond leading to the methyl carbon has the smallest force constant.

Acknowledgment. I am grateful to the Rutgers University Center for Computer and Information Services for gen-

erously providing the large amount of computer time needed for this project.

I owe thanks to Professor Imre Csizmadia (University of Toronto) and to his outstanding coworkers for exposing me to the intricacies of ab initio techniques during the summer of 1973.

I also wish to thank Professor Edward Thornton (University of Pennsylvania) for first arousing my interest in mass spectral fragmentation mechanisms.

References and Notes

- (1) See, for example, F. Jordan, Ph.D. Dissertation, University of Pennsylvania, 1967. (In Dissertation Abstracts and University Microfilms, Ann Arbor, Mich.) That study attempted to calculate the electronic structure and preferred geometry of some mass spectral ions.
- (2) Some recent references are (a) L. Radom, P. C. Hariharan, J. A. Pople, and P. v. R. Schleyer, *J. Am. Chem. Soc.*, **95**, 6531 (1973); L. Radom, J. A. Pople, and P. v. R. Schleyer, *ibid.*, **95**, 8133 (1973), for calculations on C₃H₅⁺ isomers and substituted derivatives; (b) P. A. Kollman, W. F. Trager, S. Rothenberg, and J. E. Williams, *ibid.*, **95**, 458 (1973), on CH₂OH⁺, CH₂NH₂⁺, and CH₃⁺; (c) L. M. Tel, S. Wolfe, and I. G. Csizmadia, *Int. J. Quantum Chem.*, **7**, 475 (1973), on CH₃CH₂⁺ and HOCH₂⁺; (d) P. C. Hariharan, L. Radom, J. A. Pople, and P. v. R. Schleyer, *J. Am. Chem. Soc.*, **96**, 599 (1974) on C₃H₇⁺; (e) W. J. Hehre and P. C. Hiberty, *ibid.*, **96**, 2665 (1974), for rearrangement paths in haloethyl systems.
- (3) K. Levsen and F. W. McLafferty, *J. Am. Chem. Soc.*, **96**, 139 (1974).
- (4) B. H. Solka and M. E. Russell, *J. Phys. Chem.*, **78**, 1268 (1974).
- (5) W. J. Hehre, W. A. Lathan, R. Ditchfield, M. D. Newton, and J. A. Pople, Program No 236, Quantum Chemistry Program Exchange, Indiana University, Bloomington, Ind.
- (6) W. J. Hehre, R. F. Stewart, and J. A. Pople, *J. Chem. Phys.*, **51**, 2657 (1969).
- (7) R. Ditchfield, W. J. Hehre, and J. A. Pople, *J. Chem. Phys.*, **54**, 724 (1971).
- (8) R. S. Mulliken, *J. Chem. Phys.*, **23**, 1833 (1955).
- (9) P. C. Hariharan and J. A. Pople, *Chem. Phys. Lett.*, **16**, 217 (1972); P. C. Hariharan and J. A. Pople, *Theor. Chim. Acta*, **28**, 213 (1973).
- (10) M. D. Newton, W. A. Lathan, W. J. Hehre, and J. A. Pople, *J. Chem. Phys.*, **52**, 4064 (1970).
- (11) J. A. Pople and M. S. Gordon, *J. Am. Chem. Soc.*, **89**, 4256 (1967).
- (12) (a) L. Radom, W. J. Hehre, and J. A. Pople, *J. Am. Chem. Soc.*, **93**, 289 (1971); (b) W. A. Lathan, L. Radom, P. C. Hariharan, W. J. Hehre, and J. A. Pople, *Fort. Chem. Forsch.*, **40**, 1 (1973).
- (13) L. Salem and C. Rowland, *Angew. Chem., Int. Edit. Engl.*, **11**, 92 (1972).
- (14) E. M. Arnett, *Acc. Chem. Res.*, **6**, 404 (1973).
- (15) D. H. Aue, H. M. Webb, and M. T. Bowers, *J. Am. Chem. Soc.*, **97**, 4138 (1975).

An Investigation of Ethylenediamine Complexes of Copper(II) and Nickel(II) in Solutions of Dimethyl Sulfoxide

Charles L. Watkins* and Gerald S. Vigeo

Department of Chemistry, University of Alabama in Birmingham, Birmingham, Alabama 35294 (Received April 22, 1975)

Publication costs assisted by the University of Alabama in Birmingham

Solution studies of Cu^{2+} and $\text{Cu}(\text{en})_2^{2+}$ and Ni^{2+} , $\text{Ni}(\text{en})^{2+}$, $\text{Ni}(\text{en})_2^{2+}$, and $\text{Ni}(\text{en})_3^{2+}$ in dimethyl sulfoxide (DMSO) were made. The kinetics of exchange of coordinated DMSO with DMSO bulk solvent were measured by NMR line broadening techniques. At low temperatures, axially coordinated DMSO molecules exchange from the six-coordinated Cu^{2+} with a rate constant of $4.7 \times 10^3 \text{ sec}^{-1}$ (25°C). However, the axially coordinated DMSO molecules on the $\text{Cu}(\text{en})_2^{2+}$ exchange at a rate too fast to be measured by the NMR line broadening technique. At higher temperatures, the exchange of DMSO molecules equatorially coordinated to Cu^{2+} was measurable and evidence for DMSO exchange from the partially dissociated $\text{Cu}(\text{en})_2^{2+}$ was observed. The average rates of exchange for DMSO molecules coordinated to Ni^{2+} and $\text{Ni}(\text{en})_x$ complexes follow the order $\text{Ni}^{2+} < \text{Ni}(\text{en})^{2+} < \text{Ni}(\text{en})_2^{2+}$. The increase in exchange rate upon successive addition of ethylenediamine can be explained by an amine trans effect. Conclusions drawn from the NMR line broadening results are supported by paramagnetic NMR chemical shift, solution magnetic susceptibility, and calorimetric data.

Introduction

Several studies of the exchange rate between solvent coordinated paramagnetic ions and bulk solvent molecules using magnetic resonance techniques have been reported since the fundamental work of Swift and Connick.¹⁻⁹ Of particular interest to us is a comparison of these exchange rates in various aqueous and nonaqueous solvents. In this regard, we have previously reported the exchange rate of dimethyl sulfoxide (DMSO) between the first coordination sphere and bulk solution for several first row transition metal ions,¹ and rates of first and second coordination sphere exchange of DMSO in solutions of $\text{Cr}(\text{en})_3^{3+}$ in DMSO^2 (en = ethylenediamine).

A comparison of the NMR exchange studies of Cu^{2+} in DMSO and Cu^{2+} in H_2O ^{1,3} leads to some interesting observations. DMSO, which is often compared to water in its metal ion solvation properties, was found to exchange sufficiently slowly at 25°C in Cu^{2+} -DMSO solution for the exchange rate to be measured by the NMR technique. However, because of Jahn-Teller effects, only the axial DMSO ligands were found to exchange within the NMR time frame. Similar studies of Cu^{2+} - H_2O in water concluded that the axial ligands exchange too rapidly to be measured by NMR methods. ($k^1 = 2 \times 10^8 \text{ sec}^{-1}$ has been reported, as determined by the Eigen technique.¹⁰) Swift and Connick³ did find at temperatures around 100°C the four equatorial ligands of $\text{Cu}(\text{H}_2\text{O})_6^{2+}$ exchanged at a rate measurable by NMR. These results encouraged us to reexamine the Cu^{2+} -DMSO system at high temperatures. The results of the $\text{Cr}(\text{en})_3^{3+}$ studies in DMSO also suggested a study of the $\text{Cu}(\text{en})_2^{2+}$ molecule in DMSO to determine the effect nitrogen ligand substituents in the equatorial position would have on the rate of DMSO axial exchange.

Exchange studies for the $\text{Ni}(\text{en})^{2+}$, $\text{Ni}(\text{en})_2^{2+}$, and $\text{Ni}(\text{en})_3^{2+}$ species in aqueous solution have been reported by Hunt et al.^{5,7} using NMR techniques. Analogous experiments using DMSO should be valuable in determining how the behavior of these nickel complexes in solution is dependent upon solvent. In particular, a comparison of the magnetic properties of the square-planar $\text{Ni}(\text{en})_2^{2+}$ species in DMSO and aqueous solution should provide information concerning the ligand field effects of DMSO, in that they might be of insufficient strength to achieve a d-electron triplet state of the $\text{Ni}(\text{en})_2^{2+}$ in DMSO. Such results would make Ni^{2+} complex solution studies in DMSO and water quite different.

Therefore, the thermodynamic and kinetic parameters for exchange have been determined and are reported for Cu^{2+} and Ni^{2+} and for en complexes of Cu^{2+} and Ni^{2+} in DMSO. Magnetic resonance and optical and calorimetric techniques have been employed.

Experimental Section

Preparation of Compounds. $\text{Cu}(\text{en})_2(\text{NO}_3)_2$ and $\text{Ni}(\text{en})_3(\text{NO}_3)_2$ were prepared by adding ethylenediamine in small stoichiometric excess to almost saturated aqueous solutions of $\text{Cu}(\text{NO}_3)_2$ and $\text{Ni}(\text{NO}_3)_2$, respectively. Precipitation occurred with the addition of methanol. The complexes were washed with cold methanol and ether and dried.^{1,11} The elemental analyses were performed by Galbraith Lab., Inc., and found to be the following:

Compound	Found		Calcd	
	% C	% H	% C	% H
$\text{Cu}(\text{DMSO})_3(\text{NO}_3)_2$	16.62	5.10	17.08	4.27
$\text{Cu}(\text{en})_2(\text{NO}_3)_2$	15.32	5.70	15.60	5.20
$\text{Ni}(\text{DMSO})_4(\text{NO}_3)_2$	24.94	5.90	24.33	4.83
$\text{Ni}(\text{en})_3(\text{NO}_3)_2$	19.40	5.95	19.80	6.61

NMR Line Broadening Experiments. DMSO was dried over molecular sieves and a stock solution of DMSO and 2% benzene was prepared. DMSO solutions of $\text{Cu}(\text{DMSO})_3(\text{NO}_3)_2$, $\text{Cu}(\text{en})_2(\text{NO}_3)_2$, $\text{Ni}(\text{DMSO})_4(\text{NO}_3)_2$, and $\text{Ni}(\text{en})_3(\text{NO}_3)_2$ were individually prepared with metal ion concentrations of 0.05, 0.10, and 0.15 M. DMSO solutions of $\text{Ni}(\text{DMSO})_4(\text{NO}_3)_2$ and ethylenediamine in mole ratios of Ni/en = 1:1 and 1:2 were prepared with Ni^{2+} concentra-

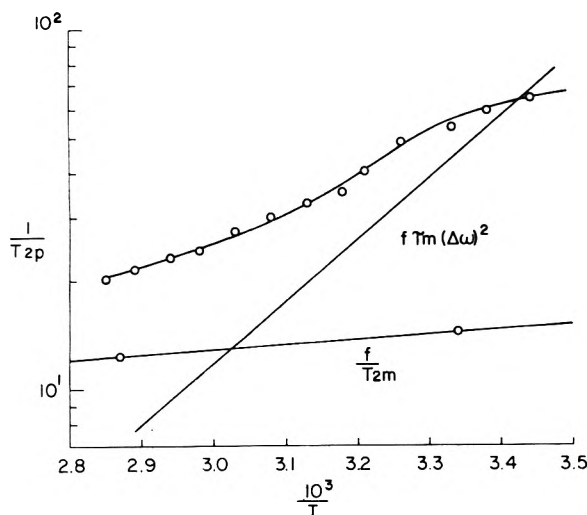


Figure 1. Line broadening of the methyl protons of DMSO for solutions of Cu^{2+} in DMSO as a function of temperature.

tions of 0.10 and 0.15 M . Line broadening and contact shift data were obtained on these solutions using a Varian HA60-IL NMR spectrometer over a temperature range of 20–130°C. The theory and methods of analysis used were as previously discussed.^{2,3}

Magnetic Susceptibility. DMSO solutions of $\text{Cu}(\text{NO}_3)_2$, $\text{Cu}(\text{en})_2(\text{NO}_3)_2$, $\text{Ni}(\text{NO}_3)_2$, $\text{Ni}(\text{en})_3(\text{NO}_3)_2$, and $\text{Ni}(\text{en})_2(\text{NO}_3)_2$ were prepared; the solution magnetic susceptibilities were determined by the Evans method¹² over a temperature range of 20–90°C. Diamagnetic susceptibility corrections were applied using Pascal's constants. The solution magnetic susceptibilities were analyzed using $1/\chi$ vs. T plots, where χ is the molar magnetic susceptibility.

Calorimetry. The heats of reaction for $\text{Ni}(\text{NO}_3)_2$ and $\text{Cu}(\text{NO}_3)_2$ with ethylenediamine in DMSO were determined using a Tronac 450A calorimeter. The calibration, data analysis, and other procedures were taken from Eattough et al.¹³

Results and Discussion

Cu^{2+} and $\text{Cu}(\text{en})_2^{2+}$ in DMSO. Line Broadening Studies. A plot of $\log 1/T_{2p}$ vs. $10^3/T$ is given in Figure 1 for Cu^{2+} in DMSO for the temperature region 20–90°C. The plot is essentially the same as previously reported¹ except that the experimental points in this work are resolved into two lines using the appropriate Swift–Connick relationships,³ $1/T_{2p} = f\tau_m(\Delta\omega)^2$ and $1/T_{2p} = f/T_{2\text{Cu}}$. In the curve fitting procedure $1/T_{2\text{Cu}}$ was first determined by the relationship of Bernheim¹⁴

$$1/T_{2\text{Cu}} = \frac{4}{9} I(I+1)S(S+1)(A^2/\hbar^2)\tau_e$$

where an average value of 2×10^{-8} sec was assumed for τ_e .³ The kinetic data for the fast exchange region, where $1/T_{2p} = f\tau_m(\Delta\omega)^2$, are summarized in Table I for the Cu^{2+} -DMSO system for the present work and the work of Viguee and Ng.¹ At 25°C the line broadening is mainly due to the exchange of the axial DMSO ligands from the Jahn-Teller distorted copper complex.¹ It is interesting that although DMSO possesses many properties similar to water, its exchange from the axial position of Cu^{2+} is much slower ($k^\ddagger = 2 \times 10^8 \text{ sec}^{-1}$ for H_2O). Similar rate differences for water and DMSO exchange were found for all of the divalent

TABLE I: Kinetic Data for Cu^{2+} -DMSO at 25°C

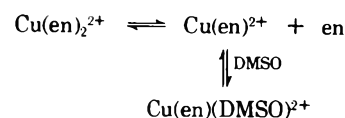
Cu (DMSO) ₆ ²⁺ ^c	k^\ddagger , sec ⁻¹	ΔH^\ddagger , kcal/mol	ΔS^\ddagger , eu	A/h , Hz
a	4.7 $\times 10^3$	7.8	-14.9	3.52 $\times 10^5$
b	7.9 $\times 10^3$	7.25	-13.6	6.65 $\times 10^5$

^a This work. ^b Reference 1. ^c The small differences given in a and b are due to corrections for $1/T_{2m}$ and a more accurate temperature calibration¹⁸ in this work.

transition metal ions previously studied.¹

The measurable exchange of the axial ligands with respect to the rather stable equatorial ligands makes the square-planar copper complexes a possible model for studying cis or other kinetic effects. With this in mind, line broadening measurements on solutions of $\text{Cu}(\text{en})_2^{2+}$ in DMSO were conducted. Plots of $\log 1/T_{2p}$ vs. $10^3/T$ are linear between 20 and 90°C with an apparent ΔH of 3.85 kcal/mol. However, the line broadening data cannot be fitted to any of the exchange dependent regions because exchange is too fast in this temperature region to be measured by the NMR technique. The greater affinity of Cu^{2+} for amine Lewis bases over analogous oxygen Lewis bases is expected to place more electron density on the Cu^{2+} in the $\text{Cu}(\text{en})_2^{2+}$. Electron repulsion for the axial ligands is greater for the $\text{Cu}(\text{en})_2^{2+}$ species than for the $\text{Cu}(\text{DMSO})_4^{2+}$ species which would account for the increased rate observed in the $\text{Cu}(\text{en})_2^{2+}$ -DMSO system. The Jahn-Teller effect becomes more operative in reducing the coordination ability of ligand bonding in the axial position of Cu^{2+} as the stronger base ethylenediamine is substituted for DMSO on Cu^{2+} . In principle, then, $\text{Cu}(\text{L})_4^{2+}$ species, where L is a monodentate electron-withdrawing ligand, could be synthesized and designed to meet the requirements for measuring axial ligand exchange by NMR techniques.

At temperatures above 100°C, Swift and Connick³ noted a new exchange process for the Cu^{2+} - H_2O system which they attributed to exchange of the more stable equatorial ligands. For the basis of comparison an analogous study of the Cu^{2+} -DMSO system was conducted between temperatures of 70 and 130°C. A plot of $\log 1/T_{2p}$ vs. $10^3/T$ in Figure 2 gives the results of the study. The experimental points are now resolved into the two processes which appear at lower temperatures, $1/T_{2p} = f\tau(\Delta\omega)^2$ and $1/T_{2p} = f/T_{2\text{Cu}}$ and a new high temperature process $1/T_{2p} = f/\tau_m'$. The data for the present study and that of Swift and Connick are listed in Table II. Only approximate values for the kinetic parameters are obtained due to the limited temperature range. $k^\ddagger = 4 \text{ sec}^{-1}$, $\Delta H^\ddagger = 15.2 \text{ kcal/mol}$, and $\Delta S^\ddagger = -16.3 \text{ eu}$ for the Cu^{2+} -DMSO system, while Swift and Connick reported $k^\ddagger = 10^4 \text{ sec}^{-1}$, $\Delta H^\ddagger = 11 \text{ kcal/mol}$, and $\Delta S^\ddagger = -4 \text{ eu}$ for the Cu^{2+} - H_2O system. Again, the slower exchange rate for DMSO is evident. Figure 3 gives a plot of $\log 1/T_{2p}$ vs. $10^3/T$ for the high temperature region for the $\text{Cu}(\text{en})_2^{2+}$ -DMSO. The results are similar to those found for the Cu^{2+} -DMSO and the Cu^{2+} - H_2O . These results suggest the following dissociation above 100°C:



A similar dissociative exchange process was found in the

TABLE II: Kinetic Data for Cu^{2+} -DMSO and Cu^{2+} - H_2O at High Temperature

	k^\ddagger , sec^{-1}	ΔH^\ddagger , kcal/mol	ΔS^\ddagger , eu	A/h , Hz
$\text{Cu}(\text{DMSO})_2^{2+ a}$	≈ 4	≈ 15	≈ -16	$\approx 1.6 \times 10^5$
$\text{Cu}(\text{H}_2\text{O})_6^{2+ b}$	$\approx 10^4$	≈ 11	≈ -4	

^a This work at 120°C. ^b Reference 3 at 100°C.

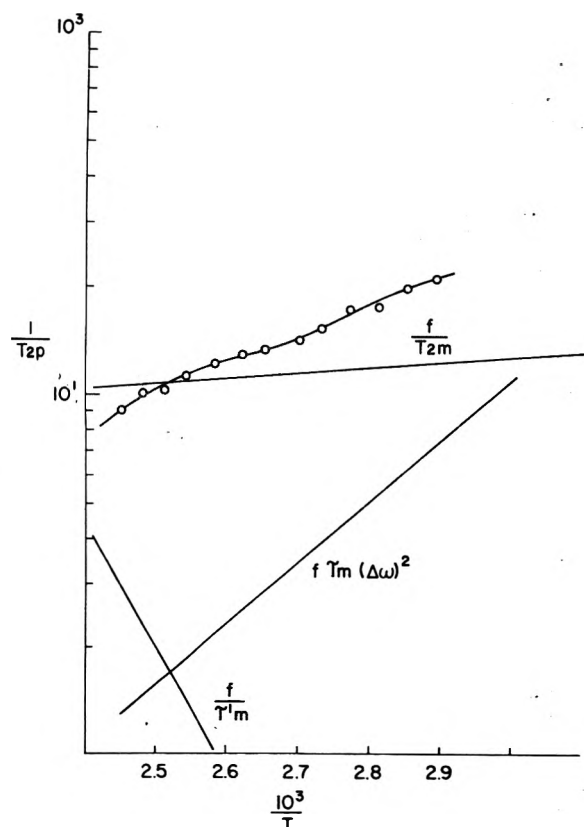


Figure 2. Line broadening of the methyl protons of DMSO for solutions of Cu^{2+} in DMSO. High temperature region.

high temperature region of the $\text{Cr}(\text{en})_3^{3+}$ -DMSO system.² Because exchange is too fast in the 20–90°C region to be measured by the NMR technique, the kinetic parameters for the dissociative process for $\text{Cu}(\text{en})_2^{2+}$ -DMSO cannot be calculated.

Cu^{2+} and $\text{Cu}(\text{en})_2^{2+}$ in DMSO. *Contact Shift and Magnetic Susceptibility.* Paramagnetic chemical shifts (C.S.) were measured for DMSO as a function of temperature in 0.1 M solutions of Cu^{2+} and in 0.1 M solutions of $\text{Cu}(\text{en})_2^{2+}$. The results are shown in Figure 4 as plots of C.S. vs $10^3/T$. The C.S. for DMSO in solutions of Cu^{2+} decreases with increase in temperature as would be expected from the Curie-Weiss relationship:

$$\frac{\text{C.S.}/f}{\nu} = \frac{\Delta\nu}{\nu} = -A_n \frac{\gamma_e g \beta S(S+1)}{\gamma_n 3KT}$$

where f is the fraction of the ligand molecules coordinated and the other terms have their usual meaning.²

The reverse C.S. behavior has been noted for water in the Cu^{2+} - H_2O system by Luz and Shulman.⁴ The paramagnetic chemical shift for DMSO in $\text{Cu}(\text{en})_2^{2+}$ solution exhibits Curie-Weiss behavior at lower temperatures but begins to deviate at higher temperatures, the C.S. increasing with increasing temperature. The most probable expla-

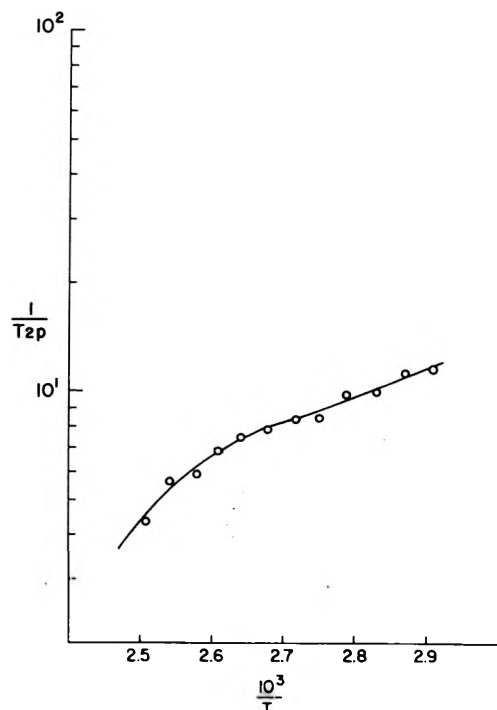


Figure 3. Line broadening of the methyl protons of DMSO for solutions of $\text{Cu}(\text{en})_2^{2+}$ in DMSO. High temperature region.

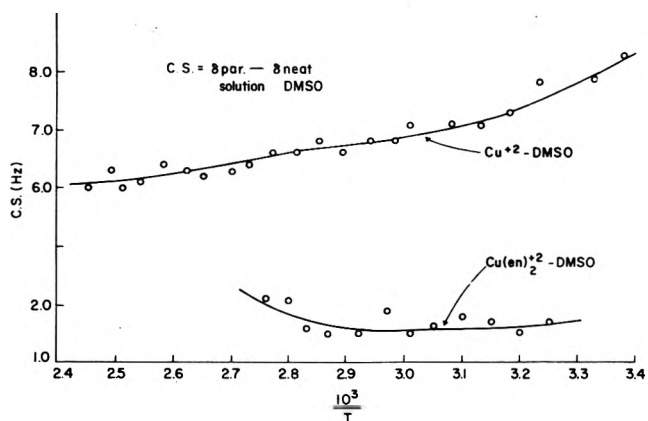


Figure 4. Paramagnetic chemical shifts of the methyl protons of DMSO for solutions of Cu^{2+} and $\text{Cu}(\text{en})_2^{2+}$ in DMSO as a function of temperature.

nation is that at higher temperatures there is a dissociation of an ethylenediamine from the $\text{Cu}(\text{en})_2^{2+}$ species, as indicated by the line broadening data. Such an explanation would support an increase in paramagnetic chemical shift without a change in the magnetic properties of the Cu^{2+} ion. The magnetic susceptibility data, plotted as $1/\chi$ vs. T , indicates Curie-Weiss behavior for the Cu^{2+} ion in $\text{Cu}(\text{en})_2^{2+}$ throughout the temperature range studied. A Weiss constant of $\theta = 118^\circ$ is obtained. No deviation from the curve is noted at high temperatures. The paramagnetic chemical shift, line broadening, and magnetic susceptibility data support a dissociative mechanism for $\text{Cu}(\text{en})_2^{2+}$ at high temperatures similar to the dissociative mechanism for the Cu^{2+} - H_2O as reported by Swift and Connick.³

Ni^{2+} , $\text{Ni}(\text{en})^{2+}$, $\text{Ni}(\text{en})_2^{2+}$, and $\text{Ni}(\text{en})_3^{2+}$ in DMSO. *Line Broadening, Contact Shift, and Magnetic Susceptibility.* Line Broadening studies as a function of tempera-

ture were conducted for the above nickel-ethylenediamine species in DMSO. The results are given in Figure 5 as plots of $\log 1/T_{2p}$ vs. $10^3/T$ for DMSO solutions of Ni^{2+} , $Ni(en)^{2+}$, and $Ni(en)_2^{2+}$. (For the sake of clarity the plot for the $Ni(en)_3^{2+}$ is not shown; it is a straight line and contributes no information.) The paramagnetic chemical shifts were determined as a function of temperature for DMSO solutions of Ni^{2+} , $Ni(en)^{2+}$, $Ni(en)_2^{2+}$, and $Ni(en)_3^{2+}$. The results are shown in Figure 6. The plot indicates very little change in the C.S. for $Ni(en)_3^{2+}$ which implies very little dissociation of the $Ni(en)_3^{2+}$. From the slight deviation from Curie-Weiss behavior, this dissociation is estimated to be less than 5% over the entire temperature range.

An analysis of the line broadening data for the $Ni(en)_x^{2+}$ -DMSO system was attempted using the method of Hunt.⁵ However, the analysis could not be completed because we were unable to determine reliable individual dissociation constants for the $Ni(en)_x^{2+}$ in DMSO. Both optical methods with computer fitting¹⁵ and calorimetric methods were used. Although the individual dissociation constants could not be determined, a reliable estimate of the overall K_{eq} was obtained and found to be about 1×10^{29} . Both the optical and calorimetric data indicate that the stabilities of the various $Ni(en)_x^{2+}$ complexes are much greater in DMSO than in water (overall $K_{eq} = 1 \times 10^{18}$ for H_2O at 25°C).¹⁶ The large individual K_{eq} 's and the difference between the K_{eq} 's suggest that in the DMSO solutions of $Ni(en)^{2+}$, $Ni(en)_2^{2+}$, and $Ni(en)_3^{2+}$ the parent ions are essentially nondissociated, especially in the temperature range 20–40°C. This assumption is supported by the paramagnetic chemical shift data in Figure 6. If dissociation is occurring, the C.S. would increase at higher temperatures (with increasing dissociation). Because the $Ni(en)^{2+}$ and $Ni(en)_2^{2+}$ follow similar (but lower) paramagnetic chemical shifts to that of Ni^{2+} as a function of temperature, very little dissociation is evident.

By using the line broadening data from Figure 5 over the 20–40°C temperature range, the following kinetic parameters are obtained:^{2,3}

Species	$k^{\ddagger}, a \text{ sec}^{-1}$	$\Delta H^{\ddagger}, \text{kcal/mol}$	$\Delta S^{\ddagger}, \text{eu}$
Ni^{2+}	6.9×10^3	11.1	-3.3
$Ni(en)^{2+}$	1.4×10^4	7.8	-12.8
$Ni(en)_2^{2+}$	1.9×10^4	5.2	-20.9

a 25°C.

The rate constants for exchanging DMSO ligands are in the order $Ni^{2+} < Ni(en)^{2+} < Ni(en)_2^{2+}$. The rates are controlled by the enthalpy of activation, ΔH^{\ddagger} , whose order is $Ni^{2+} > Ni(en)^{2+} > Ni(en)_2^{2+}$. The rate mechanism is dissociative in nature¹ and bond breaking of the Ni-DMSO bond (which is related to ΔH^{\ddagger}) is a most important factor in the rate of exchange. The Ni^{2+} -DMSO bond opposite an ethylenediamine nitrogen atom should be weak due to a trans effect. If the mechanism for exchange is dissociative, the trans effect would increase the exchange rate of the opposing DMSO molecule while the molecules cis to ethylenediamine nitrogen atoms should exchange more slowly. One would expect all six DMSO molecules about Ni^{2+} to exchange with a rate $k^{\ddagger}_{Ni^{2+}}$ ($k^{\ddagger}_{Ni^{2+}} = 6.9 \times 10^3 \text{ sec}^{-1}$). The two DMSO molecules bonded to $Ni(en)_2^{2+}$ should exchange more rapidly with a rate $k^{\ddagger}_{Ni(en)_2^{2+}}$ ($k^{\ddagger}_{Ni(en)_2^{2+}} = 1.9 \times 10^4 \text{ sec}^{-1}$). Of the four DMSO molecules bonded to $Ni(en)^{2+}$, two should exchange with a rate $k^{\ddagger}_{Ni^{2+}}$ and two with a rate $k^{\ddagger}_{Ni(en)_2^{2+}}$. Their weighted average should be the

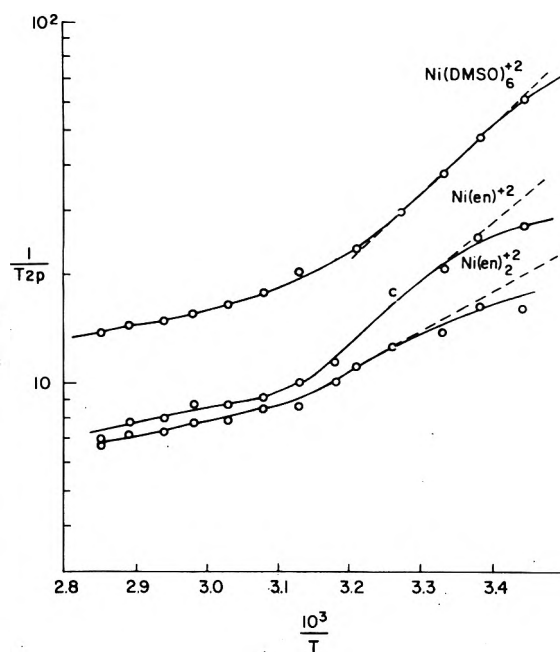


Figure 5. Line broadening of the methyl protons of DMSO for solutions of $Ni(DMSO)_6^{2+}$, $Ni(en)^{2+}$, and $Ni(en)_2^{2+}$ in DMSO as a function of temperature.

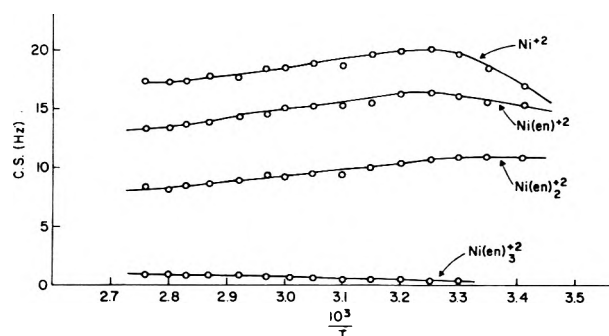


Figure 6. Paramagnetic chemical shifts of the methyl protons of DMSO for solutions of Ni^{2+} , $Ni(en)^{2+}$, $Ni(en)_2^{2+}$, and $Ni(en)_3^{2+}$ in DMSO as a function of temperature.

observed rate for $Ni(en)^{2+}$. The k^{\ddagger}_{av} obtained in this manner does give exactly the observed k^{\ddagger} for $Ni(en)^{2+}$. Although exact agreement may be fortuitous, the internal consistency of these data support the assignment of stability order and the assumption of the importance of the trans effect.

The kinetic data for Ni^{2+} , $Ni(en)^{2+}$, and $Ni(en)_2^{2+}$ in DMSO and H_2O are compared in Table III. The values of k^{\ddagger} and ΔH^{\ddagger} for both systems change in the same way but the ΔS^{\ddagger} for DMSO decreases from Ni^{2+} to $Ni(en)_2^{2+}$ while ΔS^{\ddagger} shows the opposite trend for H_2O . These trends help to explain why k^{\ddagger} for water increases faster than k^{\ddagger} for DMSO as the $Ni(en)_x^{2+}$ species are successively formed. Changes for DMSO due to ΔH^{\ddagger} increase k^{\ddagger} while changes in ΔS^{\ddagger} decrease k^{\ddagger} . ΔH^{\ddagger} effects are greater than ΔS^{\ddagger} effects for DMSO which result in the observed increase in k^{\ddagger} in going from Ni^{2+} to $Ni(en)_2^{2+}$. Placing an amine trans to DMSO has a larger effect on ΔH^{\ddagger} (and presumably on the bond energy of the Ni^{2+} -DMSO bond) than placing an amine trans to a water molecule. This is to be expected because of the relative basicities of en, H_2O , and DMSO.

TABLE III: Kinetic Data for Ni²⁺, Ni(en)²⁺, and Ni(en)₂²⁺ in H₂O^a and DMSO at 25° C

	Ni ²⁺		Ni(en) ²⁺		Ni(en) ₂ ²⁺	
	DMSO	H ₂ O	DMSO	H ₂ O	DMSO	H ₂ O
<i>k</i> [‡] , sec ⁻¹	6.9 × 10 ³	4.4 × 10 ⁴	1.4 × 10 ⁴	4.4 × 10 ⁵	1.9 × 10 ⁴	5.4 × 10 ⁴
Δ <i>H</i> [‡] , kcal/mol	11.1	10.3	7.8	10.0	5.2	9.1
Δ <i>S</i> [‡] , eu	-3.32	-5.2	-12.8	1.0	-20.9	2.6
<i>A/h</i> , Hz	9.1 × 10 ⁴	2.2 × 10 ⁷	1.1 × 10 ⁵	2.2 × 10 ⁷	1.3 × 10 ⁵	2.3 × 10 ⁷

^a Reference 5.TABLE IV: Calorimetric Data of Cu²⁺-en and Ni²⁺-en in DMSO and H₂O at 25° C

		Δ <i>H</i> ^o ₁	Δ <i>H</i> ^o ₂	Δ <i>H</i> ^o ₃	Δ <i>H</i> ^o _{total} ^a	log <i>K</i> ₁	log <i>K</i> ₂	log <i>K</i> ₃	log β
Cu ²⁺	DMSO ^b	21.3	17.5	1.7	40.5	15.6	12.8	1.25	29.65
	H ₂ O ^c	12.6	12.6		25.2	10.48	9.07		19.55
Ni ²⁺	DMSO ^b	16.9	14.8	8.8	39.5	11.7	10.8	6.5	29.0
	H ₂ O ^d	9.5	7.5	8.7	25.8	7.52	6.28	4.26	18.0

^a kcal/mol. ^b The Δ*H*^o_{total} for Cu²⁺ and Ni²⁺ are accurately determined but the Δ*H*^o's for each stepwise reaction are approximate to within 5% due to slight curvature of the Δ*H*^o₁ and Δ*H*^o₂, heats absorbed. Δ*H*^o₃ is determined by difference. log *K* for the DMSO work is determined by assuming that Δ*G*^o ≈ Δ*H*^o. The entropy contribution is probably no larger than Δ*S*^o for the analogous water data. ^c Reference 19. ^d Reference 20.

An examination of Figure 6 shows that the paramagnetic chemical shift of DMSO in Ni²⁺, Ni(en)²⁺, and Ni(en)₂²⁺-DMSO solutions does not follow the expected Curie-Weiss behavior below temperatures of 10³/T = 3.25. The magnetic susceptibility data of Ni²⁺ and Ni(en)₃²⁺-DMSO solutions as a function of temperature exhibit Curie-Weiss behavior over the entire temperature range with θ = 97 and 90°, respectively. Thus, no magnetic change in the electron configuration (such as triplet = singlet equilibria which is temperature dependent in some Ni²⁺ complexes) is occurring. Also, from the magnetic susceptibility data we can probably exclude the formation of the tetrahedral = octahedral equilibrium, which favors the tetrahedral structure at lower temperature. (This case would increase the magnetic susceptibility with temperature decrease.) A square-planar = octahedral equilibrium can also be ruled out because of a corresponding reduction in magnetic susceptibility with square-planar formation. One explanation of the unusual paramagnetic chemical shift behavior is that with a decrease in temperature, as the melting point of DMSO is approached (18°C), the nitrate ions in solution begin to compete with DMSO for Ni²⁺ sites. The NO₃⁻ ion's coordination in available sites would preserve the octahedral structure and maintain the octahedral magnetic properties of the Ni²⁺ but would allow fewer first coordination sites for DMSO exchange, thus lowering the paramagnetic chemical shift. Meek's¹⁷ study of Ni(DMSO)₆²⁺ in solutions of Cl⁻ dissolved in DMSO shows a definite exclusion of DMSO by Cl⁻ with increase in temperature because of the stronger affinity of Cl⁻ for Ni²⁺. In this case, the roles of DMSO and NO₃⁻ are probably reversed causing NO₃⁻ to be preferred at lower temperatures. Additional support for the existence of some bonding between Ni²⁺ and NO₃⁻ can be seen in the synthesis of Ni(DMSO)₄(NO₃)₂ by Vigeo and Ng¹ and Ni(DMSO)₆(ClO₄)₂ by Selbin.¹¹ Whereas the Ni(DMSO)₆(ClO₄)₂ complex crystallizes with the ClO₄⁻ outside the first coordination sphere, NO₃⁻ replaces two DMSO molecules in the crystalline formation of Ni(DMSO)₄(NO₃)₂.

Calorimetric Measurements. An attempt was made to determine the association constants for the Ni²⁺-en system in DMSO using a computer-fitted optical method. The results were not consistent and the overall association con-

stant log β ranged from 27 to 32. Calorimetric data were collected for the same purpose and the results are shown in Table IV. Assuming that Δ*G*^o ≈ Δ*H*^o, the log β for Ni(en)₃²⁺ was found to 29.65 which centers the range of values determined by the optical method. It is not the intent to justify the assumption that Δ*G*^o = Δ*H*^o but rather to show that ignoring *T*Δ*S*^o contribution to Δ*G*^o does not substantially reduce the value of log *K*. Thus, our earlier assumptions which allowed us to determine rate constants, *k*[‡], without the association constants as used by Hunt should be valid.

It can be seen from Table IV that the heats of reaction for each step between the Cu²⁺ and Ni²⁺ with ethylenediamine are significantly larger than those found in water. This is most certainly due to the larger bond energy of the metal ion-water over the bond energy of the metal ion-DMSO. It may be that the *T*Δ*S*^o is of much less importance in these reactions. It is interesting to note the comparison of the differences in log β for Cu²⁺-en in water and in DMSO with the log β differences of Ni²⁺-en in water and in DMSO. There is a difference of about 10 log units for the Cu²⁺-en systems (29.6 for DMSO and 19.6 for H₂O) while the difference for the Ni²⁺-en systems is approximately 11 log units (29.0 and 18.0). A comparison of the total Δ*H*^o difference between the Cu²⁺-en and Ni²⁺-en systems yields a similar relationship. The Δ*H*^o difference for the Cu²⁺-en system is 15.3 kcal while the Δ*H*^o difference for the Ni²⁺-en system is 14.7 kcal. If the log β and Δ*H*^o values are this similar, it would suggest that the *T*Δ*S*^o terms for water and DMSO reactions on Cu²⁺ are very similar; the same can also be said for the Ni²⁺-en system *T*Δ*S*^o for water and DMSO. Since the *T*Δ*S*^o for Cu²⁺-en and Ni²⁺-en are known for water (-1.46 and 0.2 kcal/mol, respectively), they may be used as *T*Δ*S*^o values for DMSO systems to compare with Δ*H*^o to determine their relative importance in controlling log β for Ni²⁺-en and Cu²⁺-en in DMSO. Such a comparison reveals that Δ*G*^o is composed of only 0.5% *T*Δ*S*^o at 25°C. Thus our assumption that Δ*G*^o ≈ Δ*H*^o would be acceptable.

Summary and Conclusions

The NMR line broadening of DMSO in Cu²⁺-DMSO solution is primarily due to axial exchange between 20 and

90°C, as previously reported,¹ while equatorial exchange becomes important above 90°C. The exchange of DMSO from the trans positions of the square-planar $\text{Cu}(\text{en})_2^{2+}$ was too fast to be measured by the NMR technique. The kinetics of exchange between DMSO on the nickel species Ni^{2+} , $\text{Ni}(\text{en})^{2+}$, and $\text{Ni}(\text{en})_2^{2+}$ and bulk DMSO were determined by the NMR line broadening technique. The rate constants are in the order $\text{Ni}^{2+} < \text{Ni}(\text{en})^{2+} < \text{Ni}(\text{en})_2^{2+}$. The rate mechanism is dissociative in nature and a trans effect causes a rate difference between the nickel exchanging species in solution.

The paramagnetic chemical shifts for DMSO in solutions of Cu^{2+} and $\text{Cu}(\text{en})_2^{2+}$ were measured and found to obey the Curie-Weiss law at low temperatures. At higher temperatures, the C.S. for $\text{Cu}(\text{en})_2^{2+}$ deviates from the Curie-Weiss law. The magnetic susceptibility of the Cu^{2+} and $\text{Cu}(\text{en})_2^{2+}$ in DMSO over the entire investigated temperature range shows no deviation from the Curie-Weiss law. Deviation of the C.S. of $\text{Cu}(\text{en})_2^{2+}$ supports a dissociation of the copper complex at high temperature.

The magnetic susceptibilities of Ni^{2+} and $\text{Ni}(\text{en})_3^{2+}$ follow a Curie-Weiss relationship between 20 and 90°C. The C.S. of each of the nickel complexes deviates from the Curie-Weiss relationship over all or part of the temperature range studied. $\text{Ni}(\text{en})_3^{2+}$ has a slight deviation attributable to a small amount of dissociation. The species Ni^{2+} , $\text{Ni}(\text{en})^{2+}$, and $\text{Ni}(\text{en})_2^{2+}$ deviate at temperatures below $10^3/T = 3.25$. This effect, which is not a result of the change in the magnetic properties of the Ni^{2+} ion, is interpreted as the increasing competition of NO_3^- for coordination sites on the Ni^{2+} .

The stepwise ΔH° 's for the reaction of en with Ni^{2+} and Cu^{2+} in DMSO were determined by titration calorimetry. These results were compared with the same reactions in water and found to be much larger, presumably due to the higher $\text{M}^{2+}\text{-H}_2\text{O}$ bond energy. The calorimetry and optical data support certain assumptions used in the analysis of the parameters of DMSO kinetics of exchange.

References and Notes

- (1) G. S. Vigee and P. Ng, *J. Inorg. Nucl. Chem.*, **33**, 2477 (1971).
- (2) C. L. Watkins, G. S. Vigee, and M. E. Harris, *J. Phys. Chem.*, **77**, 855 (1973).
- (3) T. J. Swift and R. E. Connick, *J. Chem. Phys.*, **37**, 307 (1962).
- (4) Z. Luz and R. G. Shulman, *J. Chem. Phys.*, **43**, 3750 (1965).
- (5) A. G. Desai, H. W. Dodgen, and J. P. Hunt, *J. Am. Chem. Soc.*, **91**, 5001 (1969).
- (6) A. McAuley and J. Hill, *Quart. Rev., Chem. Soc.*, **23**, 18 (1969).
- (7) J. P. Hunt, *Coord. Chem. Rev.*, **7**, 1 (1971).
- (8) F. Basolo and R. G. Pearson, "Mechanisms of Inorganic Reactions", 2nd ed, Wiley, New York, N.Y., 1967.
- (9) G. N. La Mar, DeW. Horrocks, Jr., and R. H. Holm, Ed., "NMR of Paramagnetic Molecules: Principles and Applications", Academic Press, New York, N.Y., 1973.
- (10) G. Geier, *Ber. Bunsenges, Phys. Chem.*, **69**, 517 (1965).
- (11) J. Selbin, W. E. Bull, and L. H. Holmes, *J. Inorg. Nucl. Chem.*, **16**, 219 (1961).
- (12) D. F. Evans, *J. Chem. Soc.*, 2003 (1959).
- (13) D. J. Eatough, J. J. Christensen, and R. M. Izatt, "Experiments in Thermometric Titrimetry and Titration Calorimetry", Brigham Young University Press, Provo, Utah, 1973.
- (14) R. A. Bernheim, et al., *J. Chem. Phys.*, **30**, 950 (1959).
- (15) K. R. Magnell, *J. Chem. Educ.*, **50**, 619 (1973).
- (16) L. E. Orgel, "An Introduction to Transition Metal Chemistry", 2nd ed, Wiley, New York, N.Y., 1966, p 85.
- (17) D. W. Meek, et al., *J. Am. Chem. Soc.*, **82**, 6013 (1960).
- (18) A. L. Van Geet, *Anal. Chem.*, **42**, 679 (1970).
- (19) H. K. J. Powell and N. F. Curtis, *J. Chem. Soc. A*, 1441 (1967).
- (20) C. R. Bertsch, et al., *J. Phys. Chem.*, **62**, 444 (1958).

COMMUNICATIONS TO THE EDITOR

Polymorphism of Cholesteryl Acrylate

Publication costs assisted by Gifu University

Sir: Recently, the phase transition of cholesteryl acrylate (CA) has been studied by several workers,¹⁻³ with an interest toward polymerization of CA in the liquid crystal phase. However, there are some discrepancies between various publications on phase transition temperatures of CA. We have attempted to find one cause of the above discrepancies, by means of differential scanning calorimetry (DSC) and polarized light microscopy. In the course of the present work, an unusual phase transition, an exothermic transition on heating process, attracted our attention. This communication reports the effect of an impurity on the phase transition, especially the unusual phase transition, of CA.

CA was prepared by the following two methods. Sample 1³ was prepared by refluxing a chloroform solution (250 ml) of cholesterol (193 g), acrylic chloride (135 g), *N,N'*-dimethylaniline (35 ml), and a small amount of *p*-*tert*-butylcatechol. The residue was recrystallized from a mixture of chloroform-acetone (1:3, yield 40%). The sample was veri-

fied pure by elementary analysis, infrared spectroscopy, thin layer chromatography, nuclear magnetic resonance spectroscopy, and mass spectroscopy. Sample 2⁴ was synthesized by refluxing a methyl ethyl ketone solution (400 ml) containing 48 g of cholesterol, 45 g of acrylic chloride, and 35 ml of *N,N'*-dimethylaniline (yield 30%). Although the sample was recrystallized from a mixture of ethyl ether and ethyl alcohol, the crystals obtained were not absolutely pure. Thin layer chromatography exhibited two spots, and the results of the elementary analysis did not agree with the calculated values. The main impurity is cholesteryl β -chloropropionate, and the amounts are at least less than 3% for sample 1 and roughly several ten percents for sample 2.⁵

Thermal properties were measured with a DSC (Perkin-Elmer, DSC 1B) calibrated with galium and indium, and by hot stage polarized light microscopy.

Typical patterns of thermal hysteresis found by DSC are shown in Figure 1. On the first heating, sample 1 exhibits a solid-solid phase transition at 58°C and is in the mesomorphic state between 125.9 (the melting point, T_m) and 127°C. On the first cooling, there is a cholesteric liquid crystal phase between 127 and about 110°C; the latter tem-

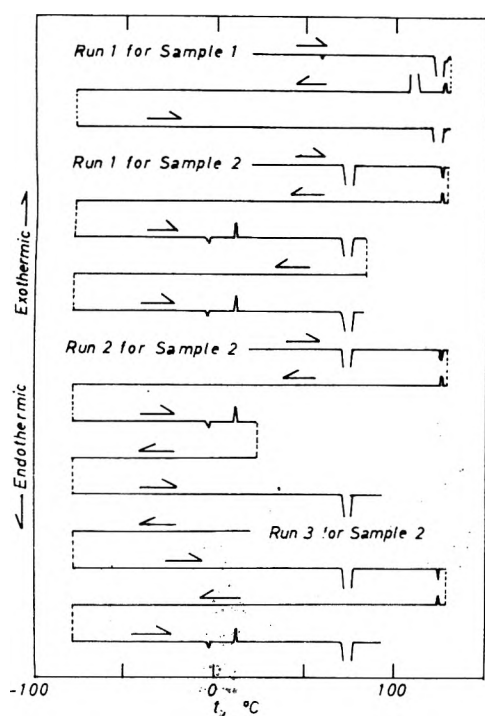


Figure 1. DSC curves of samples 1 and 2 at heating and cooling processes. The temperature was raised and lowered at a rate of $10^{\circ}\text{C}/\text{min}$. Starting samples are the crystals crystallized from recrystallization solvents. Three runs for sample 2 indicate an effect of thermal history on phase transitions.

perature changes depending on the cooling rate. On the second heating, the phase transitions are the same as those on the first heating, except that the transition at 58°C disappears. The phase transitions of sample 2 are quite different from those of sample 1. A mesomorphic phase, nematic in appearance, exists between 75 and 125°C on the first heating. On cooling, the cholesteric liquid crystal phase appears below 125°C . However, no other transition appears down to -78°C . Sample 2 can be purified further by recrystallization from a mixed solvent of chloroform-acetone (1:3). When sample 2 is treated thusly, the melting point approaches gradually toward T_m of sample 1, 124.5°C . Therefore, T_m of CA is very sensitive to impurity concentration.

On the second heating, there are an endothermic transition at -3°C ($\Delta H = 0.7$ cal/g, and $\Delta S = 1.2$ eu) and an exothermic transition at 12.5°C ($\Delta H = -3.6$ cal/g, $\Delta S = -5.6$ eu). These two transitions depend on the history of thermal hysteresis as shown in Figure 1, and were depressed in the sample cooled slowly from the melt. These results may suggest that metastable crystals are formed in impure samples during cooling from the melt and changes to another metastable solid. This solid is transformed to the stable crystals. Similar unusual transitions have been found in several tristearins,^{6,7} several sulfonamides,⁸ cholesteryl laurate,⁹ cholesteryl oleate,¹⁰ and cholesteryl tridecanoate.⁹ On the other hand, it has been reported that the thermal properties of cholesteryl *n*-aliphatic carboxylate are very sensitive to purity of sample.¹¹ Our thermal data on CA suggest that the unusual transition would be caused by crystallization from a metastable solid which occurs during cooling from the melt.

Further detailed mechanisms of phase transitions of CA will be published elsewhere.

Acknowledgments. The authors wish to thank Professor N. Koizumi of Kyoto University, Associate Professor S. Uenishi of Gifu University, and Dr. Y. Tanaka of Research Institute for Polymers and Textiles, Japan, for valuable discussions.

References and Notes

- (1) W. J. Toth and A. V. Tobolsky, *J. Polym. Sci., Part B*, **8**, 289 (1970).
- (2) A. C. de Visser, J. Feyen, K. de Groot, and A. Bartjes, *J. Polym. Sci., Part B*, **8**, 805 (1970).
- (3) G. Hardy, F. Cser, A. Kallo, K. Nytrai, G. Bodor, and M. Lengyel, *Acta Chim. Acad. Sci. Hung.*, **65**, 287 (1970).
- (4) Y. Tanaka, S. Kabaya, Y. Shimura, A. Okada, Y. Kurihara, and Y. Sakakibara, *J. Polym. Sci., Part B*, **10**, 261 (1972).
- (5) These results for sample 2 were obtained by NMR spectroscopy and infrared spectroscopy. To be published elsewhere.
- (6) D. Chapman, *Chem. Rev.*, **62**, 433 (1962).
- (7) E. M. Barral, II, and J. C. Guffy, *Adv. Chem. Ser.*, No. **63**, 1 (1967).
- (8) S. S. Yang and J. K. Guilorry, *J. Pharm. Sci.*, **61**, 26 (1972).
- (9) E. M. Barral, II, J. F. Johnson, and R. S. Porter in "Thermal Analysis", Vol. 1, R. F. Schwenker and P. D. Garn, Ed., Academic Press, New York, N.Y., 1969, p 556.
- (10) A. P. Gray, "Thermal Analysis Newsletter", No. 4, Perkin-Elmer Corp., Norwalk, Conn.
- (11) M. J. Vogel, E. M. Barral, II, and C. P. Mignosa, "Liquid Crystals and Ordered Fluids", J. F. Johnson and R. S. Porter, Ed., Plenum Press, New York, N.Y., 1970, p 333; *Mol. Cryst. Liq. Cryst.*, **15**, 49 (1971).

Department of Synthetic Chemistry
Gifu University
Kagamigahara, Gifu 504
Japan

Shinichi Yano*
Junji Yasue
Koichiro Aoki

Received June 3, 1975

Experimental Confirmation of the Gronwall-Friedman Limiting Law for Unsymmetrical Electrolytes

Sir: Several theoretical treatments of electrolyte solutions¹⁻³ predict terms of the form $l \ln l$ in the partial molar properties of unsymmetrical electrolytes. The most precise available experimental results show no convincing evidence for such terms. Friedman³ examined freezing-point measurements⁴ and emf results^{5,6} for lanthanum chloride; he found no support for the theory beyond the Debye-Hückel limiting law. Recently Pitzer⁷ studied the freezing-point measurements of a 6-1 electrolyte, with a similar lack of success. He concluded that higher-order electrostatic effects were negligible in the extrapolations to infinite dilution required to obtain activity coefficients for pure salt solutions.

We believe that previous attempts to assess the importance of higher-order effects have failed for three reasons: (1) the experimental measurements did not extend to sufficiently low concentration, (2) the concentration intervals were too widely spaced, and (3) graphical rather than analytical means were used to process the results. Accordingly, we have measured the emf's of 12 lanthanum chloride concentration cells with liquid junction over a molality range of 2×10^{-4} to 1×10^{-3} mol kg^{-1} , and with molality differences in the cell compartments of 7×10^{-5} to 4×10^{-4} mol kg^{-1} .

Table I shows the experimental cell potentials at 298.150 K and their differences from the expression

$$E/\text{volt} = -0.03425\bar{t}_+ \int_1^{II} d \ln (m\gamma_{\pm}) \quad (1)$$

TABLE I: Molalities and Cell Potentials for the Cell
 Ag|AgCl|LaCl₃ (m₁)|LaCl₃ (m₂)|AgCl|Ag

(m ₁ /mol kg ⁻¹) × 10 ⁴	(m ₂ /mol kg ⁻¹) × 10 ⁴	E, mV	(E - E _{calc d}), mV
13.277	11.266	2.361	+0.007
11.266	7.650	5.672	+0.007
7.650	5.409	5.161	-0.020
5.409	4.166	3.965	+0.011
4.166	3.505	2.650	+0.013
3.505	2.338	6.253	+0.021
6.690	4.725	5.216	-0.013
4.725	3.964	2.695	+0.026
13.381	10.087	4.081	+0.012
10.087	7.521	4.299	-0.016
7.521	5.637	4.288	-0.019
5.637	4.214	4.379	-0.022

where \bar{t}_+ is the average value of the cation transference number^{8,9} over the molality range of the two cell compartments. We find

$$\ln \gamma_{\pm} = -3.517 \text{ kg}^{1/2} \text{ mol}^{-1/2} I^{1/2} - 5.38672 \text{ kg mol}^{-1} I \ln I/I_0 - 15.42447 \text{ kg mol}^{-1} I \quad (2)$$

where I_0 is a standard value of ionic strength chosen as 1 mol kg⁻¹. The coefficients of the $I \ln I/I_0$ and I terms were obtained from the cell potentials by the method of least squares with a procedure analogous to that used by Gibbard¹⁰ for smoothing enthalpies of dilution.

An F test shows that the coefficient of the $I \ln I/I_0$ term is significantly different from zero. The significance probability of the calculated F value is less than 0.001. The agreement of the coefficient of this term with the value of -5.496 kg mol⁻¹ predicted by Gronwall¹ and Friedman³ is the first quantitative evidence for the validity of the Gron-

wall-Friedman limiting law. The standard errors of the coefficients of the $I \ln I/I_0$ and I terms are 0.76 and 3.29 kg mol⁻¹, respectively. The magnitude of these quantities illustrates the well-known difficulty of determining accurate values of least-squares coefficients when the independent variables are highly correlated.

A partial analysis of results at higher molalities than those in Table I shows that eq 2 is accurate to a few parts per thousand in $\ln \gamma_{\pm}$ only at ionic strengths lower than 0.002 mol kg⁻¹. This is to be expected, because eq 2 contains only the first few terms of a slowly converging series. A discussion of our results at higher molalities and the comparison with previous measurements on this system^{5,6,11} will be presented in a subsequent article.

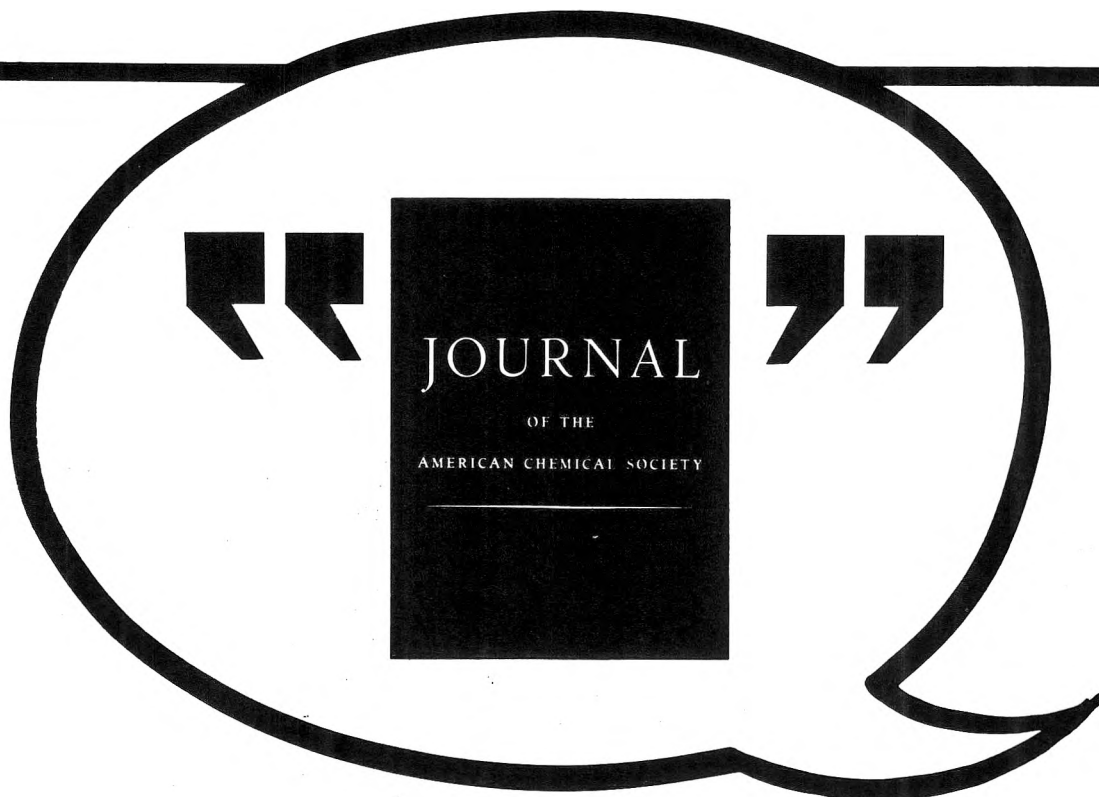
References and Notes

- (1) T. H. Gronwall, V. K. LaMer, and K. Sandved, *Phys. Z.*, **28**, 558 (1928).
- (2) J. G. Kirkwood, *Chem. Rev.*, **19**, 275 (1936).
- (3) H. L. Friedman, "Ionic Solution Theory", Interscience-Wiley, New York, N.Y., 1962.
- (4) G. Scatchard, B. Vonnegut, and D. W. Beaumont, *J. Chem. Phys.*, **33**, 1292 (1960).
- (5) T. Shedlovsky and D. A. MacInnes, *J. Am. Chem. Soc.*, **61**, 200 (1939).
- (6) T. Shedlovsky, *J. Am. Chem. Soc.*, **72**, 3680 (1950).
- (7) K. S. Pitzer, *J. Solution Chem.*, **4**, 249 (1975).
- (8) L. G. Longsworth and D. A. MacInnes, *J. Am. Chem. Soc.*, **60**, 3070 (1938).
- (9) F. H. Spedding, P. E. Porter, and J. M. Wright, *J. Am. Chem. Soc.*, **74**, 2778 (1952).
- (10) H. F. Gibbard, *J. Phys. Chem.*, **73**, 2382 (1969).
- (11) F. H. Spedding, P. E. Porter, and J. M. Wright, *J. Am. Chem. Soc.*, **74**, 2781 (1952).

Department of Chemistry and Biochemistry
 Southern Illinois University
 Carbondale, Illinois 62901

H. Frank Gibbard*
 Michael J. Wilson

Received September 2, 1975



More chemists quote the Journal of The American Chemical Society than any other journal in the world **BECAUSE ...**

Each year the JOURNAL OF THE AMERICAN CHEMICAL SOCIETY publishes nearly 9,000 pages of new chemistry—original research of the widest possible interest in all fields of chemistry.

Each biweekly issue includes up to 50 definitive articles, and about the same number of concise, up-to-the-minute communications by the world's leading chemists.

No wonder the JOURNAL OF THE AMERICAN CHEMICAL SOCIETY is one of chemistry's great subscription values . . . no wonder it is read, studied and quoted by more working chemists than any other publication.

Take advantage of this extraordinary value now . . . complete and send in the coupon today.

**Journal of the American Chemical Society
American Chemical Society**

1976

1155 Sixteenth Street, N.W.
Washington, D.C. 20036

Yes, I would like to receive the JOURNAL OF THE AMERICAN CHEMICAL SOCIETY at the one-year rate checked below:

	<i>U.S.</i>	<i>Canada**</i>	<i>Latin America**</i>	<i>Other Nations**</i>
ACS Member One-Year Rate* <input type="checkbox"/>	\$28.00 <input type="checkbox"/>	\$40.75 <input type="checkbox"/>	\$38.75 <input type="checkbox"/>	\$40.75 <input type="checkbox"/>
Nonmember <input type="checkbox"/>	\$112.00 <input type="checkbox"/>	\$124.75 <input type="checkbox"/>	\$122.75 <input type="checkbox"/>	\$124.75 <input type="checkbox"/>

Bill me Bill company Payment enclosed

Air freight rates available on request.

Name _____

Street _____

Home
Business

City _____

State _____

Zip _____

Journal subscriptions start January '76

*NOTE: Subscriptions at ACS member rates are for personal use only. **Payment must be made in U.S. currency, by international money order, UNESCO coupons, U.S. bank draft, or order through your book dealer.

RADIONUCLIDES IN THE ENVIRONMENT

ADVANCES IN CHEMISTRY SERIES NO. 93

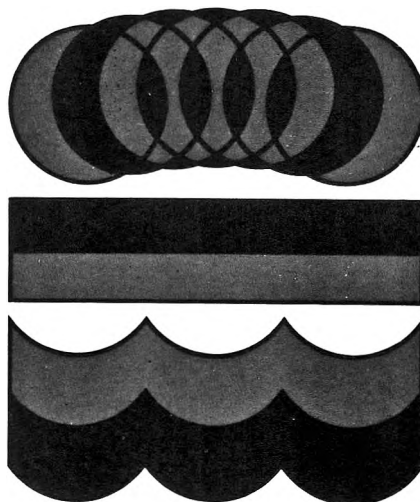
Twenty-eight papers from a symposium sponsored by the Division of Nuclear Chemistry and Technology, chaired by E. C. Freiling.

Pollution . . . a growing concern . . . a concept not generally associated with radionuclides. The successful control of this hazardous waste product of nuclear energy is essential to the continued use and development of nuclear power. Critical to this problem is an understanding of the processes by which radionuclides are produced, dispersed, and retained in the environment.

The papers in this volume discuss and evaluate the properties and problems relating to radionuclides, including

- mechanisms of release, absorption, uptake, transport
- behavior, measurement and characterization, specific weapons tests
- specific activity, public health aspects, fallout
- new methods and equipment

522 pages with index Clothbound (1968) \$15.00
Set of L.C. cards with library orders upon request.



Other books in the ADVANCES IN CHEMISTRY SERIES OF related interest include:

No. 89 Isotope Effects in Chemical Processes. Methods of separating isotopes and labeled molecules—chemical exchange, electromigration, photochemical processes, and distillation—are examined, along with factors that suit a process to isotope separation—single stage fractionation, exchange rate, and reflux.
278 pages cloth (1969) \$13.00

No. 82 Radiation Chemistry—II. Thirty-six papers and 17 abstracts on radiation chemistry in gases, solids, and organic liquids. Includes three plenary lectures. 558 pages cloth (1968) \$16.00

No. 81 Radiation Chemistry—I. Forty-one papers and 17 abstracts on radiation chemistry in aqueous media, biology, and dosimetry. From the international conference at Argonne National Laboratory. 616 pages cloth (1968) \$16.00. No. 81 and 82 ordered together \$30.00

No. 72 Mass Spectrometry in Inorganic Chemistry. A basic tool for chemical manipulations, the mass spectrometer is a conventional monitor for any stage in a research problem to help establish what is going on. 21 Research reports. 329 pages cloth (1968) \$12.00

No. 68 The Mössbauer Effect and Its Application in Chemistry. Ten papers that will familiarize chemists with Mössbauer spectroscopy as an analytical tool for studying chemical bonding, crystal structure, electron density, magnetism, and other properties.

178 pages cloth (1967) \$8.00

No. 66 Irradiation of Polymers. Eighteen papers survey radiation mechanics in polymers, the chemical nature of reactive species produced, crosslinking and scission, homopolymerization, graft copolymerization, and the effects of ultraviolet light radiation.

275 pages cloth (1967) \$10.00

No. 58 Ion-Molecule Reactions in the Gas Phase. Eighteen papers survey spectrometric and other methods for producing and studying ion-molecule reactions such as pulsed sources for studying thermal ions, reactions in flames and electrical discharges.

336 pages cloth (1966) \$10.50

No. 50 Solvated Electron. Reviews of theory, structure, reactions of solvated and hydrated electrons; detailed papers on electrical transport properties, photochemistry, theory of electron transfer reactions, structure of solvated electrons, hydrated electron research. 304 pages cloth (1965) \$10.50

Postpaid in U. S. and Canada; plus 30 cents elsewhere.

Order from:

**SPECIAL ISSUES SALES
AMERICAN CHEMICAL SOCIETY
1155 SIXTEENTH ST., N.W.
WASHINGTON, D. C. 20036**